Synthesis of cobalt complexes towards single-molecule magnets: a structural and magnetic investigation

Laura E. Sharp
M.Sci.

Submitted in fulfilment of the requirements for the
Degree of Doctor of Philosophy

School of Chemistry
College of Science and Engineering
University of Glasgow

2014

Abstract

The syntheses and characterisation of eighteen cobalt containing complexes are reported. These complexes range from simple monomers to complexes containing up to fourteen metal centres. Magnetic susceptibility measurements were carried out on ten complexes, to investigate the possibility of SMM properties.

Cobalt monomers were synthesised using the ligand, 2-Bis(2-hydroxyethyl)amino-2-(hydroxymethyl)-1,3-propanediol, "bis-tris" (H_5L) and subsequently utilised as starting materials to form polynuclear complexes, a homometallic mixed valence Co_{10} complex (**4**) and a heterometallic $\{Mn^{II}_5Co^{III}_4\}$ complex (**5**). Magnetic susceptibility measurements on both these complexes were complicated due to the presence of M^{II} ions in multiple geometries.

A collection of complexes containing two to four metal centres was synthesised using the ligands diethanolamine and triethanolamine. Magnetic susceptibility measurements were carried out on a bromide bridged dimer (**7**), the Co^{II} ions were found to be weakly ferromagnetically coupled and the complex has an effective spin ground state $S' = 1$ with $g > 4$. A mixed valent tetramer (**10**) with two tetrahedral Co^{II} ions was found to have antiferromagnetic interactions.

Five new seven-membered mixed valence disc complexes were synthesised; three homometallic and using the ligands diethanolamine, N-methyldiethanolamine and bis-tris propane; and two heterometallic discs that incorporated Mn^{II} ions, using the ligands 2-amino-2-(hydroxymethyl)-propane-1,3-diol, "tris" and diethanolamine (dea). Magnetic susceptibility measurements carried out on two homometallic Co_7 discs, (**11**) and (**12**), found them to have an effective spin ground state $S' = 2$ with $g > 4$. The magnetic properties of one heterometallic disc were measured $[Co_6Mn(dea)_6(NO_3)_3][NO_3]_2$ (**15**); it was not possible to clarify whether all M^{II}-M^{II} interactions occurring in this complex were ferromagnetic or whether other effects such as zero-field splitting were operative.

Of the larger complexes synthesised a homometallic Co_{10} (**17** and **17a**) complex was found to display predominantly ferromagnetic interactions. A novel heterometallic mixed valence 'double disc' complex with chloride bridges $[Co_{12}Mn_2(NO_3)_4(dea)_{12}Cl_2][Cl]_2[NO_3]_2$ (**18**) was also synthesised.

Acknowledgements

I would like to thank Dr Mark Murrie for his help and guidance throughout the last few years and his patience and support during the production of this thesis.
I would also like to thank Dr Victoria Milway for all her help with magnetic measurements and data. I would also like to thank Dr Floriana Tuna for further magnetic measurements.

For ensuring there were always plenty of trips to the pub, the occasional long lunch, lots of cake and lively conversations, I would like to thank the Murrie group past and present. Thanks to Fraser for helping me get started on the long Ph.D. journey, Andrew for introducing me to the wonderful world of crystallography, and to Vicki for getting the lab organised. Fraser thanks for always having an interesting story and thanks to Katie for sharing all the most important news stories. Ryan, Gavin and MJ thank you for being enthusiastic when I was struggling to see the positives. To all the project students who helped make the office an interesting place to be thanks, especially to Niall for crystallography pointers and to Claire for sharing my love of cobalt.

Without the support of my family I would never have been able to start this Ph.D. let alone finish it, thank you all for being there.

To Michael, thank you for your support, keeping me motivated and cheering me up, this thesis would not have been completed without you. Thank you.

Author's Declaration

The work contained in this thesis, submitted for the degree of doctor of philosophy, is my own original work, except where due reference is made to others. No material within has been previously submitted for a degree at this or any other university.

Definitions

acac	-	Acetylacetonate
bpy	-	2,2′-bypyridine
btH_5	-	2-Bis(2-hydroxyethyl)amino-2-(hydroxymethyl)-1,3-propanediol, bis-tris
$btpH_6$	-	2,2'-(propane-1,3-diyldiimino)bis[2-(hydroxymethyl)propane-1,3-diol, bis-tris propane
BVS	-	Bond valence sum
Bzp	-	2-benzoyl pyridine
CSD	-	Cambridge structural database
$deaH_2$	-	Diethanolamine
$etheidiH_3$	-	N-(1-hydroxymethylpropyl)iminodiacetic acid
Et_2O	-	Diethylether
EtOH	-	Ethanol
Et-sao	-	2-hydroxypropiophenone oxime
F_{calc}	-	Calculated structure-factor amplitude
F_{obs}	-	Observed structure-factor amplitude
g	-	Landé g-factor
Hdeo	-	2-hydroxy-[1,2-di(pyridine-2-yl)]ethane-1-one
$heidiH_3$	-	N-(2-hydroxyethyl)iminodiacetic acid
HF-EPR	-	High Frequency Electron Paramagnetic Resonance
Hmp	-	2-hydroxymethylpyridine
immp	-	2-iminomethyl-6-methoxy-phenolic anion
INS	-	Inelastic neutron scattering
k	-	Boltzmann constant ($1.38 \times 10^{-23}\, JK^{-1}$)
K	-	Kelvin
MeCN	-	Acetonitrile
MeOH	-	Methanol
$metheidiH_3$	-	N-(1-hydroxymethylethyl)iminodiacetic acid
$N\text{-}mdeaH_2$	-	N-Methyldiethanolamine
OAc	-	Acetate
QTM	-	Quantum tunnelling of the magnetisation
sao	-	Salicylaldoxime
SMM	-	Single-molecule magnet
SOC	-	Spin-orbit coupling
SQUID	-	Superconducting Quantum Interference Device

T	-	Temperature
tacn	-	1,4,7-triazacyclononane
TBA	-	Tetrabutylammonium
$teaH_3$	-	Triethanolamine
$thmeH_3$	-	1,1,1-tris(hydroxymethyl)ethane
TIP	-	Temperature independent paramagnetism
TMA	-	Tetramethylammonium
$trisH_3$	-	2-amino-2-(hydroxymethyl)-propane-1,3-diol
ZFS	-	Zero-field splitting

1. Introduction

1.1 Diamagnetism and Paramagnetism

When placed in a homogeneous magnetic field, *H*, a sample will acquire magnetisation, *M*. These are related by *Equation 1-1*, where χ is the magnetic susceptibility.[1]

$$\chi = \mathrm{d}M/\mathrm{d}H \tag{1-1}$$

χ is independent of *H* when the field is weak enough, leading to *Equation 1-2*.[1]

$$\chi = M/H \tag{1-2}$$

Magnetic susceptibility is a combination of two contributions from the diamagnetic susceptibility (χ^D) and paramagnetic susceptibility (χ^P).

$$\chi = \chi^D + \chi^P \tag{1-3}$$

Metal ions that do not contain unpaired electrons are diamagnetic,[2] when placed in a magnetic field the sample will be repelled by the field and therefore the magnetic susceptibility will be negative. Metal ions with unpaired electrons are paramagnetic; there will still be a diamagnetic contribution however it will be hidden by the paramagnetic contribution. A paramagnetic material placed in a magnetic field will be attracted into the field due to the interaction of the unpaired electrons' orbital and/or spin angular momentum with the applied field.

The diamagnetic contribution to a sample can be approximated using *Equation 1-4* where *a* is a factor varying between 0.4 and 0.5 and *Mw* is the molecular weight.[1]

$$\chi^D = aMw \times 10^{-6}\ \mathrm{cm}^3\ \mathrm{mol}^{-1} \tag{1-4}$$

1.2 Molecular Magnetism

The molar magnetic susceptibility, χ_M, characterises the way in which an applied magnetic field, H, interacts with the angular momenta associated with the thermally populated states of a molecule. The angular momenta that must be considered consist of the orbital angular momentum and the electron spin angular momentum. Both of these need to be taken into account when trying to calculate the magnetisation of a complex. An electronic state with total spin angular momentum *S* will have 2*S*+1 sublevels with spin quantum numbers m_s. When a magnetic field is applied Zeeman splitting of the 2*S*+1 m_s levels occurs, separating the energy levels. This is known as the first order Zeeman Effect and the splitting is proportional to the applied field.

Molar magnetic susceptibility can be deduced from one of the fundamental equations of molecular magnetism, *Equation 1-5*.[1]

$$M = N\frac{\sum_n \frac{-dE_n}{dH}\exp(-E_n/kT)}{\sum_n \exp(-E_n/kT)} \tag{1-5}$$

Where *N* is Avagadro's number, E_n (where n = 1, 2, …) is an energy level of the molecule, *T* is the absolute temperature and *k* is the Boltzmann constant. However, as this equation can often be difficult to apply; a simplification was proposed by van Vleck in 1932 based on a few approximations.[1] The first of these is that it is reasonable to expand the energies E_n according to increasing powers of *H*, and the second is that *H* is not too large and *T* is not too small. If these approximations and conditions are applied the result is the van Vleck formula, *Equation 1-6*.

$$\chi_M = \frac{N\sum_n \left[(E_n^{(1)})^2/kT - 2E_n^{(2)}\right]\exp(-E_n^{(0)}/kT)}{\sum_n \exp(-E_n^{(0)}/kT)} \tag{1-6}$$

Where $E_n^{(0)}$ is the energy of level *n* in zero field and $E_n^{(1)}$ and $E_n^{(2)}$ are first- and second-order Zeemann coefficients. The Curie law is derived by further simplification of this equation.[1]

$$\chi_M = \frac{Ng^2\mu_B^2}{3kT}S(S+1) \tag{1-7}$$

or $$\chi_M = \frac{C}{T} \tag{1-8}$$

Where g is a constant (Landé g-factor), which is dependent on the ion, μ_B is the Bohr magneton and S is the spin ground state. The Curie law holds for normal paramagnets and samples that obey the Curie law will show a horizontal straight line in a plot of $\chi_M T$ *vs.* T. However, it has been shown that not all paramagnetic materials obey Curie law, for some materials it is necessary to introduce a further factor, the Weiss constant, θ_W.

$$\chi_M = \frac{C}{T - \theta_W} \tag{1-9}$$

The Weiss constant takes into account intermolecular interactions and is positive for ferromagnets and negative for antiferromagnets. When the absolute temperature is plotted against $1/\chi$ the intercept on the temperature axis is the value of θ_W (Figure 1-1).

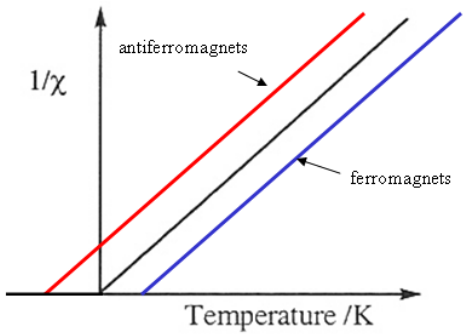

Figure 1-1 Idealised Curie-Weiss behaviour.[3]

1.3 Exchange Interactions

Exchange interactions occurring within a complex can result in magnetic phenomena.[4] Direct exchange occurs between orbitals containing unpaired electrons, without the need for an intermediate atom. Figgis and Martin[5] first proposed direct exchange for a copper complex, $[Cu_2(CH_3CO_2)_4(H_2O)_2]$ suggesting that one unpaired electron in each $d_{x^2-y^2}$ orbital of the Cu^{II} centre interact. However, subsequent work[2] has shown that the copper centres are too far apart for direct orbital overlap to occur. When there is insufficient overlap between the neighbouring magnetic orbitals, superexchange can occur. Superexchange is an exchange interaction between metal ions that proceeds through an intermediate non-magnetic ion. The strength of this type of exchange is dependent on the degree of orbital overlap (where the orbitals involved are p-orbitals), and the distance from the bridging ligand to the metal.[4] Whether the interaction is ferromagnetic or antiferromagnetic depends on the M-L-M angle (where M is the metal and L is the bridging ligand).[6-8]

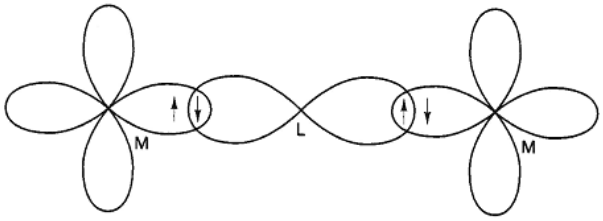

Figure 1-2 Superexchange between two metal centres *via* a bridging ion with a bridging angle of 180° resulting in an antiferromagnetic interaction.[9]

In Figure 1-2, where the interaction is linear between two identical metal centres, the *d*-electrons align antiparallel resulting in an antiferromagnetic interaction. Interactions where the angle is close to 90° result in unpaired *d*-electrons aligning parallel as shown in Figure 1-3, producing a ferromagnetic coupling.

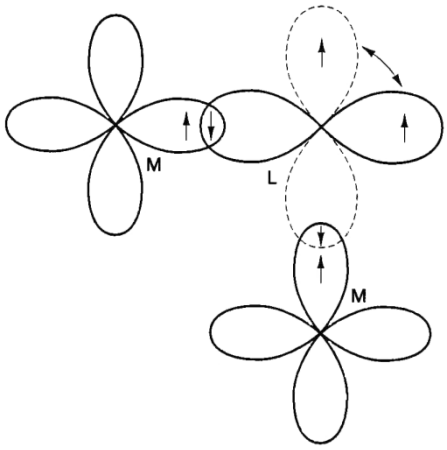

Figure 1-3 Superexchange between two metal centres *via* a bridging ion with a bridging angle of 90° resulting in a ferromagnetic interaction [9]

The unpaired electrons in different *p*-orbitals of the bridging ion tend to align parallel due to spin correlation and exchange stabilisation.[10] This results in ferromagnetic coupling between the two paramagnetic ions. The type of interaction, ferro- or antiferromagnetic is dependent on the M-L-M bridging angle; for a series of analogous complexes with varying M-L-M angle there is often a point below which the coupling is ferromagnetic and above which it becomes antiferromagnetic.[11]

The exchange interaction can be represented by a spin Hamiltonian ($\hat{H}$), where $\hat{S}_i$ and $\hat{S}_j$ are spin operators and J_{ij} is the exchange integral.

$$\hat{H} = -2\sum J_{ij}\,\hat{S}_i \cdot \hat{S}_j \tag{1-10}$$

From *Equation 1-10* for ferromagnetic exchange J is positive and for antiferromagnetic exchange J is negative.

1.4 Single-Molecule Magnets

A complex, which when placed in a magnetic field becomes magnetised and remains so even after the field is switched off, can be described as a single-molecule magnet (SMM).[12] Single-molecule magnets differ from bulk magnets in that their magnetic behaviour is of purely molecular origin, not the long range ordering associated with the latter.

Most SMMs are clusters of paramagnetic transition metal ions linked by bridging ligands, such as oxide and chloride, where the paramagnetic ions can interact via superexchange, described previously (Section 1.3). Magnetisation is normally only retained below a certain temperature, known as the blocking temperature (T_B). The first complex to display SMM behaviour was $[Mn_{12}O_{12}(CH_3CO_2)_{16}(H_2O)_4]\cdot 2CH_3CO_2H\cdot 4H_2O$ (commonly abbreviated to $Mn_{12}OAc$, synthesised by Lis in 1980[13] but first studied as an SMM in 1993[14,15]), with a blocking temperature of around 3 K.[16] The first new complex to show an increase in blocking temperature was an Mn_6 complex, $[Mn^{III}_6O_2(Et\text{-}sao)_6(O_2CPh(Me)_2)_2(EtOH)_6]$ (where Et-saoH$_2$ = 2-hydroxyphenylpropanone oxime and $O_2CPh(Me)_2$ = 3,5-dimethylbenzoate), this complex was found to have a blocking temperature of $\cong$ 4.5 K.[17] This record was subsequently broken in 2011 first by a dysprosium N_2^{3-} radical-bridged complex[18] $[\{[(Me_3Si)_2N]_2Dy(THF)\}_2(N_2)]^-$ and then a few months later by an N_2^{3-} radical-bridged terbium complex.[19] This complex holds the record for the highest blocking temperature of 13.9 K. These two complexes show that the use of lanthanides provides scope for much higher blocking temperatures to be achieved than by d-block metals alone.

The slow relaxation of magnetisation in the absence of an applied field is due to an energy barrier (E_a) to reorientation of the magnetisation, the higher this barrier the greater the blocking temperature. The energy barrier is proportional to the parameters S^2 and D, and the size of the barrier is given by *Equation 1-11* when the spin ground state, S is an integer and *Equation 1-12* for a non-integer. The value of the zero-field splitting parameter (D) is best found using EPR or INS.

$$E_a = S^2|D| \tag{1-11}$$

$$E_a = (S^2 - 1/4)|D| \quad (1\text{-}12)$$

If the complex has a high spin ground state, high magnetic anisotropy (D) and therefore a high zero-field splitting (ZFS) and there are negligible magnetic interaction between molecules, it is more likely that single-molecule magnetism will be observed.[12]

1.4.1 Slow Relaxation of Magnetisation

Slow magnetic relaxation at low temperature in an SMM can be determined in an alternating current (ac) susceptibility measurement, and is a consequence of an axial anisotropy due to a negative axial zero field splitting, *D* which results in splitting of the spin ground state, *S*, into (2*S*+1) m_s levels, from -*S* to +*S* in integer steps. This results in an energy barrier, E_a between the two lowest energy degenerate m_s states (m_s and $-m_s$).[20]

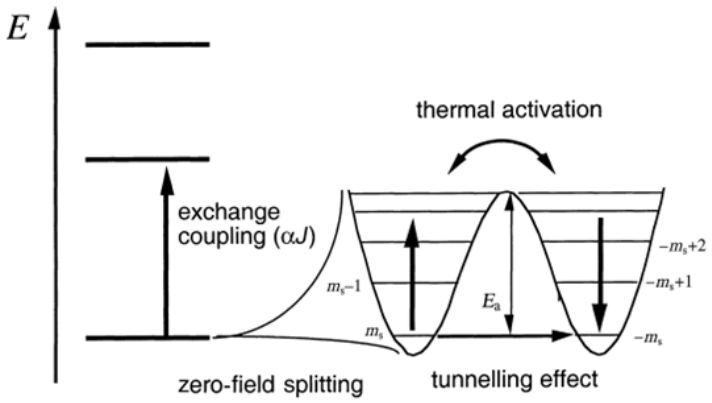

Figure 1-4 Zero-field splitting within the ground state leading to an energy barrier E_a.[20]

From *Equations 1-11 and 1-12* it can be seen that for SMMs a large spin ground state (*S*) and a large and negative axial zero-field splitting (*D*) would lead to a large energy barrier. A large energy barrier allows the spin of the molecule to be magnetised in one direction when a magnetic field is applied. The process of transitioning between positive and negative levels via the m_s = 0 level is thermally activated (Figure 1-4). When the temperature of the sample is below a certain blocking temperature spontaneous reorientation of magnetisation cannot occur. If the magnetic field is applied when the sample is below the blocking temperature the spin population is effectively frozen on one side of the energy barrier. The sample can be magnetised in either direction 'spin up' or 'spin down' at zero field depending on the direction of the applied field. Temperature and sweep rate dependent hysteresis loops are observed in *M vs. H* for SMMs. This magnetic memory effect is due to the energy barrier, E_a.[15] These hysteresis loops often display steps due to an additional

phenomena coined quantum tunnelling of magnetisation through the energy barrier, an example is shown in Figure 1-5.[21]

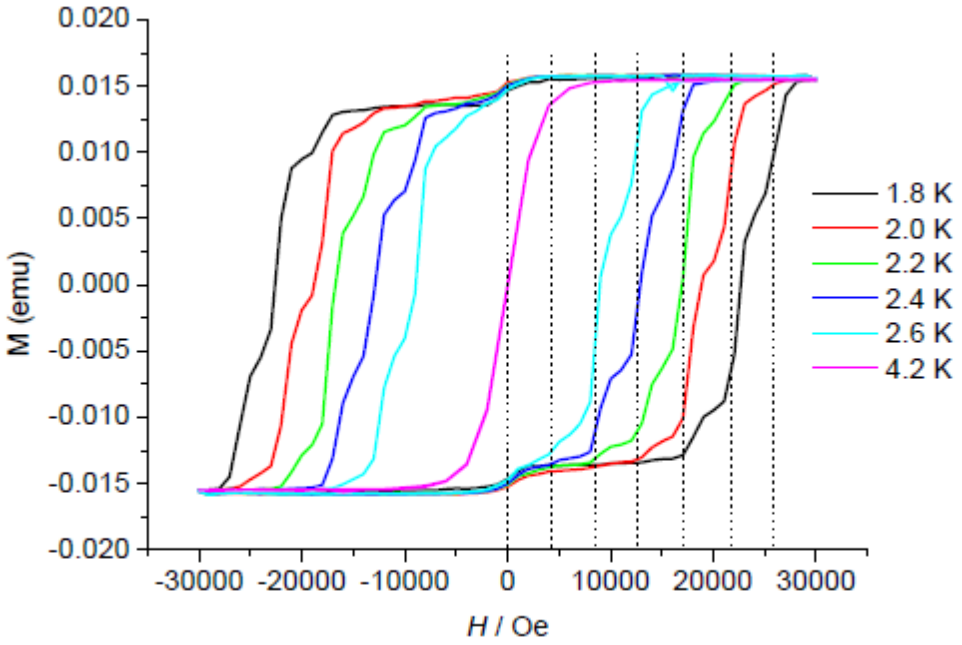

Figure 1-5 Typical example of hysteresis loops recorded for a single crystal of $Mn_{12}Ac$, showing steps associated with quantum tunnelling.[22]

Magnetic susceptibility consists of two parts; an in-phase component, χ' and an out-of-phase component, χ'' that are related according to the *Equations 1-13, 1-14 and 1-15*, where χ is the magnetic susceptibility and φ is the phase shift. Ac susceptibility measurements are used to probe the occurrence of slow relaxation in SMMs.[23] These experiments involve applying an alternating magnetic field to a sample. When the field reaches a large enough frequency the magnetic moment of the sample will not be able to keep up and will lag behind, resulting in a frequency dependent out-of-phase signal.

$$\chi' = \chi \cos\varphi \tag{1-13}$$

$$\chi'' = \sin\varphi \tag{1-14}$$

$$\chi = \sqrt{\chi'^2 + \chi''^2} \tag{1-15}$$[23]

During typical ac susceptibility experiments for an SMM the sample is measured over a temperature range (usually from 10 K to 1.8 K), while the ac field frequency is set. If the sample shows slow relaxation of magnetisation an increase of χ'' signals should be seen over all measured frequencies, these are seen as distinct peaks for many SMMs (Figure 1-6). At low frequencies χ' should approach the susceptibility measured in a static field.

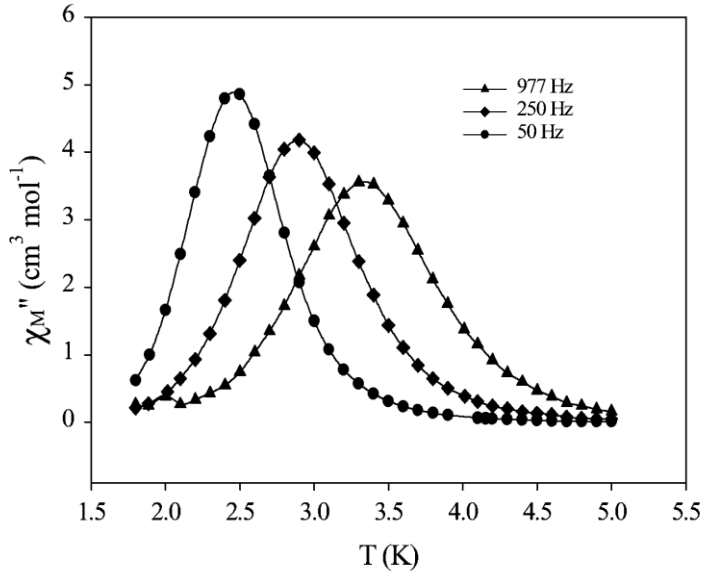

Figure 1-6 Out-of-phase (χ'') signal in ac susceptibility studies *vs.* temperature in an ac field oscillating at the indicated frequencies.[24]

The maximum out-of-phase signal is dependent on both frequency of the ac signal and temperature at which it is measured.[4] The relaxation of magnetisation of a SMM follows an Arrhenius law for a thermally activated process to overcome the energy barrier.[21]

$$\tau = \tau_0 \exp(E_a/kT) \quad \text{where} \quad \tau = (1/2)\pi\nu \qquad (1\text{-}16)$$

Where T is the temperature at which the maximum is observed in the out-of-phase ac susceptibility, k is the Boltzmann constant and ν is the ac frequency in Hertz. If the measurement is repeated at a number of frequencies the E_a and τ_0 can be determined from a plot of lnτ *vs.* 1/*T*.

Hysteresis loops in *M vs. H* studies and the presence of frequency dependent signals in the out-of-phase ac susceptibility measurements are generally taken as evidence that a complex can be regarded as an SMM.

1.4.2 Quantum Tunnelling

Another phenomenon associated with single-molecule magnets is quantum tunnelling of the magnetisation (QTM). This is where relaxation of magnetisation of an SMM occurs below the energy barrier.[25] The presence of QTM is observed as steps in the magnetisation *vs.* field hysteresis loops due to fast relaxation (Figure 1-5). For QTM to occur between two m_s levels with the same energy on either side of the potential energy diagram, there must be some admixing of the states.[26] As the magnetic field is swept from $H = 0$ to $H = nD/g\mu_B$ the degeneracy of the m_s levels on either side of the potential well is lifted and at certain fields a positive m_s state will be aligned with a

negative m_s state, mixing of these states allows relaxation of the magnetisation under the thermal barrier (Figure 1-7).[26]

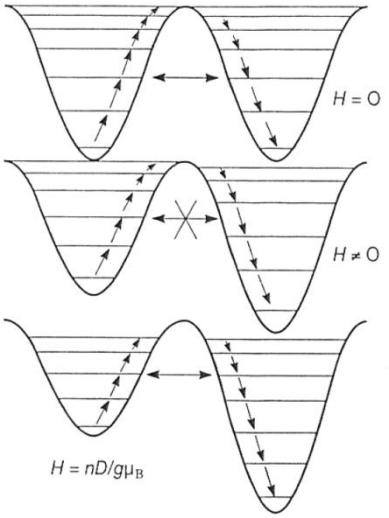

Figure 1-7 Potential energy diagram for an SMM changes as the field is swept from $H = 0$ to $H = nD/g\mu_B$[26]

The necessary admixing of states can be caused by ZFS interactions (E and higher order terms)[12] and/or when a transverse magnetic field is applied to the molecule. A transverse magnetic field is a field that is applied in the xy plane, perpendicular to the easy (z) axis, this induces mixing of states differing in m_s by ±1.[27]

The lifting of degeneracy of spin states in the absence of an applied magnetic field is known as zero-field splitting. The zero-field splitting Hamiltonian is shown in *Equation 1-17*,

$$\hat{H}_{ZFS} = D[\hat{S}_Z^2 - \frac{1}{3}S(S+1)] + E(\hat{S}_X^2 - \hat{S}_Y^2)$$

(axial term) (transverse term) (1-17)

D is the axial ZFS parameter, which changes the energy of the m_s states and the E term mixes the m_s states, specifically those states differing by ±2.[12] For complexes with axial symmetry, the E term will become zero, suggesting that to eliminate QTM from SMMs synthesising clusters with high symmetry would be a good place to start, though success is not guaranteed due to higher order terms. There are several further explanations to account for the observation of QTM for example, dipolar fields caused by neighbouring molecules,[28] nuclear spins[29,30] and phonon-assisted tunnelling.[31]

1.5 Single Crystal X-Ray Diffraction

1.5.1 Background

X-Ray crystallography is a vital tool, used in many areas of chemistry that allows full structural determination of compounds, including inorganic metal clusters. It is one method for examining the structure of materials that are based on the absorption or emission of radiation by the object being examined. To examine structures on the atomic scale it is necessary to choose radiation with wavelengths of the same order or smaller, therefore visible light would not be suitable, so X-ray radiation is used. The most commonly used sources of X-ray radiation are copper and molybdenum where the Kα radiation has wavelengths of 1.54184 Å and 0.71073 Å, respectively.

The radiation is scattered by the object at which it is directed, the scattered rays will have a particular phase and intensity compared to the other scattered rays, meaning that each object will have its own unique scattering pattern. In an optical microscope, the scattered rays are light and can be recombined using lenses, however no material exists that can focus X-rays. In X-ray diffractometers, sensitive detectors are used to recombine the X-rays using mathematical processes.[32] Therefore the process to examine the structure of a complex consists of two stages, recording the X-ray scattering pattern and then the subsequent recombination using mathematics.

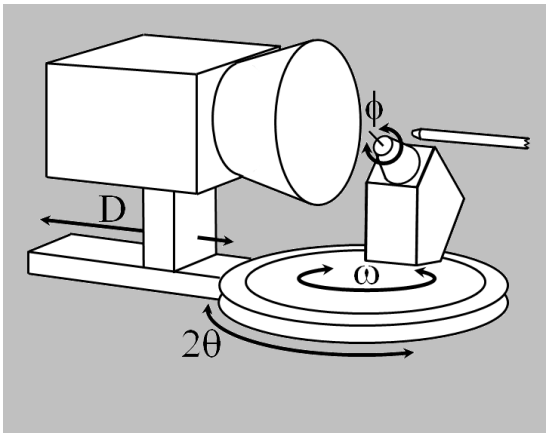

Figure 1-8 Schematic of an X-ray diffractometer showing the detector and goniometer.[33]

The object, as previously mentioned, cannot be a single molecule as it would be impossible to hold this in an X-ray beam for the length of the experiment and the resultant scattering pattern would be far too weak, so a small crystalline sample is used. The smallest repeating unit within the crystal is known as the unit cell. Every molecule contained within the unit cell has many equivalent molecules within the crystal that are aligned in the same way, meaning they will cause the X-rays to scatter in the same way. This combined scattering is sufficiently strong enough to be detected

and measured. The scattering is a result of the interaction between the incident X-rays and the electrons of the atoms, this interaction is very fast compared with the methods used to collect and record the scattering pattern, therefore the result is of time-averaged electron density. Concentrations of electron density correspond to atom positions in the sample structure.

The properties of the scattering pattern correspond to properties of the crystal structure. The geometry of the spots is related to the lattice and unit cell geometry of the crystal structure and gives information about the repeat distances between molecules. The symmetry of the spots, in terms of pattern and intensity, is related to the crystal system and space group. The intensities of the spots contain the information about the positions of atoms within the unit cell.[32]

1.5.2 Symmetry

As previously mentioned crystalline materials must be used for X-ray diffraction, the repeating unit cell allowing for strong enough diffraction patterns to be collected. Between unit cells there is translational symmetry and within the unit cell itself further symmetry elements can exist. This includes rotation (2-, 3-, 4-, and 6-fold), improper rotation ($\bar{2}, \bar{3}, \bar{4}$, and $\bar{6}$), screw axes, glide planes, inversion centres and mirror planes. An improper rotation is defined as a rotation with a simultaneous reflection in a plane perpendicular to the axis and passing through the centre of the molecule. A glide plane is reflection in a mirror plane followed by translation and a screw axis is translation, along the direction of a rotation axis, followed by rotation. If the molecule contains a centre of inversion then it is centrosymmetric.[32] In the crystalline solid state there are 230 possible ways in which these symmetry elements can be put together, these possible arrangements are called space groups, they can be divided up into seven crystal systems. For a unit cell to be assigned to a particular crystal system it must fulfil certain constraints (Table 1-1).

Table 1-1[32] Crystal Systems showing restrictions on unit cell geometry.

Crystal System	Essential Symmetry	Restrictions on unit cell
Triclinic	None	None
Monoclinic	One two-fold rotation and/or mirror	$\alpha = \gamma = 90°$
Orthorhombic	Three two-fold rotation and/or mirrors	$\alpha = \beta = \gamma = 90°$
Tetragonal	One four-fold rotation	$a = b$; $\alpha = \beta = \gamma = 90°$
Rhombohedral	One three-fold rotation	$a = b = c$; $\alpha = \beta = \gamma$ ($\neq 90°$)
Hexagonal	One six-fold rotation	$a = b$; $\alpha = \beta = 90^{\circ}$; $\gamma = 120°$
Cubic	Four three-fold rotation axes	$a = b = c$; $\alpha = \beta = \gamma = 90°$

Inversion, rotation or reflection symmetry in the structure can relate individual atoms and molecules to each other within the unit cell as well as between unit cells, therefore it is possible to select a symmetry independent fraction that may be smaller than the unit cell, this is known as the asymmetric unit. When the space group symmetry is applied to the asymmetric unit it generates the unit cell.[34]

1.5.3 Bragg's Law

The first step in acquiring a structure requires the unit cell to be indentified from the initial matrix images. Bragg's law, (*Equation 1-18*) where λ is the wavelength of the incident X-rays used, d is the spacing of the planes between the atomic lattice and θ is the angle between the incident X-ray and the atomic lattice plane, is used to determine the unit cell parameters.

$$n\lambda = 2d_{hkl}\sin\theta \tag{1-18}$$

By applying Bragg's law each reflection is assigned a set of indices (h,k,l) which give the reflection a specific location in the diffraction pattern. The correct Bravais lattice is assigned after the cell parameters have been found, allowing the correct data collection strategy to be employed. Many frames are collected during the course of the experiment as data collection can take from anywhere between a few hours and a couple of days. From these frames the individual reflections are processed to obtain accurate intensities for each reflection, this involves integrating, scaling and applying corrections such as an absorption correction to the data. The intensity of each spot is proportional to the square of the structure factor, a complex number which contains information about both the amplitude and the phase of a wave. It is not possible to directly record the phase during a diffraction experiment; this is known as the phase problem.

1.5.4 Structure Solution Methods

The phase problem can be overcome using various methods, which allow an electron intensity map to be formed from which the structure can be solved. Direct methods, require some prior knowledge of the chemical structures and solve using electron densities; generally direct methods will yield good phase information when there are no heavy atoms present. Structure factor amplitudes and phases are linked by knowledge of the electron density of the structure being examined; if nothing were known about the electron density direct methods would not work. Constraints, such as there must be discrete atom points and no negative electron density, are applied to ensure a physically reasonable electron density distribution will be generated. Phases are then assigned and refined against the constraints, until a stable set of phases is achieved. Figures of merit (FOMs), are calculated during the phase expansion process, these give an indication of the likelihood that the phases will lead to a correct solution.[35] The phases which give the best FOM are then used to produce an electron density map which, with knowledge of the chemistry involved can be used to give the most likely structure.

In Patterson methods, the phase of the heaviest atom in the structure is used as the phase for the whole crystal structure. This method is also known as a Patterson map, synthesis or function, and is most useful when the structure being examined contains mostly light atoms with a few heavy atoms (Figure 1-9). However, as the Patterson function does not use phase information, every peak observed in the Patterson map corresponds to an interatomic vector.[34]

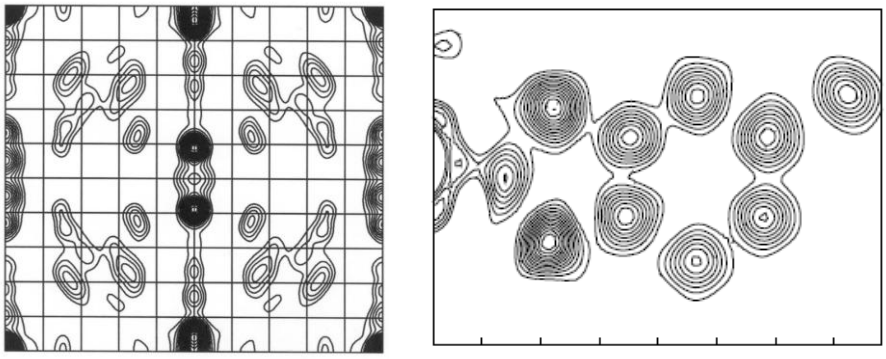

Figure 1-9 Patterson synthesis (left) and Fourier map (right) (Patterson synthesis peaks correspond to vectors between pairs of atoms, atoms relative to each other, Fourier synthesis peaks correspond to atomic positions, relative to the unit cell origin).[36]

The most recently introduced method is charge flipping. This method works in both real and reciprocal space alternating between the two, in the manner of Fourier recycling.[37,38] In real space the sign of the charge density below a certain threshold is reversed, in reciprocal space the F_{obs} moduli are constrained using the unweighted F_{obs} map, and the total charge is allowed to change. The structure is solved by an iterative process, finding a solution that applies to the constraint sets

in both real and reciprocal space. One major advantage of the charge flipping method is that it does not apply symmetry to the structure during the iterative process; the density is treated as if it has *P*1 symmetry,[39] allowing determination of the symmetry to be carried out after structure determination.

These methods allow a large proportion of the electron density of the structure to be identified; however not all the atoms may be found and any missing atoms can be found using a Fourier difference map. Once all atoms have been found and identified the structure can be refined using the least squares refinement. This is the most common approach used to determine the structure of inorganic or small molecules, and involves minimising the function,

$$\sum w(F_{obs} - F_{calc})^2 \quad (1\text{-}19)$$

Where F_{obs} is the strength of an observed diffraction spot and F_{calc} is the value calculated from the structural model for the same reflection and *w* is a chosen weight reflecting the importance of the particular diffraction spot to the total structure, compared with all the other reflections. Carrying out several cycles of least squares refinement will improve the structure to the point where the change in parameters is negligible. At this point the R-factor (residual factor) should be low, as it is a measure of the agreement between the observed and calculated reflections and the result should be a reliable structural description of the contents of the crystal.

The major disadvantage of single crystal X-ray crystallography is the need for high quality crystals of reasonable size to allow high quality data sets to be collected; in some instances this is just not possible. In situations where crystals cannot be examined using lab X-ray diffractometers, alternative methods such as synchrotrons can be used, these produce much more intense X-rays, which are useful for small or weakly diffracting samples.[40]

1.6 Synthetic Methods

1.6.1 Rational Synthesis vs. Serendipitous Approach

In general SMMs are synthesised via either rational design or serendipitous self assembly. In rational design specific ligands that can control the structural outcome are synthesised and the reagents are added in ratios to allow certain structures to be formed. Rational design could also involve starting from a known complex and carrying out ligand substitutions in order to improve desirable properties, such as ferromagnetic exchange. An example of this is a series of Mn_6 complexes, starting from a known complex $[Mn_6O_2(sao)_6(O_2CR)_2(EtOH)_4]$, bulkier ligands (Me-$saoH_2$, Et-$saoH_2$, Ph-$saoH_2$ and R = Ph or Me_2) were synthesised and the hexametallic cluster re-

made. This resulted in the 'twisting' of the Mn-O-N-Mn torsion angle, and enhanced SMM properties.[41]

The serendipitous approach generally involves one step reactions meaning there is little synthetic control especially when using polydentate ligands, with multiple binding sites and binding modes. Base can be added to these reactions in order to attempt to control the deprotonation of the ligand. Ligands can act in two ways, either as a cap to a single metal centre or as a bridge between several metal centres; some ligands are capable of functioning in both ways, such as carboxylate ligands. With so many variables the range of potential structures is huge.

A rational design of an SMM should take into account the desirability of a high spin ground state combined with easy axis magnetic anisotropy as well as consideration of the bridging angles involved in the complex. Control of bridging angles can be very difficult to achieve with small flexible ligands and therefore the use of large rigid ligands is preferred for rational design of SMMs. A successful example of rational design is found in the synthesis of a series of isostructural $[Mn^{III}_6Cr^{III}]^{3+}$ complexes.[42] In this case the counter ion and/or solvent of crystallisation has been varied systematically and the magnetic properties measured, this approach resulted in the SMM $[\{(talen^{t\text{-}Bu_2})Mn^{III}_3\}_2\{Cr^{III}(CN)_6\}](BPh_4)_3$ (where $talen^{t\text{-}Bu_2}$ = tris(tetradentate)triplesalen(t-Bu_2)). Another approach has been to use CN^- bridges between transition metal centres in complexes. These have the advantage over oxo-bridged clusters of forming linear M-CN-M subunits allowing the synthesis of complexes with predictable structures.[43] However, major drawbacks to the rational approach are the need to consider the target complex at the beginning of the synthetic process, when the behaviour of ligands and metals under particular conditions may not be fully understood and also results are ultimately based on the researchers' ability to come up with new ideas.

The alternative to rational synthesis is serendipitous assembly, in this case more flexible ligands with multiple binding modes are chosen, this work generally has most success when previous results and experiments are taken into account and provide a starting point for further work.[44] Another approach to serendipitous assembly is to create an imbalance between the numbers of donor atoms on the ligand and the number of coordination sites on the metal. If a situation is created such that there are too many donor atoms for one metal then it is likely that bridging between metals will occur. This approach has been used successfully with a range of polycarboxylates to create a series of $[Fe_{17}(O)_4(OH)_{16}(heidi)_8(H_2O)_{12}]^{3+}$ and $[Fe_{19}(O)_6(OH)_{14}(heidi)_{10}(H_2O)_{12}]^+$, $[Fe_{19}(O)_6(OH)_{14}(meheidi)_{10}(H_2O)_{12}]^+$ $[Fe_{19}(O)_6(OH)_{14}(etheidi)_{10}(H_2O)_{12}]^+$ cages (where H_3heidi = N-(2-hydroxyethyl)iminodiacetic acid) H_3metheidi = N-(1-hydroxymethylethyl)iminodiacetic acid and H_3etheidi = N-(1-hydroxymethylpropyl)iminodiacetic acid)[45,46] and with citrate $[Ni_{21}(cit)_{12}(OH)_{10}(H_2O)_{10}]Na_8(NMe_4)_8$ cages (H_4cit = $HOC(CO_2H)(CH_2CO_2H)_2$).[47]

The synthesis of metal complexes can be carried out at ambient temperature and atmospheric pressure using low boiling point solvents. Iin the case of reagents which are insoluble or unreactive at room temperature, there are alternative methods which can be used.

1.6.2 Alternative Methods

Synthesis of metal complexes can also be carried out under high pressure for example in solvothermal synthesis.[48] The solvothermal method involves heating the reaction mixture in a sealed vessel, resulting in high pressures as well as temperatures, which may help force reaction of reagents that are insoluble or unreactive at room temperature and ambient pressure. This method may also help the formation of crystals due to the controlled environment and the possibility to allow the reaction to cool to room temperature slowly. One example is the synthesis of Cr^{III} stars, including $[Cr_4\{RC(CH_2O)_3\}(4,4'\text{-}R'_2\text{-bipy})_3Cl_6]$ (where R = Et, $HOCH_2$, Et and R′ = H, ^{t}Bu), formed from a two step solvothermal synthesis which produces crystals directly.[49]

1.7 Ligands

The work contained within this thesis uses a range of structurally similar amino-polyol ligands, diethanolamine (2,2′-iminodiethanol), triethanolamine (tris(2-hydroxyethyl)amine), tris (2-Amino-2-hydroxymethyl-propane-1,3-diol), bis-tris 2-[bis(2-hydroxyethyl)amino]-2-(hydroxymethyl)propane-1,3-diol) and bis-tris propane, (2,2′-(propane-1,3-diyldiimino)bis[2-(hydroxymethyl)propane-1,3-diol]). These ligands were chosen as they all contain multiple donor atoms, both O and N, and are flexible, allowing for different structural motifs to be formed.

1.7.1 Diethanolamine and Triethanolamine

Diethanolamine is the simplest ligand that has been used with only three potential binding sites. It was hoped that the simplicity and unhindered nature of the ligand would allow it to form large clusters under the right conditions. It has previously been shown to form complexes with several transition metals including Co,[50-52] Cu, Cr,[53] Zn, Mn and Fe,[54] a search of the Cambridge structural database (CSD)[55] results in 27 complexes. These vary from dimer structures,[56] mixed metal complexes,[57-59] or clusters with 16 Fe^{III} centres.[60] With such diverse complexes already known it was hoped that there was still scope to extend the use of diethanolamine as a ligand in polymetallic clusters.

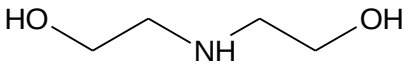

Figure 1-10 Structure of diethanolamine.

N-substituted diethanolamine has also been used in the synthesis of a unique octanuclear chloro-bridged nickel double cubane, $[Ni^{II}_4(OH)Cl_3(HL)_3Cl]_2$ (where H_3L = N-*n*-butyldiethanolamine) which has been shown to have SMM properties.[61] There are also further examples of N-substituted diethanolamine ligands being utilised to form mixed valent Fe_8,[62] and Fe_6[63,64] wheels and clusters.

Triethanolamine was utilised due to its increased flexibility compared to diethanolamine. Many examples of transition metal and lanthanide complexes with triethanolamine as a ligand exist; over 70 examples can be found in the CSD, with varying structural motifs and size. Examples of complexes with triethanolamine include a mixed valent heptanuclear Fe disc[65] and a range of metallo-ring aggregates with the formula $Fe_{16}Ln_4$ (Ln = Sm, Eu, Gd, Tb, Dy, Ho).[66] Many examples with manganese that display SMM properties also exist, both homometallic[67-69] and heterometallic complexes that incorporate Co, Ni, Fe,[70] or Dy.[71] Other examples of heterometallic complexes exist including a pentanuclear complex $Cu^{II}_2Co^{II}Co^{III}_2$,[72] which is formed from an interesting synthetic method utilising zerovalent Cu.

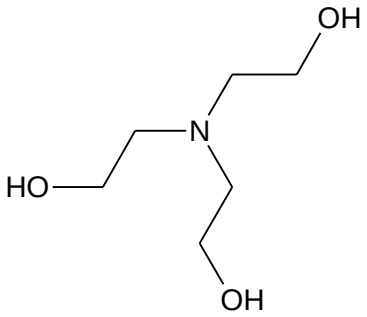

Figure 1-11Structure of triethanolamine.

1.7.2 Tris, Bis-tris and Bis-tris Propane

2-Amino-2-(hydroxymethyl)-propane-1,3-diol, hereby abbreviated to tris, is the simplest of this family of ligands, which were all originally used as biological buffers, it has been used to form a variety of complexes. Simple monomeric complexes,[73,74] polymetallic complexes, including a Co_7 disc which is an SMM,[75] Fe^{III} and Fe^{III}/Cu^{II} spin clusters,[76] a series of interesting mixed-valent $Co^{II}_2Co^{III}_4Ln^{III}_4$ aggregates[77] and polyoxometallate complexes.[78]

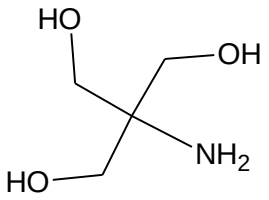

Figure 1-12 Structure of tris, 2-Amino-2-hydroxymethyl-propane-1,3-diol.

2-[*Bis*(2-hydroxyethyl)amino]-2-(hydroxymethyl)propane-1,3-diol, bis-tris, related to both tris and diethanolamine has been used to form monomeric complexes of Ni, Cu and Co.[79] In these complexes the ligand remains fully protonated, binding with an NO_4 donor set with one CH_2OH arm unbound, the distorted octahedral coordination sphere of the metal atom is completed with Cl. Other examples of monomeric complexes exist, including yttrium[80] in which case the Y^{3+} ion is surrounded by one bis-tris ligand bound through four alcohol groups of the ligand and through the central nitrogen, the coordination sphere of the ion is completed by two Cl^- ions and one methanol ligand; lanthanum,[81] in this case the coordination sphere of the La^{3+} ion is filled by two bis-tris ligands, bound through four alcohol groups and the nitrogen, the charge is balanced by three unbound Cl^- ions. Further deprotonation of the ligand, is possible and allows larger complexes to be formed by enabling bridges to form through the oxygen to more than one metal, examples of this exist with cobalt,[82] iron,[83] copper,[84] and manganese.[85]

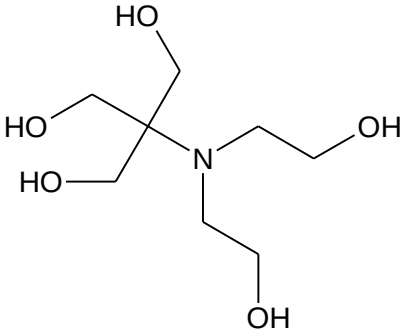

Figure 1-13 Structure of bis-tris, 2-[*Bis*(2-hydroxyethyl)amino]-2-(hydroxymethyl)propane-1,3-diol.

2,2'-(propane-1,3-diyldiimino)bis[2-(hydroxymethyl)propane-1,3-diol, bis-tris propane has two tris groups linked by a propane chain, it was hoped that with multiple binding sites and a degree of

flexibility this ligand would be able to bind to multiple metal centres at one time forming large, and possibly heterometallic clusters. This ligand has previously formed clusters with Mn, Fe,[86] Ni and Co[87] and also a large heterometallic $[Mn^{II}_{12}Mn^{III}_{6}Cu^{II}_{6}O_{14}(H_2L)_6Cl_2(H_2O)_6]Cl_6$ complex (where H_6L = btp) which was synthesised starting from a preformed bis-tris propane Cu^{II} monomer.[88] An example of an yttrium-BTP complex also exists, although this structure has only been determined by potentiometric and ^{1}H-NMR titrations.[89]

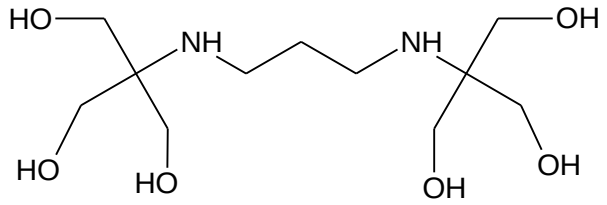

Figure 1-14 Structure of bis-tris propane, 2,2'-(propane-1,3-diyldiimino)bis[2-(hydroxymethyl)propane-1,3-diol.

1.8 Metals

The metals used in this project include cobalt, manganese, nickel, copper, and erbium. The main focus of the work was cobalt complexes, and bimetallic complexes including cobalt.

SMMs containing manganese are the most studied complexes in this area, and much more work will be needed before cobalt SMMs are as well understood.

1.8.1 Magnetic properties of cobalt

The first cobalt SMM was reported in 2002,[90] since then the field of cobalt SMMs has been growing but still lags behind that of other metals, such as manganese, in part due to the difficulty in interpreting magnetic data for polynuclear clusters containing octahedral Co^{II} ions. As mentioned previously for a molecule to be an SMM it should ideally have a large negative *D* value and it is known that Co^{II} has $D_i>0$,[91] however a cluster can show an overall negative *D* value depending on the relative orientation of individual D_i tensors with respect to the easy axis.[21,92,93]

The complexity in interpreting magnetic data for polynuclear Co^{II} complexes arises due to the first order orbital contribution. Metal ions with A or E ground terms have minimal 2nd order orbital contribution to their magnetic moment and often it can be ignored. This allows the magnetic moment to be calculated using the spin-only formula, where *g* is a constant generally ≈ 2 and *S* is the total spin quantum number. For metal ions with these ground states the magnetic moment is independent of temperature and obeys the Curie law. However metal ions with a T ground state,

have a larger 1st order orbital contribution and this must be included when calculating the magnetic moment.

In an octahedral field, at high temperature (>77 K) Co^{II} ions have a $^4T_{1g}$ ground state and display magnetic behaviour consistent with S_i = 3/2. First order spin-orbit coupling splits this ground state into a set of three states (J = 5/2, J = 3/2 and J = ½).[94] Depopulation of the levels occurs as the temperature is lowered, the magnetic moment is temperature dependent, meaning non-Curie behaviour is observed. At low temperature Co^{II} ions can be considered to have S_i = ½ with an effective anisotropic g-value ~ 4.3 which is much greater than the free-electron value of g_e ~ 2.00. This is due to the ground state Kramer's doublet being the only level which will be populated at low temperature due to the energy difference between the different levels. The ground state Kramer's doublet is separated from the other multiplets by around 100 K.[4]

In practice, real complexes rarely contain Co^{II} ions in perfect octahedral arrangements, deviations from strict octahedral environments means that the degeneracy of the $^4T_{1g}$ state is lifted. The symmetry and local environment of Co^{II} ions has been found to have an important role on whether or not the complex is a single-molecule magnet. For Co^{II} ions in tetrahedral geometry the 1st order angular momentum contribution to the magnetic moment will be largely quenched (there will be some residual orbital momentum). The aim of this research project was to synthesise novel cobalt containing complexes and investigate their magnetic properties.

1.9 References

(1) Kahn, O. *Molecular Magnetism*; VCH Publishers Inc.,USA, **1993**.

(2) Mabbs, F. E.; Machin, D. J. *Magnetism and Transition Metal Complexes*; Dover Publications, Inc., USA, **2008**.

(3) Murrie, M. *Molecular Magnetism*, lecture course, **2013**.

(4) Gatteschi, D.; Sessoli, R.; Villain, J. *Molecular Nanomagnets*; Oxford University Press, **2008**.

(5) Figgis, B. N.; Martin, R. L. *Journal of the Chemical Society (Resumed)* **1956**, 3837.

(6) Goodenough, J. B. *Physical Review* **1955**, *100*, 564.

(7) Kanamori, J. *Journal of Physics and Chemistry of Solids* **1959**, *10*, 87.

(8) Goodenough, J. B. *Journal of Physics and Chemistry of Solids* **1958**, *6*, 287.

(9) Kettle, S. F. A. *Physical Inorganic Chemistry: a coordination chemistry approach*; Oxford Univeristy Press, Inc., **1998**.

(10) Orchard, A. F. *Magnetochemistry*; Oxford University Press, **2007**.

(11) Halcrow, M. A.; Sun, J.-S.; Huffman, J. C.; Christou, G. *Inorganic Chemistry* **1995**, *34*, 4167.

(12) Bruce, D. W.; O'Hare, D.; Walton, R. I. *Molecular Materials*; Wiley, **2010**.

(13) Lis, T. *Acta Crystallographica Section B* **1980**, *36*, 2042.

(14) Sessoli, R.; Tsai, H. L.; Schake, A. R.; Wang, S.; Vincent, J. B.; Folting, K.; Gatteschi, D.; Christou, G.; Hendrickson, D. N. *Journal of the American Chemical Society* **1993**, *115*, 1804.

(15) Sessoli, R.; Gatteschi, D.; Caneschi, A.; Novak, M. A. *Nature* **1993**, *365*, 141.

(16) Friedman, J. R.; Sarachik, M. P.; Tejada, J.; Ziolo, R. *Physical Review Letters* **1996**, *76*, 3830.

(17) Milios, C. J.; Vinslava, A.; Wernsdorfer, W.; Moggach, S.; Parsons, S.; Perlepes, S. P.; Christou, G.; Brechin, E. K. *Journal of the American Chemical Society* **2007**, *129*, 2754.

(18) Rinehart, J. D.; Fang, M.; Evans, W. J.; Long, J. R. *Nature Chemistry* **2011**, *3*, 538.

(19) Rinehart, J. D.; Fang, M.; Evans, W. J.; Long, J. R. *Journal of the American Chemical Society* **2011**, *133*, 14236.

(20) Marvaud, V.; Decroix, C.; Scuiller, A.; Guyard-Duhayon, C.; Vaissermann, J.; Gonnet, F.; Verdaguer, M. *Chemistry – A European Journal* **2003**, *9*, 1677.

(21) Gatteschi, D.; Sessoli, R. *Angewandte Chemie International Edition* **2003**, *42*, 268.

(22) van Slageren, J., *Introduction to molecular magnetism*, University of Stuttgart.

(23) Martien, D. *Quantum Design* **2004**.

(24) Brechin, E. K.; Soler, M.; Davidson, J.; Hendrickson, D. N.; Parsons, S.; Christou, G. *Chemical Communications* **2002**, 2252.

(25) Hill, S.; Datta, S.; Liu, J.; Inglis, R.; Milios, C. J.; Feng, P. L.; Henderson, J. J.; del Barco, E.; Brechin, E. K.; Hendrickson, D. N. *Dalton Transactions* **2010**, *39*, 4693.

(26) Christou, G.; Gatteschi, D.; Hendrickson, D. N.; Sessoli, R. *MRS Bulletin* **2000**, *25*, 66.

(27) del Barco, E.; Kent, A. D.; Hill, S.; North, J. M.; Dalal, N. S.; Rumberger, E. M.; Hendrickson, D. N.; Chakov, N.; Christou, G. *Journal of Low Temperature Physics* **2005**, *140*.

(28) Liu, J.; Wu, B.; Fu, L.; Diener, R. B.; Niu, Q. *Physical Review B* **2002**, *65*, 224401.

(29) Prokof'ev, N. V.; Stamp, P. C. E. *Physical Review Letters* **1998**, *80*, 5794.

(30) Sinitsyn, N. A.; Prokof'ev, N. V. *Physical Review B* **2003**, *67*, 134403.

(31) Chiorescu, I.; Giraud, R.; Jansen, A. G. M.; Caneschi, A.; Barbara, B. *Physical Review Letters* **2000**, *85*, 4807.

(32) Clegg, W. *Crystal Structure Determination*; Oxford University Press, **1998**.

(33) Copley, R. X-Ray Structure Analysis, 14th BCA/CCG Intensive School, **2013**.

(34) Ladd, M.; Palmer, R. *Structure Determination by X-Ray Crystallography*; kluwer Academic/Plenum Publishers, **2003**.

(35) Massa, W. *Crystal Structure Determination*; Second ed.; Springer-Verlag, **2004**.

(36) Clegg, W. X-Ray Structure Analysis, 14th BCA/CCG Intensive School, **2013**.

(37) Oszlanyi, G.; Suto, A. *Acta Crystallographica Section A* **2004**, *60*, 134.

(38) Palatinus, L.; Chapuis, G. *Journal of Applied Crystallography* **2007**, *40*, 786.

(39) Palatinus, L.; van der Lee, A. *Journal of Applied Crystallography* **2008**, *41*, 975.

(40) Thompson, A. L. In *X-Ray Structure Analysis, 14th BCA/CCG Intensive School*, **2013**.

(41) Milios, C. J.; Inglis, R.; Bagai, R.; Wernsdorfer, W.; Collins, A.; Moggach, S.; Parsons, S.; Perlepes, S. P.; Christou, G.; Brechin, E. K. *Chemical Communications* **2007**, 3476.

(42) Glaser, T. *Chemical Communications* **2011**, *47*, 116.

(43) Atanasov, M.; Comba, P.; Hausberg, S.; Martin, B. *Coordination Chemistry Reviews* **2009**, *253*, 2306.

(44) Winpenny, R. E. P. *Journal of the Chemical Society, Dalton Transactions* **2002**, 1.

(45) Powell, A. K.; Heath, S. L.; Gatteschi, D.; Pardi, L.; Sessoli, R.; Spina, G.; Del Giallo, F.; Pieralli, F. *Journal of the American Chemical Society* **1995**, *117*, 2491.

(46) Goodwin, J. C.; Sessoli, R.; Gatteschi, D.; Wernsdorfer, W.; Powell, A. K.; Heath, S. L. *Journal of the Chemical Society, Dalton Transactions* **2000**, 1835.

(47) Murrie, M.; Stoeckli-Evans, H.; Güdel, H. U. *Angewandte Chemie International Edition* **2001**, *40*, 1957.

(48) Laye, R. H.; McInnes, E. J. L. *European Journal of Inorganic Chemistry* **2004**, 2811.

(49) Batchelor, L. J.; Sander, M.; Tuna, F.; Helliwell, M.; Moro, F.; van Slageren, J.; Burzuri, E.; Montero, O.; Evangelisti, M.; Luis, F.; McInnes, E. J. L. *Dalton Transactions* **2011**, *40*, 5278.

(50) Tudor, V.; Marin, G.; Lloret, F.; Kravtsov, V. C.; Simonov, Y. A.; Julve, M.; Andruh, M. *Inorganica Chimica Acta* **2008**, *361*, 3446.

(51) Bertrand, J. A.; Fujita, E.; VanDerveer, D. G. *Inorganic Chemistry* **1979**, *18*, 230.

(52) Tudor, V.; Madalan, A.; Lupu, V.; Lloret, F.; Julve, M.; Andruh, M. *Inorganica Chimica Acta* **2010**, *363*, 823.

(53) Semenaka, V. V.; Nesterova, O. V.; Kokozay, V. N.; Dyakonenko, V. V.; Zubatyuk, R. I.; Shishkin, O. V.; Boča, R.; Jezierska, J.; Ozarowski, A. *Inorganic Chemistry* **2010**, *49*, 5460.

(54) Ako, A. M.; Mereacre, V.; Lan, Y.; Wernsdorfer, W.; Clérac, R.; Anson, C. E.; Powell, A. K. *Inorganic Chemistry* **2009**, *49*, 1.

(55) Allen, F. *Acta Crystallographica Section B* **2002**, *58*, 380.

(56) Tudor, V.; Marin, G.; Kravtsov, V.; Simonov, Y. A.; Lipkowski, J.; Brezeanu, M.; Andruh, M. *Inorganica Chimica Acta* **2003**, *353*, 35.

(57) Nesterov, D. S.; Kokozay, V. N.; Dyakonenko, V. V.; Shishkin, O. V.; Jezierska, J.; Ozarowski, A.; Kirillov, A. M.; Kopylovich, M. N.; Pombeiro, A. J. L. *Chemical Communications* **2006**, 4605.

(58) Nesterov, D. S.; Makhankova, V. G.; Vassilyeva, O. Y.; Kokozay, V. N.; Kovbasyuk, L. A.; Skelton, B. W.; Jezierska, J. *Inorganic Chemistry* **2004**, *43*, 7868.

(59) Nesterov, D. S.; Kokozay, V. N.; Skelton, B. W. *Acta Crystallographica Section C* **2006**, *62*, m246.

(60) Ako, A. M.; Mereacre, V.; Lan, Y.; Anson, C. E.; Powell, A. K. *Chemistry – A European Journal*, **2011**, *17*, 4366.

(61) Scheurer, A.; Gieb, K.; Alam, M. S.; Heinemann, F. W.; Saalfrank, R. W.; Kroener, W.; Petukhov, K.; Stocker, M.; Muller, P. *Dalton Transactions* **2012**, *41*, 3553.

(62) Prakash, R.; Saalfrank, R. W.; Maid, H.; Scheurer, A.; Heinemann, F. W.; Trautwein, A. X.; Böttger, L. H. *Angewandte Chemie International Edition* **2006**, *45*, 5885.

(63) Saalfrank, R. W.; Prakash, R.; Maid, H.; Hampel, F.; Heinemann, F. W.; Trautwein, A. X.; Böttger, L. H. *Chemistry – A European Journal* **2006**, *12*, 2428.

(64) Saalfrank, R. W.; Deutscher, C.; Maid, H.; Ako, A. M.; Sperner, S.; Nakajima, T.; Bauer, W.; Hampel, F.; Heß, B. A.; van Eikema Hommes, N. J. R.; Puchta, R.; Heinemann, F. W. *Chemistry – A European Journal* **2004**, *10*, 1899.

(65) Liu, T.; Wang, B.-W.; Chen, Y.-H.; Wang, Z.-M.; Gao, S. *Zeitschrift für anorganische und allgemeine Chemie* **2008**, *634*, 778.

(66) Baniodeh, A.; Hewitt, I. J.; Mereacre, V.; Lan, Y.; Novitchi, G.; Anson, C. E.; Powell, A. K. *Dalton Transactions* **2011**, *40*, 4080.

(67) Murugesu, M.; Wernsdorfer, W.; Abboud, K. A.; Christou, G. *Angewandte Chemie International Edition* **2005**, *44*, 892.

(68) Stamatatos, T. C.; Poole, K. M.; Foguet-Albiol, D.; Abboud, K. A.; O'Brien, T. A.; Christou, G. *Inorganic Chemistry* **2008**, *47*, 6593.

(69) Langley, S. K.; Moubaraki, B.; Berry, K. J.; Murray, K. S. *Dalton Transactions* **2010**, *39*, 4848.

(70) Langley, S. K.; Chilton, N. F.; Moubaraki, B.; Murray, K. S. *Dalton Transactions* **2012**, *41*, 1033.

(71) Langley, S. K.; Moubaraki, B.; Murray, K. S. *Dalton Transactions* **2010**, *39*, 5066.

(72) Makhankova, V. G.; Vassilyeva, O. Y.; Kokozay, V. N.; Skelton, B. W.; Reedijk, J.; Van Albada, G. A.; Sorace, L.; Gatteschi, D. *New Journal of Chemistry* **2001**, *25*, 685.

(73) Herrick, R. S.; Ziegler, C. J.; Lopez, J.; Barone, N. V.; Gambella, A.; masi, C. *J. Organomet. Chem.* **2012**, *700*, 168.

(74) Ivarsson, G. *Acta Crystallographica Section B* **1982**, *38*, 1828.

(75) Ferguson, A.; Parkin, A.; Sanchez-Benitez, J.; Kamenev, K.; Wernsdorfer, W.; Murrie, M. *Chemical Communications* **2007**, 3473.

(76) Ferguson, A.; McGregor, J.; Brechin, E. K.; Thomas, L. H.; Murrie, M. *Dalton Transactions* **2009**, 9395.

(77) Xiang, H.; Lan, Y.; Li, H.-Y.; Jiang, L.; Lu, T.-B.; Anson, C. E.; Powell, A. K. *Dalton Transactions* **2010**, *39*, 4737.

(78) Song, Y.-F.; Abbas, H.; Ritchie, C.; McMillian, N.; Long, D.-L.; Gadegaard, N.; Cronin, L. *Journal of Materials Chemistry* **2007**, *17*, 1903.

(79) Inomata, Y.; Gochou, Y.; Nogami, M.; Howell, F. S.; Takeuchi, T. *Journal of Molecular Structure* **2004**, *702*, 61.

(80) Chen, Q.; Chang, Y. D.; Zubieta, J. *Inorganica Chimica Acta* **1997**, *258*, 257.

(81) Jin Oh, S.; Choi, Y.-S.; Hwangbo, S.; Chul Bae, S.; Kang Ku, J.; Won Park, J. *Chemical Communications* **1998**, 2189.

(82) Ferguson, A.; Parkin, A.; Murrie, M. *Dalton Transactions* **2006**, 3627.

(83) Ferguson, A.; McGregor, J.; Parkin, A.; Murrie, M. *Dalton Transactions* **2008**, 731.

(84) Kirillov, A. M.; Karabach, Y. Y.; Kirillova, M. V.; Haukka, M.; Pombeiro, A. J. L. *Dalton Transactions* **2011**, *40*, 6378.

(85) Stamatatos, T. C.; Abboud, K. A.; Christou, G. *Dalton Transactions* **2009**, 41.

(86) Ferguson, A.; Darwish, A.; Graham, K.; Schmidtmann, M.; Parkin, A.; Murrie, M. *Inorganic Chemistry* **2008**, *47*, 9742.

(87) Ferguson, A.; Schmidtmann, M.; Brechin, E. K.; Murrie, M. *Dalton Transactions* **2011**, *40*, 334.

(88) Milway, V. A.; Tuna, F.; Farrell, A. R.; Sharp, L. E.; Parsons, S.; Murrie, M. *Angewandte Chemie International Edition*, **2013**, *52*, 1949.

(89) Gomez-Tagle, P.; Yatsimirsky, A. K. *Journal of the Chemical Society, Dalton Transactions* **2001**, *0*, 2663.

(90) Wu, C.-C.; Datta, S.; Wernsdorfer, W.; Lee, G.-H.; Hill, S.; Yang, E.-C. *Dalton Transactions* **2010**, *39*, 10160.

(91) Boča, R. *Coordination Chemistry Reviews* **2004**, *248*, 757.

(92) Yang, E.-C.; Hendrickson, D. N.; Wernsdorfer, W.; Nakano, M.; Zakharov, L. N.; Sommer, R. D.; Rheingold, A. L.; Ledezma-Gairaud, M.; Christou, G. *Journal of Applied Physics* **2002**, *91*, 7382.

(93) Oshio, H.; Nakano, M. *Chemistry – A European Journal* **2005**, *11*, 5178.

(94) Lloret, F.; Julve, M.; Cano, J.; Ruiz-GarcÃ-a, R.; Pardo, E. *Inorganica Chimica Acta* **2008**, *361*, 3432.

2. Synthesis of monomers and their use as starting materials

The first group of complexes described make use of the bis-tris (2-[Bis(2-hydroxyethyl)amino]-2-(hydroxymethyl)propane-1,3-diol, H_5L) ligand (Figure 2-1, a), which has five alcohol groups around a central N-donor atom making it capable of forming multiple bridges. This ligand can be thought of as a combination of dipodal and tripodal alcohol ligands, such as *N*-methyldiethanolamine and tris (see Section 1.7.2). These types of ligand have proved very successful in forming polynuclear 3*d* clusters with a range of structures and interesting magnetic properties.[1-5]

Monomeric compounds utilising the ligand bis-tris with Ni, Cu, Zn, Co,[6] and Mn,[7] and La,[8] and Y,[9] have been reported. Monomers have the form $[M(H_5L)Cl]^+$ or $[M(H_5L)H_2O]^{2+}$ where M = Ni, Cu; $[Co^{II}(H_5L)(HCOO)]^+$;[6] and a Mn example has the form $[Mn^{III}(N_3)(H_3L)]$ where the ligand is partially deprotonated giving a neutral complex.[7] The La monomer is a different case where two ligands coordinate to one metal ion $[La^{III}(H_5L)_2]Cl_3$[8] and the yttrium monomer has the form as previous transition metal examples with the additional coordination sites filled by anions and a bound molecule of solvent $[Y^{III}(H_5L)Cl_2(MeOH)]Cl$.[9]

Polynuclear complexes with Fe, Mn, Cu and Co have been formed using the bis-tris ligand. These complexes show a variety of geometries and binding modes, with so many variables there is still potential for exciting new complexes to be discovered. $\{Fe^{III}_{10}\}$ and $\{Fe^{III}_{10}Na\}$ complexes[10] were reported to have a core topology that was unique in iron chemistry and a $\{Cu_3\}$ complex[11] remains the only example of a multicopper complex with this ligand. Heterometallic examples of complexes with this ligand are the $\{Mn_4Ln_4\}$ series where Ln = Gd, Tb, Dy, Ho and Er,[12] which was the first successful use of this ligand in 3*d*-4*f* chemistry. The two complexes with Tb and Dy display slow relaxation of magnetisation and potential SMM behaviour. Focussing on cobalt, $[Co_4Na_2(HL)_2(H_2L)_2(MeOH)_4]$ and pentanuclear $[Co_5(HL)_2(H_2L)_2]$ complexes have been previously synthesised,[13] as well as the previously mentioned monomeric Co compound.[6] However, no further work had been undertaken with these monomers. It has been shown that a mononuclear bis-tris manganese complex $[Mn^{III}(N_3)(H_3L)]$ can be further reacted with $Mn^{II}Cl_2{\cdot}4H_2O$ to create a pentanuclear $Mn^{II/III}$ cluster $[Mn^{II}_2Mn^{III}_3(H_2L)_3(H_5L)(MeOH)_{2.5}]Cl_4$ (Figure 2-1, b/c).[7]

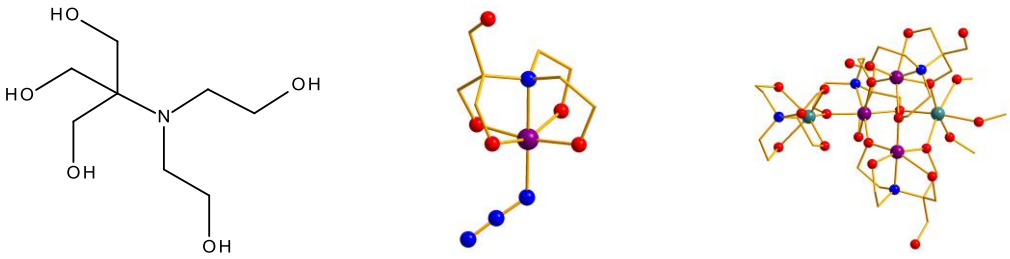

a **b** **c**

Figure 2-1 a, Bis-tris ligand; b, Mn^{III} monomer; c, $[Mn^{II}_2Mn^{III}_3]$ complex.[7] Mn^{II} dark purple; Mn^{III} teal; O red; N blue.

It was anticipated that a Co bis-tris monomer could be used as a building block to form both higher nuclearity Co clusters and heterometallic clusters. By pre-forming the monomer it was hoped that a degree of control over the product complex could be gained by altering initial reaction ratios and concentrations. Previous successful examples of this method exist for chromium complexes[14] where the nuclearity of the complex was controlled by altering the ratio of metal salt to ligand in the reaction.

Examples of other ligands being used as precursors to form high nuclearity clusters, has already proved successful, for example with this $[Cu^{II}_6Mn^{III}_{12}Mn^{II}_6O_{14}(btpH_2)_6Cl_2(H_2O)_6]Cl_6$ complex, which is formed from a copper monomer with the ligand bis-tris propane ($btpH_6$).[15] Alternatively larger building blocks[16,17] have also been utilised to form large clusters, with the advantage of greater control over the form of the final complex due to larger sections already having fixed geometry in the starting material. Building blocks can also take forms, which provide 'built in' favourable magnetic properties to the final complex. For example metal triangles,[16,18,19] a complex which contained many triangular building blocks would have a greater chance of having a non-zero spin ground state. Another building block that has been used successfully are hepta-cyanometalates, such as $[Mo^{III}(CN)_7]^{4-}$,[20,21] which is lower symmetry than the hexa-cyanometalate equivalent and is magnetically anisotropic, this produced small complexes with interesting magnetic behaviour when combined with Mn^{II} ions.[22-24]

2.1 Synthesis of Cobalt Monomers with Bis-tris

2.1.1 Synthesis of [$Co^{II}(H_5L)Cl$] Cl (1)

(where H_5L = bis-tris, $C_8H_{19}NO_5$)

Bis-tris (0.84 g, 4.01 mmol) was dissolved in 1-propanol (30 mL). $CoCl_2.6H_2O$ (0.95 g, 3.99 mmol) was dissolved in *n*-propanol (30 mL), and added to the bis-tris solution. Within a few minutes a pink precipitate formed, the reaction mixture is left to stir at room temperature for 2 days. The pink precipitate was collected by filtration and allowed to air dry, resulting in 84% yield. The remaining solution was left to evaporate slowly. After approximately one week, large well defined bright pink plates were formed. Air dried precipitate analyses as $C_8H_{19}NO_5Cl_2Co$, analysis (%) calc. (found) C, 28.33 (28.07); H, 5.66 (5.71); N, 4.13 (4.05). Selected IR data: ν = 3327, 3078, 2958, 2837, 2754, 2704, 1425, 1404, 1317, 1286, 1037, 995, 877, 705, 655 cm^{-1}. IR data confirmed that the precipitate and crystals were the same compound.

2.1.2 Synthesis of [$Co^{II}(H_5L)(NO_3)$][NO_3] (2)

Bis-tris (1.26 g, 5.98 mmol) was dissolved in acetonitrile (60 mL) at 50°C. $Co(NO_3)_2.6H_2O$ (1.74 g, 6.02 mmol) was dissolved in acetonitrile (60 mL) at 50°C , and added to the bis-tris solution. Within a few minutes a peach/pink precipitate formed and the reaction mixture was left to stir at room temperature for 3 days. The pink precipitate was collected by filtration and allowed to air dry, resulting in 87% yield. The remaining solution was left to evaporate slowly and after approximately one week, well defined bright pink plates were formed. Air dried precipitate analyses as $C_8H_{19}N_3O_{11}Co$**,** analysis (%) calc. (found) C, 24.50 (24.69); H, 4.88 (5.02); N, 10.71 (10.55). Selected IR data: υ = 3097, 2958, 2090, 1456, 1417, 1392, 1327, 1294, 1174, 1155, 1099, 1070, 1051, 1030, 993, 875, 812, 744, 732, 704, 651 cm^{-1}. IR data confirmed that the precipitate and crystals were the same compound.

2.1.3 Synthesis of [$Co^{II}(H_5L)(Br)$]Br (3)

Bis-tris (1.68 g, 8.03 mmol) was dissolved in *n*-propanol (80 mL) at 50°C. $CoBr_2$ (1.76 g, 8.05 mmol) was dissolved in *n*-propanol (80 mL) at 50°C, and added to the bis-tris solution. Within a few minutes a peach/pink precipitate formed and the reaction mixture was left to stir at room temperature for 3 days. The pink precipitate was collected by filtration and allowed to air dry, resulting in 68% yield. The remaining solution was left to evaporate slowly and air dried precipitate analyses as $C_8NO_5H_{19}Br_2Co$**,** analysis (%) calc. (found) C, 22.45 (22.26); H, 4.48 (4.50); N, 3.27 (3.21). Selected IR data: ν = 3263, 3149, 1450, 1419, 1386, 1336, 1286, 1249, 1236, 1219, 1143, 1051, 1024, 1003, 945, 916, 877, 740, 650 cm^{-1}.

2.2 Cobalt monomers

2.2.1 Discussion of crystal structure of [Co^{II}(H$_5$L)Cl][Cl](1)

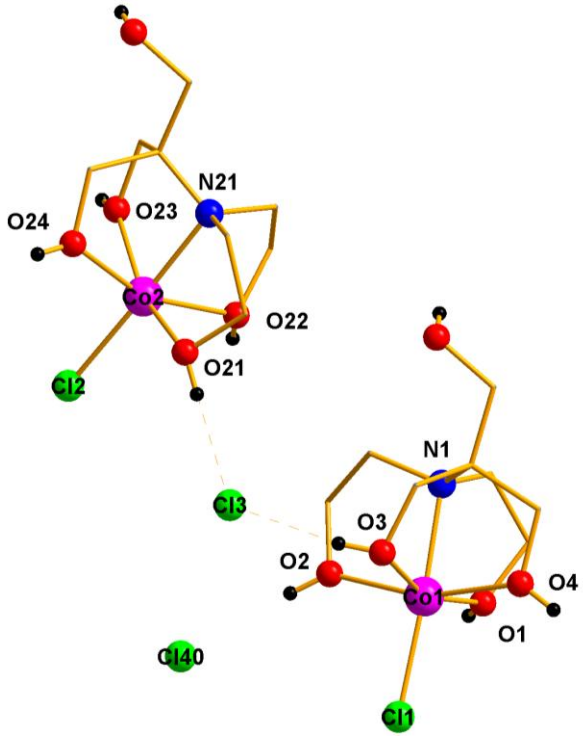

Figure 2-2 Representation of complex 1 with CH atoms omitted for clarity. Co^{II} pink; N blue; O red; Cl bright green; H black.

The complex crystallises in the monoclinic space group *Pn* and there are two monomers per asymmetric unit and four in the unit cell. The Co^{II} atom is coordinated by an {NO$_4$} ligand donor set (with all ligand O remaining protonated) and a Cl ligand, arranged in a distorted octahedral geometry. The charge is balanced by the presence of one unbound Cl anion per complex. One of these, Cl40, is disordered over three positions (with occupancy modelled as Cl40 = 0.75; Cl41 = 0.2; Cl42 = 0.05). Cl3 is almost equidistant between the two monomers with short contacts to O3 (O3(H) ⋯Cl3 2.996(2) Å) and O21 (O21(H) ⋯Cl3 3.066(3) Å) (Figure 2-2).

The complex packs in rows with the orientation of the unbound OH group alternating along the rows parallel to the *c*-axis and down the rows parallel to the *b*-axis, the ligand chlorides all point in the same direction (Figure 2-3).

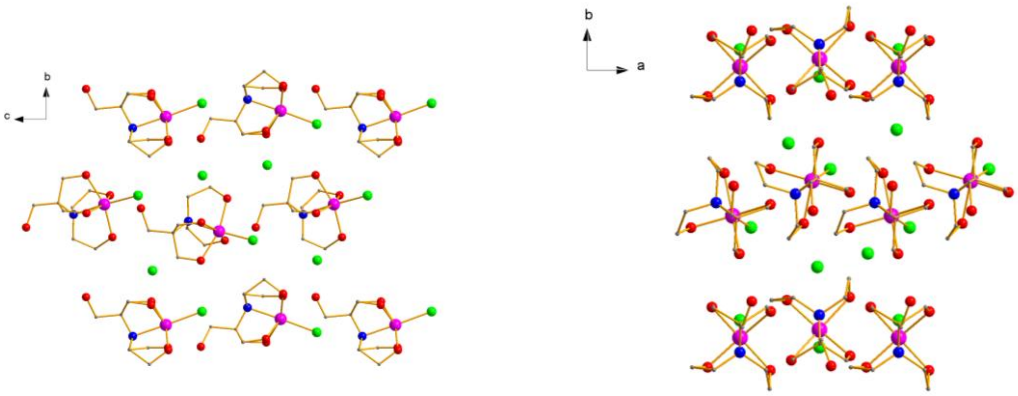

Figure 2-3 Packing diagram of 1 viewed along the *a*-(left) and *c*-axes (right).

Table 2-1 Data for crystal structure determination of 1.

Empirical Formula	$C_8H_{19}Cl_2CoNO_5$
Fw (g mol^{-1})	339.11
Crystal system	Monoclinic
Space group	*Pn*
a (Å)	7.4713(8)
b (Å)	12.719(1)
c (Å)	14.058(1)
β (deg)	91.656(6)
V (Å^3)	1335.3(2)
Z	4
T (K)	100(2)
λ (Å)	0.71073
ρ_{calcd} (Mg m^{-3})	1.687
μ (mm^{-1})	3.386
R_1[a]	0.0459
wR_2[b]	0.0859
Goodness of fit	0.908

[a] $R_1 = \Sigma \left| |F_o| - |F_c| \right| / \Sigma |F_o|$ [b] $wR_2 = \left[\Sigma \left[w\left(F_o^2 - F_c^2\right)^2 \right] - \Sigma \left[\left(F_o^2\right)^2 \right] \right]^{1/2}$ where $w = 1/\left[\sigma^2\left(F_o^2\right) + \left(0.2P\right)^2\right]$ and $P = \left[F_o^2 + 2F_c^2\right]/3$

Table 2-2 Metal-ligand bond lengths in 1.

Bond	Distance (Å)	Bond	Distance (Å)
Co1 – Cl1	2.3201(2)	Co2 – Cl2	2.3569(2)
Co1 – N1	2.1572(2)	Co2 – N21	2.1444(2)
Co1 – O1	2.0693(2)	Co2 – O21	2.1043(1)
Co1– O2	2.1039(2)	Co2 – O22	2.0699(1)
Co1 – O3	2.1237(2)	Co2 – O23	2.1555(1)
Co1 – O4	2.1257(2)	Co2 – O24	2.0779(1)

Table 2-3 BVS calculations, the underlined value is that closest to the charge for which it was calculated.[25]

Atom	Co^{II}	Co^{III}
Co1	2.17	2.25
Co2	2.16	2.23

In **2** the chloride ligand and anion are replaced by nitrate groups. The complex crystallises in the orthorhombic space group *Pbca*, with one monomer per asymmetric unit and 8 per unit cell (FFigure 2-4). The nitrate anion is linked to three monomers by hydrogen bonding through two bound and one unbound alcohol groups. The monomer packs in rows, with the direction of the bound nitrate group alternating. Channels of bound and unbound nitrate groups are present in the structure as can be seen when viewed along the *b*-axis (Figure 2-5).

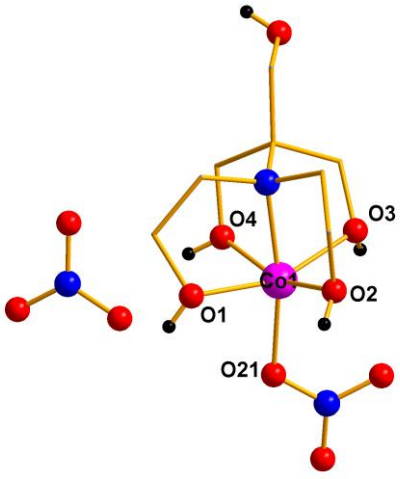

Figure 2-4 Structure of 2 (CH atoms omitted for clarity) Co^{II} pink; O red; N blue; H black.

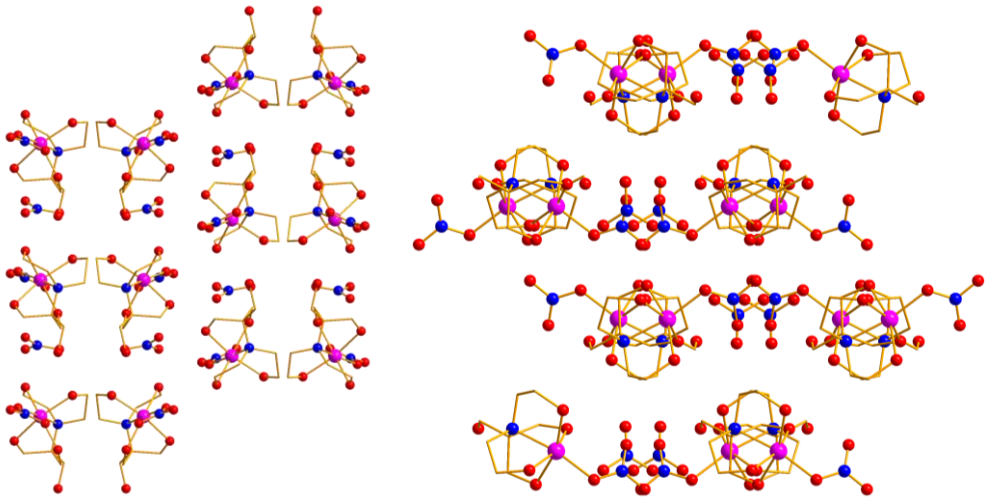

Figure 2-5 Packing diagram of 2 viewed along *a*- and *b*-axes.

Table 2-4 Data for crystal structure determination of 2.

Empirical Formula	$C_8H_{19}CoN_3O_{11}$
Fw (g mol^{-1})	378.09
Crystal system	Orthorhombic
Space group	*Pbca*
a (Å)	9.3890(2)
b (Å)	14.7564(4)
c (Å)	20.7690(6)
V (Å^3)	2877.5(1)
Z	8
T (K)	100(2)
λ (Å)	0.71073
ρ_{calcd} (Mg m^{-3})	1.81
μ (mm^{-1})	1.259
R_1[a]	0.0517
wR_2[b]	0.0413
Goodness of fit	0.946

a $R_1 = \Sigma \left| |F_o| - |F_c| \right| / \Sigma |F_o|$ b $wR_2 = \left[\Sigma \left[w\left(F_o^2 - F_c^2\right)^2 \right] - \Sigma \left[\left(F_o^2\right)^2 \right] \right]^{1/2}$ where $w = 1/\left[\sigma^2\left(F_o^2\right) + \left(0.2P\right)^2\right]$ and $P = \left[F_o^2 + 2F_c^2\right]/3$

Table 2-5 Metal-ligand bond distances in 2.

Bond	Distance (Å)
Co1– N1	2.1222 (1)
Co1– O1	2.1019(1)
Co1– O2	2.0932(1)
Co1– O3	2.0929(1)
Co1– O4	2.1322(1)
Co1– O21	2.0606(1)

Table 2-6 BVS calculation, underlined value is that which is closest to the charge for which it was calculated.[25]

Atom	Co^{II}	Co^{III}
Co1	<u>2.15</u>	2.18

2.3 Monomers as starting materials

2.3.1 Synthesis of $[Co^{II}_6Co^{III}_4(OH)_2(HL)_3(H_2L)Cl_7(CH_3OH)(MeCN)(H_2O)] \cdot 0.5MeOH \cdot H_2O$ (4·0.5MeOH·H_2O)

(where H_5L = bis-tris)

To a stirred pink solution of **1** (0.17 g, 0.50 mmol) in MeCN (20 mL) and MeOH (10 mL), $NMe_4OH.5H_2O$ (0.18 g, 0.99 mmol) was added. The resulting dark purple solution was stirred for one hour; $CoCl_2.6H_2O$ (0.24 g, 1.01 mmol) was then added. The solution was stirred for a further 4.5 hours, filtered and the blue filtrate stored in a sealed vial. After approximately one week blue/green crystals formed in 96% yield. Air dried crystals analyse as $\mathbf{C_{35}H_{87}N_5O_{31.5}Cl_7Co_{10}}$, analysis (%) calc. (found) C, 21.90 (21.34); H, 4.57 (3.97); N, 3.65 (3.31); Cl, 12.93 (12.36); Co, 30.70 (30.81). Selected IR data: ν = 3323, 2929, 2881, 2407, 1627, 1485, 1456, 1371, 1303, 1288, 1249, 1224, 1035, 1020, 995, 902, 765, 694, 675, 628 cm^{-1}.

2.3.2 Synthesis of $[Mn^{II}_5Co^{III}_4(OH)_2(HL)_2(H_2L)_2Cl_6(CH_3OH)(H_2O)] \cdot 0.5MeCN{\cdot}MeOH$ (5·0.5MeCN·MeOH)

(where H_5L = bis-tris)

To a stirred pink solution of **1** (0.36 g, 1.06 mmol) in MeCN (20 mL) and MeOH (10 mL) $NMe_4OH{\cdot}5H_2O$ (0.36 g, 1.98 mmol) was added. The resulting dark purple solution was stirred for one hr; $MnCl_2.4H_2O$ (0.40 g, 2.02 mmol) was then added. The solution was stirred for a further 5 hrs, filtered and the purple filtrate stored in a sealed vial. After one week red crystals formed in a 79% yield. Air dried crystals analyse as $\mathbf{C_{33}H_{76}N_4O_{24}Cl_6Co_4Mn_5}$, analysis (%) calc. (found) C, 23.16 (22.85); H, 4.65 (4.25); N, 3.27 (3.41); Cl, 12.50 (12.94); Co, 13.85 (13.89); Mn, 16.14 (15.73). Selected IR data: υ = 3354, 2868, 23214, 1618, 1454, 1371, 1334, 1105, 1053, 1030, 1008, 883, 734, 686, 648, 628 cm^{-1}.

2.4 Complexes formed

2.4.1 Discussion of the crystal structure of $[Co^{II}_6Co^{III}_4(OH)_2(HL)_3(H_2L)Cl_7(CH_3OH)(MeCN)(H_2O)]$(4)

Complex **4** contains a mixed valent decanuclear complex and crystallises in the monoclinic space group $P2_1/c$. The complex is best described as two non-identical distorted tetrahedra linked via Co1 and with an additional Co^{II} (Co9) on one face of the second tetrahedron (Figure 2-6 - Figure 2-8). There are six Co^{II}, three (Co1,4,9) with distorted octahedral geometry, one with distorted square pyramidal geometry (Co7), one with distorted trigonal bipyramidal geometry (Co8), and one with distorted tetrahedral geometry (Co3). Co1 has an $\{O_4NCl\}$ ligand donor set, with the four O ligands coming from two different bis-tris ligands and the N from a bound acetonitrile. Co3 has an $\{O_2Cl_2\}$ ligand donor set again with both O coming from two different bis-tris ligands. In the case of Co4, the distorted octahedral geometry is made up of $\{O_5Cl\}$, where one O is from an OH ligand, and the remaining four are from bis-tris. In Co9 four O ligands are from bis-tris, one from another OH ligand and the coordination sphere is completed by a bound methanol. The four Co^{III} all have a distorted octahedral geometry, with the ligand donor set $\{O_5N\}$, the bis-tris ligand provides an $\{NO_4\}$ donor set and the distorted octahedral geometry is completed by an OH ligand. The oxygen of the unbound protonated arm of the ligands encapsulating Co5 and Co10 is disordered over two sites. For Co5 the unbound oxygen is split 0.8 (O252) and 0.2 (O251) occupancy between the two sites and for Co10 the occupancy is split equally (O451 and O452) (Figure 2-8) between the two sites. This disorder is probably due to favourable interactions such as H-bonding possible at both sites. The oxidation states of the metal ions were assigned on the basis of bond valence sum calculations (Table 2-10 BVS for metals in 4.[25] The underlined value is the

closest to the charge for which it was calculated. Overestimation of Co^{III} values will be discussed in appendix one.), by consideration of bond lengths (Table 2-8) and charge balance.

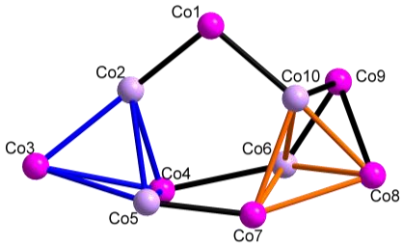

Figure 2-6 Diagram showing tetrahedra (blue and orange lines) linked through Co1 for 4 (Co^{II} pink Co^{III} lilac).

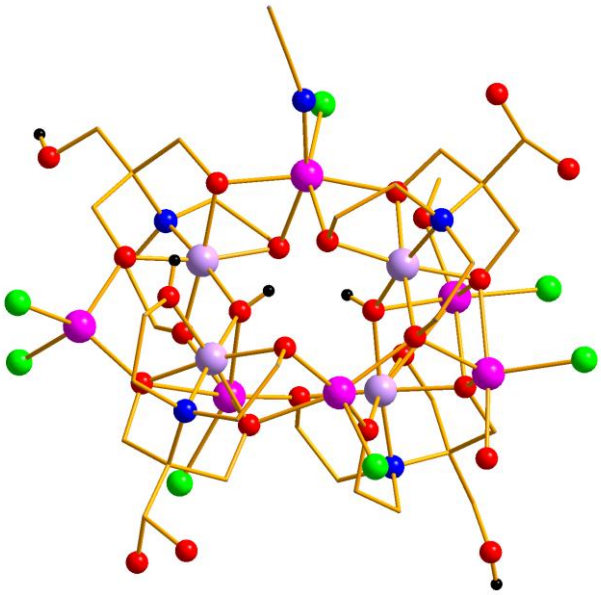

Figure 2-7 Structure of 4 (only OH protons shown (omitted on disordered ligand atoms), Co^{II} pink, Co^{III} lilac, N blue, O red, Cl bright green).

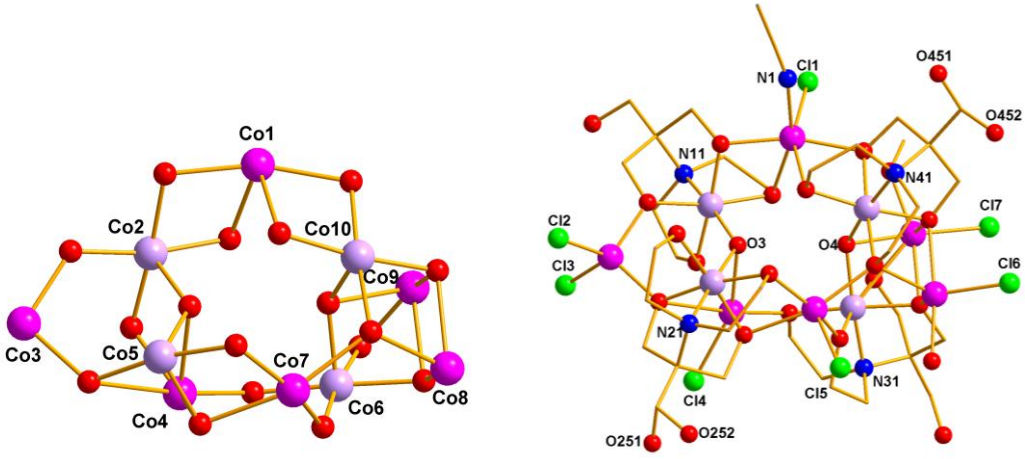

Figure 2-8 Labelled diagrams of 4, showing metal-oxygen core (left) and full structure (right).

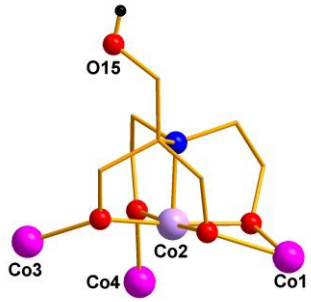

Binding mode 1 η^2: η^2: η^2: η^2: η^1: μ_4

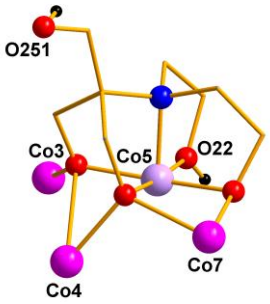

Binding mode 2 η^3: η^3: η^2: η^1: η^1: μ_4

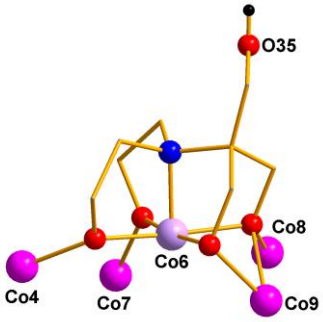

Binding mode 3 η^3: η^2: η^2: η^2: η^1: μ_5

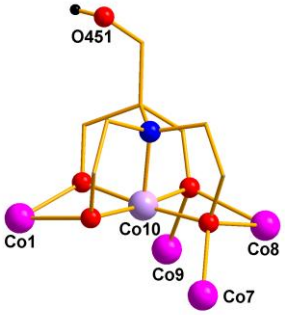

Binding mode 4 η^3: η^3: η^2: η^2: η^1: μ_5

Figure 2-9 Different binding modes in 4 (disordered ligand atoms omitted and only OH protons shown) Co^{II} pink; Co^{III} lilac; O red; N blue; H black.

In this complex all four of the bis-tris ligands show different binding modes. In binding mode one all of the alkoxide arms bridge between two metal centres, one Co^{III} and one Co^{II}. In two, one ethanolic arm from the nitrogen binds only to a Co^{III}, this O (O22) remains protonated, the second N-alkoxide (deprotonated ethanolic arm bound to nitrogen) bridges between one Co^{II} and one Co^{III}. Two of the three C-alkoxide arms bridge between three metal centres, two Co^{II} and one Co^{III}, and the third arm is unbound and protonated. Binding mode three consists of both N-alkoxide arms bridging between a Co^{II} and a Co^{III}, one of the C-alkoxide arms bridging between two Co^{II} and a Co^{III}, one bridging between a Co^{II} and a Co^{III}, the third arm is unbound and protonated. In the final binding mode, one N-alkoxide arm bridges three metal centres two Co^{II} and one Co^{III}, the other arm bridges between one Co^{II} and one Co^{III} centre. The C-alkoxide arms are bound to three and two metal centres whilst the third C-alkoxide arm remains unbound and protonated.

There are four complexes per unit cell and when viewed along the *a*-axis they form columns, with the shortest Co···Co distance between complexes in two adjacent columns being ~8.5 Å between Co3···Co8′ (Figure 2-10). The distance between two clusters in the columns is ~7.7 Å between Co3···Co8″. The disordered oxygen O451 and O452 mentioned previously are involved in intermolecular H-bonding across the rows (O452(H)···O15 2.789(1) Å and O451(H)···O452

2.579(1) Å). The disordered oxygen O251 and O252 have hydrogen bonds to a molecule of lattice solvent MeOH (0.5 occupancy) (O251(H)···O200 2.454(3) Å and O252(H)···O200 2.799(1) Å). PLATON squeeze[26,27] was used to take account of disordered solvent present in the complex that could not be modelled satisfactorily. The results showed that within the unit cell there is a void space with a volume of approximately 1000 Å^3, this void contains disordered solvent, potentially a mixture of MeOH, MeCN and H_2O due to the presence of all three within the structure. The voids space can be seen between the complexes in the packing diagrams (Figure 2-11).

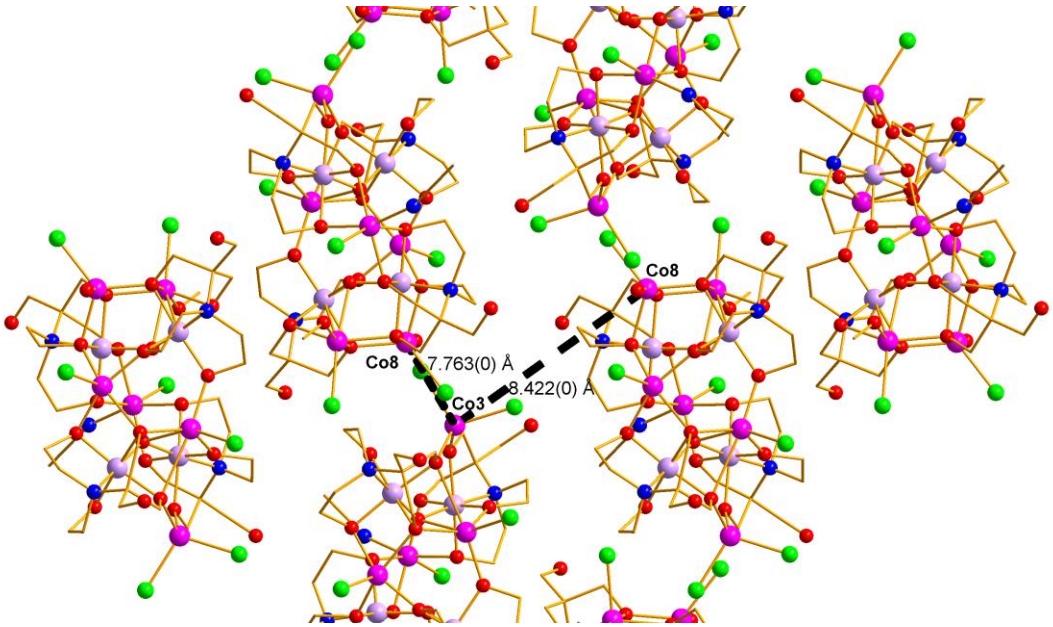

Figure 2-10 Packing diagram highlighting closest Co···Co distances in 4, viewed along *a*-axis.

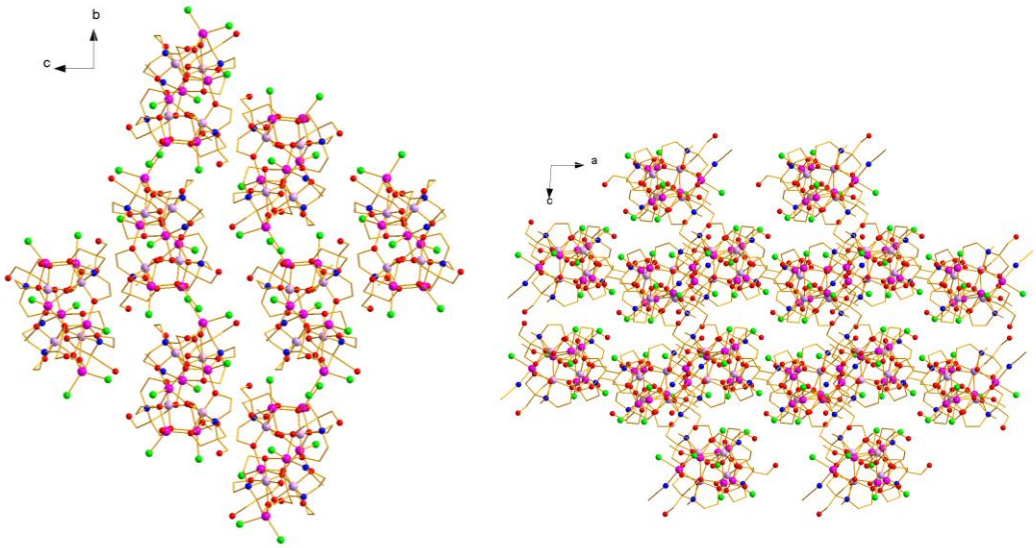

Figure 2-11 Packing diagrams for 4 viewed along *a*- and *b*-axes.

Table 2-7 Data for crystal structure determination of 4·0.5MeOH·H_2O.

Empirical Formula	$C_{35.5}H_{76}Cl_7Co_{10}N_5O_{25.5}$
Fw (g mol^{-1})	1818.5
Crystal system	Monoclinic
Space group	$P2_1/c$
a (Å)	14.8420(7)
b (Å)	23.354(1)
c (Å)	19.544(1)
β (deg)	93.782(3)
V ($Å^3$)	6759.4(6)
Z	4
T (K)	100(2)
λ (Å)	0.71073
ρ_{calcd} (Mg m^{-3})	1.825
μ (mm^{-1})	2.74
R_1[a]	0.0935
wR_2[b]	0.0908
Goodness of fit	0.996

[a] $R_1 = \Sigma \left| |F_o| - |F_c| \right| / \Sigma |F_o|$ [b] $wR_2 = \left[\Sigma \left[w\left(F_o^2 - F_c^2\right)^2 \right] - \Sigma \left[\left(F_o^2\right)^2 \right] \right]^{1/2}$ where $w = 1/\left[\sigma^2\left(F_o^2\right) + \left(0.2P\right)^2\right]$ and $P = \left[F_o^2 + 2F_c^2\right]/3$

Table 2-8 Metal-ligand bond lengths in 4.

Bond	Distance (Å)	Bond	Distance (Å)
Co1– Cl1	2.431(2)	Co6 – N31	1.912(5)
Co1 – N1	2.150(6)	Co6 – O31	1.889(5)
Co1 – O11	2.161(4)	Co6 – O32	1.877(4)
Co1 – O14	2.044(4)	Co6 – O33	1.921(5)
Co1 – O42	2.169(5)	Co6 – O34	1.923(4)
Co1 – O43	2.061(4)	Co6 – O4	1.916(4)
Co2 – N11	1.889(6)	Co7 – Cl5	2.362(2)
Co2 – O11	1.918(4)	Co7 – O21	2.009(5)
Co2 – O12	1.873(4)	Co7 – O24	2.218(4)
Co2 – O13	1.911(4)	Co7 – O31	1.958(4)
Co2 – O14	1.928(5)	Co7 – O41	2.112(4)
Co2 – O3	1.951(5)	Co8 – Cl6	2.269(2)
Co3 – Cl2	2.274(2)	Co8 – O1	2.061(6)
Co3 – Cl3	2.253(2)	Co8 – O34	1.987(4)
Co3 – O13	1.929(5)	Co8 – O41	2.106(4)
Co3 – O23	1.959(5)	Co8 – O44	2.258(5)
Co4 – Cl4	2.399 (2)	Co9 – Cl7	2.353(2)
Co4 – O12	1.943(5)	Co9 – O2	2.022(5)
Co4 – O24	2.085(5)	Co9 – O33	2.050(4)
Co4 – O3	2.334(4)	Co9 – O34	2.201(5)
Co4 – O32	2.010(4)	Co9 – O4	2.229(4)
Co5 – N21	1.905(6)	Co9 – O44	2.104(4)
Co5 – O21	1.900(5)	Co10 – N41	1.903(5)
Co5 – O22	1.917(5)	Co10 – O4	1.921(4)
Co5 – O23	1.915(5)	Co10 – O41	1.945(5)
Co5 – O24	1.911(4)	Co10 – O42	1.903(4)
Co5 – O3	1.911(5)	Co10 – O43	1.884(5)
		Co10 – O44	1.903(4)

Table 2-9 Selected bond angles in 4.

Atoms	Angle (°)	Atoms	Angle (°)
Co1-O11-Co2	97.0 (2)	Co7-O31-Co6	126.0(2)
Co1-O14-Co2	100.7 (2)	Co7-O41-Co10	113.7(2)
Co1-O42-Co10	97.3(2)	Co7-O41-Co8	114.7 (2)
Co1-O43-Co10	101.7(2)	Co8-O34-Co6	114.3(2)
Co2-O3-Co5	134.7(2)	Co8-O41-Co10	100.0(2)
Co3-O13-Co2	124.5(2)	Co8-O44-Co10	96.1(2)
Co3-O23-Co5	122.0(2)	Co8-O44-Co9	99.9(2)
Co4-O12-Co2	108.7(2)	Co9-O33-Co6	86.8(2)
Co4-O24-Co5	94.8(2)	Co9-O34-Co6	82.6(2)
Co4-O3-Co2	92.3(2)	Co9-O34-Co8	105.7 (2)
Co4-O3-Co5	87.2 (2)	Co9-O4-Co10	94.6 (2)
Co4-O32-Co6	128.6(2)	Co9-O4-Co6	82.0(2)
Co7-O21-Co5	99.5 (2)	Co9-O44-Co10	99.4(2)
Co7-O24-Co4	108.8(2)	Co10-O4-Co6	137.3(2)
Co7-O24-Co5	92.3(2)		

Table 2-10 BVS for metals in 4.[25] The underlined value is the closest to the charge for which it was calculated. Overestimation of Co^{III} values will be discussed in appendix one.

Atom	Co^{II}	Co^{III}	Atom	Co^{II}	Co^{III}
Co1	<u>2.078</u>	2.144	Co6	3.619	<u>3.680</u>
Co2	3.564	<u>3.624</u>	Co7	<u>1.870</u>	1.947
Co3	<u>2.019</u>	2.157	Co8	<u>1.871</u>	1.958
Co4	<u>1.807</u>	1.883	Co9	<u>1.995</u>	2.075
Co5	3.612	<u>3.672</u>	Co10	3.619	<u>3.680</u>

Table 2-11 BVS for the inorganic oxygen atoms in 4.[28]

Atom	BVS	Assignment*
O3	1.256	OH^-
O4	1.352	OH^-

*The oxygen atom is an O^{2-} if BVS ~2, an OH^- if the BVS ~1 and an H_2O if the BVS ~0.

2.4.1.1 Magnetic Susceptibility Measurements for 4

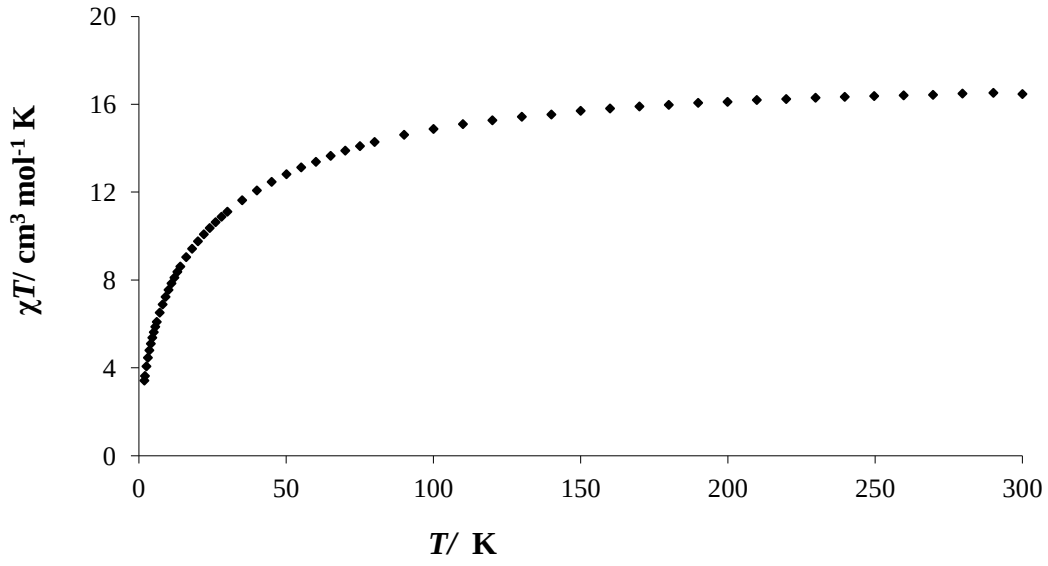

Figure 2-12 Temperature dependence of χT for 4·7.5H_2O from 1.8-300K measured in applied field of 1 Tesla.

Magnetic susceptibility measurements were carried out on an air dried sample of **4,** which analysed as **4**·7.5H_2O. The χT value at 300 K is 16.5 cm^3 mol^{-1} K, which is consistent with six uncoupled Co^{II} ions with g = 2.4. χT gradually decreases to 60 K then decreases more rapidly to 3.2 cm^3 mol^{-1} K at 1.8 K (Figure 2-12). The field dependence of the magnetisation of the cluster was measured (Figure 2-13) at both 2 K and 4 K. The magnetisation does not reach saturation at 7 T; at 2 K it reaches a value of 9.88 and at 4 K it reaches a value of 9.61.

This complex is complicated due to the presence of both six-coordinate, five-coordinate and four-coordinate Co^{II} ions. At low temperature octahedral Co^{II} has $S' = ½$, but four-coordinate Co^{II} will have $S' = 3/2$. From the χT *vs*. *T* data it is impossible to determine the different contributions of Co^{II} (six-coordiante) spin-orbit effects (1^{st} order), Co^{II} (four-coordinate) and any possible antiferromagnetic exchange.

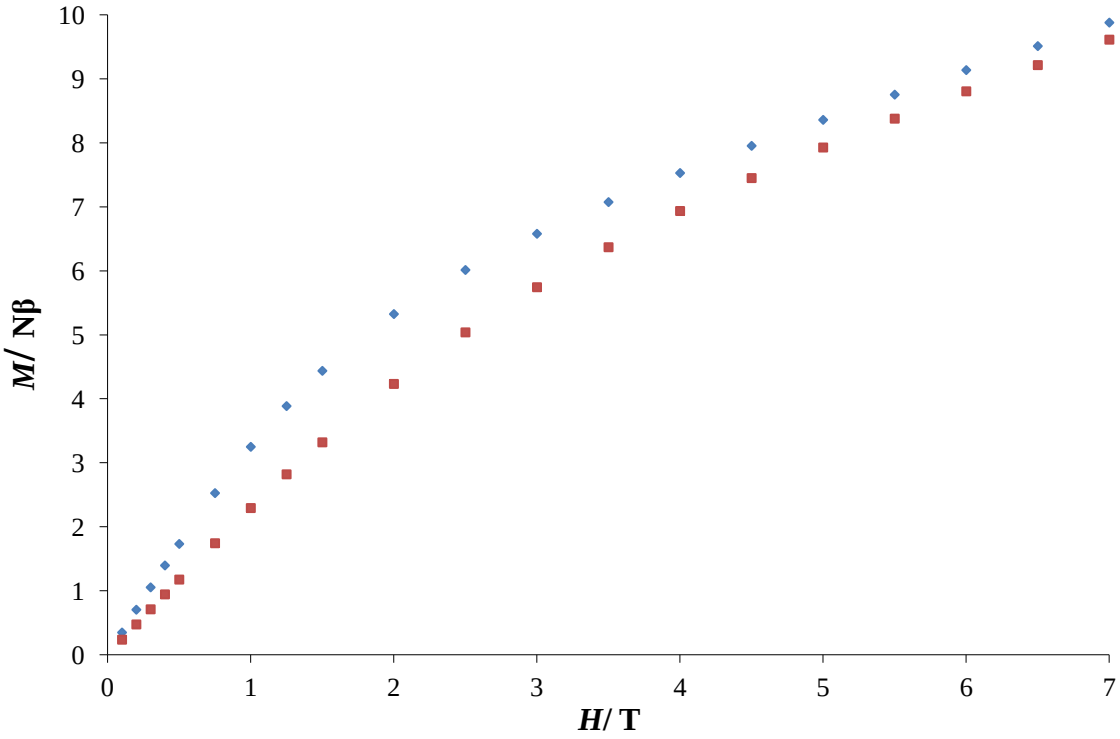

Figure 2-13 *M vs. H* for 4·7.5H_2O measured at 2 K (◆) and 4 K (■).

2.4.2 *Discussion of the crystal structure of [$Mn^{II}_5Co^{III}_4Cl_6(OH)_2(HL)_2(H_2L)_2(CH_3OH)(H_2O)$] (5)*

Complex **5** is a heterometallic complex with five Mn centres and four Co centres (Figure 2-15), which crystallises in the monoclinic space group $P2_1/n$. The complex can be described as two distorted square pyramids linked at Mn4 which is the apex of both pyramids (Figure 2-14). The four Co^{III} have distorted octahedral geometry, with a ligand donor set of $\{NO_5\}$, in each case four O ligands come from the arms of bis-tris and the final O from one of two bridging OH. Of the five Mn^{II}, Mn1 and Mn3 are penta-coordinate with distorted square pyramidal and distorted trigonal bipyramidal geometry, respectively (Figure 2-16). Mn1 has an $\{O_4Cl\}$ ligand donor set and Mn3 has an $\{O_3Cl_2\}$ ligand donor set. The remaining three manganese ions have distorted octahedral geometry with an $\{O_5Cl\}$ ligand donor set, in each case four ligand arms form part of the octahedral geometry, a bound Cl fills another position and the remaining position is filled by either a bridging OH group or methanol in the case of Mn4. BVS calculations, consideration of bond lengths and charge balance were used to assign the oxidation states.

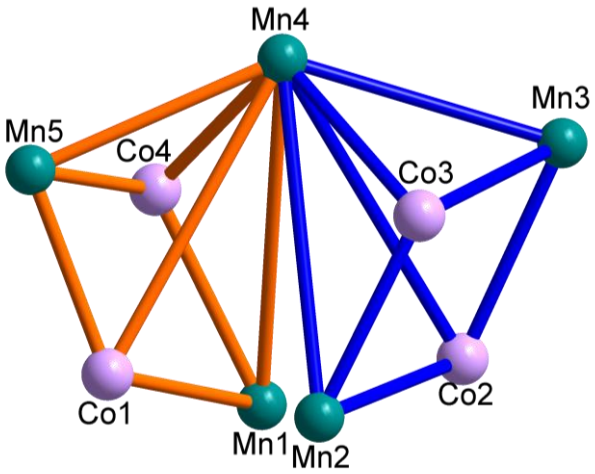

Figure 2-14 Diagram showing the two distorted square pyramids, linked at the apex (Mn4) of 5 (Co^{III} lilac; Mn^{II} teal).

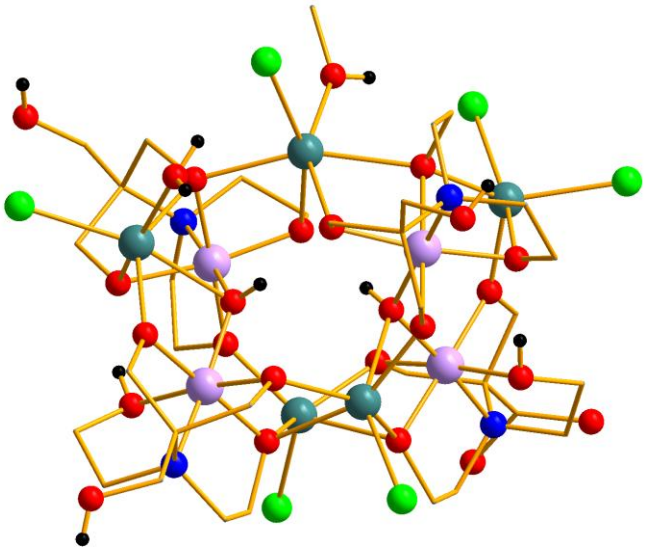

Figure 2-15 Structure of 5 (OH atoms shown but omitted on disordered ligand atoms, Co^{III} lilac; Mn^{II} teal; N blue; O red; Cl bright green).

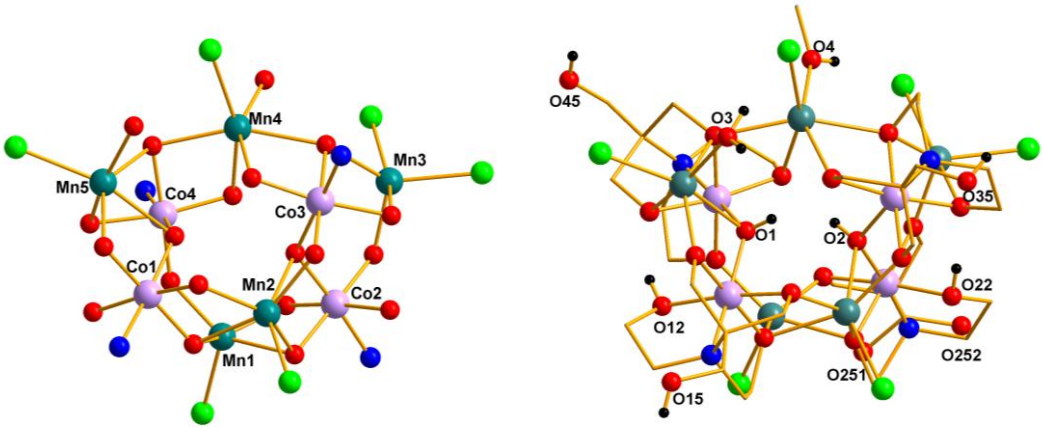

Figure 2-16 Diagrams showing atom numbers and OH groups (O251 and O252 are disordered with half occupancy and protonated).

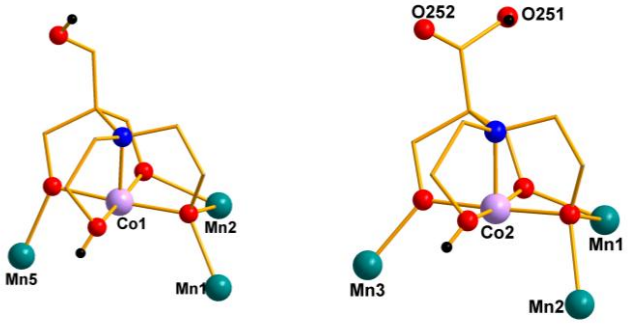

Binding mode 1: $\eta^3{:}\eta^2{:}\eta^2{:}\eta^1{:}\eta^1{:}\mu_4$

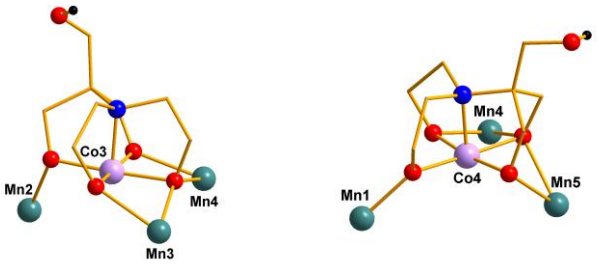

Binding mode 2: $\eta^3{:}\eta^2{:}\eta^2{:}\eta^2{:}\eta^1{:}\mu_4$ Binding mode 3: $\eta^3{:}\eta^2{:}\eta^2{:}\eta^2{:}\eta^1{:}\mu_4$

Figure 2-17 Binding modes in 5 (binding modes 2 and 3 differ in the η^3 atom, in 2 it is from an N-alkoxide arm and in 3 it is from a C-alkoxide arm).

The ligand exhibits three different binding modes (Figure 2-17). In binding mode one, an N-ethanolic arm is bound only to a Co and does not bridge between any metal centres, this O remains protonated (O12 and O22). The other N-alkoxide (deprotonated ethanolic) arm is bridging between three metal centres one Co and two Mn. Of the three arms bound to the central C, one is unbound and protonated and the remaining two alkoxide arms both bridge between Co and Mn. In the second type of binding mode, one N-alkoxide arm bridges between Co3 and Mn3, and the other N-alkoxide arm bridges between Co3 and two Mn centres (Mn3 and Mn4). Two of the three C-

alkoxide arms bind to two metal centres, one Co (Co3) and one Mn (Mn2 or Mn4), the third arm is protonated and does not bind. In the third case both N-alkoxide arms bridge between two metal centres Co4 and Mn1; and Co4 and Mn4, one of the C-alkoxide arms is protonated and unbound, of the remaining two arms one bridges between two metal centres (Co4 and Mn5) and the other bridges between three, Mn4, Mn5 and Co4. The unbound methanolic arm of the ligand around Co2 is disordered equally over two sites and is modelled as O251 and O252. Each disordered OH site has interactions with one of two specific Cl ligands on an adjacent complex, with distances of 3.24(2) Å (O251(H)···Cl31) and 2.95(2) Å (O252(H)···Cl32). Solvent is present in channels that can be seen when viewing the packing of the complex along the *b*-axis (Figure 2-18), one molecule of MeOH and one molecule of MeCN (with half occupancy) have been modelled in this area.

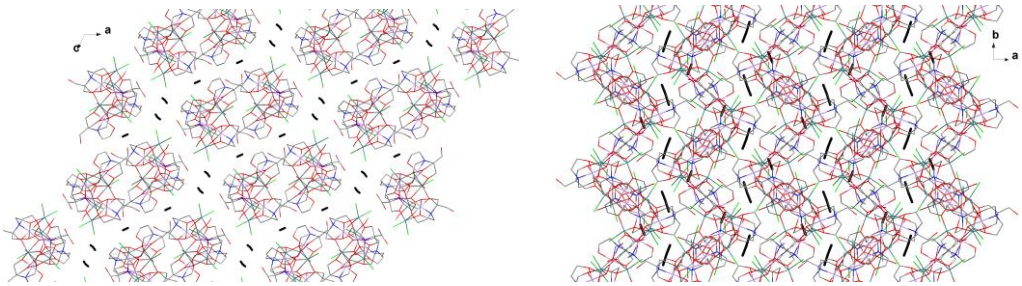

Figure 2-18 Diagram of solvent in 5 viewed along *b*-, and *c*-axes (solvent molecules highlighted in black).

From Figure 2-18, when viewed along the *b*-axis it appears that the complex packs in pairs however from the view along the *c*-axis it can be seen that the complex actually packs in pairs of offset rows with the distance between Cl2 and Cl4 on diagonally opposite clusters being 5.343(3) Å. The closest metal-metal distances are Mn1···Co3′ 7.305(1) Å on adjacent complexes (Figure 2-19). There are also H-bonds between the water molecule containing O3 (bound to Mn5) and Cl2 (O3(H)···Cl2 distance is 3.140(8) Å) and the unbound ligand arm with O35 and Cl5 (O35(H)···Cl5 distance is 3.208(8) Å) (Figure 2-20). There is also an intra-molecular interaction between Cl32 and O4 which is 3.112(7) Å.

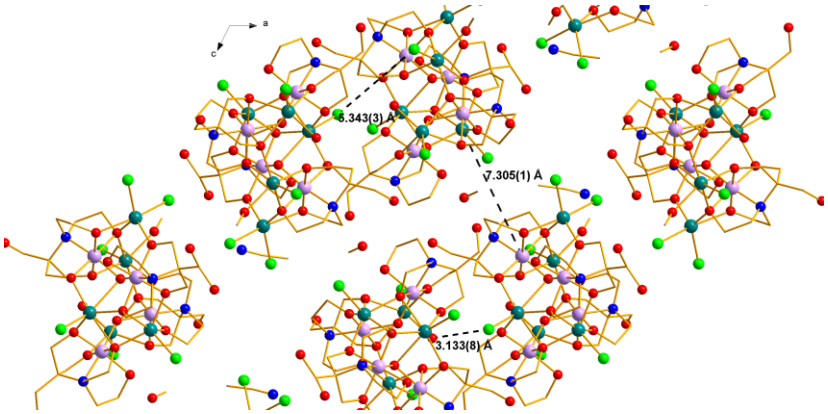

Figure 2-19 Packing diagram for 5 viewed along *b*-axis showing intermolecular distances.

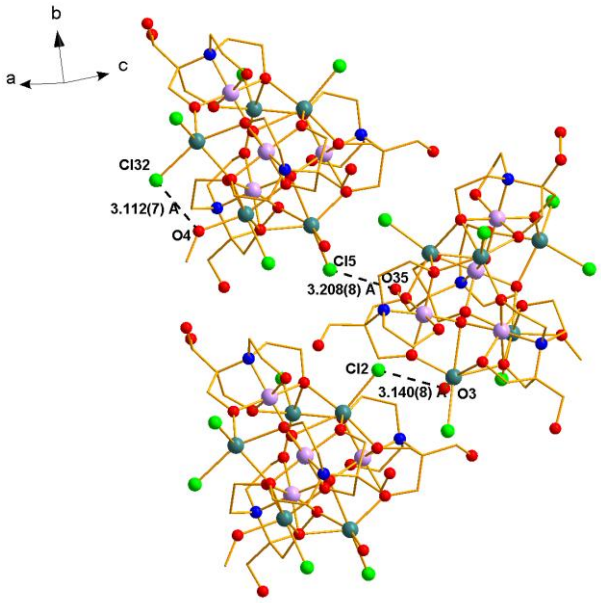

Figure 2-20 Diagram showing hydrogen bonding interactions in 5.

Table 2-12 Data for the crystal structure determination of 5·0.5MeCN·MeOH

Empirical formula	$C_{35}H_{76.5}Co_4Cl_6Mn_5N_{4.5}O_{25}$
Fw (g mol^{-1})	1683.64
Crystal system	Monoclinic
Space group	$P2_1/n$
a (Å)	22.3296(3)
b (Å)	13.2346(2)
c (Å)	23.1797(3)
β (deg)	116.144(1)
V (Å^3)	6149.3(2)
Z	4
T (K)	100(2)
λ (Å)	0.71073
ρ_{calcd} (Mg m^{-3})	1.821
μ (mm^{-1})	2.379
R_1[a]	0.0884
wR_2[b]	0.1602
Goodness of fit indicator	1.049

[a] $R_1 = \Sigma \left| |F_o| - |F_c| \right| / \Sigma |F_o|$ [b] $wR_2 = \left[\Sigma \left[w\left(F_o^2 - F_c^2\right)^2 \right] - \Sigma \left[\left(F_o^2\right)^2 \right] \right]^{1/2}$ where $w = 1/\left[\sigma^2\left(F_o^2\right) + \left(0.2P\right)^2\right]$ and $P = \left[F_o^2 + 2F_c^2\right]/3$

Table 2-13 Metal–ligand bond lengths in 5.

Bond	Distance (Å)	Bond	Distance (Å)	Bond	Distance (Å)
Co1–O1	1.894(5)	Co4–O1	1.893(5)	Mn3–Cl31	2.403(2)
Co1–N11	1.905(6)	Co4–N41	1.907(6)	Mn3–Cl32	2.452(3)
Co1–O11	1.911(5)	Co4–O41	1.895(5)	Mn3–O23	2.065(6)
Co1–O12	1.965(5)	Co4–O42	1.875(5)	Mn3–O31	2.218(6)
Co1–O13	1.887(5)	Co4–O43	1.930(5)	Mn3–O32	2.281(6)
Co1–O14	1.859(5)	Co4–O44	1.907(5)	Mn4–Cl4	2.468(2)
Co2–O2	1.906(5)	Mn1–Cl1	2.354(2)	Mn4–O4	2.170(6)
Co2–N21	1.899(7)	Mn1–O11	2.140(5)	Mn4–O31	2.329(5)
Co2–O21	1.890(5)	Mn1–O24	2.278(5)	Mn4–O34	2.208(5)
Co2–O22	1.948(6)	Mn1–O21	2.107(5)	Mn4–O41	2.187(5)
Co2–O23	1.892(5)	Mn1–O42	2.057(6)	Mn4–O44	2.280(5)
Co2–O24	1.860(5)	Mn2–Cl2	2.397(2)	Mn5–Cl5	2.436(2)
Co3–O2	1.927(5)	Mn2–O2	2.452(5)	Mn5–O1	2.366(6)
Co3–N31	1.903(6)	Mn2–O11	2.297(5)	Mn5–O3	2.111(6)
Co3–O31	1.927(5)	Mn2–O14	2.186(5)	Mn5–O13	2.082(5)
Co3–O32	1.900(5)	Mn2–O21	2.217(5)	Mn5–O43	2.262(5)
Co3–O33	1.883(5)	Mn2–O33	2.097(5)	Mn5–O44	2.297(5)
Co3–O34	1.899(5)				

Table 2-14 Selected bond angles in 5.

Atoms	Angle(°)	Atoms	Angle(°)
Co1-O1-Co4	129.5(3)	Mn3-O23-Co2	122.0(3)
Co3-O2-Co2	127.3(3)	Mn3-O31-Co3	94.6(2)
Mn1-O11-Co1	122.6(3)	Mn3-O31-Mn4	140.0(2)
Mn1-O11-Mn2	95.8(2)	Mn3-O32-Co3	93.4(2)
Mn1-O21-Co2	93.9(2)	Mn4-O31-Co3	96.1(2)
Mn1-O24-Co2	100.6(2)	Mn4-O34-Co3	101.1(2)
Mn1-O42-Co4	125.3(3)	Mn4-O41-Co4	99.4(2)
Mn2-O11-Co1	95.3(2)	Mn4-O44-Co4	95.9(2)
Mn2-O14-Co1	100.7(2)	Mn4-O44-Mn5	120.6(2)
Mn2-O2-Co2	94.8(2)	Mn5-O1-Co1	93.7(2)
Mn2-O2-Co3	94.3(2)	Mn5-O1-Co4	85.4(2)
Mn2-O21-Co2	103.4(2)	Mn5-O13-Co1	103.8(2)
Mn2-O21-Mn1	94.2(2)	Mn5-O43-Co4	87.5 (2)
Mn2-O33-Co3	108.3(2)	Mn5-O44-Co4	87.1(2)

Table 2-15 BVS for metals in 5.[25] The underlined value is the one closest to the charge for which it was calculated, overestimation for Co^{III} will be discussed in appendix one.

Atom	Co^{II}	Co^{III}	Mn^{II}	Mn^{III}
Co1	3.687	<u>3.749</u>	4.619	4.331
Co2	3.722	<u>3.784</u>	4.663	4.372
Co3	3.642	<u>3.703</u>	4.277	4.561
Co4	3.710	<u>3.773</u>	4.360	4.651
Mn1	1.599	1.671	<u>2.131</u>	2.008
Mn2	1.515	1.581	<u>2.003</u>	1.898
Mn3	1.458	1.549	<u>1.951</u>	1.894
Mn4	1.456	1.514	<u>1.920</u>	1.813
Mn5	1.556	1.619	<u>2.053</u>	1.939

Table 2-16 BVS for the inorganic oxygen atoms in 5.[28]

Atom	BVS	Assignment*
O1	1.366	OH^-
O2	1.257	OH^-

*The oxygen atom is an O^{2-} if BVS ~2, an OH^- if the BVS ~1 and an H_2O if the BVS ~0.

2.4.2.1 Magnetic Susceptibility Measurements for 5

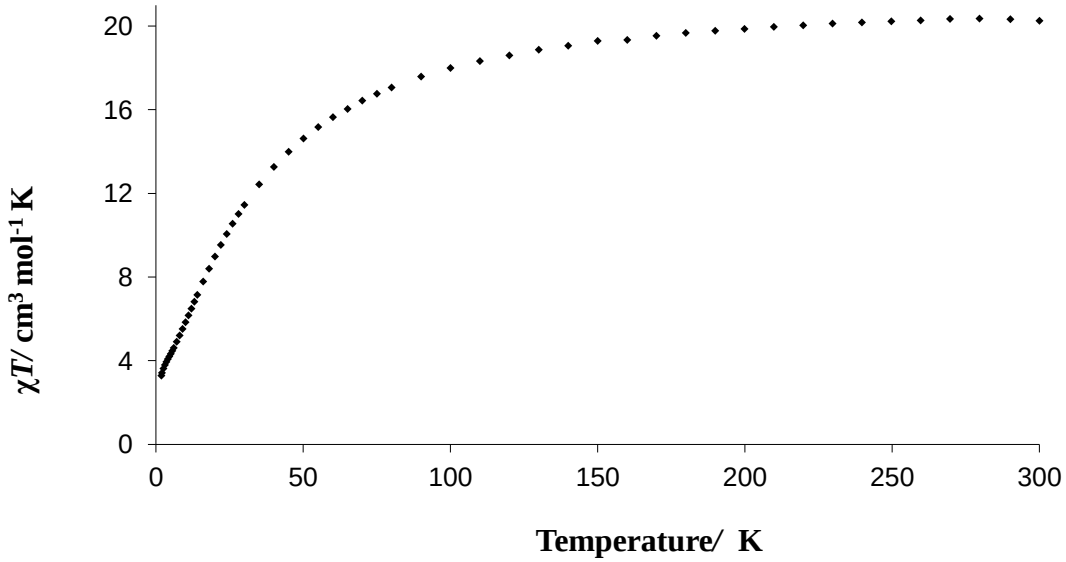

Figure 2-21 Temperature dependence of χT for complex 5 from 1.8 -300 K measured in an applied field of 1 T.

Magnetic susceptibility measurements were carried out on an air dried sample of **5** which analysed as **5**·$4H_2O$ (Figure 2-21). The χT value at 300 K is 20.3 $cm^3\,mol^{-1}$ K, this is slightly low when compared to the expected value for five uncoupled Mn^{II} ions with $g = 2$ which is 21.9 $cm^3\,mol^{-1}$ K. However, previous examples of Mn complexes have used lower values of g for fitting of data,[29-31] a value of $g = 1.95$ gives much better agreement. Variation of g from 2.0 suggests some second order spin-orbit coupling effects, this is not possible for Mn^{II} in strictly octahedral environments. However, in this complex the 6-coordinate Mn^{II} ions all have distorted geometry and there are also two variations of 5-coordinate Mn^{II}. χT gradually decreases to 60 K where it starts to drop more rapidly to 3.42 $cm^3\,mol^{-1}$ K at 1.8 K. The magnetisation was measured as a function of applied field at 2 K and 4 K (Figure 2-22). The magnetisation does not reach saturation at 7 T but equals 6.65 at 2 K and 7.03 at 4 K. The magnetisation goes through an inflexion at around 4 T which suggests there could be field induced population of low-lying excited states with $S > 5/2$.

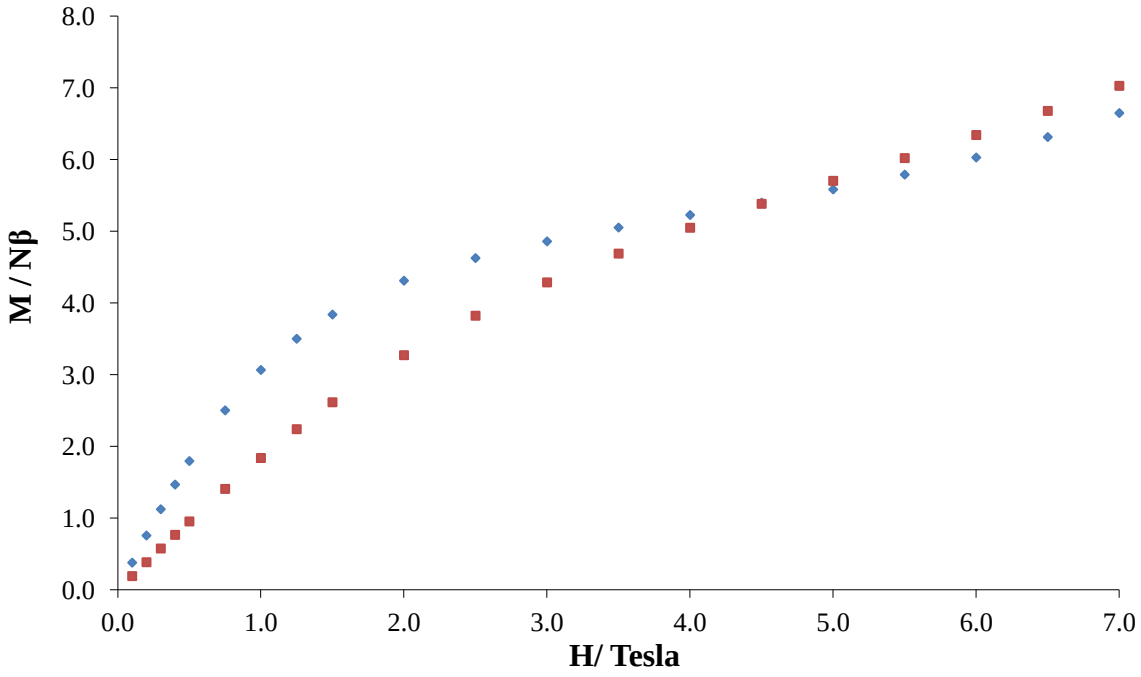

Figure 2-22 *M vs. H* for 5·4H_2O measured at 2 K (◆) and 4 K (■).

2.5 Related monomers

2.5.1 Synthesis of [Ni(H_5L)Cl]Cl (6) and [Cu(H_5L)Cl]Cl (7) monomers

$NiCl_2 \cdot 6H_2O$ (0.48 g, 2.02 mmol) was dissolved in 10 mL of *n*-propanol this was added to a stirred solution of bis-tris (0.42 g, 2.01 mmol) dissolved in 10 mL *n*-propanol. The resulting solution was stirred overnight, filtered and the green precipitate was allowed to air dry. The filtrate was stored in a sealed vial, after several weeks large green needle crystals appeared. The precipitate forms in approximately 67 % yield. Air dried precipitate analysed as **$C_8H_{19}NO_5Cl_2Ni$,** analysis (%) calc. (found) C, 28.36 (28.29); H, 5.66 (5.71); N, 4.13 (4.12). Selected IR data of precipitate: ν = 3398, 3259, 3093, 1626, 1340, 1311, 1236, 1167, 1155, 1055, 1028, 1012, 999, 898, 871, 754, 719, 684, 650 cm^{-1}. IR data of the precipitate matched that collected for crytsals.

The Cu monomer was synthesised following the same method, using $CuCl_2 \cdot 2H_2O$ (0.34 g, 1.99 mmol), no crystals formed from the solution. Air dried precipitate analysed as **$C_8H_{19}NO_5Cl_2Cu$**, analysis (%) calc. (found) C, 27.96 (28.17); H, 5.58 (5.68); N, 4.11 (4.12).

2.5.2 Discussion of crystal structure of [Ni(H_5L)Cl]Cl (6)

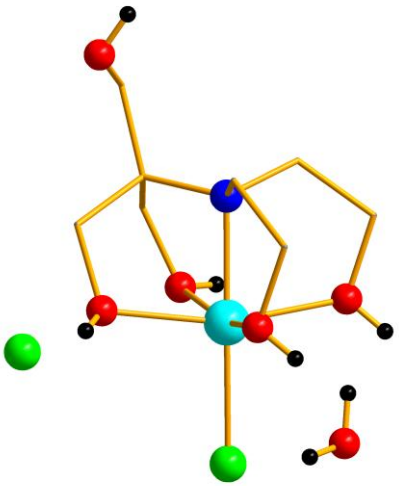

Figure 2-23 Structure of 6 (OH protons shown) Ni^{II} light blue; O red; N blue; Cl bright green; H black.

This complex is analogous to **1** described previously, the ligand remains fully protonated and the Ni^{II} charge is balanced by a bound chloride and one chloride in the lattice. From X-ray crystallography there is one molecule of water present per monomer. The complex crystallises in the monoclininc space group $P2_1/n$.

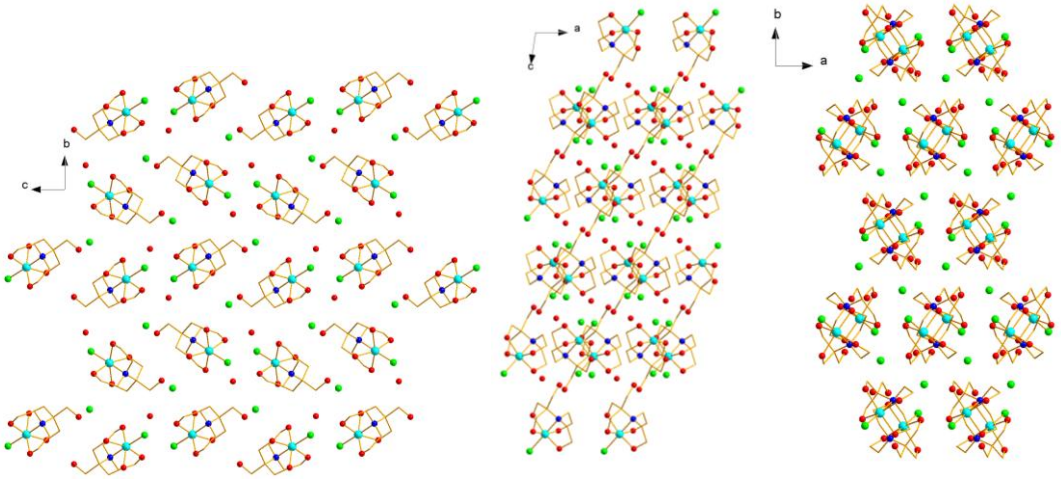

Figure 2-24 Packing diagrams of 6 viewed along *a*-, *b*- and *c*- axes

The closest neighbouring complexes are 6.7 Å apart in the direction of the *a*-axis, 7.4 Å in the *b*-axis direction and over 8 Å in the *c*-axis.

This complex and the copper analogue have been previously synthesised by Inomata *et al.* using a different synthetic method,[6] though as yet they have not been used to synthesise larger clusters, unlike the Mn monomer.[7] Inomata *et al.* have synthesised a series of eleven bivalent bis-tris monomer complexes with transition metals and different anions, $[M(H_5L)(H_2O)]SO_4 \cdot nH_2O$ (M: Co, Ni, Cu, Zn), $[MCl(H_5L)]Cl \cdot nH_2O$ (M = Co, Ni, Cu), and $[M(HCOO)(H_5L)](HCOO)$ (M: Co, Ni, Cu, Zn) (where H_5L = bis-tris). Of the chloride analogues with Co, Ni and Cu, the Ni and Cu monomers have been characterised by single crystal X-ray diffraction and the cobalt complex by powder X-ray diffractometry. The nickel complex is the same as the one described above with only very slight differences in unit cell length 6.7225(3) Å (complex **6**) compared with 6.753(1) Å[6] for the shortest axis.

Both the nickel and copper monomers were utilised as starting materials in reactions as previously described for the cobalt monomer, as yet no crystals have been produced from these reactions.

Table 2-17 Data for the crystal structure determination of 6.

Empirical Formula	$C_8H_{21}Cl_2NiO_6$
Fw (g mol^{-1})	338.86
Crystal system	Monoclinic
Space group	$P2_1/n$
a (Å)	6.7225(3)
b (Å)	14.2510(7)
c (Å)	14.3172(5)
β (deg)	98.444(2)
V (Å^3)	1356.8(1)
Z	4
T (K)	100(2)
λ (Å)	0.71073
ρ_{calcd} (Mg m^{-3})	1.747
μ (mm^{-1})	1.841
R_1[a]	0.0385
wR_2[b]	0.0594
Goodness of fit	1.088

[a] $R_1 = \Sigma \left| |F_o| - |F_c| \right| / \Sigma |F_o|$ [b] $wR_2 = \left[\Sigma \left[w\left(F_o^2 - F_c^2\right)^2 \right] - \Sigma \left[\left(F_o^2\right)^2 \right] \right]^{1/2}$ where $w = 1/\left[\sigma^2\left(F_o^2\right) + \left(0.2P\right)^2\right]$ and $P = \left[F_o^2 + 2F_c^2\right]/3$

Table 2-18 Metal-ligand bond lengths for 6.

Bond	Distance (Å)
Ni1–Cl1	2.3166(8)
Ni1–O1	2.054(2)
Ni1–O2	2.077(2)
Ni1–O3	2.109(2)
Ni1–O4	2.089(2)
Ni1–N1	2.060(3)

2.6 Conclusions

The aim of producing larger nuclearity complexes from a monomer starting material, was successful and two new mixed-valence complexes with interesting structural geometry have been synthesised and characterised. The monomer starting material proves to be a route to both homo- and heteronuclear complexes. The monomer was synthesised in good yield from simple reaction methods, making it an ideal starting material. It was found that the two polynuclear complexes are the favoured outcome of several reactions with varying concentrations of metal, monomer, base, and so it was not possible to control the outcome of the reaction by altering these quantities. Some work was undertaken to vary reaction conditions using solvothermal methods. In previous work solvothermal methods have proved to be successful where room temperature reactions have not,[32] with further investigation this could be a promising route to more novel complexes utilising monomer starting materials. The magnetic properties of both structures were examined and SMM behaviour was not observed.

Further work with different monomer starting materials (eg. the Ni and Cu monomers already synthesised), either different metal centres or using a related ligand may produce some interesting results.

2.7 References

(1) Nakajima, T.; Seto, K.; Horikawa, F.; Shimizu, I.; Scheurer, A.; Kure, B.; Kajiwara, T.; Tanase, T.; Mikuriya, M. *Inorganic Chemistry* **2012**, *51*, 12503.

(2) Stamatatos, T. C.; Foguet-Albiol, D.; Poole, K. M.; Wernsdorfer, W.; Abboud, K. A.; O'Brien, T. A.; Christou, G. *Inorganic Chemistry* **2009**, *48*, 9831.

(3) Liu, J.; Ma, C.; Chen, H.; Hu, M.; Wen, H.; Cui, H.; Song, X.; Chen, C. *Dalton Transactions* **2013**, *42*, 2423.

(4) Chen, H.; Ma, C.-B.; Hu, M.-Q.; Wen, H.-M.; Cui, H.-H.; Liu, J.-Y.; Song, X.-W.; Chen, C.-N. *Dalton Transactions* **2013**, *42*, 4908.

(5) Totaro, P.; Westrup, K. C. M.; Boulon, M.-E.; Nunes, G. G.; Back, D. F.; Barison, A.; Ciattini, S.; Mannini, M.; Sorace, L.; Soares, J. F.; Cornia, A.; Sessoli, R. *Dalton Transactions* **2013**, *42*, 4416.

(6) Inomata, Y.; Gochou, Y.; Nogami, M.; Howell, F. S.; Takeuchi, T. *Journal of Molecular Structure* **2004**, *702*, 61.

(7) Stamatatos, T. C.; Abboud, K. A.; Christou, G. *Dalton Transactions* **2009**, 41.

(8) Jin Oh, S.; Choi, Y.-S.; Hwangbo, S.; Chul Bae, S.; Kang Ku, J.; Won Park, J. *Chemical Communications* **1998**, 2189.

(9) Chen, Q.; Chang, Y. D.; Zubieta, J. *Inorganica Chimica Acta* **1997**, *258*, 257.

(10) Ferguson, A.; McGregor, J.; Parkin, A.; Murrie, M. *Dalton Transactions* **2008**, 731.

(11) Kirillov, A. M.; Karabach, Y. Y.; Kirillova, M. V.; Haukka, M.; Pombeiro, A. J. L. *Dalton Transactions*, *40*, 6378.

(12) Khan, A.; Lan, Y.; Kostakis, G. E.; Anson, C. E.; Powell, A. K. *Dalton Transactions* **2012**, *41*, 8333.

(13) Ferguson, A.; Parkin, A.; Murrie, M. *Dalton Transactions* **2006**, 3627.

(14) Graham, K.; Sharp, L. E.; Thomas, L. H.; Murrie, M. *Inorganic Chemistry Communications* **2012**, *25*, 89.

(15) Milway, V. A.; Tuna, F.; Farrell, A. R.; Sharp, L. E.; Parsons, S.; Murrie, M. *Angewandte Chemie International Edition* **2013**, *52*, 1949.

(16) Murugesu, M.; Abboud, K. A.; Christou, G. *Polyhedron* **2004**, *23*, 2779.

(17) Wang, S.; Huffman, J. C.; Folting, K.; Streib, W. E.; Lobkovsky, E. B.; Christou, G. *Angewandte Chemie International Edition* **1991**, *30*, 1672.

(18) Rajaraman, G.; Murugesu, M.; Sañudo, E. C.; Soler, M.; Wernsdorfer, W.; Helliwell, M.; Muryn, C.; Raftery, J.; Teat, S. J.; Christou, G.; Brechin, E. K. *Journal of the American Chemical Society* **2004**, *126*, 15445.

(19) Brechin, E. K.; Sañudo, E. C.; Wernsdorfer, W.; Boskovic, C.; Yoo, J.; Hendrickson, D. N.; Yamaguchi, A.; Ishimoto, H.; Concolino, T. E.; Rheingold, A. L.; Christou, G. *Inorganic Chemistry* **2005**, *44*, 502.

(20) Freedman, D. E.; Jenkins, D. M.; Iavarone, A. T.; Long, J. R. *Journal of the American Chemical Society* **2008**, *130*, 2884.

(21) Mironov, V. S.; Chibotaru, L. F.; Ceulemans, A. *Journal of the American Chemical Society* **2003**, *125*, 9750.

(22) Larionova, J.; Clérac, R.; Sanchiz, J.; Kahn, O.; Golhen, S.; Ouahab, L. *Journal of the American Chemical Society* **1998**, *120*, 13088.

(23) Larionova, J.; Kahn, O.; Gohlen, S.; Ouahab, L.; Clérac, R. *Journal of the American Chemical Society* **1999**, *121*, 3349.

(24) Larionova, J.; Clérac, R.; Donnadieu, B.; Guérin, C. *Chemistry – A European Journal* **2002**, *8*, 2712.

(25) Brese, N. E.; O'Keeffe, M. *Acta Crystallographica Section B* **1991**, *47*, 192.

(26) Sluis, P. v. d.; Spek, A. L. *Acta Crystallographica Section A* **1990**, *A46*, 194.

(27) Speck, A. *Journal of Applied Crystallography* **2003**, *36*, 7.

(28) Brown, I. D.; Wu, K. K. *Acta Crystallographica Section B* **1976**, *32*, 1957.

(29) Ferguson, A.; Thomson, K.; Parkin, A.; Cooper, P.; Milios, C. J.; Brechin, E. K.; Murrie, M. *Dalton Transactions* **2007**, 728.

(30) Brechin, E. K. *Chemical Communications* **2005**, 5141.

(31) Wittick, L. M.; Murray, K. S.; Moubaraki, B.; Batten, S. R.; Spiccia, L.; Berry, K. J. *Dalton Transactions* **2004**, 1003.

(32) Laye, R. H.; McInnes, E. J. L. *European Journal of Inorganic Chemistry* **2004**, *2004*, 2811.

3. Complexes with two to four cobalt centres

On first appearances it might be thought that small complexes with up to four metal centres would not be as magnetically interesting as larger complexes. However, examples of small clusters acting as single molecule magnets are known, such as mononuclear Co complexes;[1,2] $[Mn_4(pc)_4(mda)_2(mdaH)_2]$ (where pc = pyrenecarboxylic acid and $mdaH_2$ = N-methyldiethanolamine), which has a defective dicubane structure and displays SMM properties;[3] and a family of trinuclear Ni examples which utilise a terdentate N,N,O donor Schiff base ligand (-2-[(3-dimethylaminopropylimino)methyl]phenol)[4]

By decreasing the complexity of the complexes, factors which affect the magnetic properties can be better studied and understood. Larger complexes also often have issues such as disorder within the structure, including unbound solvent.

It was previously stated that the energy barrier to reorientation of magnetisation was,

$$E_a = S^2|D| \tag{3-1}$$

However, in certain cases this model is not ideal, for example when *S* is no longer a good quantum number such as with octahedral high spin Co^{II} or lanthanide ions.[5] It has also been suggested that the magnitude of the energy barrier is determined mostly by the strength of the spin-orbit coupling and therefore cannot be improved by independently optimising *D* and *S*.[6] The most common approach to synthesising SMMs has been to try and create clusters with large ground spin states, *S*. However as this is not as efficient as first thought, it may be interesting to focus on increasing D in the strong-exchange limit (where *S* and *D* are related) or move to the weak-exchange limit, where Co^{II}, is an exciting option.

Mn_3 triangles have been used as the building blocks for many large complexes, and are of interest themselves due to their intrinsic magnetic properties.[7] Several examples have been synthesised and different properties are seen depending on the ligand.[8] The first example is $[Mn_3(O)(bamen)_3][ClO_4]$, (where $bamenH_2$ = 1,2-bis(biacetylmonoximeimino)ethane), in this case the coupling between Mn centres is ferromagnetic.[8] A second example shows that when the ligand is altered causing distortion, the simple $[Mn_3]$ complex can act as an SMM. The complex is altered from $[Mn_3O(O_2CMe)_6(py)_3][ClO_4]$ to $[Mn_3O(O_2CMe)_3(mpko)_3][ClO_4]$ (where py = pyridine and mpkoH = methyl-2-pyridylketone oxime). The first complex is antiferromagnetically coupled and the $\{Mn_3O\}$ core is planar, and the second is ferromagnetically coupled, with the central O^{2-} lying above the $\{Mn_3\}$ plane.[9] Whether or not the triangle exhibits ferromagnetic or antiferromagnetic interactions between the metal centres seems to be dependent on the degree of torsion in the ligands.[10]

Another family of small clusters that has received attention over recent years are cubanes, containing four metal centres they often form the building blocks for larger complexes, as do the Mn triangles mentioned above.

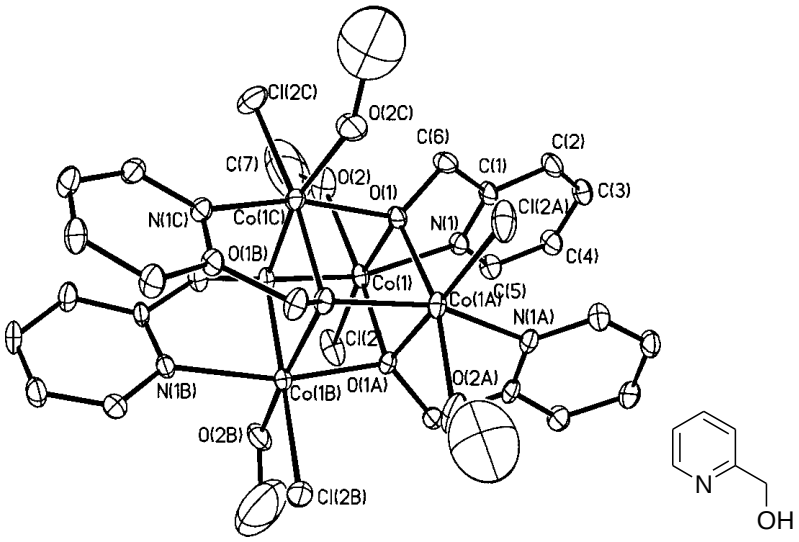

Figure 3-1 Structural diagram of the first Co^{II} SMM (where the ligand is the anion of hydroxymethylpyridine = hmp^-)[11]

The first Co^{II} complex to display slow magnetic relaxation was a cubane reported in 2002 (Figure 3-1).[11] Since then several examples have been synthesised that display SMM behaviour.[12-14] Two of these cubanes utilise the citrate ligand [$C(O^-)(CO_2^-)(CH_2CO_2^-)_2$ = cit^{4-}]. This ligand has been used successfully in cubane cluster formation with Ni ions.[15] The third example utilises hmp (as in the first Co SMM Figure 3-1) and dmb (3,3-dimethyl-1-butanol). Cobalt clusters with four metal centres can also take the form of molecular squares.[16,17] One Co molecular square that displays SMM properties utilises the deprotonated ligand N,N′-di[1-(2-hydroxyphenyl)ethlidene]hydrazone, to give [Co_4L_4].[16] In this structure (Figure 3-2) all Co^{II} ions are pentacoordinated with distorted trigonal bipyramidal geometry and there is overall intramolecular ferromagnetic coupling in the low temperature range, frequency dependent out-of-phase ac signals and slow relaxation of magnetisation are evidence of the SMM properties of this complex.

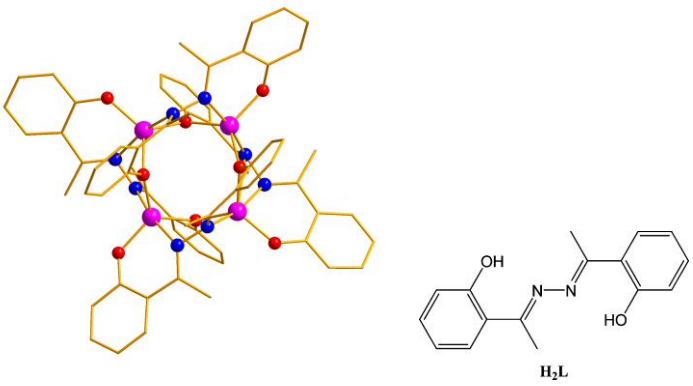

Figure 3-2 Co^{II} molecular square and N,N′-di[1-(2-hydroxyphenyl)ethlidene]hydrazone ligand.[16]

The following chapter covers synthesised complexes ranging in size from two metal centres to four, utilising the ligands diethanolamine, triethanolamine, acetylacetone (as the acetylacetonate anion), and acetate.

3.1 Complexes containing two cobalt centres

3.1.1 Synthesis of $[Co^{II}_2Br_2(teaH_3)_2]Br_2$ (8) ($teaH_3$ = triethanolamine)

Treithanolamine (0.30 g, 2.01 mmol) was dissolved in 20 mL of 2-propanol, $CoBr_2$ (0.44 g, 2.01 mmol) was then added. The reaction was stirred at room temperature overnight and then filtered. The filtrate was stored in a sealed vial and portions were taken for vapour diffusion with Et_2O. After 2 weeks pink crystals formed from the vapour diffusion crystallisation, in 10% yield. Air dried crystals analyse as $\mathbf{C_{12}H_{30}N_2O_6Br_4Co_2}$, analysis (%) calc. (found) C, 19.59 (19.54); H, 4.11 (4.13); N, 3.81 (3.73). Selected IR data: ν = 3173, 2978, 2901, 1471, 1458, 1413, 1396, 1313, 1263, 1215, 1159, 1139, 1074, 1049, 1001, 912, 887, 864, 746, 609 cm^{-1}.

Green crystals and white crystals also form from this reaction; the green crystals have been identified as the same tetramer that will be discussed in Section 3.3, whereas the white crystals are an impurity that was removed before any further analysis was undertaken. Due to time constraints the white impurity could not be identified.

3.1.2 Synthesis of $[Co^{II}Co^{III}(acac)_3(deaH)_2]$ (9) ($deaH_2$ = diethanolamine)

$Co(acac)_2$ (0.26 g, 1.01 mmol) was dissolved in acetone (20 mL) and diethanolamine (0.19 mL, 2.00 mmol) was added. The reaction was stirred for 3 hours, it was then filtered and the brown filtrate was stored in a sealed vial. After one week, small red plate crystals formed, in 31% yield. Air dried crystals analyse as $\mathbf{C_{26}H_{47}Co_2N_2O_{11}}$, analysis (%) calc. (found) C, 45.82 (45.56); H, 6.95 (6.79); N, 4.11 (4.46). Selected IR data: υ = 3254, 2983, 2947, 2864, 2796, 2648, 1570, 1516, 1429, 1384, 1280, 1192, 1153, 1093, 1087, 1051, 1033, 935, 914, 873, 823, 771, 692, 653, 630, 607 cm^{-1}. (acac = acetylacetonate, $C_5H_7O_2$)

3.1.3 Discussion of crystal structures

*3.1.3.1 Discussion of crystal structure of $[Co^{II}_2Br_2(teaH_3)_2]Br_2$ **(8)***

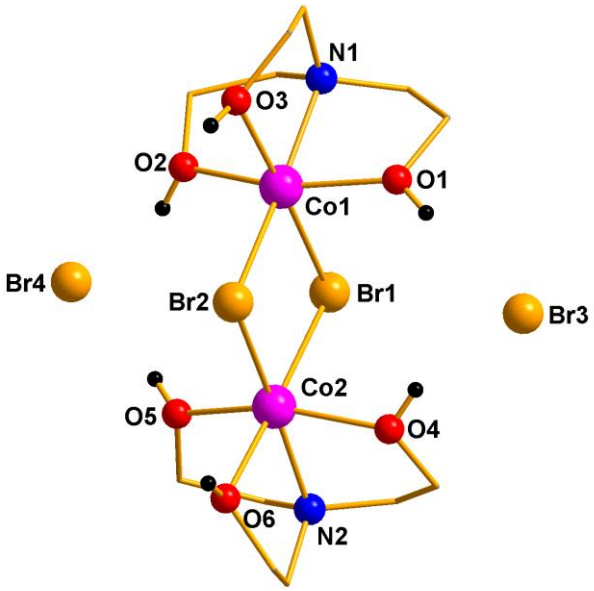

Figure 3-3 Structure of 8 (OH protons shown) Co^{II} pink; N blue; O red; Br light orange; H black.

This complex consists of two Co^{II} ions connected by two Br ligand bridges. Each cobalt ion has a distorted octahedral environment, with an $\{O_3Br_2N\}$ ligand donor set. The ligand in this complex is triethanolamine and it remains fully protonated, resulting in a 2+ charge on the complex that is balanced by two unbound Br anions. These anions are located in the lattice in rows between rows of the complex. There are hydrogen bonds between two of the protonated ligand (O1, O2, O4 and O5) arms on each Co ion and the unbound Br anions (Br3 and Br4) (O(H)···Br 3.1548(1)-3.2075(1)Å). The third ligand arm with O3 and O6 hydrogen bonds to further symmetry equivalent Br anions (Br3 and Br4), O6/3(H)···Br4/3 3.2111(1)/3.2129(1) Å.

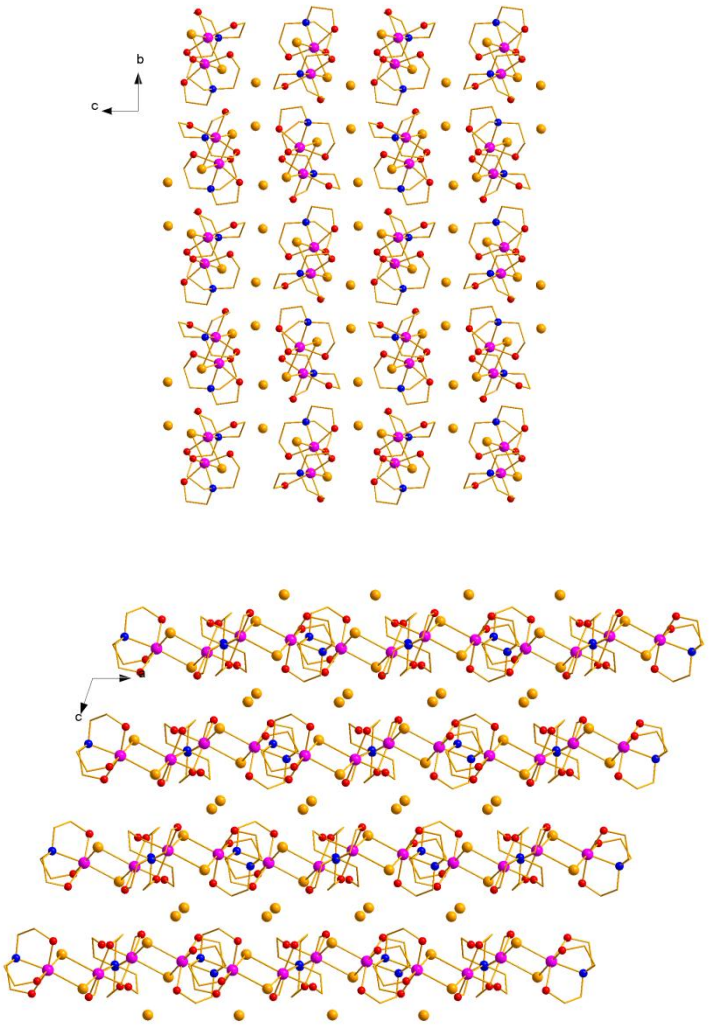

Figure 3-4 Packing diagrams of 8 viewed along the *a*-(top) and *b*-axes(bottom).

The orientation of the complex alternates in the *b*- and *c*-axis directions, however in the direction of the *a*-axis the orientation of the complex remains the same. The unbound Br anions are arranged in columns between the complexes.

Complexes with bridging Br anions[18-22] are much rarer than complexes with bridging Cl anions[23-27] (CSD search 10 results for Br bridged and 78 for Cl bridged). A similar Co dimer complex with bridging Br ions has been previously synthesised, $[CoBr(TPyEA)]_2(BPh_4)_2$ (where TPyEA = tris(1-pyrazolylethyl)amine).[19] This complex has an inversion centre and therefore both Co-Br-Co angles are the same, 96.7(2)° (compared with 89.72(2)° and 94.71(2)° for **8**) and resulting in a Co···Co distance of 4.008(3) Å compared with a distance of 3.7134(1) Å for **8**. Other complexes with bridging Br include $[Co(IPr)Br]_2Br_2$ (where IPr = 1,3-bis(2,6-diisopropylphenyl)imidazol-2-ylidene)[18] the two Co^{II} ions in this example have tetrahedral geometry and a Co-Br-Co bridging angle 82.00(1)°, the magnetic behaviour is attributed to antiferromagnetic interactions between the two. The Cl bridged analogue with the ligand IPr has also been synthesised (Co-Cl-Co angle 84.76(1)° and the interactions between the two metal centres are also found to be antiferromagnetic.[18]

Table 3-1 Data for the crystal structure determination of 8.

Empirical Formula	$C_{12}H_{30}Br_4Co_2N_2O_6$
Fw (g mol^{-1})	735.86
Crystal system	Monoclinic
Space group	*P2$_1$/c*
a (Å)	11.7009(3)
b (Å)	14.254(4)
c (Å)	14.3326(3)
β (deg)	108.6810(10)
V (Å^3)	2264.74(10)
Z	4
T (K)	100(2)
λ (Å)	0.71073
ρ_{calcd} (Mg m^{-3})	2.158
μ (mm^{-1})	8.55
R_1[a]	0.0352
wR_2[b]	0.0391
Goodness of fit indicator	1.041

[a] $R_1 = \Sigma \left| |F_o| - |F_c| \right| / \Sigma |F_o|$ [b] $wR_2 = \left[\Sigma \left[w\left(F_o^2 - F_c^2\right)^2 \right] - \Sigma \left[\left(F_o^2\right)^2 \right] \right]^{1/2}$ where $w = 1/\left[\sigma^2\left(F_o^2\right) + \left(0.2P\right)^2\right]$ and $P = \left[F_o^2 + 2F_c^2\right]/3$

Table 3-2 Selected metal-ligand bond lengths for 8.

Bond	Distance (Å)	Bond	Distance (Å)
Co1–Br1	2.6525(7)	Co2–Br1	2.6123(7)
Co1–Br2	2.5198(7)	Co2–Br2	2.5291(6)
Co1–N1	2.153(3)	Co2–N2	2.157(3)
Co1–O1	2.067(3)	Co2–O4	2.097(3)
Co1–O2	2.072(3)	Co2–O5	2.065(3)
Co1–O3	2.095(3)	Co2–O6	2.083(3)

Table 3-3 Selected bond angles for 8.

Atoms	Angle (°)
Co2-Br1-Co1	89.72(2)
Co1-Br2-Co2	94.71(2)

Table 3-4 BVS calculation[28] results for 8.

Atom	Co^{II}	Co^{III}
Co1	<u>2.165</u>	2.188
Co2	<u>2.172</u>	2.195

Underlined values are that closest to the oxidation state for which they were calculated.

*3.1.3.2 Discussion of the crystal structure of $[Co^{II}Co^{III}(acac)_3(deaH)_2]$ (**9**)*

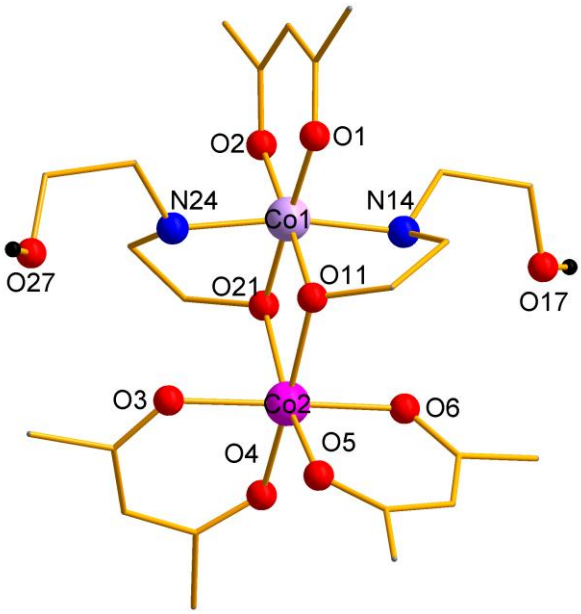

Figure 3-5 Structure of 9 showing protonated ligand arms Co^{II} pink; Co^{III} lilac; O red; N blue; H black (all other H-atoms removed for clarity).

This complex is a mixed valent cobalt dimer that crystallises in the triclinic space group *P*-1. The Co^{III} ion is bound to one acac and two dithanolamine ligands, one ethanolic arm of each diethanolamine ligand remains unbound and protonated. The Co^{III} ion has an $\{N_2O_4\}$ ligand donor set arranged as a distorted octahedral coordination sphere. The Co^{II} ion also has a distorted octahedral arrangement and has an $\{O_6\}$ ligand environment, made up of two acac ligands and two ethanolic arms from two diethanolamine ligands. The oxidation states of the metal centres were assigned on the basis of charge balance and consideration of bond lengths and BVS calculations.[28]

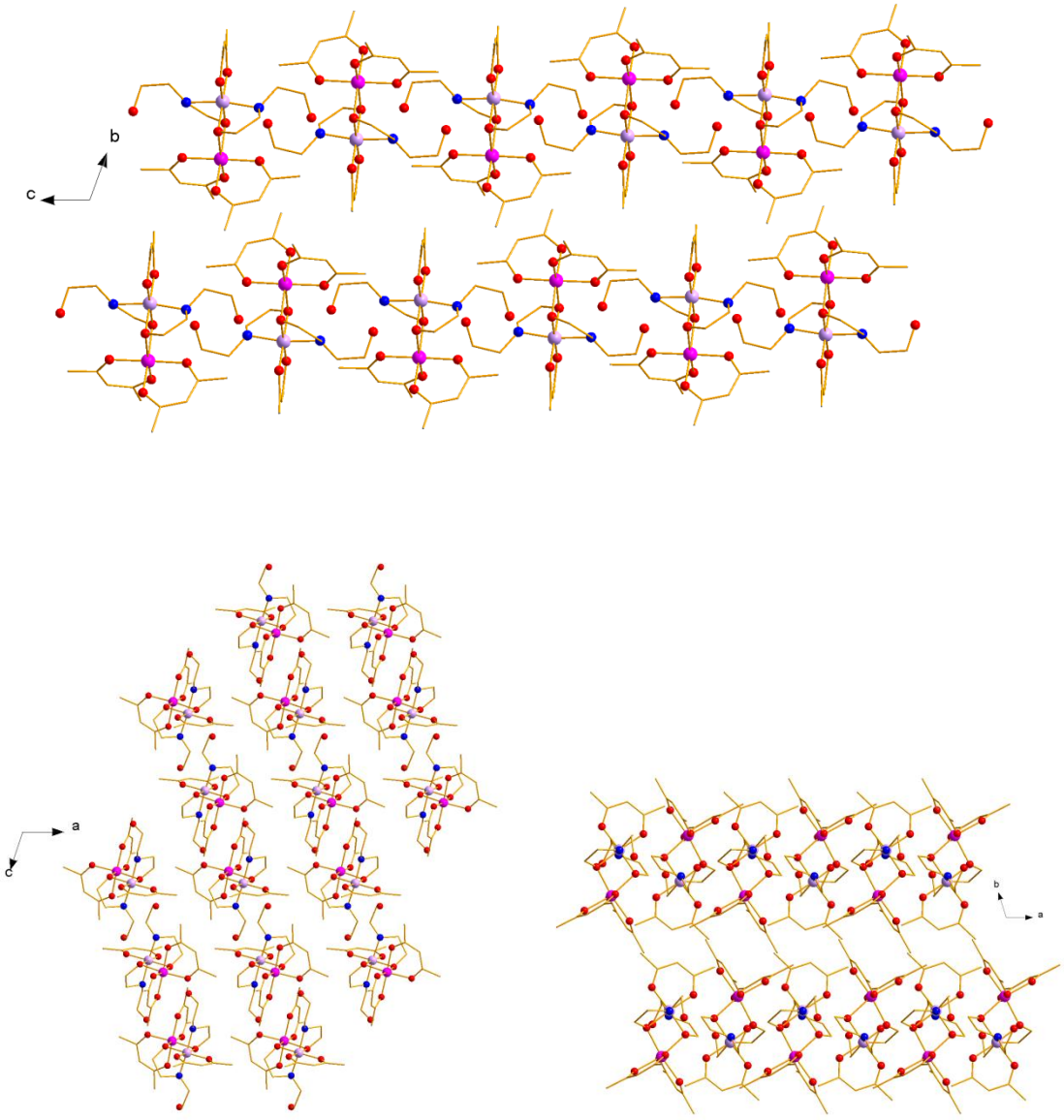

Figure 3-6 Packing diagrams for 9 viewed along *a*-, *b*-, and *c*-axes.

The complexes are linked by hydrogen bonding, between the hydrogens on O17 and O27 to the oxygens O21 and O11, on neighbouring clusters, O(H)···O11 2.785(3) Å and O(H)···O21 2.720(2) Å. There are no molecules of solvent present in the lattice. Magnetic susceptibility measurements were not carried out on this complex due to the presence of only one paramagnetic ion per complex.

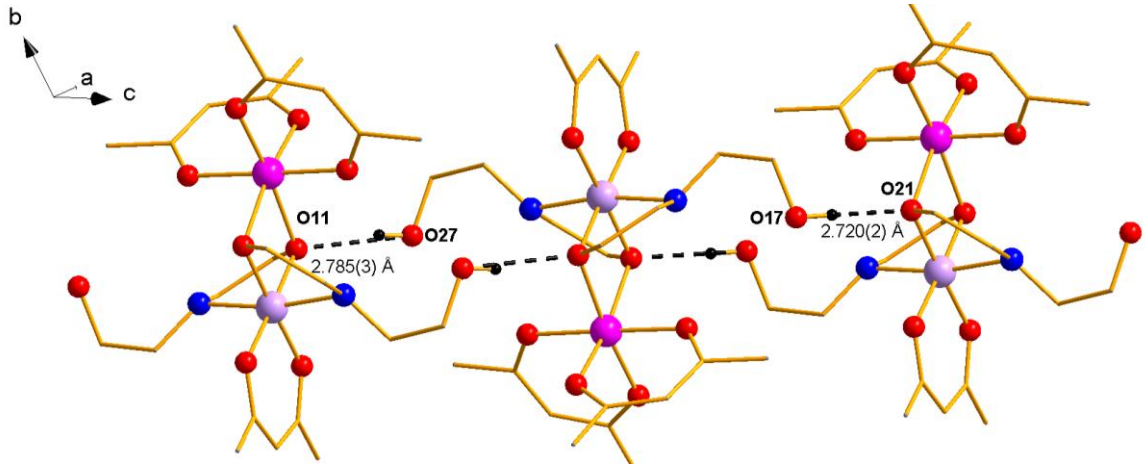

Figure 3-7 Diagram showing inter-molecular hydrogen bonding for complex 9.

Table 3-5 Data for the crystal structure determination of 9.

Empirical Formula	$C_{23}H_{41}Co_2N_2O_{10}$
Fw (g mol^{-1})	623.45
Crystal system	triclinic
Space group	*P*-1
a (Å)	9.0252(2)
b (Å)	11.5519(2)
c (Å)	14.6866(3)
α (deg)	106.504 (1)
β (deg)	103.695 (1)
γ (deg)	102.084 (1)
V (Å^3)	1362.04(5)
Z	2
T (K)	100(2)
λ (Å)	0.71073
ρ_{calcd} (Mg m^{-3})	1.52
μ (mm^{-1})	1.274
R_1[a] (%)	0.0356
wR_2[b] (%)	0.0482
Goodness of fit	1.014

[a] $R_1 = \Sigma \left| |F_o| - |F_c| \right| / \Sigma |F_o|$ [b] $wR_2 = \left[\Sigma \left[w\left(F_o^2 - F_c^2\right)^2 \right] - \Sigma \left[\left(F_o^2\right)^2 \right] \right]^{1/2}$ where $w = 1/\left[\sigma^2\left(F_o^2\right) + \left(0.2P\right)^2\right]$ and $P = \left[F_o^2 + 2F_c^2\right]/3$

Table 3-6 Metal-ligand bond lengths for 9.

Bond	Distance (Å)	Bond	Distance (Å)
Co1–O11	1.891(2)	Co2–O11	2.136(2)
Co1–N14	1.983(2)	Co2–O21	2.148(2)
Co1–O21	1.893 (2)	Co2–O3	2.061(2)
Co1–N24	1.978(2)	Co2–O4	2.043(2)
Co1–O1	1.916(2)	Co2–O5	2.052(2)
Co1–O2	1.908(2)	Co2–O6	2.062(2)

Table 3-7 Selected bond angles for 9.

Atoms	Angle (°)
Co2-O11-Co1	99.42(7)
Co2-O21-Co1	98.89(7)

Table 3-8 BVS calculation results for 9.[28] The underlined value is that closest to the oxidation state for which it was calculated, overestimation in Co^{III} result is discussed in appendix one.

Atom	Co^{II}	Co^{III}
Co1	3.639	<u>3.688</u>
Co2	<u>2.094</u>	2.14

3.1.4 Magnetic Susceptibility Measurements of $[Co^{II}_2Br_2(teaH_3)_2]Br_2$ (8)

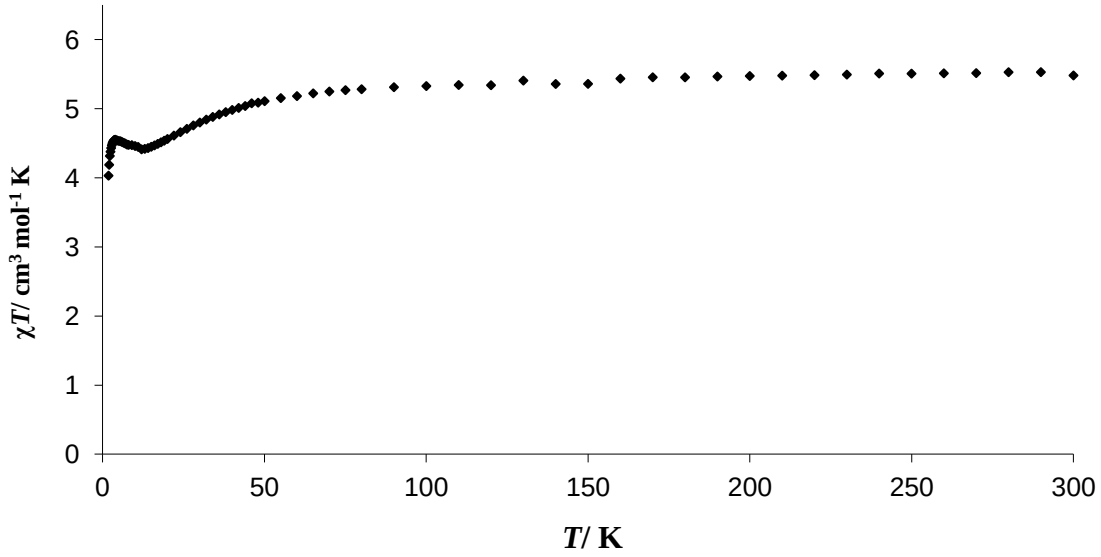

Figure 3-8 Temperature dependence of χT for 8 from 1.8-300K measured in an applied field of 1000 G.

Magnetic susceptibility measurements were carried out on an air dried sample, which analysed as **8**. The χT value at 300 K is 5.48 $cm^3\ mol^{-1}$ K and is consistent with two uncoupled Co^{II} ions with g = 2.4. The χT value gradually decreases to a local minimum at 12 K of 4.45 $cm^3\ mol^{-1}$ K, it then increases to a local maximum at 3.6 K of 4.55 $cm^3\ mol^{-1}$ K and then rapidly decreases to 4.03 $cm^3\ mol^{-1}$ K at 1.8 K.

The low temperature peak of 4.56 $cm^3\ mol^{-1}$ K is consistent with an effective $S' = 1$ ground state with an anisotropic g value of 4.27. The decrease in χT down to 12 K is due to spin-orbit coupling and is often seen in Co^{II} complexes as the temperature is decreased.[29] The subsequent increase in χT is due to the spin-orbit coupling effects being quenched at low temperature due to weak ferromagnetic coupling. The Co^{II}-Br-Co^{II} bridging angles in this complex are ~89° and ~94°, angles around 90° generally favour ferromagnetic coupling.[30,31] The decrease in χT after the maximum at 3.6 K is potentially due to zero-field splitting of the effective $S' = 1$ ground state, though it is possible that intermolecular antiferromagnetic interactions could also be responsible.[32] Ac susceptibility measurements were also carried out, however no increase in out-of-phase signals were observed down to 1.8 K.

3.2 Complexes containing three cobalt centres

A search of the CSD reveals that there are around 30 linear type complexes with three cobalt centres bridged by oxygen. Some of these have similarities of structure with the complex described below,[33,34] though many of them utilise much bulkier and complex ligands,[35] some also have different bridging groups between the Co^{II} and Co^{III} ions such as azides.[36]

3.2.1 Synthesis of $[Co^{II}Co^{III}_2(acac)_2(O_2CMe)_2(teaH)_2]\cdot 4MeCN$ (10·4MeCN)

$Co(acac)_2$ (0.26 g, 1.01 mmol) was dissolved in acetonitrile (20 mL) and triethanolamine (0.13 mL, 1.00 mmol) was added. The reaction was stirred for 5 hours, it was then filtered and the brown filtrate was stored in a sealed vial. After one week, small crystals formed, in 13% yield. Air dried crystals analyse as $\mathbf{C_{26}H_{50}N_2O_{14}Co_3}$, analysis (%) calc. (found) C, 37.92 (37.79); H, 6.12 (5.82); N, 3.40 (3.48). Selected IR data: ν = 1560, 1518, 1437, 1421, 1379, 1323, 1282, 1060, 1014, 947, 918, 786, 756, 690, 640 cm^{-1}.

3.2.2 Discussion of crystal structure of $[Co^{II}Co^{III}_2(acac)_2(O_2CMe)_2(teaH)_2]\cdot 4MeCN$ (10·4MeCN)

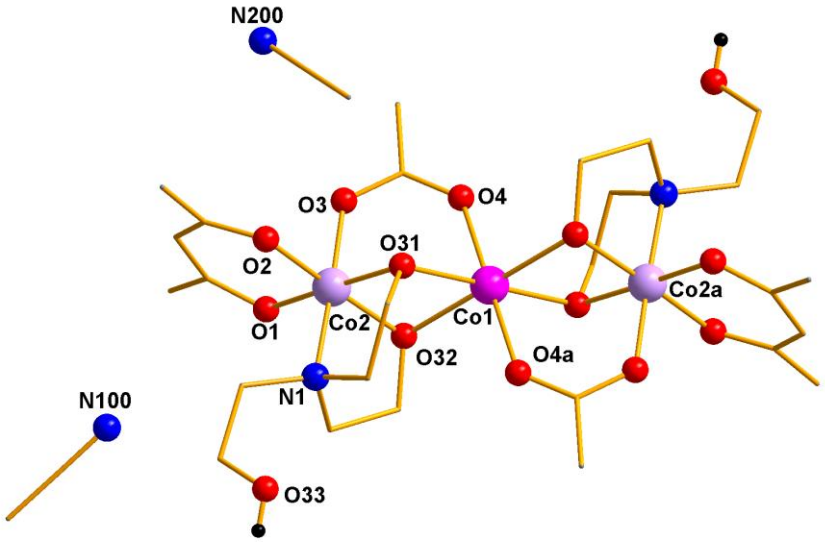

Figure 3-9 Structure of 10 with key atoms labelled. Atom label a signifies symmetry equivalent a = 2-x, 1-y, 1-z. Co^{II} pink; Co^{III} lilac; O red; N blue; H black.

This mixed valent complex consists of two Co^{III} ions and one Co^{II} ion, and crystallises in the orthorhombic space group *Pcba*. The central Co^{II} ion has an $\{O_6\}$ ligand donor set arranged in a distorted octahedral geometry. Four of these oxygen donor atoms come from deprotonated ethanolic arms of two triethanolamine ligands, the remaining oxygen donors from two acetate

groups. The terminal Co^{III} ions are related by symmetry; they have an $\{NO_5\}$ ligand donor set also arranged in a distorted octahedral arrangement. The nitrogen and two oxygens are provided by the triethanolamine ligand, two oxygen donor atoms are from an acac group, and the final oxygen is from an acetate group.

Each triethanolamine ligand has two bound and deprotonated arms and one unbound arm that remains protonated, the acac groups are chelating and the acetate groups bridge between Co^{II} and Co^{III} ions. The oxidation states of the metal ions were assigned by consideration of bond lengths, charge balance and BVS calculations.

From the synthesis reported it is clear that no acetate was present in the starting materials and that it must therefore be formed *in situ* during the reaction. It is thought that this is formed from the oxidative hydrolytic cleavage of the acetylacetonate ligand.[37,38]

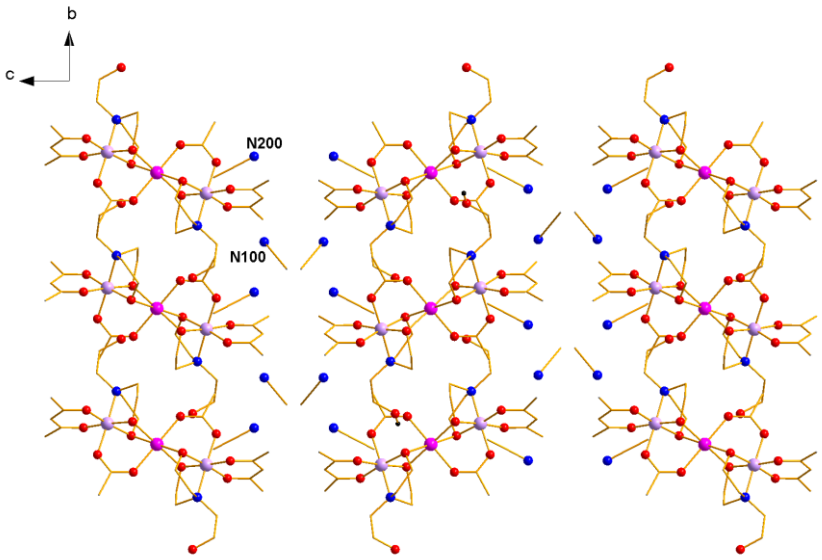

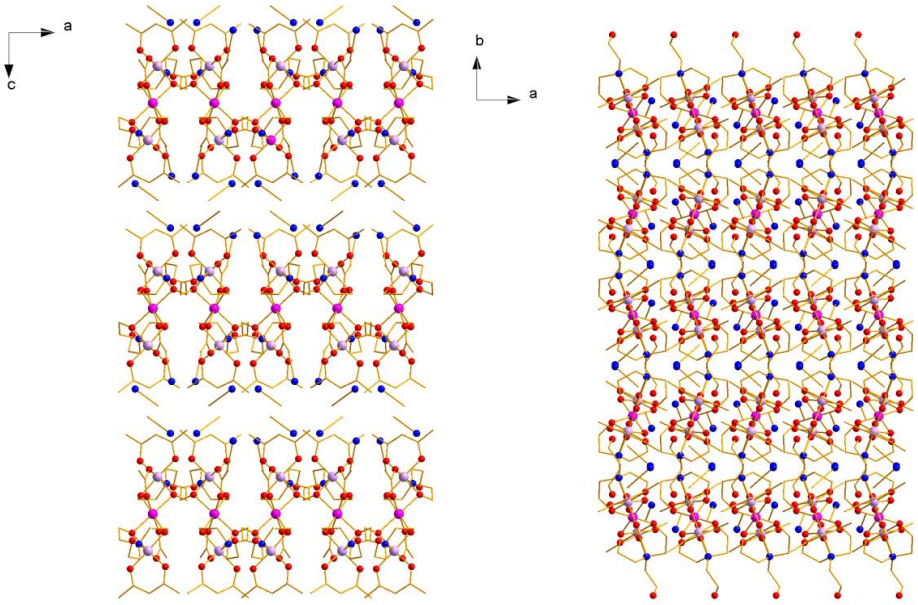

Figure 3-10 Packing diagrams for 10·4MeCN viewed along *a*-(previous page), *b*-(left), and *c*-axes(right).

There are two molecules of acetonitrile solvent and their symmetry equivalents in the lattice per complex; this solvent is ordered in channels, with N100 facing out of the channel and N200 pointing into the channel (Figure 3-10, view along *a*-axis). The closest Co···Co distances between neighbouring rows are 8.496(2) Å between rows, and 10.822(2) Å along the row. The shortest distance between Co ions within a complex is 3.018(1) Å.

This complex is very similar to the core of a heteropentanuclear complex (Figure 3-11),[39] three cobalt centres linked by two acetate groups and two triethanolamine groups as above. This core is then extended by a further acetate and triethanolamine ligand bridging to a copper atom at each end of the linear cobalt core.

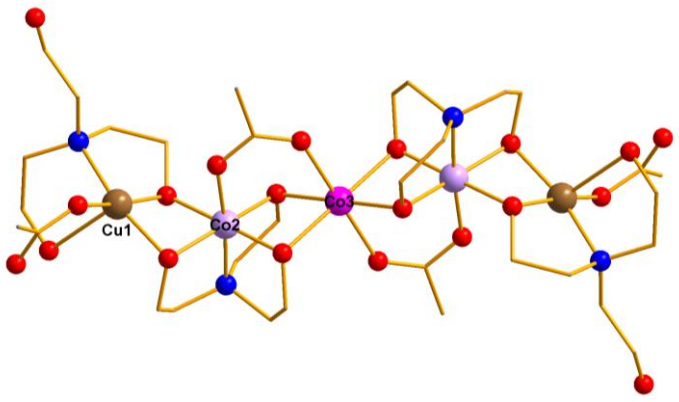

Figure 3-11 Structure of $[Cu^{II}_2Co^{II}Co^{III}_2(O_2CMe)_4(H_2L)_2(L)_2]$[39] where H_3L = triethanolamine. Co^{II} pink; Co^{III} lilac; Cu^{II} brown; O red; N blue; H omitted for clarity.

In this cobalt and copper heterometallic complex the unbound triethanolamine OH is disordered over two positions and the five metal ions are linked by 8 oxygen atoms of four triethanolamine ligands and two acetate ligands.[39] The distance between the Co^{II} and Co^{III} ions is 2.964(1) Å, comparable to the distance in complex **10**. The complex was found to have antiferromagnetic interactions between the Co^{II} and Cu^{II} ions, with diamagnetic Co^{III} playing an effective role in transmitting this interaction at low temperature.[39]

The general structural form of the core of complex **10**, Co^{III}-Co^{II}-Co^{III} is found in a variety of other complexes prepared from both Co^{III} and Co^{II} salts, implying that the formation of this core is favourable and stable. Some examples utilising similar ligands to those used here are $[Co^{II}Co^{III}_2(NO_2)_4(NH_2CH_2CH_2O)_4]$, where the ligand is ethanolamine, and the synthesis started with a Co^{III} salt.[40] The same ethanolamine ligand was also used to synthesise $[Co^{II}(Co^{III}(NH_2CH_2CH_2O)_3)_2]^{2+}$ as the acetate salt.[34] Further examples of mixed valent trimers include those in which the terminal Co^{III} ions are encapsulated by a tetradentate Schiff base ligand.[35,41-44] When the ligand used is salen (H_2salen = 1,6-bis(2-hydroxyphenyl)-2,5-diazahexa-1,5-diene), these complexes are of interest due to an ability to interact with proteins.[41] A more unusual Co_3 linear trimer is $[Co^{II}_3(OH)_2(pa)_2(ina)_2]$ (pa = 3-(1*H*-benzimidazol-2-yl)propanoic carboxylate; and ina = isonicotinate) which has an interesting T_d-O_h-T_d geometry arrangement (Figure 3-12),[45] the trinuclear cluster forms part of an extended 2D network.

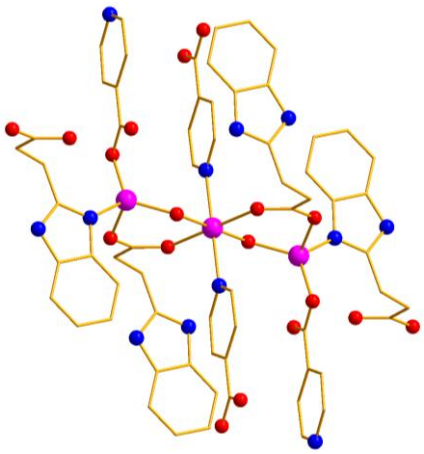

Figure 3-12 Diagram of $[Co^{II}_3(OH)_2(pa)_2(ina)_2]$ showing the coordination environments of Co^{II}.[45]

Table 3-9 Data table for the crystal structure determination of 10·4MeCN.

Empirical Formula	$C_{34}H_{58}Co_3N_6O_{14}$
Fw (g mol^{-1})	951.67
Crystal system	orthorhombic
Space group	*Pbca*
a (Å)	9.190 (1)
b (Å)	15.119 (2)
c (Å)	30.661(4)
V (Å^3)	4260.4(10)
Z	4
T (K)	100(2)
λ (Å)	0.71073
ρ_{calcd} (Mg m^{-3})	1.484
μ (mm^{-1})	1.223
R_1[a]	0.0565
wR_2[b]	0.1277
Goodness of fit	0.945

[a] $R_1 = \Sigma \left| |F_o| - |F_c| \right| / \Sigma |F_o|$ [b] $wR_2 = \left[\Sigma \left[w\left(F_o^2 - F_c^2\right)^2 \right] - \Sigma \left[\left(F_o^2\right)^2 \right] \right]^{1/2}$ where $w = 1/\left[\sigma^2\left(F_o^2\right) + \left(0.2P\right)^2\right]$ and $P = \left[F_o^2 + 2F_c^2\right]/3$

Table 3-10 Selected metal-ligand bond lengths for 10.

Bond	Distance (Å)	Bond	Distance (Å)
Co1–O32	2.168(5)	Co2–N1	1.986(6)
Co1–O4	2.088(5)	Co2–O31	1.878(5)
Co1–O31	2.061(5)	Co2–O32	1.913(5)
Co1–O32a	2.168(5)	Co2–O1	1.900(5)
Co1–O4a	2.088(5)	Co2–O2	1.907(5)
Co1–O31a	2.061(5)	Co2–O3	1.922(5)

Table 3-11 Selected bond angles for 10.

Atoms	Angle (°)
Co1-O31-Co2	99.9(2)
Co1-O32-Co2	95.2(2)

Table 3-12 BVS calculations for 10.[28]

Atom	Co^{II}	Co^{III}
Co1	<u>1.976</u>	2.019
Co2	3.495	<u>3.557</u>

Underlined value is the one closest to the charge for which it was calculated. Overestimations for Co^{III} will be discussed in the appendix one.

Magnetic measurements were not carried out for this complex due to the presence of only one Co^{II} per complex, and the distance between Co^{II} ions in different complexes making coupling between centres unlikely.

3.3 Complexes containing four cobalt centres

3.3.1 Synthesis of $[Co^{II}_2Co^{III}_2Br_4(tea)_2(H_2O)_2]$ ·4(2-propanol)(11·4(2-propanol)

(where H_3tea = triethanolamine)

Triethanolamine (0.45 g, 3.02 mmol) was dissolved in 20 mL of 2-propanol, $CoBr_2$ (0.33 g, 1.51 mmol) and $Co(NO_3)_2.6H_2O$ (0.45g, 1.55 mmol) were then added. The reaction was stirred at room temperature overnight and then filtered. The filtrate was stored in a sealed vial and portions were taken for vapour diffusion with Et_2O. After 2 weeks green crystals formed in small yield, smaller white crystals were also present. The green crystals of interest were separated and analysed separately. Selected IR data: green crystals ν = 3439, 3342, 2991, 2935, 2916, 2872, 1610, 1460, 1400, 1375, 1307, 1263, 1249, 1149, 1076, 1049, 1003, 927, 906, 752, 696, 657, 626 cm^{-1}. Due to the difficulty in collecting a pure sample for magnetic measurements it was not possible to carry out microanalysis.

Selected IR data: white crystals ν =3346, 3149, 2931, 2899, 2829, 1485, 1458, 1435, 1402, 1365, 1321, 1292, 1246, 1193, 1093, 1078, 1064, 1003, 916, 854, 759, 609 cm^{-1}.

This reaction was similar to the reaction used to synthesise complex **8**, single crystal X-ray diffraction of the green crystals formed by this reaction and the one used to synthesise complex **8** revealed them to be the same complex.

3.3.2 Discussion of the crystal structure of $[Co^{II}_2Co^{III}_2Br_4(tea)_2(H_2O)_2]\cdot 4(CH_3CH(OH)CH_3)$ (11·4(CH$_3$CH(OH)CH$_3$))

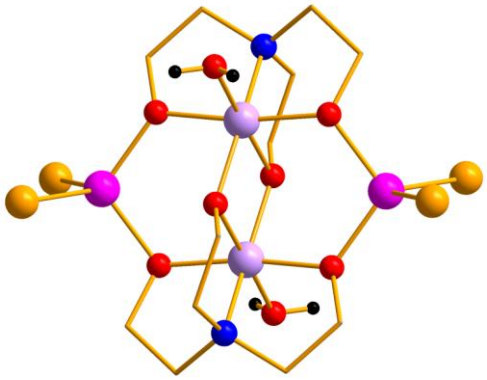

Figure 3-13 Structure of 11 H-atoms of bound H_2O shown all others omitted for clarity. Co^{II} pink; Co^{III} lilac; O red; N blue; Br orange.

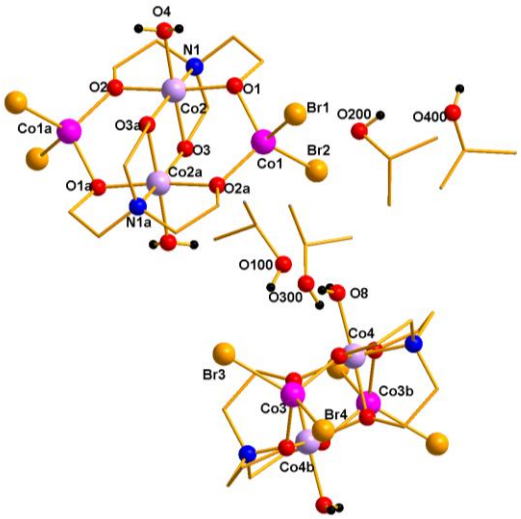

Figure 3-14 Labelled diagram of 11 including four molecules of 2-propanol solvent. H-atoms of OH groups shown all others omitted for clarity; labels a and b signify symmetry equivalents: a = -x, 1-y, -z; b = -x,-y, 1-z.

This complex consists of four cobalt ions (two Co^{II} and two Co^{III}), four bromide ions, two triethanolamine ligands and two bound water molecules. The Co^{II} ions each have an $\{Br_2O_2\}$ coordination environment with a distorted tetrahedral geometry (smallest angle O1-Co1-Br1 98.7(2)°; largest angle Br1-Co1-Br2 115.8(6)° compared to 109.5° for ideal tetrahedral geometry). The Co^{III} ions have a distorted octahedral geometry with an $\{NO_5\}$ ligand donor set, one triethanolamine ligand provides three oxygen donors, a further oxygen comes from the symmetry equivalent triethanolamine ligand and a water molecule completes the coordination sphere. The oxidation states were assigned on the basis of bond length, BVS calculations[28] and consideration of charge balance.

The asymmetric unit of this sample consists of two half complexes and four molecules of 2-propanol solvent, the unit cell consists of four complete complexes.

There are hydrogen bonding interactions between the complex and molecules of solvent, each complex interacts with a pair of solvent molecules and their symmetry equivalents. The interactions are between a bound water molecule and two 2-propanol solvent molecules (Figure 3-15) for example O8(H)···O100 2.638(9) Å, O8(H)···O300 2.659(9) Å. These solvent molecules have further interactions with the Br ions, O100(H)···Br3 3.380(5) Å and O300(H)···Br4 3.567(7) Å.

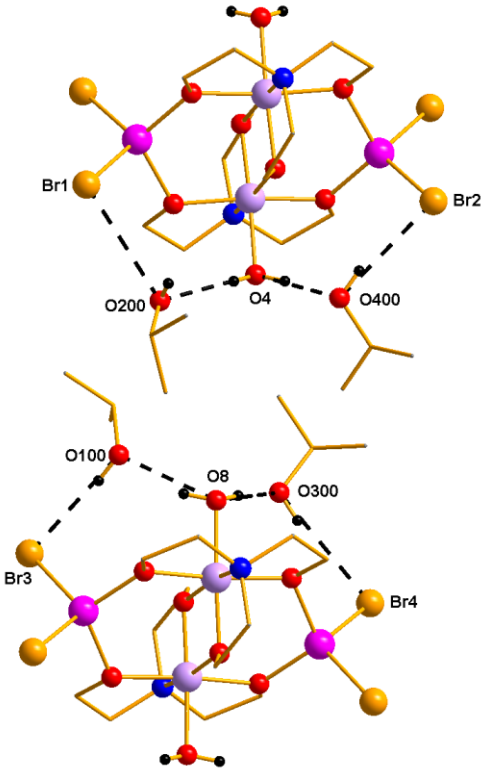

Figure 3-15 Hydrogen bonding interactions shown for 11 and one symmetry equivalent set of solvent molecules.

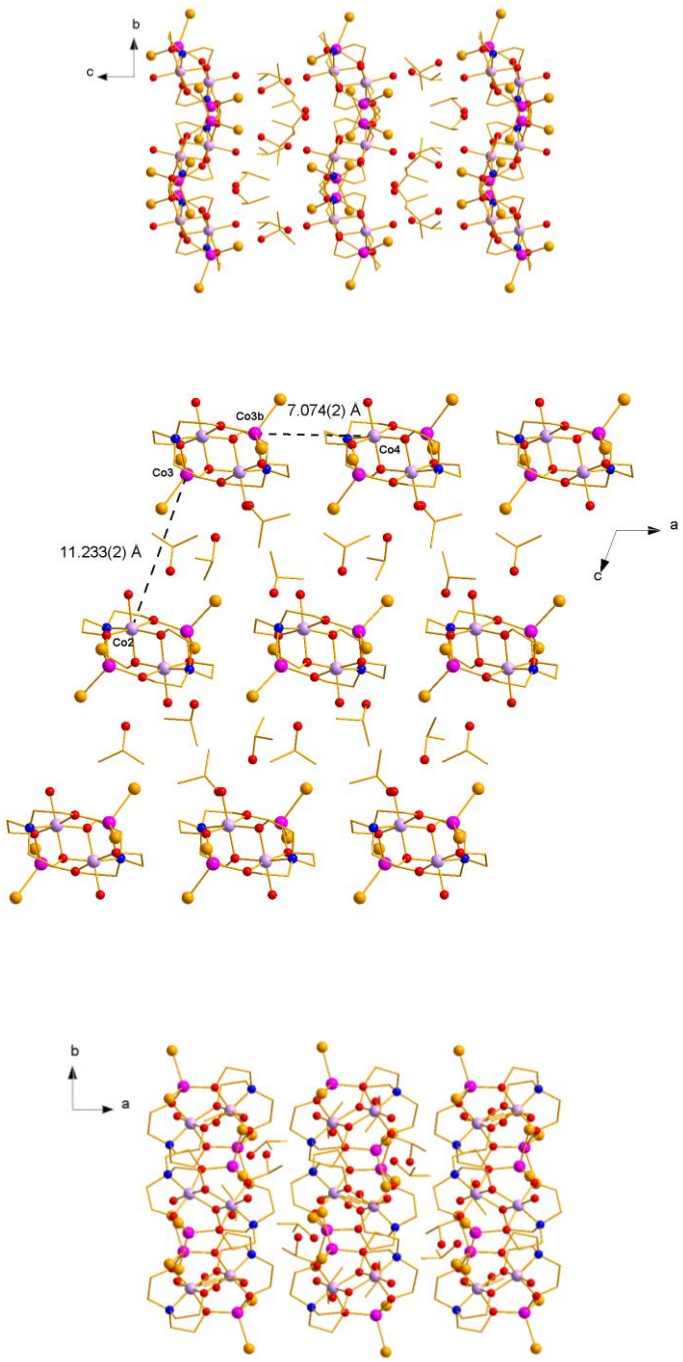

Figure 3-16 Packing diagrams for 11 viewed along *a*-, *b*- and *c*-axes. Closest Co···Co′ distances are shown in *b*-axis view.

The closest Co···Co distance between neighbouring complexes is 7.074(2) Å between divalent Co3b and trivalent Co4′ (Figure 3-14). From the above packing diagrams in can be seen that the solvent molecules are arranged in layers between sheets of complexes, the distance from Co3···Co2″ over this row of solvent is 11.233(2) Å. The closest $Co^{II}\cdots Co^{II}$ distance between complexes is approximately 9.5 Å.

This structural motif of four Co ions with an almost planar arrangement, as above, is relatively uncommon, with only around 30 hits in the CSD[46] (compared with over 50 for cubane type

structures). However these all contain Co in either octahedral or trigonal bipyramidal[47] environments, with a mixture of Co^{II} and Co^{III} ions, and no examples containing tetrahedral Co^{II} could be found.

One example of a cobalt tetramer is $[Co^{II}_4(\mu_3\text{-}Cl)_2(\mu\text{-}Cl)_4Cl_2(THF)_6]$, this example is interesting due to the number of bridging Cl anions and the presence of two different Co^{II} environments trigonal bipyramindal and octahedral, which is relatively rare.[47] Magnetic measurements suggest that the interactions between metal centres in this tetramer are ferromagnetic. Complexes with bridging oxygen atoms are more common. Some examples using simple ligands similar to those utilised here are $[Co^{II}_4(\mu_3\text{-}OH)(H_2O)_6(ntp)_2]$ (where H_3ntp = nitrilotripropionic acid, $(N(CH_2CH_3COOH)_3)$),[32] a mixed valent example using diethanolamine ($deaH_2$) $[Co^{II}_2Co^{III}_2(deaH_2)_2(dea)_4](ClO_4)_2$,[48] and an example which uses the acetylacetonate ligand is $[Co^{II}_4(acac)_6(OMe)_2(MeOH)_2]$.[49] The only examples of Co tetramers with Br as a ligand were cubanes $[Co_4Br_4(C_6H_6NO)_4(CH_3OH)_4]Br_4$ and $[CoBr(NPR_3)]_4$ (where R = Me, Et),[50,51] a molecular square of the form $[Co_4L_4](BF_4)_4$, where L = PMAH (2-[(2-aminoethylamino)methyl]-5-bromo-N-[2-(1H-imidazol-5-yl)ethyl]pyrimidine-4-carboxamide),[52,53] and a linear complex $\{Co_2Br_2[^{tBu}NON]\}_2$[20] (where ^{tBu}NON is a diamidosilylether ligand). The linear complex is the only one of the four mentioned here to have Br as a bridging ligand rather than a terminal ligand.

Table 3-13 Data for the crystal structure determination of 11·4($CH_3CH(OH)CH_3$)

Empirical Formula	$C_{24}H_{60}Br_4Co_4N_2O_{12}$
Fw (g mol^{-1})	1124.1
Crystal system	Monoclinic
Space group	$P2_1/a$
a (Å)	18.8451(5)
b (Å)	10.1948(2)
c (Å)	22.7852(5)
β (deg)	110.530(1)
V ($Å^3$)	4099.5(2)
Z	4
T (K)	120(2)
λ (Å)	0.71073
ρ_{calcd} (Mg m^{-3})	1.821
μ (mm^{-1})	5.54
R_1[a]	0.1092
wR_2[b]	0.068
Goodness of fit	1.006

[a] $R_1 = \Sigma\left||F_o| - |F_c|\right| / \Sigma|F_o|$ [b] $wR_2 = \left[\Sigma\left[w\left(F_o^2 - F_c^2\right)^2\right] - \Sigma\left[\left(F_o^2\right)^2\right]\right]^{1/2}$ where $w = 1/\left[\sigma^2\left(F_o^2\right) + \left(0.2P\right)^2\right]$ and $P = \left[F_o^2 + 2F_c^2\right]/3$

Table 3-14 Selected metal ligand bond lengths for complex 11.

Bond	Distance (Å)	Bond	Distance (Å)
Co1–Br1	2.430 (2)	Co3–Br3	2.400(2)
Co1–Br2	2.413(2)	Co3–Br4	2.428(2)
Co1–O1	1.967(5)	Co3–O5	1.934(5)
Co1–O2	1.932(5)	Co3–O6	1.967(5)
Co2–N1	1.907(7)	Co4–N2	1.906(7)
Co2–O1	1.902(5)	Co4–O5	1.902(5)
Co2–O2	1.909(6)	Co4–O6	1.910(6)
Co2–N1	1.950(5)	Co4–O7a	1.946(5)
Co2–O3a	1.864(5)	Co4–O7	1.860(5)
Co2–O3	1.942(5)	Co4–O8	1.934(6)

Table 3-15 Selected bond angles for complex 11.

Atoms	Distance (Å)
Co1-O1-Co2	116.8(2)
Co1a-O2-Co2	122.3(3)
Co2-O3-Co2a	99.8(2)
Co3-O5-Co4	121.4(3)
Co3b-O6-Co4	117.0(2)
Co4-O7-Co4b	99.8(3)

Table 3-16 BVS calculation results for 11.[28]

Atom	Co^{II}	Co^{III}
Co1	<u>2.070</u>	2.092
Co2	3.648	<u>3.710</u>
Co3	<u>2.052</u>	2.074
Co4	3.623	<u>3.684</u>

Underlined value is that closest to the oxidation state for which it was calculated, overestimations for Co^{III} will be discussed in appendix one.

3.3.3 Magnetic Measurements for $[Co^{II}_2Co^{III}_2Br_4(tea)_2(H_2O)_2]\cdot 4(CH_3CH(OH)CH_3)$ (11·4(CH₃CH(OH)CH₃))

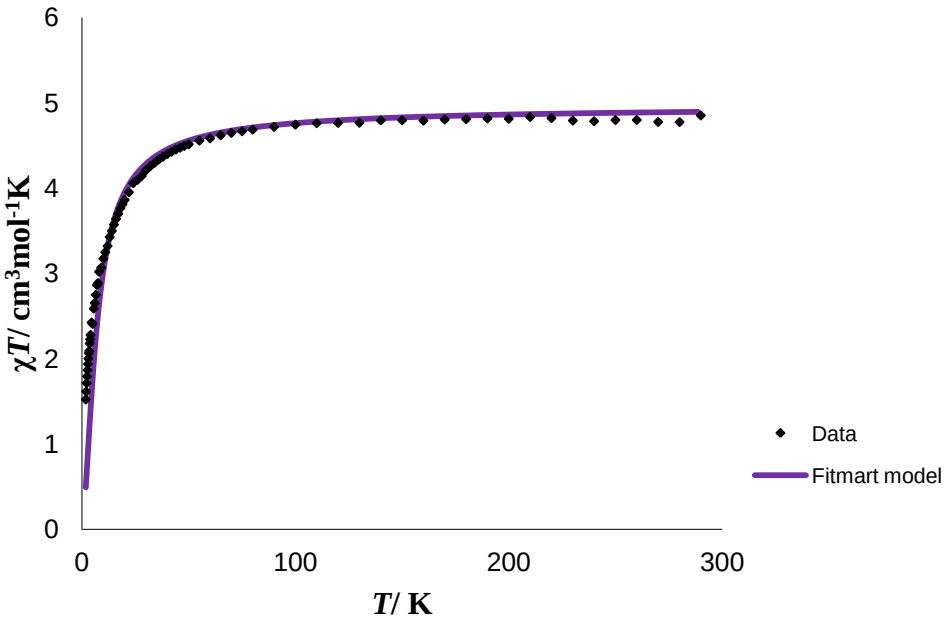

Figure 3-17 Temperature dependence of χT for 11 from 1.8 – 290K measured in an applied field of 1000 G.

Magnetic susceptibility measurements were carried out on an oven dried sample of **11**. Due to the low yield, no microanalysis could be carried out. After oven drying it is suggested no solvent remains in the lattice. The χT value at 290 K is 4.85 $cm^3\ mol^{-1}\ K$ (Figure 3-17), which is consistent with two uncoupled Co^{II} ions with g = 2.3. χT gradually decreases down to approximately 36 K then decreases more rapidly to 1.52 $cm^3\ mol^{-1}\ K$ at 1.8 K. The field dependence of the magnetisation of the cluster was measured (Figure 3-18) at both 2 K and 5 K, the magnetisation does not reach saturation at 5 T, at 2 K it reaches a value of 3.90 and at 5 K it reaches a value of 3.33. This suggests there is field-induced population of excited states with $S > 0$, however there is also the possibility of ZFS at low temperature which makes analysis of the data complicated.

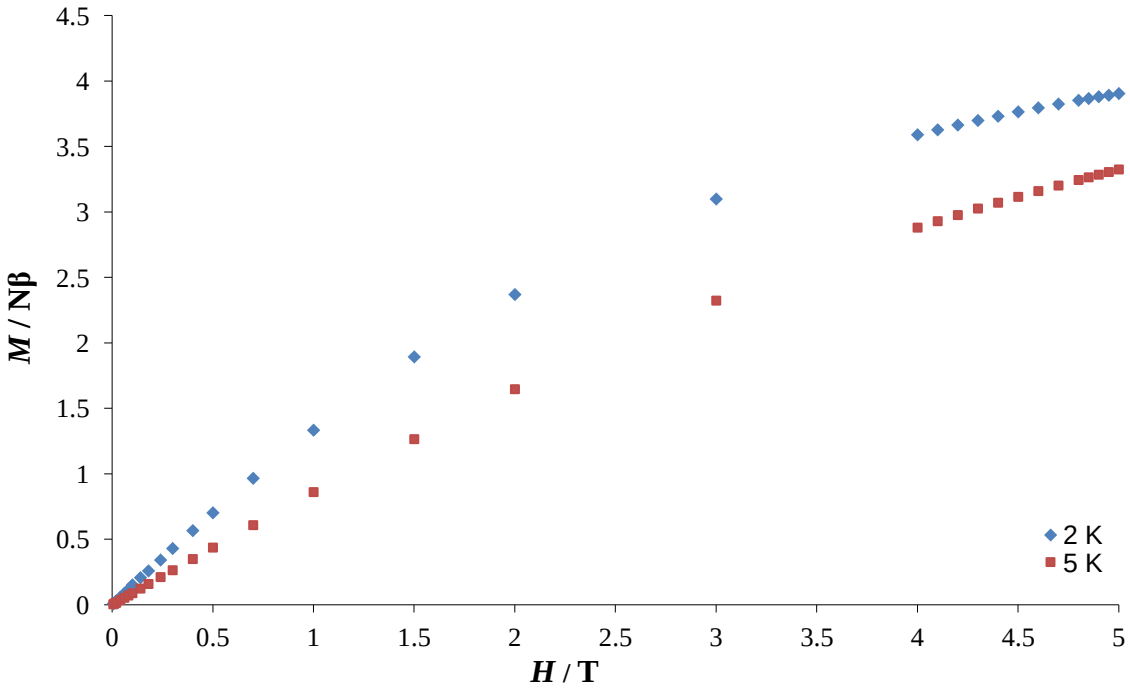

Figure 3-18 *M vs. H* for 11 measured at 2 K and 5 K.

Fitting of the χT *vs.* T data was undertaken using FitMart,[54] with the best fit parameters found to be g = 2.3 and J = 2.25 cm^{-1} (Figure 3-17), a positive J value is indicative of antiferromagnetic coupling in this program, which uses the Hamiltonian below.

$$\hat{\mathbf{H}} = \boldsymbol{J_1} \cdot \widehat{\boldsymbol{s_1}} \cdot \widehat{\boldsymbol{s_2}} - \boldsymbol{g\mu_\beta H} \cdot (\widehat{\boldsymbol{s_{1_z}}} + \widehat{\boldsymbol{s_{2_z}}}) \qquad (3\text{-}2)$$

However, using these parameters did not give a good match for the magnetisation *vs.* field data, possibly due to zero-field splitting and/or the presence of a paramagnetic impurity. The above Hamiltonian (3-2) is specific to FitMart, and using the previously given spin Hamiltonian (1-10) gives J = -1.12 cm^{-1}.

3.4 Conclusions

Four new cobalt complexes have been synthesised. Two of these are dimer complexes, one with two divalent cobalt ions which exhibits ferromagnetic coupling between the two ions and one mixed valent $Co^{II}Co^{III}$ dimer. One complex with three cobalt centres, with the acetate ligand being formed *in situ*. An interesting tetramer complex with a novel arrangement of two tetrahedral Co^{II} ions and two Co^{III} ions was also synthesised.

Complexes **8** $[Co^{II}_2Br_2(teaH_3)_2]Br_2$ and **11** $[Co^{II}_2Co^{III}_2Br_4(tea)_2(H_2O)_2]$ are clearly related, they can both be formed under the same reaction conditions, over the same timescale. The method described in Section 3.3 was preferred for the synthesis of **11** because although the yield was very low, there were only two types of crystal to separate rather than three. The dimer complex **8** was easier to collect, as the pink crystals were larger and it was the major product. Several alterations to the synthesis were attempted in order to synthesise either product cleanly, such as changing the reaction concentration, solvent, reaction time, and crystallisation method. However, none of these proved successful and reducing the reaction concentration resulted in monomer forming.

Complex **8** is a new addition to the small family of Br bridged Co dimers and complex **11** is one of only a few examples of Co tetramer complex with Br ligands. As the triethanolamine ligand remains fully protonated in **8** there is potential to extend the complex with further deprotonation, this complex could be used as a new starting material if the synthesis could be improved.

Future work would be to optimise the conditions for the synthesis of complexes **11** and **8**, and also to synthesise the Cl analogues for comparison. In particular the impact on the bridging angles for **8** and measurement of the subsequent effect on the magnetism of this complex.

3.5 References

(1) Banerjee, I.; Jana, A.; Singh, S.; Marek, J.; del Barco, E.; Ali, M. *Polyhedron* **2013**, *66*, 162.

(2) Boča, R.; Miklovič, J.; Titiš, J. *Inorganic Chemistry* **2014**, *53*, 2367.

(3) Nguyen, T. N.; Abboud, K. A.; Christou, G. *Polyhedron* **2013**, *66*, 171.

(4) Biswas, R.; Ida, Y.; Baker, M. L.; Biswas, S.; Kar, P.; Nojiri, H.; Ishida, T.; Ghosh, A. *Chemistry – A European Journal* **2013**, *19*, 3943.

(5) Waldmann, O. *Inorganic Chemistry* **2007**, *46*, 10035.

(6) Ruiz, E.; Cirera, J.; Cano, J.; Alvarez, S.; Loose, C.; Kortus, J. *Chemical Communications* **2008**, 52.

(7) Milios, C. J.; Inglis, R.; Jones, L. F.; Prescimone, A.; Parsons, S.; Wernsdorfer, W.; Brechin, E. K. *Dalton Transactions* **2009**, 2812.

(8) Sreerama, S. G.; Pal, S. *Inorganic Chemistry* **2002**, *41*, 4843.

(9) Stamatatos, T. C.; Foguet-Albiol, D.; Stoumpos, C. C.; Raptopoulou, C. P.; Terzis, A.; Wernsdorfer, W.; Perlepes, S. P.; Christou, G. *Journal of the American Chemical Society* **2005**, *127*, 15380.

(10) Inglis, R.; Taylor, S. M.; Jones, L. F.; Papaefstathiou, G. S.; Perlepes, S. P.; Datta, S.; Hill, S.; Wernsdorfer, W.; Brechin, E. K. *Dalton Transactions* **2009**, 9157.

(11) Yang, E.-C.; Hendrickson, D. N.; Wernsdorfer, W.; Nakano, M.; Zakharov, L. N.; Sommer, R. D.; Rheingold, A. L.; Ledezma-Gairaud, M.; Christou, G. *Journal of Applied Physics* **2002**, *91*, 7382.

(12) Liu, J.; Datta, S.; Bolin, E.; Lawrence, J.; Beedle, C. C.; Yang, E.-C.; Goy, P.; Hendrickson, D. N.; Hill, S. *Polyhedron* **2009**, *28*, 1922.

(13) Galloway, K. W.; Whyte, A. M.; Wernsdorfer, W.; Sanchez-Benitez, J.; Kamenev, K. V.; Parkin, A.; Peacock, R. D.; Murrie, M. *Inorganic Chemistry* **2008**, *47*, 7438.

(14) Moubaraki, B.; Murray, K. S.; Hudson, T. A.; Robson, R. *European Journal of Inorganic Chemistry* **2008**, *29*, 4525.

(15) Murrie, M.; Biner, D.; Stoeckli-Evans, H.; Güdel, H. U. *Chemical Communications* **2003**, 230.

(16) Wu, D.; Guo, D.; Song, Y.; Huang, W.; Duan, C.; Meng, Q.; Sato, O. *Inorganic Chemistry* **2009**, *48*, 854.

(17) Wang, C.-F.; Dai, G.-L.; Jin, Z.-N. *Inorganica Chimica Acta*, *394*, 255.

(18) Matsubara, K.; Sueyasu, T.; Esaki, M.; Kumamoto, A.; Nagao, S.; Yamamoto, H.; Koga, Y.; Kawata, S.; Matsumoto, T. *European Journal of Inorganic Chemistry* **2012**, *18*, 3079.

(19) Di Vaira, M.; Mani, F. *Inorganica Chimica Acta* **1983**, *70*, 99.

(20) Moatazedi, Z.; Katz, M. J.; Leznoff, D. B. *Dalton Transactions* **2010**, *39*, 9889.

(21) Laine, T. V.; Klinga, M.; Leskelä, M. *European Journal of Inorganic Chemistry* **1999**, *6*, 959.

(22) Al-Juaid, S. S.; Eaborn, C.; El-Hamruni, S. M.; Hitchcock, P. B.; Smith, J. D.; Sözerli Can, S. E. *Journal of Organometallic Chemistry* **2002**, *649*, 121.

(23) Brewer, B.; Brooks, N.; Abdul-Halim, S.; Sykes, A. *Journal of Chemical Crystallography* **2003**, *33*, 651.

(24) Yilmaz, V. T.; Hamamci, S.; Thöne, C. *Polyhedron* **2004**, *23*, 841.

(25) Crochet, A.; Fromm, Katharina M. *Zeitschrift für anorganische und allgemeine Chemie* **2010**, *636*, 1484.

(26) Zhu, L.-L.; Sun, Y.; Zhang, H.-H.; Wang, Y.; Sun, B.-W. *Acta Crystallographica Section E* **2009**, *65*, m991.

(27) Xiao, L.; Jie, S.; Song, Y.; Cao, X.; Sun, W.-H. *Journal of Organometallic Chemistry* **2008**, *693*, 3858.

(28) Brese, N. E.; O'Keeffe, M. *Acta Crystallographica Section B* **1991**, *47*, 192.

(29) Aromi, G.; Stoeckli-Evans, H.; Teat, S. J.; Cano, J.; Ribas, J. *Journal of Materials Chemistry* **2006**, *16*, 2635.

(30) Boudalis, A. K.; Raptopoulou, C. P.; Psycharis, V.; Abarca, B.; Ballesteros, R. *European Journal of Inorganic Chemistry* **2008**, *24*, 3796.

(31) Clemente-Juan, J. M.; Coronado, E.; Forment-Aliaga, A.; Galán-Mascarós, J. R.; Giménez-Saiz, C.; Gómez-García, C. J. *Inorganic Chemistry* **2004**, *43*, 2689.

(32) King, P.; Clerac, R.; Wernsdorfer, W.; Anson, C. E.; Powell, A. K. *Dalton Transactions* **2004**, 2670.

(33) Cotton, F. A.; Eiss, R. *Journal of the American Chemical Society* **1968**, *90*, 38.

(34) Bertrand, J. A.; Kelley, J. A.; Vassian, E. G. *Journal of the American Chemical Society* **1969**, *91*, 2394.

(35) Assey, G. E.; Butcher, R. J.; Gultneh, Y. *Acta Crystallographica Section E* **2011**, *67*, m303.

(36) Shin, J. W.; Rowthu, S. R.; Hyun, M. Y.; Song, Y. J.; Kim, C.; Kim, B. G.; Min, K. S. *Dalton Transactions* **2011**, *40*, 5762.

(37) Rao, C. N. R.; Natarajan, S.; Vaidhyanathan, R. *Angewandte Chemie International Edition* **2004**, *43*, 1466.

(38) Vasvari, G.; Hajdu, I. P.; Gal, D. *Journal of the Chemical Society, Dalton Transactions* **1974**, 465.

(39) Makhankova, V. G.; Vassilyeva, O. Y.; Kokozay, V. N.; Skelton, B. W.; Reedijk, J.; Van Albada, G. A.; Sorace, L.; Gatteschi, D. *New Journal of Chemistry* **2001**, *25*, 685.

(40) Golobič, A.; Štefane, B.; Polanc, S. *Polyhedron* **1999**, *18*, 3661.

(41) Chattopadhyay, S.; Drew, M. G. B.; Ghosh, A. *European Journal of Inorganic Chemistry* **2008**, *10*, 1693.

(42) Chattopadhyay, S.; Bocelli, G.; Musatti, A.; Ghosh, A. *Inorganic Chemistry Communications* **2006**, *9*, 1053.

(43) Babushkin, D. E.; Talsi, E. P. *Journal of Molecular Catalysis A: Chemical* **1998**, *130*, 131.

(44) Wu, D.; Zhang, X.; Huang, P.; Huang, W.; Ruan, M.; Ouyang, Z. W. *Inorganic Chemistry* **2013**, *52*, 10976.

(45) Yao, M.-X.; Zeng, M.-H.; Zou, H.-H.; Zhou, Y.-L.; Liang, H. *Dalton Transactions* **2008**, 2428.

(46) CSD search 2013 September.

(47) Sobota, P.; Olejnik, Z.; Utko, J.; Lis, T. *Polyhedron* **1993**, *12*, 613.

(48) Bertrand, J. A.; Fujita, E.; VanDerveer, D. G. *Inorganic Chemistry* **1979**, *18*, 230.

(49) Werndrup, P.; Kessler, V. G. *Journal of the Chemical Society, Dalton Transactions* **2001**, 574.

(50) Wang, F.-M.; Lu, C.-S.; Li, Y.-Z.; Meng, Q.-J. *Acta Crystallographica Section E* **2010**, *66*, m594.

(51) Riese, U.; Harms, K.; Neumüller, B.; Dehnicke, K. *Zeitschrift für anorganische und allgemeine Chemie* **1998**, *624*, 1279.

(52) Brown, S. J.; Olmstead, M. M.; Mascharak, P. K. *Inorganic Chemistry* **1989**, *28*, 3720.

(53) Brown, S. J.; Stephan, D. W.; Mascharak, P. K. *Journal of the American Chemical Society* **1988**, *110*, 1996.

(54) Engelhardt, L.; Garland, C.; Rainey, C.; Freeman, A.; FitMArt - Fully Integrated Tool for Magnetic Analysis in Research & Teaching: **2014**.

4. Heptanuclear discs

4.1 Introduction

The planar heptanuclear disc complex is the most studied structural motif for Co^{II}-based SMMs, the discs consist of a central cobalt ion surrounded by a ring of six cobalt ions, the oxidation states of the metals present in the different structures varies and includes $[Co^{II}_7]$,[1-3] $[Co^{III}Co^{II}_6]$,[4,5] $[Co^{II}_3Co^{III}_4]$[6] and $[Co^{II}_4Co^{III}_3]$,[7-9] some discs have an overall charge and some are neutral, some exhibit SMM behaviour and others do not. Whether or not a disc displays SMM behaviour and to what extent is very dependent on the structure, symmetry and overall composition. Different synthetic methods have been employed to synthesise Co_7 discs, including solvothermal and microwave syntheses, although most commonly the discs are the product of room temperature reactions.

4.1.1 Co^{II}_7 discs

One example of the Co_7 discs to display slow relaxation of magnetisation is $[Co^{II}_7(bzp)_6(N_3)_9(CH_3O)_3][ClO_4]_2$ (bzp = 2-benzoyl pyridine)[1] (Figure 4-1) which crystallises in the monoclinic C_2/c space group. Here all cobalt centres are in the +2 oxidation state with distorted octahedral geometry. The central cobalt ion is bridged to two outer cobalt ions by μ_3-azide groups, the remaining bridging sites are filled by disordered azide/hydroxide groups. A similar azide bridged complex has also been reported $[Co^{II}_7(hdeo)_6(N_3)_6][ClO_4]_2$ (hdeo = 2-hydroxy-[1,2-di(pyridine-2-yl)]ethane-1-one),[2] in this case the complex crystallises in the space group *P*-1, the outer cobalt ions have an $\{O_2N_4\}$ ligand environment and the central cobalt ion has an $\{N_6\}$ environment. In both these examples the magnetic data are consistent with ferromagnetic coupling between the $S' = ½$ Co^{II} centres leading to an $S' = 7/2$ ground state and evidence of slow relaxation below 4 K suggests that both these complexes display SMM behaviour.[1,2]

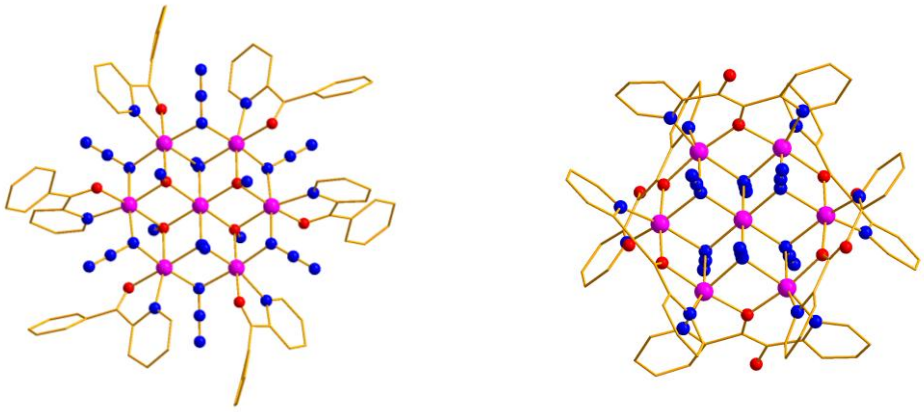

Figure 4-1 Diagram of azide bridged Co^{II}_7 discs $[Co^{II}_7(bzp)_6(N_3)_9(CH_3O)_3]^{2+}$(left) and $[Co^{II}_7(hdeo)_6(N_3)_6]^{2+}$ (right). Co^{II} pink; N blue; O red; H omitted for clarity.

Another example in which all the cobalt ions are in the +2 oxidation state is $[Co^{II}_7(immp)_6(CH_3O)_6][ClO_4]_2$ (immp = 2-iminomethyl-6-methoxy-phenolic-anion) (Figure 4-2),[3] which has higher symmetry than the previous two examples and crystallises in the *P*-3 trigonal space group. However, in this example the cobalt ions are methoxy-bridged, the six outer Co^{II} are bridged by μ-phenoxo groups, and the central cobalt ion has an $\{O_6\}$ ligand donor set in a distorted octahedral geometry. Magnetic data for this complex suggests that there are ferromagnetic interactions between the seven cobalt ions, however there are no out-of-phase ac signals above 2 K, suggesting this complex does not act as an SMM however further measurements would need to be carried out below 2 K.[3]

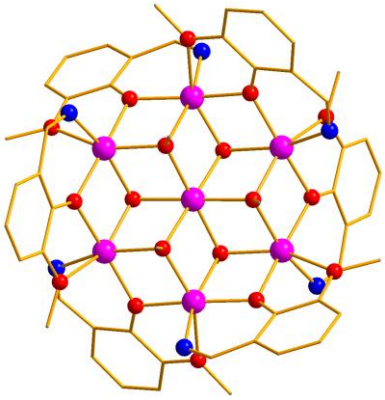

Figure 4-2 Structure of $[Co^{II}_7(immp)_6(CH_3O)_6]^{2+}$. Co^{II} pink; N blue; O red; H omitted for clarity.

When considering mixed-valent heptanuclear cobalt discs there are three variations, $[Co^{II}_4Co^{III}_3]$ which is the most common, $[Co^{II}_6Co^{III}]$ and $[Co^{II}_3Co^{III}_4]$ which is the least common.[10,11]

4.1.2 $Co^{II}_4Co^{III}_3$ discs

Two examples of this kind are $[Co^{II}_4Co^{III}_3(Htris)_6(NO_3)_3(H_2O)_3][NO_3]_2$ (Figure 4-3) (H_3tris = 2-amino-2-(hydroxymethyl)propane-1,3-diol, tris)[8] which does display SMM behaviour, and $[Co^{II}_4Co^{III}_3(dea)_6(CH_3COO)_3][ClO_4]_{0.75}[CH_3COO]_{1.25}$ (H_2dea = diethanolamine)[9] (Figure 4-3) which shows evidence of ferromagnetic interactions between the four Co^{II} ions. However, the second example does not display an out-of-phase ac signal above 2 K (further low temperature measurements would be required to investigate the possibility of the complex acting as an SMM below 2 K). Both of these complexes have high axial symmetry, the first crystallises in the trigonal space group *P*-3 with C_3 symmetry and the second in the cubic space group *I*-43*d* with the disc having C_3 symmetry. The ligand environments of the different cobalt ions are the same, Co^{II} $\{O_6\}$ and Co^{III} $\{N_2O_4\}$. In the first Co_7 complex all Co^{II} ions have distorted octahedral geometry [8] and in the second complex the central Co^{II} ion has octahedral geometry and the outer Co^{II} ions have distorted octahedral geometry.[9] The bridging angles between Co^{II} ions in the two complexes are slightly different (the bridging angles Co^{II}–O–Co^{II} in the tris complex are ~93° compared with ~95°

and ~96° in the complex with dea). This suggests that small changes in bridging angle and coordination geometry play an important role in whether or not a complex is an SMM.

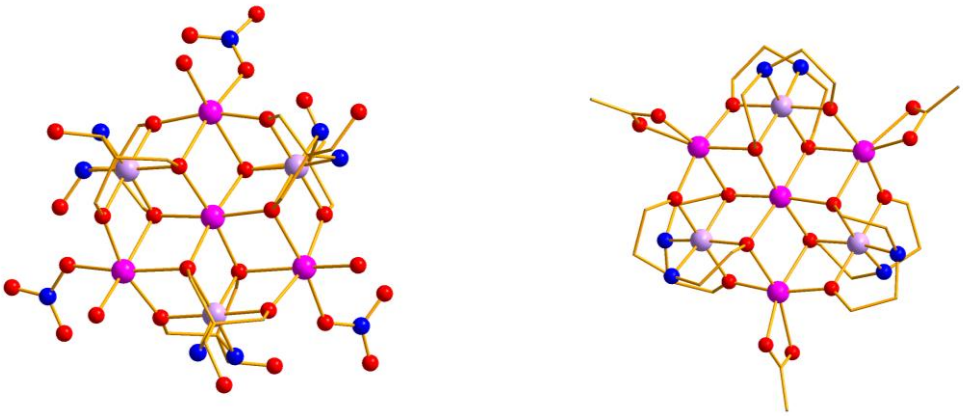

Figure 4-3 Structure of $[Co^{II}_4Co^{III}_3(Htris)_6(NO_3)_3(H_2O)_3]^{2+}$ (left) and $[Co^{II}_4Co^{III}_3(dea)_6(CH_3COO)_3]^{2+}$(right). Co^{II} pink; Co^{III} lilac; N blue; O red; H omitted for clarity.

4.1.3 $Co^{II}_6Co^{III}$discs

These examples consist of a central Co^{III} ion surrounded by six Co^{II} ions. In $[Co^{II}_6Co^{III}(OH^-)_6(L)_6]^{3+}$ (L = 2-(pyridine-2-yl)pentane-2-ol-4-one)[4] (Figure 4-4) which crystallises in the triclinic space group *P*-1 (Figure 4-4). The central ion is linked to the outer cobalt ions by six μ_3-bridging OH groups, which are arranged in a distorted octahedral arrangement about the central cobalt. The Co^{II} ions have an $\{NO_5\}$ ligand donor set, also in a distorted octahedral arrangement. The measured χT value at low temperature is consistent with six effective spin S'=1/2 states, with ferromagnetic interactions and g_{eff} = 4.34. Out-of-phase ac susceptibility signals were observed for this complex below ~4 K and SMM behaviour was confirmed by very low temperature measurements (below 1.8 K) where hysteresis was seen.[4] The bridging angles Co^{II}-O-Co^{II} in the complex range from 93°-104°.[4]

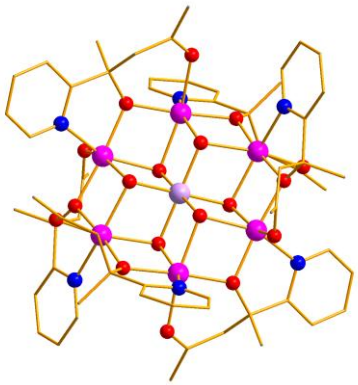

Figure 4-4 Structure of $[Co^{II}_6Co^{III}(OH)_6(L)_6]^{3+}$ Co^{II} pink; Co^{III} lilac; O red; N blue; H omitted for clarity.

Two further examples are $(N^nBu_4)[Co^{II}_6Co^{III}(thme)_2(OCCMe_3)_8Br_2]$, which crystallises in the $P2_1/n$ space group with two crystallographically distinct molecules in the asymmetric unit, and $Na_2[Co^{II}_6Co^{III}(thme)_2(O_2CMe)_{10}(OH_2)_4]^+$ (H_3thme = 1,1,1-tris(hydroxymethyl)ethane),[5] which crystallises in the $C2/c$ space group. These show ferromagnetic coupling between the Co^{II} ions but no hysteresis was observed even at very low temperatures, and no out-of-phase ac susceptibility signals were seen in measurements between 10 and 1.8 K.[5] The bridging angles in this complex fall in the range Co^{II}–X–Co^{II} (where X = Br or O) 88°-99°.[5]

4.1.4 $Co^{II}_3Co^{III}_4$ discs

This is the least common combination of oxidation states in mixed valent heptanuclear discs, with only one example listed in the CSD.[11] $[Co^{II}_3Co^{III}_4(L_6)(MeO)_6]$ (LH_2 = 1,1,1-trifluoro-7-hydroxy-4-methyl-5-aza-hept-3-en-2-one) (Figure 4-5).[6] This complex crystallises in the $P2_1/n$ space group, the central cobalt ion has an $\{O_6\}$ coordination sphere and the six outer cobalt ions have identical$\{NO_5\}$ environments. This complex is not an SMM even though there is ferromagnetic exchange interaction between the Co^{II} centres, the Co^{II}–O–Co^{II} bridging angles in this complex are ~95° and ~97°.[6] In the study of this complex, it was discovered to have a large tunnelling parameter,[6] several orders of magnitude larger than the tunnelling parameter for typical SMMs (Mn_{12} and Fe_8).[12] This is taken as the reason why slow relaxation of magnetisation is not observed for this compound.[6]

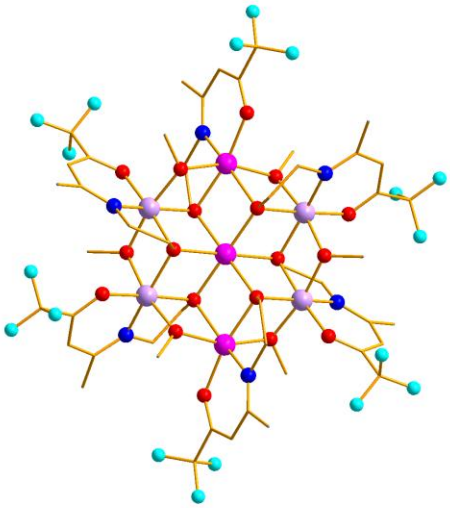

Figure 4-5 Structure of $[Co^{II}_3Co^{III}_4(L_6)(MeO)_6]$ Co^{II} pink; Co^{III} lilac; O red; N blue; F light blue; H omitted for clarity.

Complex	**Charge on disc**	**Space group**	**Symmetry**	**μ_3-X bridge**	**Co–(μ_3-X)–Co (°)**	**Co–(μ_2-Ψ)–Co (°)***	**Magnetic Behaviour** (measurement)
$[Co^{II}_7(bzp)_6(N_3)_9(CH_3O)_3][ClO_4]_2$ [1]	2+	*C2/c*	S_2	MeO-/N_3-	93.2-95.3	99.1	F/ tending towards SMM behaviour (microSQUID)
$[Co^{II}_7(hdeo)_6(N_3)_6][ClO_4]_2$ [2]	2+	*P*-1	S_2	N_3-	96.2-98.6	107.5	F/ tending towards SMM behaviour (1.9 K)
$[Co^{II}_7(immp)_6(CH_3O)_6][ClO_4]_2$ [3]	2+	*P*-3	S_6	MeO-	95.4-99.0	102.9	F (2 K)
$[Co^{II}_4Co^{III}_3(Htris)_6(NO_3)_3(H_2O)_3][NO_3]_2$ [8]	2+	*P*-3	C_3	RO-	95.3-97.7	105.2	F/SMM (microSQUID)
$[Co^{II}_4Co^{III}_3(dea)_6(CH_3COO)_3][ClO_4]_{0.75}$ $[CH_3COO]_{1.25}$ [9]	2+	*I*-43*d*	C_3	RO-	94.4-97.9	106.8	F (2 K)
$[Co^{II}_6Co^{III}(OH)_6(L_2)_6][ClO_4]_3$ [4]	3+	*P*-1	S_2	OH-	93.8-101.1	104	F/SMM (microSQUID)
$TBA[Co^{II}_6Co^{III}(thme)_2(OCCMe_3)_8Br_2]$ [5]	-1	$P2_1/n$	C_2	RO-	95.2-101.2	85.1	F (microSQUID)
$Na_2[Co^{II}_6Co^{III}(thme)_2(O_2CMe)_{10}(OH_2)_4]$ [5]	-2	*C2/c*	C_2	RO-	84.5-95.5	92.2	F (2 K)
$[Co^{II}_3Co^{III}_4(L36)(MeO)6]$ [6]	0	$P2_1/n$	S_6	RO-	89.4-101.5	103.9	F (microSQUID)

* - average value; R- polydentate organic ligand; Ψ- most often a donor atom coming from the polydentate ligand; H_3tris= 2-amino-2-(hydroxymethyl)propane-1,3-diol, tris; L^2 = 2-(pyridine-2-yl)pentane-2-ol-4-one; L^3H_2 = 1,1,1-trifluoro-7-hydroxy-4-methyl-5-aza-hept-3-en-2-one; bzp = 2-benzoyl pyridine; hdeo = 2-hydroxy-[1,2-di(pyridine-2-yl)]ethane-1-one; immp = 2-iminomethyl-6-methoxy-phenolic-anion; H_2dea = diethanolamine; H_3thme = 1,1,1-tris(hydroxymethyl)ethane; F- ferromagnetic; SMM-single molecule magnet, hysteresis has been shown; tending towards SMM- slow relaxation has been observed but no hysteresis.

Table 4-1 Summary table of Co_7 discs (adapted from reference 4)

4.2 $Co^{II}_4Co^{III}_3$ Discs

4.2.1 Synthetic Methods

*4.2.1.1 Synthesis of $[Co^{II}_4Co^{III}_3(btpH_2)_3(NO_3)_5(EtOH)]\cdot 3(EtOH)$ (**12**·3EtOH)*

(where $btpH_6$ = bis-tris propane, $C_{11}H_{26}N_2O_6$)

$Co(NO_3)_2.6H_2O$ (1.16 g, 4.00 mmol) was dissolved in 10 mL of EtOH. Bis-tris propane (1.13 g, 4.00 mmol) was added followed by $NMe_4OH.5H_2O$ (0.30 g, 1.66 mmol). After stirring overnight the reaction mixture was filtered and stored in a sealed vial. Dark purple rods appeared after 3 weeks in 33% yield. Air dried crystals analyse as $\mathbf{C_{35}H_{86}N_{11}O_{41}Co_7}$, analysis (%) calc. (found) C, 24.38 (24.31); H, 4.73 (4.78); N, 8.93 (9.12). Selected IR data: υ = 3510, 3325, 3194, 2931, 2862, 1639, 1620, 1429, 1373, 1305, 1288, 1014, 692, 665, 601cm^{-1}.

*4.2.1.2 Synthesis of $[Co^{II}_4Co^{III}_3(dea)_6(NO_3)_3][NO_3]_2\cdot 4.5(MeOH)$ (**13**·4.5MeOH)*

(where $deaH_2$ = diethanolamine, $C_4H_{11}NO_2$)

$Co(NO_3)_2.6H_2O$ (1.16 g, 4.00 mmol) was dissolved in 10 mL of MeOH. Diethanolamine (0.21 g, 2.00 mmol) was added followed by NaOMe (0.11 g, 2.04 mmol). After stirring overnight the reaction mixture was filtered and stored in a sealed vial. Dark green square plate crystals appeared after 2 weeks in 26% yield. Air dried crystals analyse as $\mathbf{C_{24}H_{66}N_{11}O_{33}Co_7}$, analysis (%) calc. (found) C, 19.89 (19.57); H, 4.49 (4.29); N, 10.63 (10.43). Selected IR data: *ν* = 3376, 3217, 2866, 1635, 1465, 1383, 1307, 1278, 1109, 1062, 1037, 889, 694, 628 cm^{-1}.

*4.2.1.3 Synthesis of $[Co^{II}_4Co^{III}_3(N\text{-}mdea)_6(NO_3)_3][NO_3]_2$ (**14**)*

(where $N\text{-}mdeaH_2$ = N-methyldiethanolamine, $C_5H_{13}NO_2$)

$Co(NO_3)_2.6H_2O$ (0.29 g, 1.00 mmol) was dissolved in 10 mL of MeOH. N-Methyl-diethanolamine (0.12 mL, 1.05 mmol) was added and the reaction mixture stirred overnight. It was then filtered and stored in a sealed vial. Dark green plate crystals appeared after 3 weeks in 29% yield. Air dried crystals analyse as $\mathbf{C_{30}H_{74}N_{11}O_{31}Co_7}$, analysis (%) calc. (found) C, 24.06 (23.87); H, 4.98 (4.68); N, 10.29 (10.09). Selected IR data: *ν* = 3610, 3416, 2875, 1637, 1481, 1458, 1329, 1296, 1284, 1084, 1060, 1022, 908, 827, 806, 744, 669, 609 cm^{-1}.

4.2.2 Discussion of Crystal Structures

*4.2.2.1 Discussion of crystal structure of $[Co^{II}_4Co^{III}_3(btpH_2)_3(NO_3)_5(C_2H_5OH)]\cdot 3EtOH$ (**12**·3EtOH) (where $btpH_6$= bis-tris propane)*

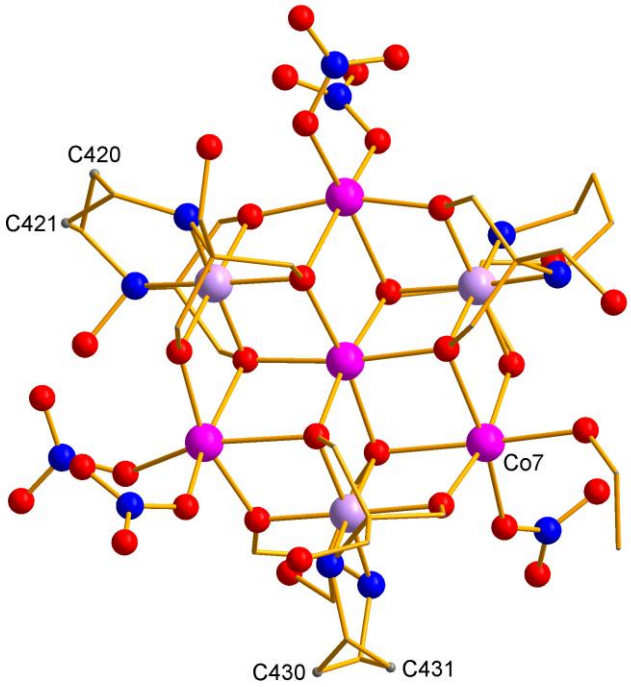

Figure 4-6 Structure of 12 (showing disordered C atoms, H-atoms and solvent have been omitted for clarity) Co^{II} pink; Co^{III} lilac; O red; N blue. The central carbon of the propane backbone is disordered in two of the three ligands, the disordered atoms are labelled as follows and the occupancy of the sites are given in brackets, C420(0.7):C421(0.3) and C430(0.6):C431(0.4).

The first structure described uses the ligand bis-tris propane (H_6btp), and is one of only a few examples of cobalt complexes with this ligand (Figure 4-6). Previously this ligand has formed a pentanuclear cluster with cobalt which has the form of a partial fragment of the common Co_7 disc motif.[13] Other than this complex there are currently no other published structures including cobalt and btp. However, other work being carried out within the group has resulted in chloride and bromide $\{Co^{II}_4Co^{III}_3\}$ complexes with btp as a ligand.[14] The chloride complex is similar to that above with five chloride ligands and a bound molecule of methanol, $[Co^{II}_4Co^{III}_3(btpH_2)_3Cl_5(MeOH)]$(Figure 4-7), and crystallises in the $P2_1/c$ space group. The bromide complex has been synthesised with six bound bromide ligands and the charge of the complex is balanced by an unbound tetramethylammonium ion, $[NMe_4][Co^{II}_4Co^{III}_3(btpH_2)_3Br_6]$ (Figure 4-7), this complex crystallises in the *R*-3*c* space group.

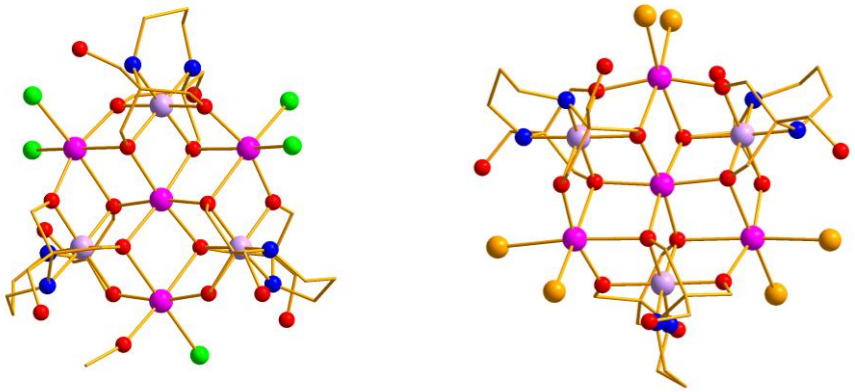

Figure 4-7 Chloride and bromide Co_7 complexes with bis-tris propane.[14] Co^{II} pink; Co^{III} lilac; O red; N blue; Cl bright green; Br light orange; H atoms omitted for clarity.

In the nitrate example (**12**, Figure 4-6) the distorted octahedral environment around each cobalt ion is analogous to that of the Co_7 with tris described earlier, in terms of number and type of atom.[8] However in this example, all the anions required for charge balance are bound directly to the complex. The complex crystallises in the monoclinic space group $P2_1/c$, it consists of three Co^{III} ions with distorted octahedral geometry with an $\{N_2O_4\}$ ligand donor set and four Co^{II} ions which have an $\{O_6\}$ environment arranged in a distorted octahedral geometry. For the central Co^{II} the ligand donor set is completed by six CH_2O^- arms from the three ligands, for two of the outer Co^{II} four of the oxygen atoms are from ligand arms and the remaining two positions are filled by two monodentate nitrate anions. The final Co^{II} ion (Co7) is bound to only one nitrate and the distorted octahedral geometry is completed by a bound molecule of ethanol.

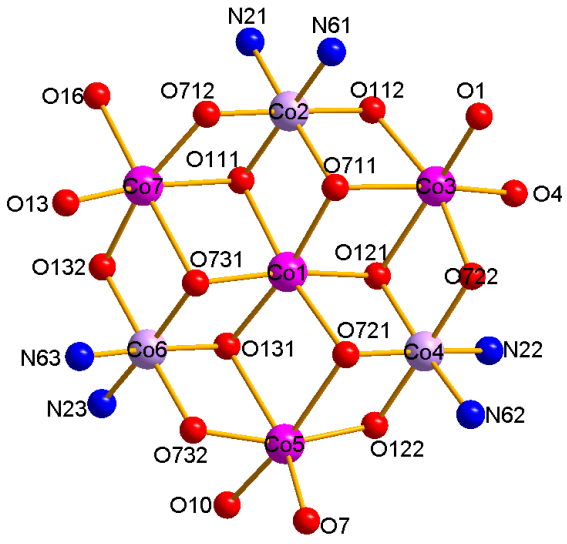

Figure 4-8 Labelled diagram of 12 showing environments of the metal centres (solvent, hydrogen and carbon atoms removed for clarity) Co^{II} pink; Co^{III} light purple; O red; N blue. N21 is the second atom in the first btp ligand.

From the packing diagrams below it can be seen that there are extensive interactions between clusters. Each cluster has short contact and hydrogen bond interactions with eight others, for each

ligand there are two unbound arms, these interact with either a bound nitrate anion on a neighbouring cluster or an unbound ligand arm, for example O723(H)···O733 2.715(4) Å and O123(H)···O2 2.829(5) Å. From the single crystal X-ray data collected at 100 K there are three unbound molecules of ethanol associated with each cluster; these have hydrogen bonding interactions with clusters of ~2.7 Å. The closest $Co^{II}\cdots Co^{II}$ distance is 7.957(1) Å between Co3 and Co3′ on neighbouring clusters and the closest $Co^{II}\cdots Co^{III}$ distance is 7.794(1) Å between Co2 and Co5″ (Figure 4-9).

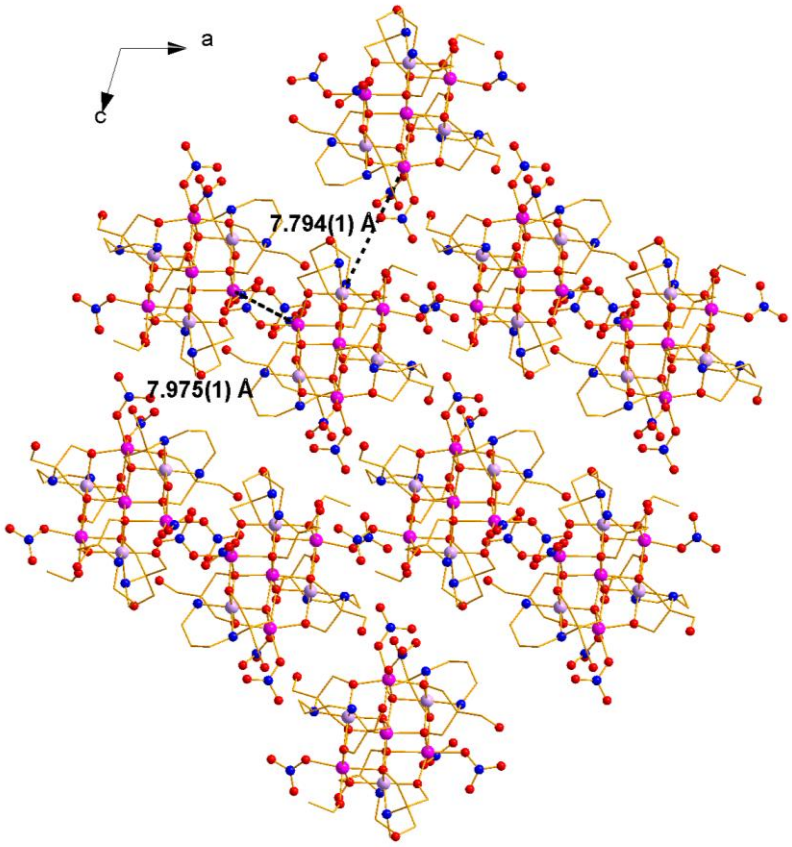

Figure 4-9 Packing diagram of 12 viewed along *b*-axis, showing closest Co···Co′ distances.

Table 4-2 Data for crystal structure determination of 12·3EtOH

Empirical Formula	$C_{41}H_{90}Co_7N_{11}O_{37}$
Fw (g mol^{-1})	1741.75
Crystal system	Monoclinic
Space group	*P2$_1$/c*
a (Å)	18.123(2)
b (Å)	13.752(2)
c (Å)	26.469(3)
β (deg)	106.262(4)
V (Å^3)	6332.9(13)
Z	4
T (K)	100(2)
λ (Å)	0.71073
ρ_{calcd} (Mg m^{-3})	1.825
μ (mm^{-1})	1.896
R_1[a]	0.0578
wR_2[b]	0.1072
Goodness of fit	0.982

[a] $R_1 = \Sigma \left| |F_o| - |F_c| \right| / \Sigma |F_o|$ [b] $wR_2 = \left[\Sigma \left[w\left(F_o^2 - F_c^2\right)^2 \right] - \Sigma \left[\left(F_o^2\right)^2 \right] \right]^{1/2}$ where $w = 1/\left[\sigma^2\left(F_o^2\right) + \left(0.2P\right)^2\right]$ and $P = \left[F_o^2 + 2F_c^2\right]/3$

Table 4-3 Selected metal-ligand bond lengths for 12.

Bond	Distance (Å)	Bond	Distance (Å)	Bond	Distance (Å)
Co1–O111	2.106(2)	Co3–O121	2.272(2)	Co5–O7	2.112(2)
Co1–O711	2.137(2)	Co3–O722	1.965(2)	Co5–O10	2.077(3)
Co1–O121	2.106(2)	Co3–O1	2.084(3)	Co6–O131	1.902(2)
Co1–O721	2.096(2)	Co3–O4	2.086(3)	Co6–O132	1.897(2)
Co1–O131	2.099(2)	Co4–O121	1.917(2)	Co6–N23	1.929(3)
Co1–O731	2.116(2)	Co4–O122	1.883(2)	Co6–N63	1.937(3)
Co2–O111	1.905(2)	Co4–N22	1.931(3)	Co6–O731	1.914(2)
Co2–O112	1.880(2)	Co4–N62	1.932(3)	Co6–O732	1.874(2)
Co2–N21	1.951(3)	Co4–O721	1.908(2)	Co7–O111	2.229(2)
Co2–N61	1.931(3)	Co4–O722	1.882(2)	Co7–O712	1.996(2)
Co2–O711	1.903(2)	Co5–O122	1.978(3)	Co7–O132	1.998(2)
Co2–O712	1.889(2)	Co5–O721	2.304(2)	Co7–O731	2.217(2)
Co3–O112	1.972(3)	Co5–O131	2.307(2)	Co7–O13	2.102(3)
Co3–O711	2.296(2)	Co5–O732	1.994(3)	Co7–O16	2.103(2)

Table 4-4 Selected bond angles for 12.

Atoms	Angle (°)	Atoms	Angle (°)
Co1-O111-Co2	96.60(1)	Co2-O111-Co7	94.94(1)
Co1-O111-Co7	93.16(9)	Co2-O112-Co3	106.80(1)
Co1-O121-Co3	93.77(9)	Co2-O711-Co3	94.42(9)
Co1-O121-Co4	94.64(1)	Co2-O712-Co7	103.61(1)
Co1-O131-Co5	93.29(9)	Co3-O121-Co4	94.4(1)
Co1-O131-Co6	95.92(1)	Co3-O722-Co4	106.5(1)
Co1-O711-Co2	95.63(1)	Co4-O122-Co5	107.63(1)
Co1-O711-Co3	92.27(9)	Co4-O721-Co5	95.00(1)
Co1-O721-Co4	95.24(1)	Co5-O131-Co6	95.05(9)
Co1-O721-Co5	93.47(9)	Co5-O732-Co6	107.33(1)
Co1-O731-Co6	95.01(1)	Co6-O132-Co7	103.50(1)
Co1-O731-Co7	93.24(9)	Co6-O731-Co7	95.3(1)

Table 4-5 BVS[15] calculation results for Co atoms in 12.

Atom	Co^{II}	Co^{III}	Atom	Co^{II}	Co^{III}
Co1	<u>1.940</u>	1.982	Co5	<u>1.959</u>	2.002
Co2	3.839	<u>3.890</u>	Co6	3.857	<u>3.907</u>
Co3	<u>2.043</u>	2.087	Co7	<u>2.046</u>	2.09
Co4	3.859	<u>3.909</u>			

The underlined value is that closest to the charge for which it was calculated. Overestimation of Co^{III} values will be discussed in appendix one.

*4.2.2.2 Discussion of crystal structure of $[Co^{II}_4Co^{III}_3(dea)_6(NO_3)_3][NO_3]_2 \cdot 4.5MeOH$ (**13·4.**5MeOH) (where $deaH_2$ = diethanolamine)*

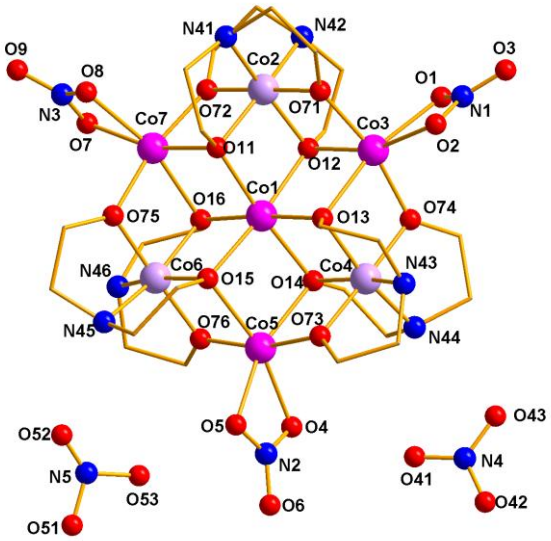

Figure 4-10 Structure of 13. Co^{II} pink; Co^{III} lilac; O red; N blue; H-atoms and solvent omitted for clarity.

In this example (Figure 4-10) the ligand is diethanolamine and there are 6 ligands per cluster, the complex crystallises in the monoclinic space group $P2_1/c$. The ligand environments for all the cobalt ions in this structure are identical to complex **12**, all Co^{II} have an $\{O_6\}$ ligand environment in a distorted octahedral geometry and all Co^{III} have a distorted octahedral geometry with an $\{N_2O_4\}$ ligand donor set. All the peripheral Co^{II} ions are bound to one bidentate nitrate anion as well as the ethanolic arms of the diethanolamine ligand. The cluster has a charge of 2+ which is balanced by the presence of two unbound nitrate anions in the lattice.

Both unbound nitrate anions have one hydrogen bond to the cluster through the amine group of the ligand (N45(H)···O 2.908(1) Å and N44(H)···O 3.268(1) Å) (Figure 4-11), these nitrate anions also have short contact interactions with the disordered solvent that is present. Interactions between clusters are between the bound nitrates on one cluster and the CH backbone of the ligand on another cluster. All the molecules of disordered solvent are grouped together in pockets between complexes, (Figure 4-12, *b*-axis view). The closest $Co^{II}\cdots Co^{II}$ distance between neighbouring clusters is 6.7971(1) Å between Co5 and Co5′.

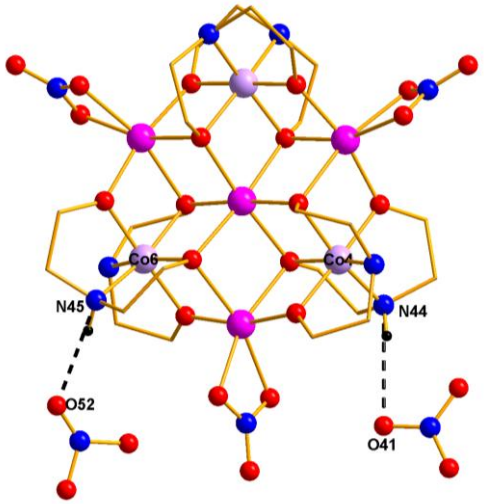

Figure 4-11 Diagram showing hydrogen bonds to nitrate groups for 13.

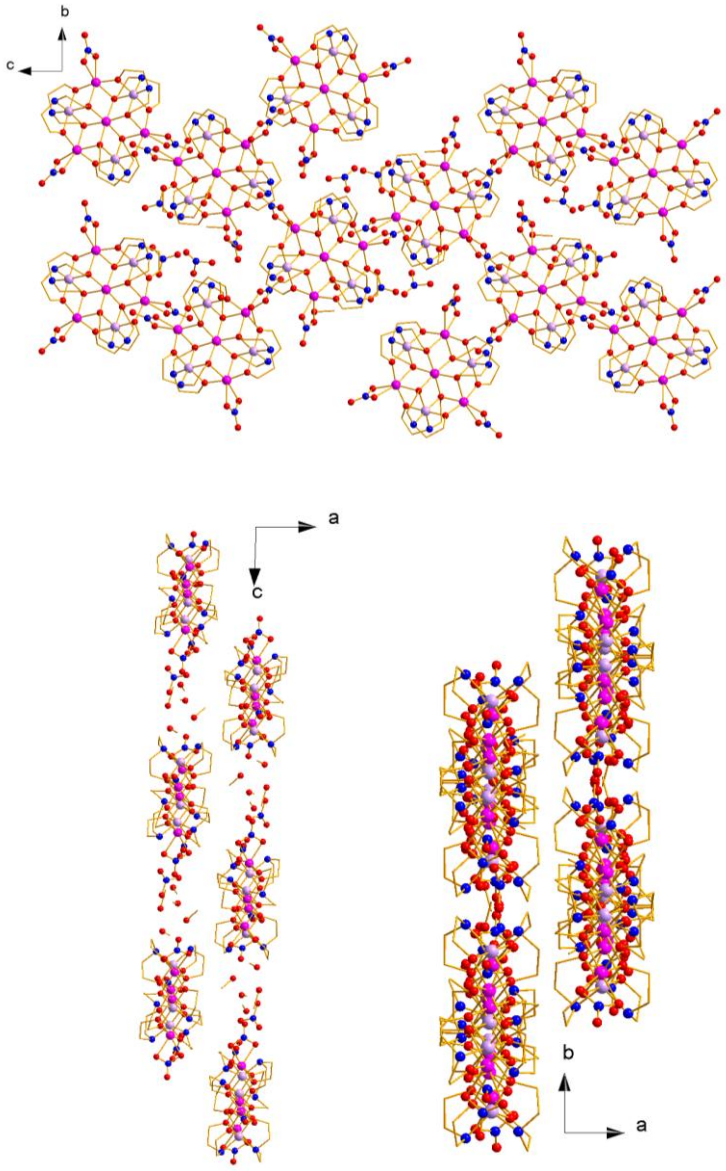

Figure 4-12 Packing diagrams of 13 viewed along *a*-, *b*- and *c*-axes

Diethanolamine complexes with cobalt are more common than those with btp, with around 20 examples listed in the CSD.[11,16] These examples include a simple monomer,[17] mixed metal complexes,[18,19] small polynuclear complexes,[20,21] and the Co_7 example described in the introduction,[9] which is the acetate analogue of complex **13**.

Table 4-6 Data for crystal structure determination of 13·4.5MeOH.

Empirical Formula	$C_{28.5}H_{72}Co_7N_{11}O_{31.5}$
Fw (g mol^{-1})	1485.46
Crystal system	Monoclinic
Space group	*P2$_1$/c*
a (Å)	11.8751(3)
b (Å)	13.0048(3)
c (Å)	33.9097(7)
β (deg)	92.1040(1)
V (Å^3)	5233.3(2)
Z	4
T (K)	100(2)
λ (Å)	0.71073
ρ_{calcd} (Mg m^{-3})	1.867
μ (mm^{-1})	2.268
R_1[a]	0.0444
wR_2[b]	0.0735
Goodness of fit	0.99

[a] $R_1 = \Sigma \left| |F_o| - |F_c| \right| / \Sigma |F_o|$ [b] $wR_2 = \left[\Sigma \left[w\left(F_o^2 - F_c^2\right)^2 \right] - \Sigma \left[\left(F_o^2\right)^2 \right] \right]^{1/2}$ where $w = 1/\left[\sigma^2\left(F_o^2\right) + \left(0.2P\right)^2\right]$ and $P = \left[F_o^2 + 2F_c^2\right]/3$

Table 4-7 Metal-ligand bond lengths for 13.

Bond	Distance (Å)	Bond	Distance (Å)	Bond	Distance (Å)
Co1–O11	2.081(2)	Co3– O13	2.162(2)	Co5–O4	2.149(2)
Co1–O12	2.109(2)	Co3– O74	1.978(2)	Co5–O5	2.149(3)
Co1– O13	2.091(2)	Co3– O1	2.143(2)	Co6–O15	1.925(2)
Co1–O14	2.086(2)	Co3– O2	2.150(2)	Co6–N45	1.951(3)
Co1–O15	2.106(2)	Co4–O13	1.916(2)	Co6–O75	1.885(2)
Co1–O16	2.098(2)	Co4– N43	1.946(3)	Co6–O16	1.928(2)
Co2–O11	1.922(2)	Co4– O73	1.870(2)	Co6–N46	1.954(3)
Co2–N41	1.952(3)	Co4–O14	1.920(2)	Co6–O76	1.885(2)
Co2–O71	1.882(2)	Co4–O44	1.947(3)	Co7– O11	2.156(2)
Co2–O12	1.925(2)	Co4–O74	1.886(2)	Co7–O72	1.974(2)
Co2–N42	1.947(3)	Co5–O73	1.988(2)	Co7–O75	1.970(2)
Co2—O72	1.890(2)	Co5–O14	2.165(2)	Co7– O16	2.182(2)
Co3– O71	1.978(2)	Co5–O15	2.179(2)	Co7– O7	2.172(2)
Co3–O12	2.168(2)	Co5– O76	1.981(2)	Co7–O8	2.162(2)

Table 4-8 Selected bond angles for 13.

Atoms	Angle (°)	Atoms	Angle (°)
Co1-O11-Co2	97.13(9)	Co2-O11-Co7	97.40(9)
Co1-O11-Co7	95.60(9)	Co2-O12-Co3	97.07(9)
Co1-O12-Co2	96.10(9)	Co2-O71-Co3	105.39(10)
Co1-O12-Co3	95.29(8)	Co2-O72-Co7	105.11(10)
Co1-O13-Co3	95.98(9)	Co3-O13-Co4	96.91(9)
Co1-O13-Co4	96.41(9)	Co3-O74-Co4	104.52(11)
Co1-O14-Co4	96.46(9)	Co4-O14-Co5	97.20(9)
Co1-O14-Co5	94.97(9)	Co4-O73-Co5	105.33(11)
Co1-O15-Co5	93.98(9)	Co5-O15-Co6	97.89(9)
Co1-O15-Co6	96.37(9)	Co5-O76-Co6	106.55(11)
Co1-O16-Co6	96.54(9)	Co6-O16-Co7	97.06(9)
Co1-O16-Co7	94.34(8)	Co6-O75-Co7	106.27(11)

Table 4-9 BVS calculations[15] for 13.

Atom	Co^{II}	Co^{III}	Atom	Co^{II}	Co^{III}
Co1	2.019	2.063	Co5	2.035	2.079
Co2	3.741	3.79	Co6	3.724	3.773
Co3	2.065	2.111	Co7	2.044	2.088
Co4	3.796	3.846			

The underlined value is that closest to the value for which it was calculated. Overestimations for Co^{III} will be discussed in appendix one.

*4.2.2.3 Discussion of the crystal structure of $[Co^{II}_4Co^{III}_3(N\text{-}mdea)_6(NO_3)_3][NO_3]_2$ (**14**)*

(where N-mdeaH$_2$ = N-methyldiethanolamine)

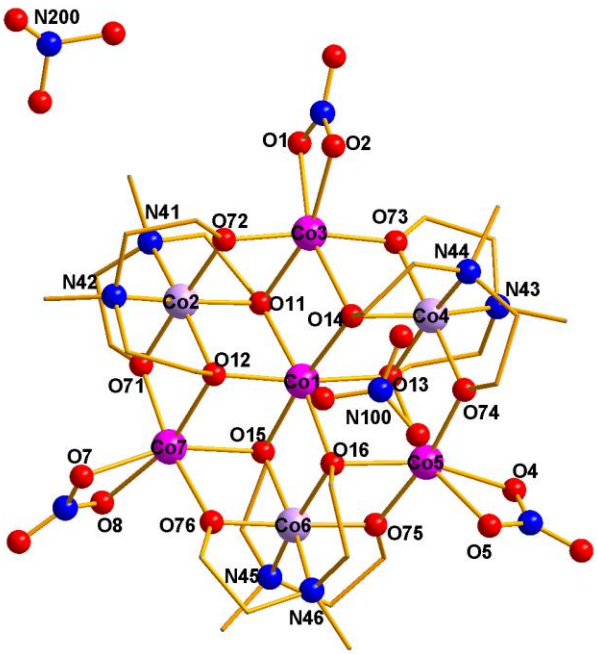

Figure 4-13 Structure of 14, nitrate with N200 is disordered over 2 sites. Co^{II} pink; Co^{III} lilac; O red; N blue; H atoms and solvent omitted for clarity.

This structure is analogous to complex **13**, however, in this example, **14**, the ligand is N-methyldiethanolamine, which is a relatively unused ligand in terms of cobalt coordination chemistry. All known cobalt- containing structures with this ligand are mixed metal complexes,[22,23] including hexanuclear $[Mn^{III}_2Mn^{II}_2Co^{II}_2(O_2CCHMe_2)_8(N\text{-}mdeaH)_2(N\text{-}mdea)_2]$ and $[Fe^{III}_2Co^{II}_4(O_2CCHMe_2)_8(N\text{-}mdeaH)_2(N\text{-}mdea)_2]$, these complexes were synthesised as part of an investigation altering the ligands of a parent complex.[22]

In **14** there are differences in the positions of the unbound anions, one unbound nitrate anion is disordered over two sites (Figure 4-14) and the interactions between clusters are different, this can be seen in the packing diagrams below (Figure 4-15).

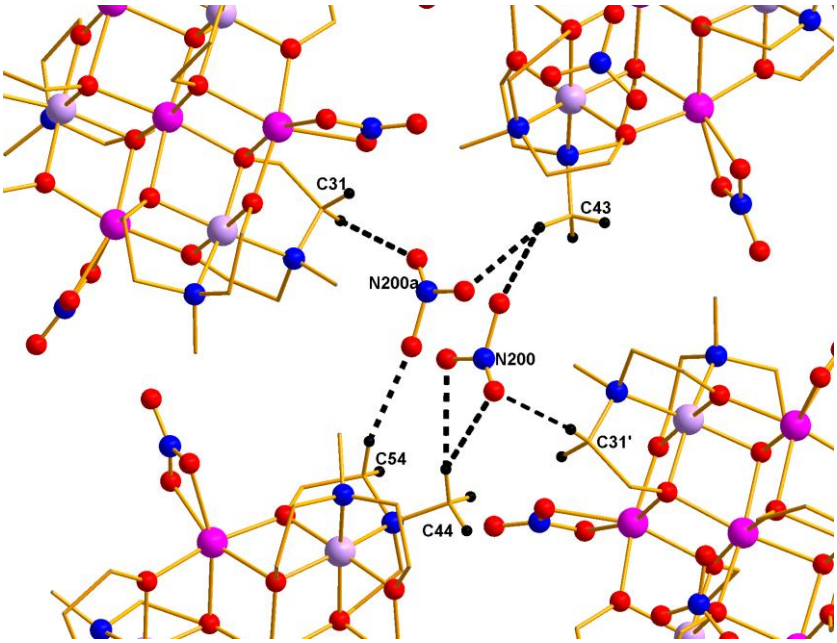

Figure 4-14 Diagram showing interactions of disordered nitrate anion and Co_7 cluster 14.

The distance between metal ions in different clusters is approximately 8 Å; this is the average distance between neighbouring clusters in all directions. The shortest distance between bound nitrate groups on neighbouring clusters is 3.026(6) Å between N3 and O6′. One unbound nitrate anion, with the nitrogen labelled as N100 lies sandwiched between two clusters, approximately equidistant from both with the distance between nearest metal ions and the nitrogen of the nitrate between 5.7 Å and 6.4 Å. The disordered nitrate anion (N200) is disordered over two positions; in each position there are interactions between the O atoms (O201, O202 and O203) of the nitrate and H atoms on surrounding ligands on C31, C43, C44 and C54 on three neighbouring clusters.

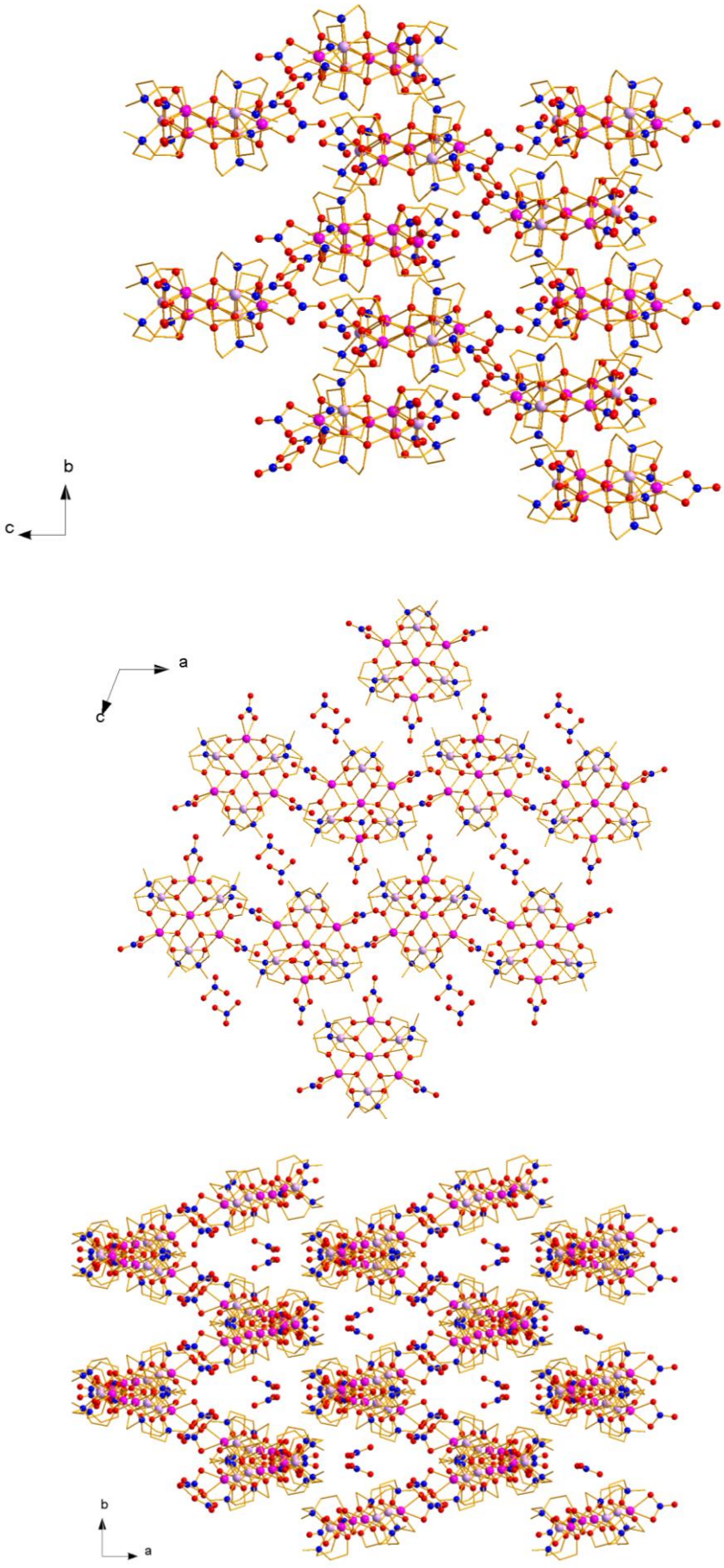

Figure 4-15 Packing diagrams of 14 viewed along *a*-, *b*- and *c*-axes.

Table 4-10 Data for crystal structure determination of 14.

Empirical Formula	$C_{30}H_{66}Co_7N_{11}O_{27}$
Fw (g mol^{-1})	1425.44
Crystal system	Monoclinic
Space group	$P2_1/c$
a (Å)	20.4836(2)
b (Å)	11.3919(1)
c (Å)	26.4917(2)
β (deg)	111.2220(10)
V (Å^3)	5762.54(10)
Z	4
T (K)	100(2)
λ (Å)	0.71073
ρ_{calcd} (Mg m^{-3})	1.643
μ (mm^{-1})	2.051
R_1[a]	0.0734
wR_2[b]	0.1086
Goodness of fit	1.049

[a] $R_1 = \Sigma \left| |F_o| - |F_c| \right| / \Sigma |F_o|$ [b] $wR_2 = \left[\Sigma \left[w\left(F_o^2 - F_c^2\right)^2 \right] - \Sigma \left[\left(F_o^2\right)^2 \right] \right]^{1/2}$ where $w = 1/\left[\sigma^2\left(F_o^2\right) + \left(0.2P\right)^2\right]$ and $P = \left[F_o^2 + 2F_c^2\right]/3$

Table 4-11 Metal-ligand bond lengths for 14.

Bond	Distance (Å)	Bond	Distance (Å)	Bond	Distance (Å)
Co1–O11	2.091(4)	Co3–O73	1.978(4)	Co5–O4	2.176(4)
Co1–O12	2.090(4)	Co3–O14	2.182(4)	Co5– O5	2.142(4)
Co1–O13	2.088(4)	Co3—O1	2.159(4)	Co6–O15	1.939(4)
Co1–O14	2.091(4)	Co3–O2	2.159(4)	Co6–N45	2.007(5)
Co1–O15	2.091(4)	Co4–O13	1.931(4)	Co6–O75	1.893(4)
Co1–O16	2.073(4)	Co4–N43	2.010(5)	Co6–O16	1.936(4)
Co2–O11	1.928(4)	Co4–O73	1.884(4)	Co6–N46	2.004(5)
Co2–N41	2.008(5)	Co4–O14	1.933(4)	Co6–O76	1.880(4)
Co2–O71	1.891(4)	Co4– N44	2.008(5)	Co7–O71	1.974(4)
Co2–O12	1.928(4)	Co4–O74	1.882(4)	Co7–O12	2.178(4)
Co2–N42	2.021(5)	Co5–O13	2.163(4)	Co7–O15	2.179(4)
Co2–O72	1.887(4)	Co5– O74	2.000(4)	Co7–O76	1.979(4)
Co3–O11	2.150(4)	Co5–O75	1.972(4)	Co7–O7	2.156(4)
Co3–O72	1.979(4)	Co5–O16	2.187(4)	Co7–O8	2.156(4)

Table 4-12 Selected bond angles for 14.

Atoms	Angle (°)	Atoms	Angle (°)
Co1-O11-Co2	99.2(2)	Co2-O11-Co3	98.0(2)
Co1-O12-Co2	99.3(2)	Co2-O72-Co3	105.6(2)
Co1-O11-Co3	95.2(2)	Co2-O12-Co7	97.4(2)
Co1-O14-Co3	94.3(2)	Co2-O71-Co7	106.1(2)
Co1-O14-Co4	99.0 (2)	Co3-O14-Co4	97.6(2)
Co1-O13-Co4	99.2(2)	Co3-O73-Co4	106.8(2)
Co1-O13-Co5	94.6(2)	Co4-O74-Co5	105.9(2)
Co1-O16-Co5	94.3(2)	Co4-O13-Co5	98.24(2)
Co1-O16-Co6	99.0(2)	Co5-O75-Co6	107.0(2)
Co1-O15-Co6	98.3(2)	Co5-O16-Co6	97.6(2)
Co1-O15-Co7	94.7(2)	Co6-O15-Co7	97.5(2)
Co1-O12-Co7	94.8(2)	Co6-O76-Co7	106.9(2)

Table 4-13 Bond valence sum calculations for 14.

Atom	Co(II)	Co(III)	Atom	Co(II)	Co(III)
Co1	2.061	2.106	Co5	2.015	2.059
Co2	3.479	3.528	Co6	3.490	3.538
Co3	2.048	2.089	Co7	2.037	2.082
Co4	3.507	3.556			

The underlined value is the one closest to the value for which it was calculated. Overestimation of values for Co^{III} will be discussed in the appendix.

4.2.3 Magnetic Data

Magnetic measurements were carried out on air dried samples of **12** and **13.**

4.2.3.1 Magnetic Susceptibility Measurements for $[Co^{II}_4Co^{III}_3(H_2btp)_3(NO_3)_5(C_2H_5OH)]$ (12)

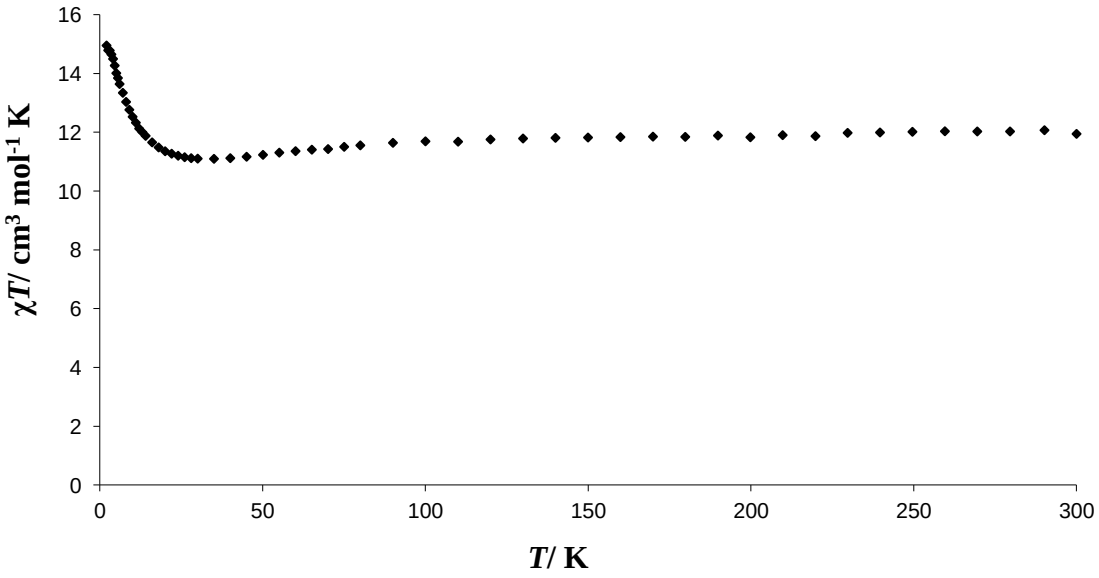

Figure 4-16 Temperature dependence of χT for 12 from 1.8 - 300 K measured in an applied field of 1000 G.

Magnetic susceptibility measurements were carried out on an oven dried sample of **12**. The χT value at 300 K is 11.9 $cm^3\ mol^{-1}\ K$ (Figure 4-16) and is consistent with four uncoupled Co^{II} ions with $g = 2.52$, suggesting the orbital angular momentum of the ions is not quenched and contributes to the magnetic susceptibility. There is a general decrease in χT towards 35 K, this decrease is often seen for Co^{II} complexes as the temperature is lowered and can be attributed to spin-orbit coupling.[24,25] χT reaches a maximum at 2 K of 15.0 $cm^3\ mol^{-1}\ K$, as mentioned in Chapter 1, at low temperature each Co^{II} centre can be treated as having an effective spin $S_i' = ½$ with anisotropic g values. The value of χT at 2 K is consistent with an effective spin ground state $S' = 2$ with $g = 4.47$. The magnetisation was measured against applied field at 2 K and 4 K (Figure 4-17), at 7 T the magnetisation equals ~8.7, this is consistent with an effective spin ground state $S' = 2$ and $g > 4$.

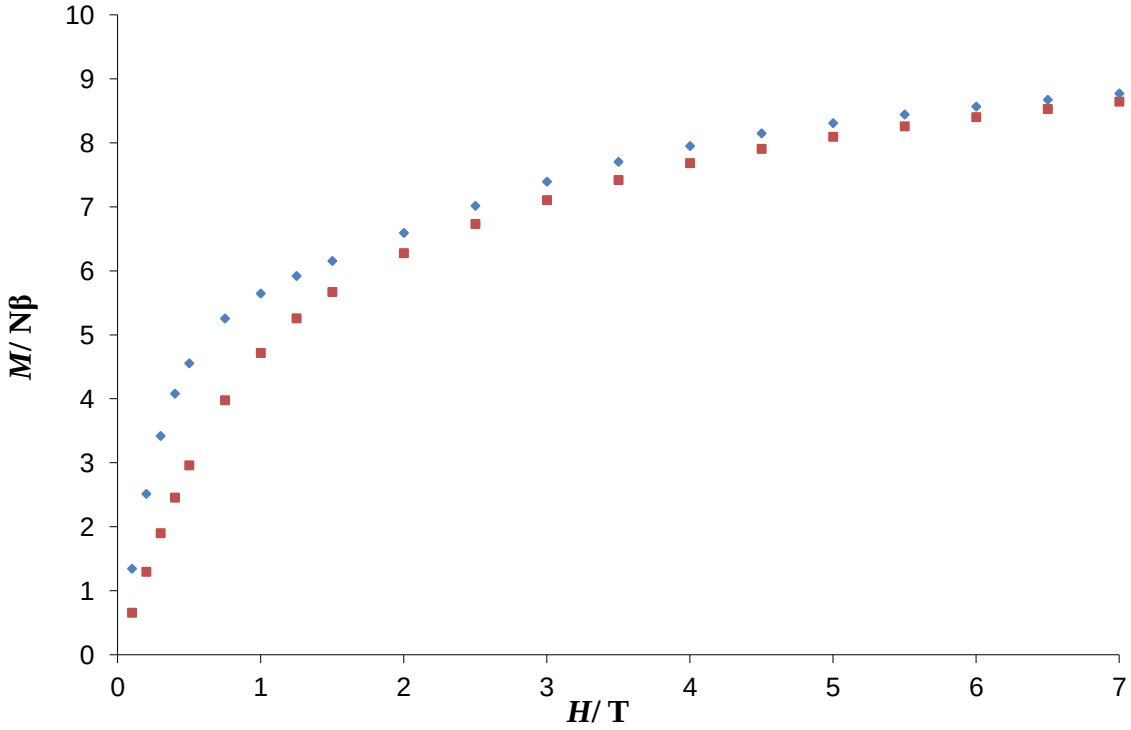

Figure 4-17 *M vs. H* measured for complex 12 at 2 K (◆) and 4 K (■).

4.2.3.2 Magnetic Susceptibility Measurements for $[Co^{II}_4Co^{III}_3(dea)_6(NO_3)_3][NO_3]_2$ (13)

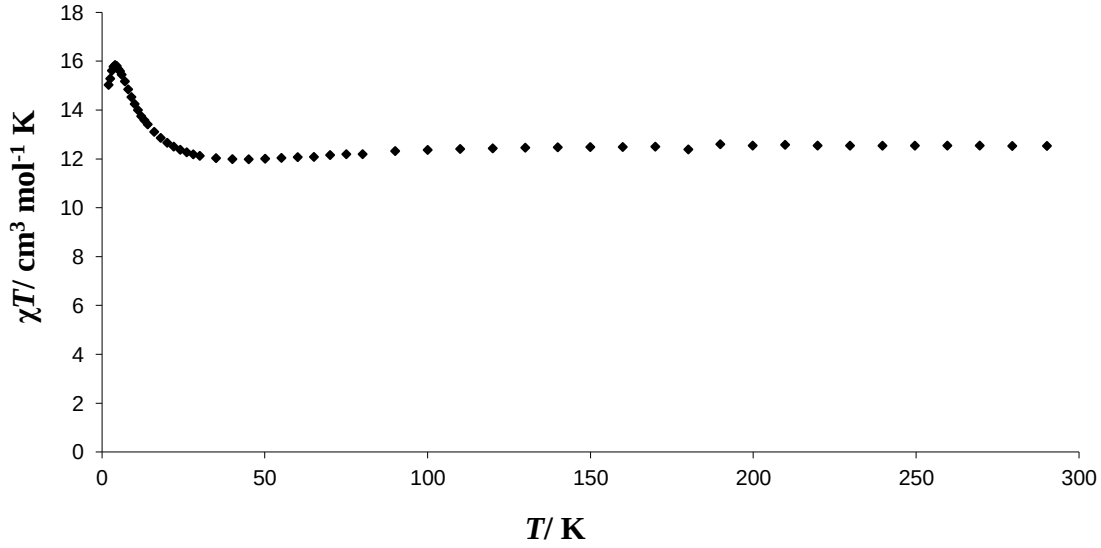

Figure 4-18 Temperature dependence of χT for 13 from 1.8 - 300 K measured in an applied field of 1000 G.

Magnetic susceptibility measurements were carried out on an oven dried sample of **13**. The χT value at 290 K is 12.5 cm^3 mol^{-1} K (Figure 4-18) and is consistent with the χT value for four

uncoupled Co^{II} ions with g = 2.58. There is a slight decrease in χT to 12.0 $cm^3\ mol^{-1}$ K at 35 K, χT then reaches a maximum at 4 K of 15.8 $cm^3\ mol^{-1}$ K followed by a decrease to 15.0 $cm^3\ mol^{-1}$ K at 2 K. These χT values are very similar to those found for the previous complex **11**, although for **12** the values are slightly higher and the maximum χT value is reached at a higher temperature. The magnetisation was measured as a function of applied field at 2 K and 4 K (Figure 4-19). At 7 T the magnetisation is equal to ~8.6 which is consistent with S' = 2 and g> 4.

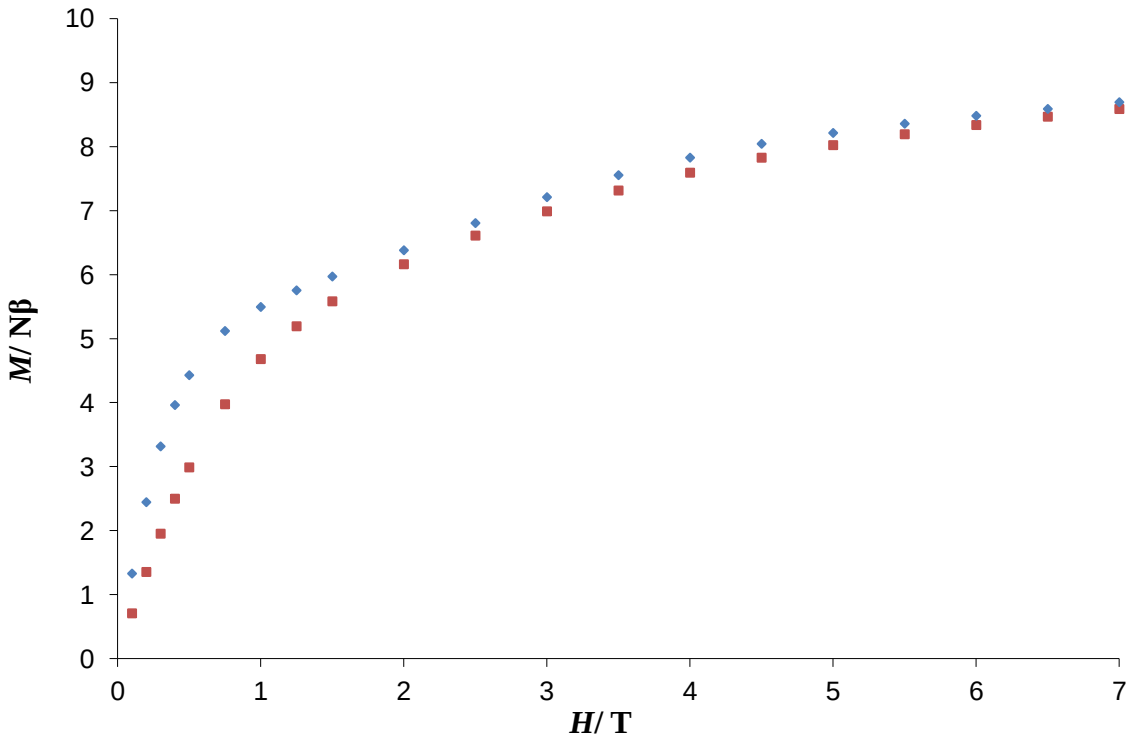

Figure 4-19 *M vs. H* measured for complex 13 at 2 K (◆) and 4 K (■).

4.3 Bimetallic Discs

Although there are several examples of Co and Mn mixed metal complexes, there are no examples of heptametallic disc complexes other than $[Mn^{II}_4Co^{III}_3(Htris)_6(NO_3)_3(H_2O)_3][NO_3]_2$[26] which has been synthesised previously within the group. There are examples of the seven membered disc structure for other metals including Mn,[27-32] Fe,[28,33] Ni[34-37] and Zn.[37,38] There are also heterometallic examples including Mn and Fe.[39] In order to obtain complexes including Co and with interesting magnetic properties it is desirable to have Co in the +2 oxidation state and for the additional metal ions to be magnetically interesting. In the example given above it can be seen that this has not been achieved, as the cobalt is present as Co^{III} ions and manganese as Mn^{II} ions. Only a few examples of different structures including Co and Mn with the desired oxidation states have been found. For example, the hexametallic complex $[Mn^{III}_2Co^{II}_4O_2(O_2CPh)_{10}(DMF)_4]$ which does not display any SMM properties.[40] Other examples include an octanuclear $[Mn^{II}_4Co^{III}_2Co^{II}_2O_2(teaH_2)_2(teaH)_{0.82}(dea)_{3.18}(O_2CMe)_2(OMe)_2][BF_4]_2[O_2CMe]_2$ complex and a tetranuclear complex $[Mn^{II}_2Co^{II}_2(teaH)_2(sal)_2(acac)_2(MeOH)_2]$[41] (Figure 4-20) (where $teaH_3$ = triethanolamine; $deaH_2$ = diethanolamine; salH = salicylic acid; acacH = acetylacetone). In both of these complexes χT *vs.* *T* measurements are indicative of dominant antiferromagnetic coupling.

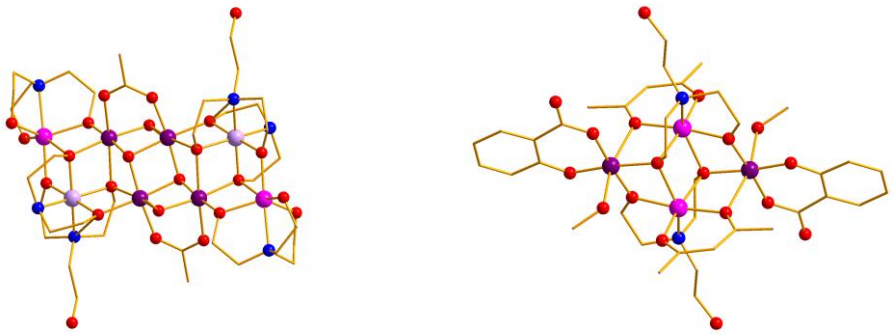

Figure 4-20 Structures of $[Mn^{II}_4Co^{II}_2Co^{III}_2O_2(teaH_2)_2(teaH)_{0.82}(dea)_{3.18}(O_2CMe)_2(OMe)_2]^{4+}$ and $[Mn^{II}_2Co^{II}_2(teaH)_2(sal)_2(acac)_2(MeOH)_2]$ Co^{II} pink; Co^{III} lilac; Mn^{III} dark purple; O red; N blue; H atoms omitted for clarity.

4.3.1 Synthetic Methods

*4.3.1.1 Attempted synthesis of $[Co^{II}_4Mn^{III}_3]$ with $trisH_3$ results in $[Co_{4.7}Mn_{2.3}(trisH)_6(NO_3)_3(H_2O)_3][NO_3]_2$·3MeOH (**15**·3MeOH)*

(where $trisH_3$ = tris(hydroxymethyl)aminomethane)

$Co(NO_3)_2.6H_2O$ (1.16 g, 3.99 mmol) and $Mn(NO_3)_2.4H_2O$ (1.00 g, 3.98 mmol) were dissolved in 20 mL of H_2O, tris (0.97 g, 8.01 mmol) was added and the reaction was stirred for 30 minutes. Water was then removed under vacuum and the dark purple residue was dissolved in approximately 10 mL of MeOH. The solution was then filtered and stored in a sealed vial. After approximately

three weeks purple thin rod shaped crystals formed in 36% yield. Air dried crystals analyse as **$C_{30}H_{76.5}N_{12.5}O_{40.5}Co_{4.7}Mn_{2.3}$** analysis (%) calc. (found) C, 21.66 (21.14); H, 4.27 (4.58); N, 10.52 (11.23); Co, 16.65 (16.17); Mn, 7.59 (7.44). Selected IR data: *v* = 3309, 3227, 3147, 2928, 2875, 1637, 1587, 1550, 1410, 1311, 1068, 1008, 976, 815, 761, 682, 613 cm^{-1}.

*4.3.1.2 Attempted synthesis of $[Co^{II}_4Mn^{III}_3]$ with $deaH_2$ results in $[Co_6Mn_1(dea)_6(NO_3)_3][NO_3]_2 \cdot 3MeOH \cdot 1.5H_2O$ (**16**·3MeOH· 1.5H_2O)*

(where $deaH_2$ = diethanolamine)

$Co(NO_3)_2.6H_2O$ (0.58 g, 1.99 mmol) and $Mn(NO_3)_2.4H_2O$ (0.50 g, 1.99 mmol) were dissolved in 10 mL of MeOH, diethanolamine (0.21 g, 2.00 mmol) was added followed by NaOMe (0.11 g, 2.04 mmol) and the reaction was stirred for four hours. The solution was then filtered and stored in a sealed vial. After approximately three weeks green square plate crystals formed in 9% yield. Air dried crystals analyse as **$C_{24}H_{66}N_{11}O_{32}Co_6Mn_1$**, analysis (%) calc. (found) C, 20.83 (20.89); H, 4.62 (4.43); N, 10.69 (10.88); Co, 24.53 (24.22); Mn, 3.81 (4.18). Selected IR data: *v* = 3375, 3209, 2875, 1636, 1467, 1384, 1305, 1278, 1145, 1107, 1062, 1037, 918, 891, 825, 806, 783, 694, 626 cm^{-1}.

4.3.2 Discussion of Crystal Structures

*4.3.2.1 Discussion of crystal structure of $[Co^{III}_3Mn^{II}_4(trisH)_6(NO_3)_3(H_2O)_3][NO_3]_2$·MeOH (**15**·MeOH)*

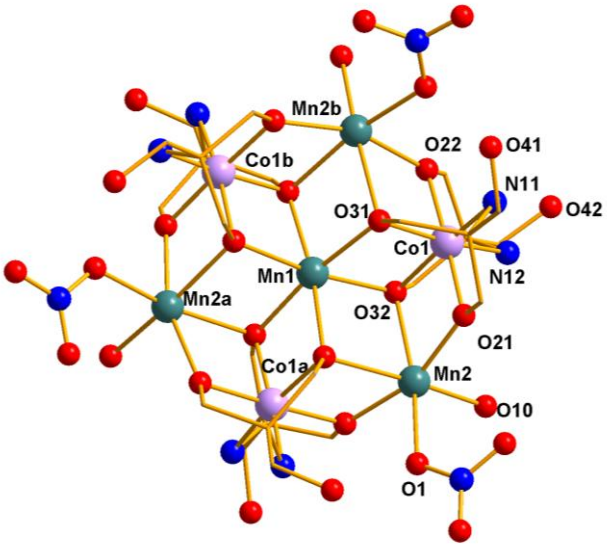

Figure 4-21 Structure of $[Co^{III}_3Mn^{II}_4(trisH)_6(NO_3)_3(H_2O)_3][NO_3]_2$(15) obtained from single crystal X-ray diffraction. Co^{III} lilac; Mn^{II} teal. Atom labels a and b signify symmetry equivalents; a = 1-x+y, 1-x, z; b = 1-y, x-y, z.

This example is the bimetallic equivalent of the previously published $[Co^{II}_4Co^{III}_3]$ complex[8] and is similar to a previously published structure.[26] Metal ions have been assigned as three Co^{III} ions and four Mn^{II} ions, supported by consideration of bond lengths and charge balance, however it is very difficult to distinguish between Co^{II} and Mn^{II} using crystallographic data. BVS calculation[15] (Table 4-17) results are ambiguous, the assignment of four M^{II} is supported, however it would be difficult to assign the ions as Mn over Co based on this alone. Metal analysis suggests that in a bulk sample different ratios of metal ions are present in different clusters, with a ratio of ~ 4.7Co: 2.3Mn ions rather than the desired 4Co:3Mn, the formula $[Co_{4.7}Mn_{2.3}(trisH)_6(NO_3)_3(H_2O)_3][NO_3]_2$ is proposed, however it is not possible to identify the positions of these ions from crystallography.

The following discussion will describe the structure as shown in Figure 4-21. The coordination spheres of the Mn ions are filled by $\{O_6\}$ in a distorted octahedral arrangement, with the oxygen atoms coming from deprotonated alcohol ligand arms; this is the case for the central Mn; or four oxygen donors are provided by the ligand and the remaining coordination sites are filled by a monodentate nitrate ion and a bound molecule of water; this is the case for the outer Mn ions. The Co^{III} ions have an $\{N_2O_4\}$ ligand donor set, coordinated to the central amine group of two ligands and the deprotonated alcohol groups of four ligand arms from two separate ligands. The charge of the complex is balanced by the presence of two lattice nitrates. One nitrate anion lies directly above the central Mn^{II} ion, and it is hydrogen bonded to three lattice molecules of methanol. Due to the way the clusters pack together there are large channels running through the structure parallel to the *c*-axis (Figure 4-22), the second nitrate is disordered and found in these channels along with several molecules of disordered MeOH and water per complex, these were dealt with by applying the PLATON squeeze program.[42,43]

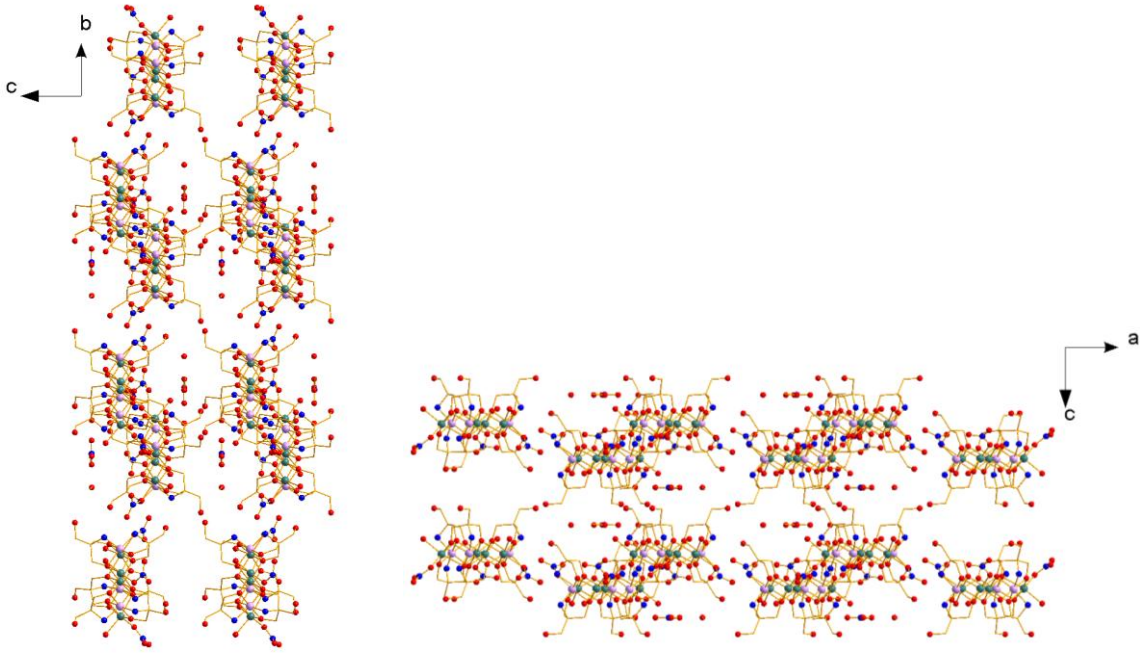

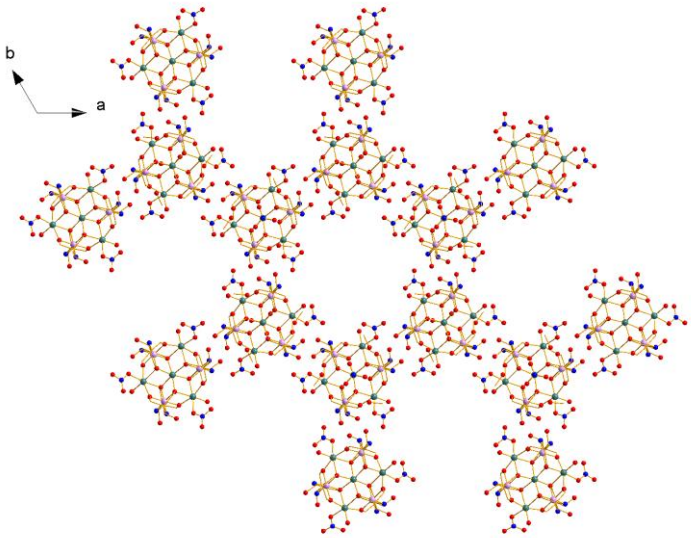

Figure 4-22 Packing diagrams of 15 viewed along *a*-, *b*- and *c*-axes

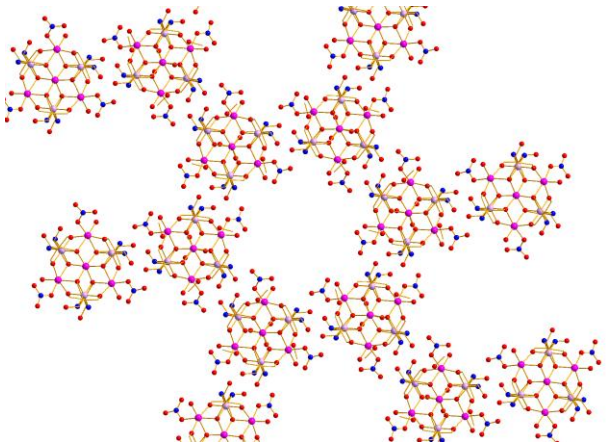

Figure 4-23 Packing diagram of $Co^{II}_4Co^{III}_3$ equivalent complex viewed along *c*-axis.

Comparing this complex with the equivalent [$Co^{II}_4Co^{III}_3$] complex[8] it can be seen that there are several similarities. When the packing of each complex is viewed along the *c*-axis, the same channels can be seen in both (Figure 4-22 and Figure 4-23). In the mixed metal example the diameter of the channel is 11.943(4) Å compared with 13.084(3) Å in the cobalt example measured between equivalent nitrate groups on complexes either side of the channel. The hydrogen bonding that occurs in heterometallic complex is also similar to that shown for the cobalt complex. The unbound nitrate anion lies above the central Mn ion, and is hydrogen bonded to one molecule of methanol which has further hydrogen bonding to the unbound ligand arm (Figure 4-24 upper), O41(H)···O100 2.714(6) Å and O100(H)···O4 2.795(4) Å. There are extensive hydrogen bonding interactions between complexes, approximately 3 Å in length (Figure 4-24 lower).

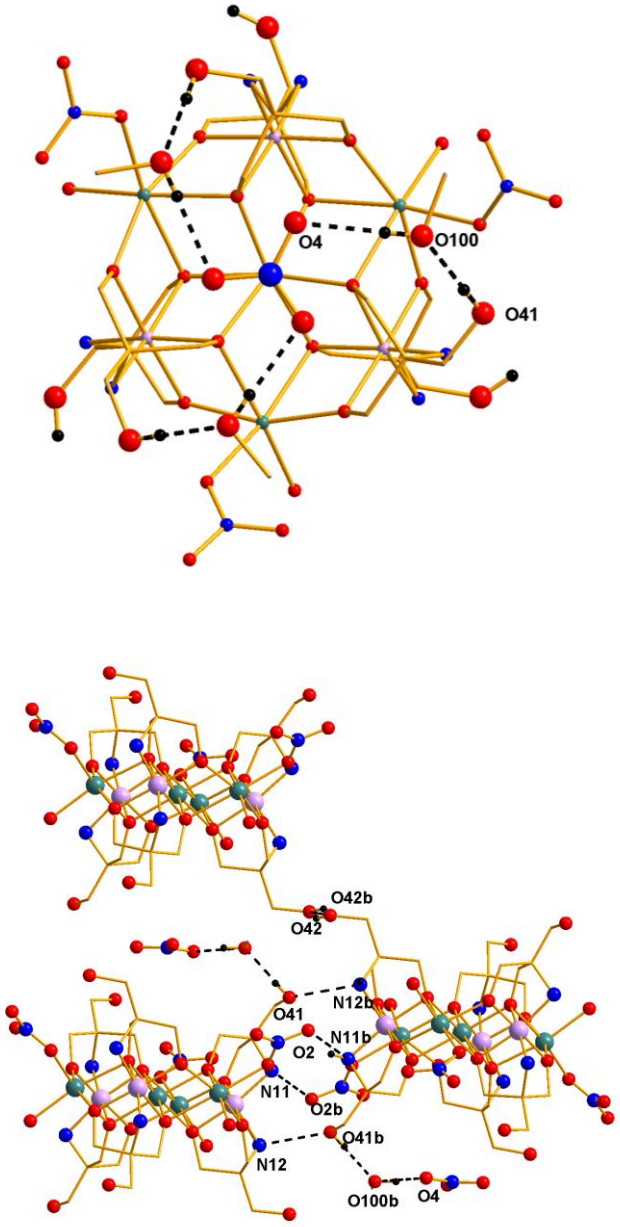

Figure 4-24 Hydrogen bonding interactions in complex 15. Upper figure = interactions between unbound nitrate, methanol and complex; lower figure = extensive hydrogen bonding between solvent, nitrate and complexes.

Table 4-14 Data for crystal structure determination of 15·3MeOH

Empirical Formula	$C_{27}H_{66}Co_3Mn_4N_{11}O_{39}$
Fw (g mol^{-1})	1565.42
Crystal system	Trigonal
Space group	*P*-3
a (Å)	19.6102(4)
b (Å)	19.6102(4)
c (Å)	11.5071(2)
α (deg)	90
β (deg)	90
γ (deg)	120
V (Å^3)	3832.3(1)
Z	2
T (K)	100(2)
λ (Å)	0.71073
ρ_{calcd} (Mg m^{-3})	1.303
μ (mm^{-1})	1.348
R_1[a]	0.0598
wR_2[b]	0.0717
Goodness of fit	1.01

One NO_3 is not found crystallographically assumed to be present in the squeezed electron density.

[a] $R_1 = \Sigma \left| |F_o| - |F_c| \right| / \Sigma |F_o|$ [b] $wR_2 = \left[\Sigma \left[w\left(F_o^2 - F_c^2\right)^2 \right] - \Sigma \left[\left(F_o^2\right)^2 \right] \right]^{1/2}$ where $w = 1/\left[\sigma^2\left(F_o^2\right) + \left(0.2P\right)^2\right]$ and $P = \left[F_o^2 + 2F_c^2\right]/3$

Table 4-15 Selected metal-ligand bond lengths for 14.

Bond	Distance (Å)	Bond	Distance (Å)
Co1–O21	1.897(3)	Mn1–O32a	2.159(3)
Co1–O22	1.891(3)	Mn1–O31b	2.162(3)
Co1–O31	1.914(2)	Mn1–O32b	2.159(3)
Co1–O32	1.914(2)	Mn2–O1	2.153(3)
Co1–N11	1.912(3)	Mn2–O10	2.121(3)
Co1–N12	1.933(3)	Mn2–O21	2.017(3)
Mn1–O31	2.162(3)	Mn2–O22a	2.027(3)
Mn1–O32	2.159(3)	Mn2–O31a	2.293(3)
Mn1–O31a	2.162(3)	Mn2–O32	2.308(3)

Table 4-16 Selected bond angles for 15.

Atoms	Angle(°)	Atoms	Angle(°)
Mn1-O31a-Mn2	93.37(9)	Co1-O21-Mn2	105.8(1)
Mn1-O32-Mn2	93.04(9)	Co1-O22-Mn2b	106.5(1)
Mn1- O31-Co1	94.9(1)	Co1-O31-Mn2b	96.2(1)
Mn1-O32-Co1	95.00(1)	Co1-O32-Mn2	94.9(1)

Table 4-17 Bond valence calculations for 15.

Atom	Co^{II}	Co^{III}	Mn^{II}	Mn^{III}
Mn1	1.696	1.733	<u>2.210</u>	2.038
Mn2	<u>1.804</u>	1.843	<u>2.351</u>	2.168
Co1	3.848	<u>3.897</u>	4.531	4.302

The underlined value is the one closest to the value for which it was calculated. The results for Mn2 are ambiguous. Overestimation for Co^{III} values will be discussed in appendix one.

From Table 4-17 it is clear that the values for Co^{II} and Mn^{II} are not conclusive, it would be very difficult to assign the atoms 1 and 2 as either Mn^{II} or Co^{II} based on these results, particularly for Mn2.

4.3.2.2 *Discussion of crystal structure of $[Co^{II}_3Co^{III}_3Mn^{II}(dea)_6(NO_3)_3][NO_3]_2 \cdot 3MeOH \cdot 1.5H_2O$ (**16**$\cdot 3MeOH \cdot 1.5H_2O$) (where H_2dea = diethanolamine)*

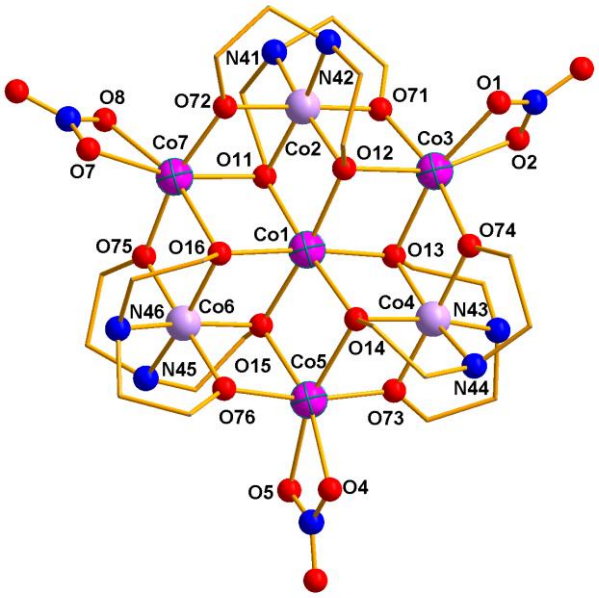

Figure 4-25 Structure of $[Co^{II}_3Co^{III}_3Mn^{II}(dea)_6(NO_3)_3][NO_3]_2$ 16) Co^{II} /Mn^{II} pink with cross (there are three Co^{II} ions and one Mn^{II} ion, but it is not possible to determine the position of the Mn^{II} ion); Co^{III} lilac; O red; N blue; H-atoms, solvent and unbound nitrate omitted for clarity.

In this example the structure of the heptanuclear disc is analogous to complex **13** with the exception that there is one Mn ion per disc (Figure 4-25). The position of the Mn^{II} ion cannot be identified from crystallography and it could be disordered over several sites. See Section 4.2.2.2 for structural description. The charge of the complex is balanced by the presence of two unbound nitrate anions. Three molecules of methanol and 1.5 molecules of water have been modelled per complex.

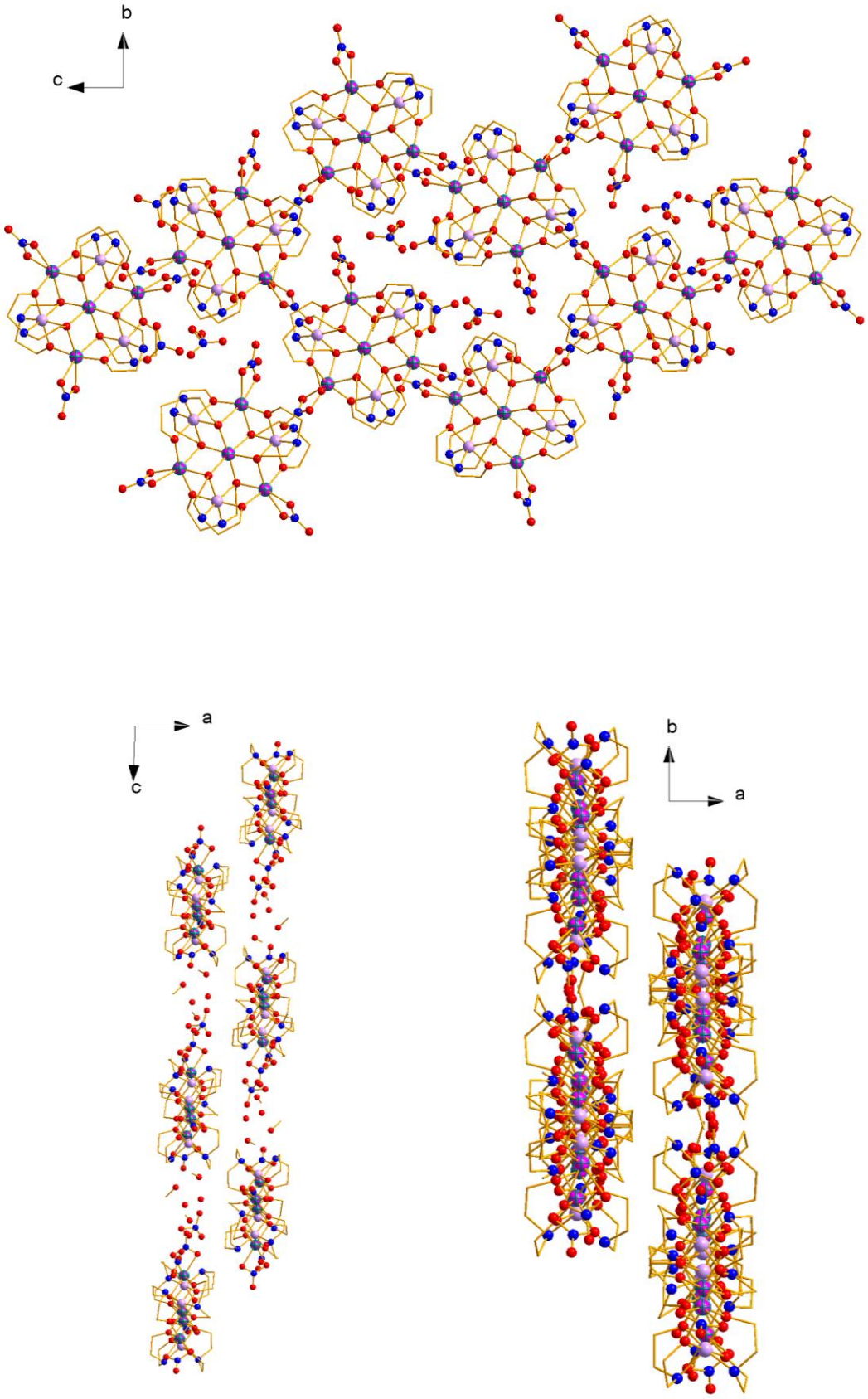

Figure 4-26 Packing diagram of 16 viewed along *a*-, *b*- and *c*-axes

The packing arrangement and locations of nitrate anions and solvent molecules is very similar to the cobalt complex **13** as would be expected, with only one Mn^{II} present in complex **16** and the similarities in size and configuration of Mn^{II} and Co^{II}. The hydrogen bonding interactions (Figure 4-27) between the solvent, unbound nitrates and complexes are in the range of 2.7 – 2.9 Å. The shortest are between unbound molecules of water and methanol O(H)···O 2.765(7) Å and 2.743 (4) Å. The longest interaction is between an unbound nitrate and water (2.963(2) Å). The interactions between NH groups in the complex and either unbound nitrate or solvent are approximately 2.9 Å. The closest metal···metal distance between neighbouring clusters is 6.8724(7) Å between Co3 and Co3′, which is comparable with complex **13**.

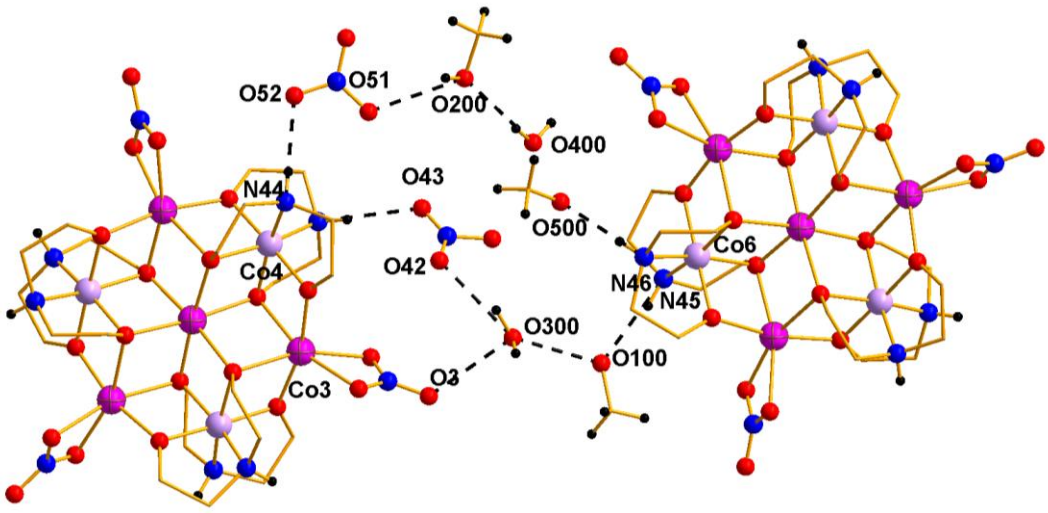

Figure 4-27 Diagram showing hydrogen bonding interactions between solvent, nitrates and complexes for 16.

Table 4-18 Data for the crystal structure determination of 16·3MeOH·1.5H_2O

Empirical Formula	$C_{27}H_{69}Co_6MnN_{11}O_{31.5}$*
Fw (g mol^{-1})	1452.44
Crystal system	Monoclinic
Space group	$P2_1/c$
a (Å)	11.8407(6)
b (Å)	13.0171(6)
c (Å)	33.9894(16)
β (deg)	92.021(3)
V ($Å^3$)	5235.6(4)
Z	4
T (K)	100(2)
λ (Å)	0.71073
ρ_{calcd} (Mg m^{-3})	1.858
μ (mm^{-1})	2.266
R_1[a]	0.0461
wR_2[b]	0.0887
Goodness of fit	0.991

*There is one Mn per complex but it is not possible to place this using crystallographic data, all metal ions have been modelled as Co.

[a] $R_1 = \Sigma \left| |F_o| - |F_c| \right| / \Sigma |F_o|$ [b] $wR_2 = \left[\Sigma \left[w\left(F_o^2 - F_c^2\right)^2 \right] - \Sigma \left[\left(F_o^2\right)^2 \right] \right]^{1/2}$ where $w = 1/\left[\sigma^2\left(F_o^2\right) + \left(0.2P\right)^2\right]$ and $P = \left[F_o^2 + 2F_c^2\right]/3$

Table 4-19 Selected metal-ligand bond lengths for 16.

Bond	Distance(Å)	Bond	Distance(Å)	Bond	Distance(Å)
Co1–O11	2.103(2)	Co3–O13	2.191(2)	Co5–O73	1.984(2)
Co1–O12	2.102(2)	Co3–O2	2.157(3)	Co5–O76	1.996(2)
Co1–O13	2.112(2)	Co3–O71	1.991(2)	Co6–N45	1.948(3)
Co1–O14	2.113(2)	Co3–O74	1.989(2)	Co6–N46	1.945(3)
Co1–O15	2.099(2)	Co4–N43	1.942(3)	Co6–O15	1.921(2)
Co1–O16	2.113(2)	Co4–N44	1.955(3)	Co6–O16	1.928(2)
Co2–N41	1.941(3)	Co4–O13	1.927(2)	Co6–O75	1.884(2)
Co2–N42	1.946(3)	Co4–O14	1.926(2)	Co6–O76	1.890(2)
Co2–O11	1.920(2)	Co4–O73	1.881(2)	Co7–O11	2.159(2)
Co2–O12	1.923(2)	Co4–O74	1.890(2)	Co7–O16	2.175(2)
Co2–O71	1.872(2)	Co5–O14	2.200(2)	Co7–O7	2.144(2)
Co2–O72	1.879(2)	Co5–O15	2.169(2)	Co7–O72	1.987(2)
Co3–O1	2.158(2)	Co5–O4	2.174(2)	Co7–O75	1.982(2)
Co3–O12	2.173(2)	Co5–O5	2.182(2)	Co7–O8	2.154(2)

Table 4-20 Selected bond angles for 16.

Atoms	Angle(°)	Atoms	Angle(°)
Co1-O11-Co2	96.51(9)	Co5-O14-Co1	93.94(8)
Co1-O12-Co2	96.46(9)	Co5-O14-Co4	97.40(9)
Co1-O13-Co4	96.48(9)	Co5-O15-Co1	95.26(8)
Co1-O14-Co4	96.47(9)	Co5-O15-Co6	97.82(9)
Co1-O15-Co6	97.08(9)	Co5-O73-Co4	106.90(10)
Co1-O16-Co6	96.41(9)	Co5-O76-Co6	105.18(10)
Co3-O12-Co1	94.67(9)	Co7-O11-Co1	96.01(8)
Co3-O12-Co2	97.20(9)	Co7-O11-Co2	97.07(9)
Co3-O13-Co1	93.84(8)	Co7-O16-Co1	95.22(8)
Co3-O13-Co4	97.83(9)	Co7-O16-Co6	96.99(9)
Co3-O71-Co2	105.5(1)	Co7-O72-Co2	104.6(1)
Co3-O74-Co4	106.5(1)	Co7-O75-Co6	105.5(1)

Table 4-21 BVS calculations for 16.

Atom	Co^{II}	Co^{III}	Mn^{II}	Mn^{III}
Co1	<u>1.955</u>	1.997	2.547	2.349
Co2	3.806	<u>3.856</u>	4.629	4.396
Co3	<u>1.994</u>	2.038	2.599	2.397
Co4	3.739	<u>3.788</u>	4.546	4.318
Co5	<u>1.961</u>	2.003	2.551	2.356
Co6	3.747	<u>3.797</u>	4.556	4.328
Co7	<u>2.043</u>	2.088	2.663	2.455

The underlined value is that closest to the oxidation state for which it was calculated. Overestimations for Co^{III} will be discussed in appendix one.

From **Table 4-21** it is clear that an alternative method for assigning metals and their oxidation states must be employed due to the lack of a clear result from BVS calculations, atoms 1, 3, 5 and 7 have good agreement for Co^{II} but the values for Mn^{II} are also quite close. Metal analysis shows that there is one Mn^{II} ion per complex however; it is not possible to determine the position of this ion from single crystal X-ray crystallography.

4.3.3 Magnetic susceptibility measurements for $[Co^{II}_3Co^{III}_3Mn^{II}(dea)_6(NO_3)_3][NO_3]_2$ (16)

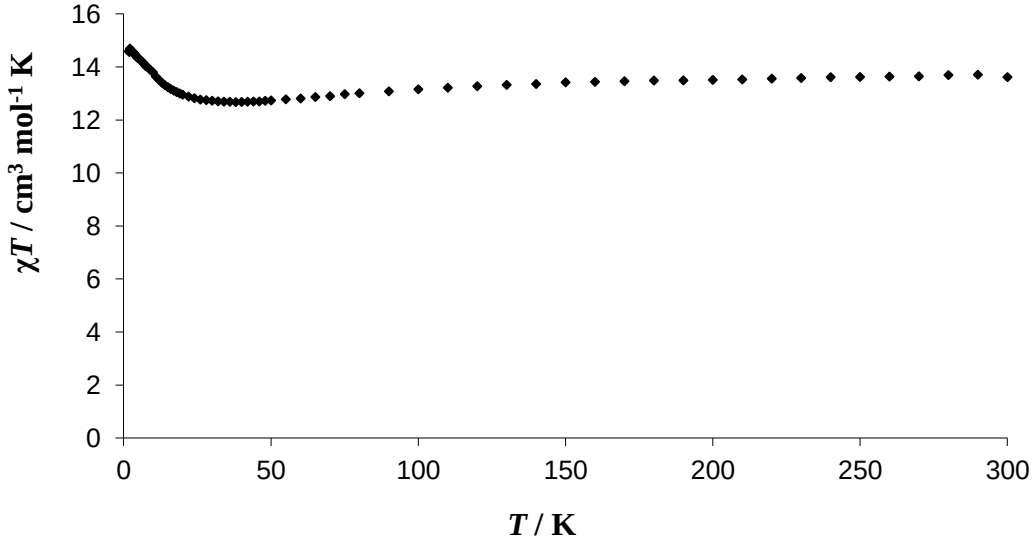

Figure 4-28 Temperature dependence of χT for 16 from 1.8-300 K measured in an applied field of 1000 G.

Magnetic susceptibility measurements were carried out on a sample of **16** $[Co_6Mn(dea)_6(NO_3)_3][NO_3]_2$. The χT value at 300 K is 13.6 $cm^3\ mol^{-1}\ K$ which is consistent with three uncoupled Co^{II} ions and one Mn^{II} (with g = 2.56 for Co^{II} and g = 2 for Mn^{II}). The χT value decreases slightly to 12.7 $cm^3\ mol^{-1}\ K$ at 38 K below this temperature χT values begin to increase. As the temperature is decreased the χT value increases to 14.6 $cm^3\ mol^{-1}\ K$ at 1.8 K.

If there were four uncoupled Mn^{II} ions the expected χT value at 300 K would be 17.5 $cm^3\ mol^{-1}\ K$ for g = 2.0, four uncoupled Co^{II} ions would be expected to have a χT value at 300 K of 9.92 $cm^3\ mol^{-1}\ K$ for g = 2.3. Measured values are therefore consistent with a mix of Mn^{II} and Co^{II}. At low temperature four Co^{II} ions with effective $S_i' = 1/2$ and $g \sim 4.3$ would give a calculated χT value of 13.9 $cm^3\ mol^{-1}\ K$ for $S' = 2$ if there is ferromagnetic exchange. The low temperature χT value is higher than this calculated value again suggesting the presence of some Mn^{II}, but it is not possible to say whether all M^{II}-M^{II} interactions are ferromagnetic or whether ZFS is playing a role.

4.4 Conclusions

In conclusion three new Co_7 discs have been synthesised adding to the growing family of Co_7 disc complexes, the magnetic susceptibility measurements of complexes **12** and **13** suggest ferromagnetic interactions between the Co^{II} centres.

Two new heterometallic complexes have also been formed and magnetic susceptibility measurements were carried out on complex **16**. The magnetic susceptibility measurements confirmed the presence of Mn^{II} within the complex.

The original aim to replace the Co^{III} ions was unsuccessful, due to Co^{II} ions oxidising before the Mn^{II} ions, attempting the reaction under more controlled conditions such as under nitrogen could be more successful. Attempting these reactions with alternative M^{III} ions, eg. Cr^{III} and Fe^{III} has not yet yielded any successful results. This could be due to the relative inertness of the Cr^{III}, performing the reaction under more forcing conditions (eg. solvothermal) could result in the desired products.[44] The lack of success with Fe^{III} is more disappointing as others have had success in forming mixed Co and Fe complexes with the desired oxidation states and similar ligands,[22] this suggests that with alteration of reaction and crystallisation conditions, isolation of heterometallic complexes could be possible.

Further work would be required to synthesise the desired $[Co^{II}_4Mn^{III}_3]$ complexes. Synthesis of a $[Co^{III}_3Mn^{II}_4]$ complex similar to **15** has been described previously,[26] using very similar conditions to those described here. The only difference in synthesis was the absence of base in the synthesis reported here, suggesting that the formation of the product is very sensitive to pH. For complex **16** reaction conditions were altered, and proved to be less successful in incorporating Mn ions into the structure. Attempting to synthesise both **15** and **16** under different reaction pH could hopefully provide the desired $[Co^{II}_4Mn^{III}_3]$ products.

4.5 References

(1) Zhang, Y.-Z.; Wernsdorfer, W.; Pan, F.; Wang, Z.-M.; Gao, S. *Chemical Communications* **2006**, 3302.

(2) Wang, X.-T.; Wang, B.-W.; Wang, Z.-M.; Zhang, W.; Gao, S. *Inorganica Chimica Acta* **2008**, *361*, 3895.

(3) Zhang, S.-H.; Song, Y.; Liang, H.; Zeng, M.-H. *CrystEngComm* **2009**, *11*, 865.

(4) Kitos, A. A.; Efthymiou, C. G.; Papatriantafyllopoulou, C.; Nastopoulos, V.; Tasiopoulos, A. J.; Manos, M. J.; Wernsdorfer, W.; Christou, G.; Perlepes, S. P. *Polyhedron* **2011**, *30*, 2987.

(5) Moragues-Canovas, M.; Talbot-Eeckelaers, C. E.; Catala, L.; Lloret, F.; Wernsdorfer, W.; Brechin, E. K.; Mallah, T. *Inorganic Chemistry* **2006**, *45*, 7038.

(6) Chibotaru, L. F.; Ungur, L.; Aronica, C.; Elmoll, H.; Pilet, G.; Luneau, D. *Journal of the American Chemical Society* **2008**, *130*, 12445.

(7) Alley, K. G.; Bircher, R.; Waldmann, O.; Ochsenbein, S. T.; Güdel, H. U.; Moubaraki, B.; Murray, K. S.; Fernandez-Alonso, F.; Abrahams, B. F.; Boskovic, C. *Inorganic Chemistry* **2006**, *45*, 8950.

(8) Ferguson, A.; Parkin, A.; Sanchez-Benitez, J.; Kamenev, K.; Wernsdorfer, W.; Murrie, M. *Chemical Communications* **2007**, 3473.

(9) Tudor, V.; Marin, G.; Lloret, F.; Kravtsov, V. C.; Simonov, Y. A.; Julve, M.; Andruh, M. *Inorganica Chimica Acta* **2008**, *361*, 3446.

(10) Cambridge structural database search, 2013 September.

(11) Allen, F. *Acta Crystallographica Section B* **2002**, *58*, 380.

(12) Gatteschi, D.; Sessoli, R. *Angewandte Chemie International Edition* **2003**, *42*, 268.

(13) Ferguson, A.; Schmidtmann, M.; Brechin, E. K.; Murrie, M. *Dalton Transactions* **2011**, *40*, 334.

(14) Murrie Group unpublished work Co7 and BTP analogues.

(15) Brese, N. E.; O'Keeffe, M. *Acta Crystallographica Section B* **1991**, *47*, 192.

(16) Bruno, I. J.; Cole, J. C.; Edgington, P. R.; Kessler, M.; Macrae, C. F.; McCabe, P.; Pearson, J.; Taylor, R. *Acta Crystallographica Section B* **2002**, *B58*, 389.

(17) Mazus, M. D.; Kovalenko, A. L.; Polyakov, V. N.; Simonov, Y. A.; Malinovskii, T. I. *Zh. Neorg. Khim. (Russ) (Russ. J. Inorg. Chem.)* **1986**, *31*, 716.

(18) Nesterov, D. S.; Kokozay, V. N.; Dyakonenko, V. V.; Shishkin, O. V.; Jezierska, J.; Ozarowski, A.; Kirillov, A. M.; Kopylovich, M. N.; Pombeiro, A. J. L. *Chemical Communications* **2006**, 4605.

(19) Nesterov, D. S.; Kokozay, V. N.; Skelton, B. W. *Acta Crystallographica Section C* **2006**, *62*, m246.

(20) Bertrand, J. A.; Fujita, E.; VanDerveer, D. G. *Inorganic Chemistry* **1979**, *18*, 230.

(21) Tudor, V.; Madalan, A.; Lupu, V.; Lloret, F.; Julve, M.; Andruh, M. *Inorganica Chimica Acta* **2010**, *363*, 823.

(22) Malaestean, I. L.; Speldrich, M.; Ellern, A.; Baca, S. G.; Kögerler, P. *Polyhedron* **2010**, *29*, 1990.

(23) Malaestean, I. L.; Kutluca, M.; Speldrich, M.; Ellern, A.; Kögerler, P. *Inorganica Chimica Acta* **2012**, *380*, 72.

(24) Aromi, G.; Stoeckli-Evans, H.; Teat, S. J.; Cano, J.; Ribas, J. *Journal of Materials Chemistry* **2006**, *16*, 2635.

(25) Figgis, B. N.; Gerloch, M.; Lewis, J.; Mabbs, F. E.; Webb, G. A. *Journal of the Chemical Society A: Inorganic, Physical, Theoretical* **1968**, 2086.

(26) Ferguson, A., Ph.D. thesis, 2007.

(27) Stamatatos, T. C.; Foguet-Albiol, D.; Poole, K. M.; Wernsdorfer, W.; Abboud, K. A.; O'Brien, T. A.; Christou, G. *Inorganic Chemistry* **2009**, *48*, 9831.

(28) Liu, T.; Wang, B.-W.; Chen, Y.-H.; Wang, Z.-M.; Gao, S. *Zeitschrift für anorganische und allgemeine Chemie* **2008**, *634*, 778.

(29) A. Bolcar, M.; M. J. Aubin, S.; Folting, K.; N. Hendrickson, D.; Christou, G. *Chemical Communications* **1997**, 1485.

(30) Saalfrank, R. W.; Nakajima, T.; Mooren, N.; Scheurer, A.; Maid, H.; Hampel, F.; Trieflinger, C.; Daub, J. *European Journal of Inorganic Chemistry* **2005**, *2005*, 1149.

(31) Saalfrank, R. W.; Scheurer, A.; Prakash, R.; Heinemann, F. W.; Nakajima, T.; Hampel, F.; Leppin, R.; Pilawa, B.; Rupp, H.; Müller, P. *Inorganic Chemistry* **2007**, *46*, 1586.

(32) Stamatatos, T. C.; Poole, K. M.; Foguet-Albiol, D.; Abboud, K. A.; O'Brien, T. A.; Christou, G. *Inorganic Chemistry* **2008**, *47*, 6593.

(33) Hoshino, N.; Ako, A. M.; Powell, A. K.; Oshio, H. *Inorganic Chemistry* **2009**, *48*, 3396.

(34) Meally, S. T.; Karotsis, G.; Brechin, E. K.; Papaefstathiou, G. S.; Dunne, P. W.; McArdle, P.; Jones, L. F. *CrystEngComm* **2010**, *12*, 59.

(35) Zhang, J.; Teo, P.; Pattacini, R.; Kermagoret, A.; Welter, R.; Rogez, G.; Hor, T. S. A.; Braunstein, P. *Angewandte Chemie International Edition* **2010**, *49*, 4443.

(36) Wei, L.-Q.; Zhang, K.; Feng, Y.-C.; Wang, Y.-H.; Zeng, M.-H.; Kurmoo, M. *Inorganic Chemistry* **2011**, *50*, 7274.

(37) Meally, S. T.; McDonald, C.; Karotsis, G.; Papaefstathiou, G. S.; Brechin, E. K.; Dunne, P. W.; McArdle, P.; Power, N. P.; Jones, L. F. *Dalton Transactions* **2010**, *39*, 4809.

(38) Tesmer, M.; Muller, B.; Vahrenkamp, H. *Chemical Communications* **1997**, 721.

(39) Saalfrank, R. W.; Prakash, R.; Maid, H.; Hampel, F.; Heinemann, F. W.; Trautwein, A. X.; Böttger, L. H. *Chemistry – A European Journal* **2006**, *12*, 2428.

(40) Gavrilenko, K. S.; Punin, S. V.; Cador, O.; Golhen, S.; Ouahab, L.; Pavlishchuk, V. V. *Inorganic Chemistry* **2005**, *44*, 5903.

(41) Langley, S. K.; Chilton, N. F.; Moubaraki, B.; Murray, K. S. *Dalton Transactions* **2012**, *41*, 1033.

(42) Spek, A. *Journal of Applied Crystallography* **2003**, *36*, 7.

(43) Spek, A. *Acta Crystallographica Section D* **2009**, *65*, 148.

(44) Laye, R. H.; McInnes, E. J. L. *European Journal of Inorganic Chemistry* **2004**, *14*, 2811.

5. Complexes with more than seven metal centres

In the synthesis of SMMs increasing the number of metal centres within the complex is advantageous, as it has the potential to increase the spin ground state of the cluster, an important factor in whether or not a complex is an SMM is having a large spin ground state. However, the interaction between the metal centres must be taken into consideration.

There are several different cluster types that contain more than seven cobalt centres, one of the most common forms are linked cobalt cubanes, that form Co_8 and Co_{12} complexes, further structures are possible if the cubane building blocks are capped. Other structures involve expanded or overlapping versions of the well known Co_7 discs.[1]

A study has been carried out on cobalt-pivalate complexes which resulted in a series of complexes ranging from dinuclear Co^{II} species to tetradecanuclear cage cluster.[2] This study suggests a pattern to the formation of cubanes and higher nuclearity clusters from dimerisation of a cobalt dimer to stepwise addition of cubanes and capping atoms. Some forms which they suggest from their hypothesis are already known for cobalt, these are both Co_8 complexes, one a quadruply capped cubane[3] and the other a face-sharing triple cubane cluster.[4,5] Further examples include $[Co_{12}(OH)_6(O_2CCH_3)_6(mhp)_{12}]$ (Hmhp = 6-methyl-2-hydroxypyridine),[6] in this complex the metal centres form a centred pentacapped-trigonal prism polyhedron. This complex was further studied in 2000, and led to the synthesis of three related Co_{10} complexes.[7]

A tridecanuclear cluster can be formed, $[Co^{II}_{13}(mosao)_8(Hmosoa)_6][ClO_4]_4 \cdot 3DMF \cdot MeOH \cdot 3H_2O$ (H_2mosao = 3-methoxysalicyladoxime).[1] This complex could be described as two overlapping Co_7 moieties that share two atoms Co7 and Co8 (Figure 5-1), with an additional Co atom acting as a bridge between the two. The magnetic behaviour of this Co_{13} complex was studied down to 2 K and it was shown to exhibit antiferromagnetic coupling between the Co^{II} ions.[1] A similar complex[8] has also been synthesised using the ethoxy derivative of the ligand, $[Co^{II}_{13}(eosao)_8(Heosao)_6][ClO_4]_4$ (H_2eosao = 3-ethoxysalicylaldoxime), this complex is also found to have strong antiferromagnetic interactions.

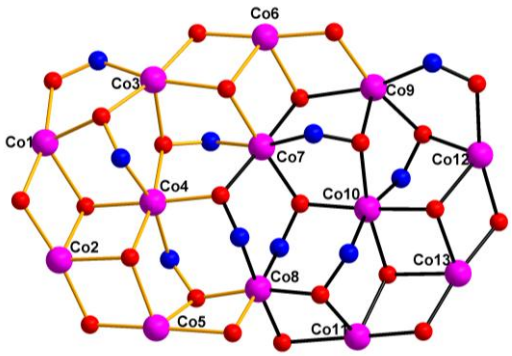

Figure 5-1 Structure of $[Co^{II}_{13}(eosao)_8(Heosao)_6][ClO_4]_4$ with overlapping Co_7 moieties highlighted.[9] Co pink; N blue; O red.

One of the more novel clusters that has been synthesised in recent years is a Co_{12} cluster, three cubanes are bridged by a central nitrate ligand, this complex displays SMM behaviour.[10] A complex with a similar structural motif was synthesised by Cooper *et al.*, in this example the bridging nitrate is replaced by a planar CO_3^{2-} ion, this complex was not found to display SMM behaviour.[11]

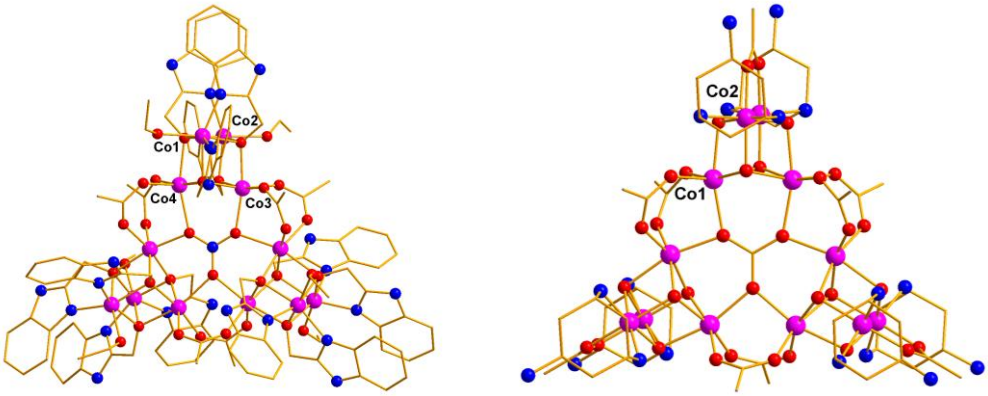

Figure 5-2 Structures of Co_{12} complexes, with central nitrate (left)[10] and central acetate (right),[11] unique cobalt ions only labelled. Co^{II} pink; O red; N blue

A Co_{10} complex has been synthesised which also contains the CO_3^{2-} ion. It appears that this ion is formed *in situ* and is required for cluster formation,[12] this complex also does not display SMM behaviour. However, a butterfly-like Co_{10} complex $[Co^{II}_6Co^{III}_4(OH)(X)(pa)_4(pdm)_6(pdmH)_2][ClO_4]_4$ (paH = phenylalinol, $pdmH_2$ = pyridine-2,6-diyldimethanol; X = OH, OMe), has been found to display slow relaxation of magnetisation.[13] More recently an unusual Co_{15} cluster has been synthesised, in which there is an μ_6-CO_3^{2-} anion, as previously this anion is found to be required for cluster formation and can be formed *in situ* however, the yield of the reaction can be improved by addition of carbonate to the reaction.[14] This complex has the formula $[Co^{II}_{15}(H_{1.33}L)_6(\mu_6\text{-}CO_3)_6\text{-}(\mu_3\text{-}OMe)_2(\mu\text{-}dmf)_3(dmf)_5(MeOH)_{0.5}(H_2O)_{2.5}]$ (where H_4L = 6,6′-methylenebis(4-(*tert*-butyl)-2-(hydroxymethyl)-phenol) and the irregularly shaped core is shown in Figure 5-3. Magnetic susceptibility measurements of this complex show that it does not display SMM behaviour and suggests the interactions between Co^{II} ions are antiferromagnetic.

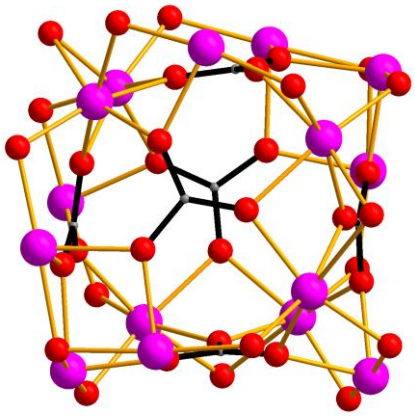

Figure 5-3 Metallic core of $[Co^{II}_{15}(H_{1.33}L)_6(\mu_6\text{-}CO_3)_6\text{-}(\mu_3\text{-}OMe)_2(\mu\text{-}dmf)_3(dmf)_5(MeOH)_{0.5}(H_2O)_{2.5}]$[14] with the position of $\mu_6\text{-}CO_3^{2-}$ highlighted in black. Co^{II} pink; O red; C grey.

One of the largest cobalt clusters is $[Co^{II}_{24}(\mu_3\text{-}OH)_{14}(\mu\text{-}OH)_4(\mu_3\text{-}OMe)_2(\mu_3\text{-}Cl)_2Cl_4(mhp)_{22}]$ (Hmhp = 2-methyl-6-hydroxypyridine). This structure is based on $[Co_3(OH)_4]^{2+}$ cubes with one corner missing, though further studies on this complex would be needed to confirm if this complex has any SMM behaviour.[15]

Although many examples of cobalt clusters exist, many of them do not display any SMM behaviour. One way to increase the potential for SMM activity in cobalt clusters would be to introduce another metal into the cluster, either another transition metal (replacing any Co^{III} ions with other M^{III} ions, which are not diamagnetic) or a lanthanide (Ln). The incorporation of lanthanides into 3*d* metal clusters has attracted interest due to the large and sometimes anisotropic magnetic moments they contribute. The majority of 3*d*-4*f* clusters behaving as SMMs have Cu, Mn or Fe as the 3*d* metal and a wide range of structures have been reported, from simple linear complexes[16] to more unusual complexes with high nuclearity.[17-19] Of the complexes with Co that have been reported, a range of linear trinuclear complexes $Co^{II}_2Ln^{III}$ (Ln = Gd, Tb, Dy, Ho) have been shown to have SMM properties.[20,21]

Gadolinium(III) has a large isotropic S_i = 7/2 ground state, and can be used to increase the spin ground state of a cluster, if the Gd couples ferromagnetically to Co^{II}, giving the favourable combination of large spin ground state and magnetic anisotropy. Several examples of tetra-nuclear Co^{II}-Gd^{III} complexes have shown SMM behaviour.[22] However others examples exist which do not display SMM properties,[23] whether or not the Co^{II} ion is high-spin or low-spin is an important factor.[24] Erbium(III) has been less studied though some examples of single-ion complexes that display slow relaxation of magnetisation do exist.[25,26] A search of the CSD[27,28] reveals there are only three structures containing cobalt and erbium. Two of these are extended network systems[29,30] and the third is a tetra-nuclear complex with the formula $[Co^{II}_2Er^{III}_2(O_2CCMe_3)_8(C_9H_7N)_2(NO_3)_2]$ (Figure 5-4).[31] Magnetic studies of this complex concluded that there are weak antiferromagnetic interactions between the metal ions.

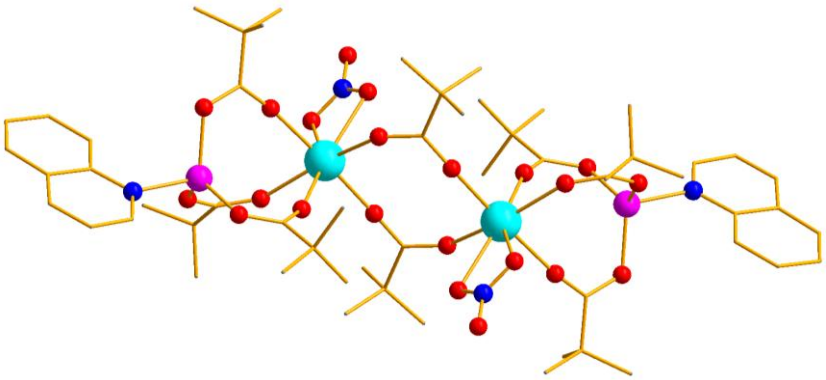

Figure 5-4 Structure of $[Co^{II}_2Er^{III}_2(O_2CCMe_3)_8(C_9H_7N)_2(NO_3)_2]$[31] Er^{III} cyan; Co^{II} pink; O red; N blue.

A series of closely isostructural complexes $\{Co^{II}_2Co^{III}_4Ln^{III}_4\}$ (Ln = Y, Gd and Dy) provide a platform to study the effect of changing the lanthanide ion have also been synthesised,[32] and will be discussed in more detail in Section 5.4.2.

5.1 Complex with eight cobalt centres

5.1.1 Synthesis of $[Co^{II}_4Co^{III}_4(btpH_2)_4Cl_2(NO_3)_2]$ (17)

($btpH_6$ = bis-tris propane)

$Co(NO_3)_3.6H_2O$ (0.87 g, 2.99 mmol) and $CoCl_2.6H_2O$ (0.24 g, 1.01 mmol) were dissolved in 10 mL of MeOH, bis-tris propane (0.57 g, 2.02 mmol) was then added followed by $NMe_4OH.5H_2O$ (0.15g, 0.83 mmol). The reaction was stirred overnight at room temperature, it was then filtered and the filtrate stored in a sealed vial. After approximately three weeks in a sealed vial, purple crystals formed in 4% yield. Air dried crystals analyse as $\mathbf{C_{44}H_{109}N_{10}O_{40.5}Cl_2Co_8}$, analysis (%) calc. (found) C, 26.84 (26.34); H, 5.58 (4.97); N, 7.11 (7.62). Selected IR data: υ = 3414, 3350, 3173, 2978, 2872, 1637, 1483, 1450, 1394, 1383, 1315, 1147, 1078, 1018, 987, 974, 871, 827, 794, 740, 694, 682, 661, 611, 601 cm^{-1}.

5.1.2 Discussion of crystal structure

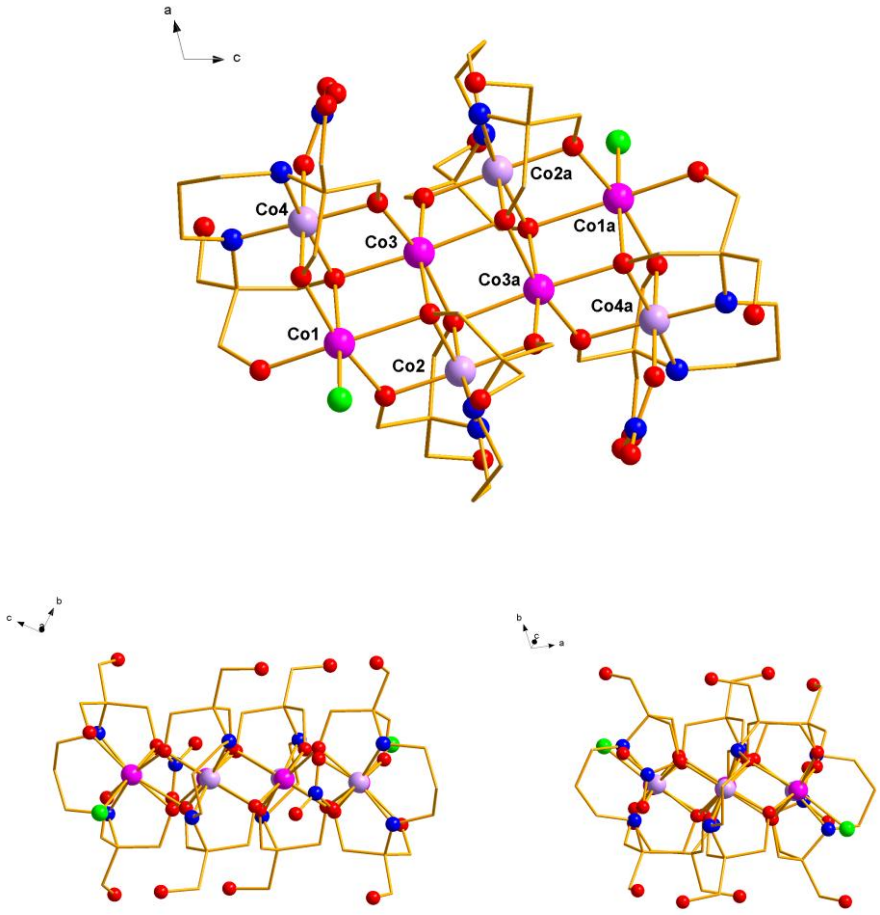

Figure 5-5 Structure of 17; (H atoms omitted for clarity) viewed along the *b*-axis and approximate *a*- and *c*-axes. Co^{II} pink; Co^{III} lilac; O red; N blue; Cl bright green.

Four Co^{III} and four Co^{II} ions are present in this complex, linked by four btp ligands, with two nitrate and two Cl groups as terminal ligands. All metal centres display distorted octahedral geometry. The most distorted are Co1 and Co3 where the angle between the opposite ligand donor atoms is only 169°. Co^{III} ions have an $\{N_2O_4\}$ ligand donor set, where for Co2, the four oxygen donors come from the btp ligand. Co4 has three oxygen donors that come from the btp ligand and one from a monodentate nitrate group. The central Co3 ion has an $\{O_6\}$ ligand donor set contributed by three btp ligands. Co1 has an $\{O_5Cl\}$ ligand environment, where the oxygen donors are provided by two different ligands.

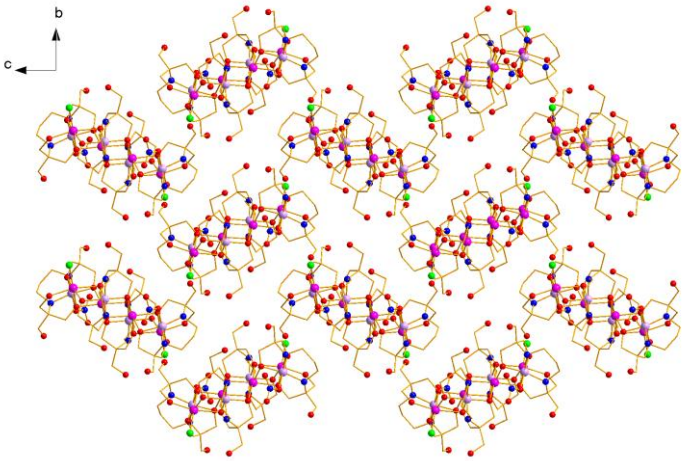

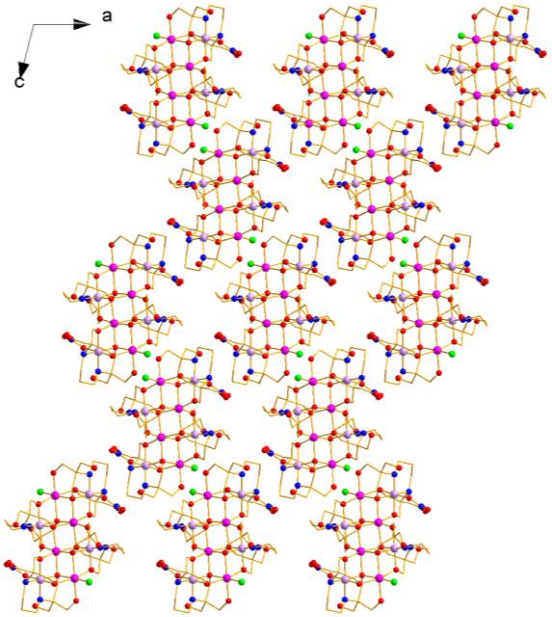

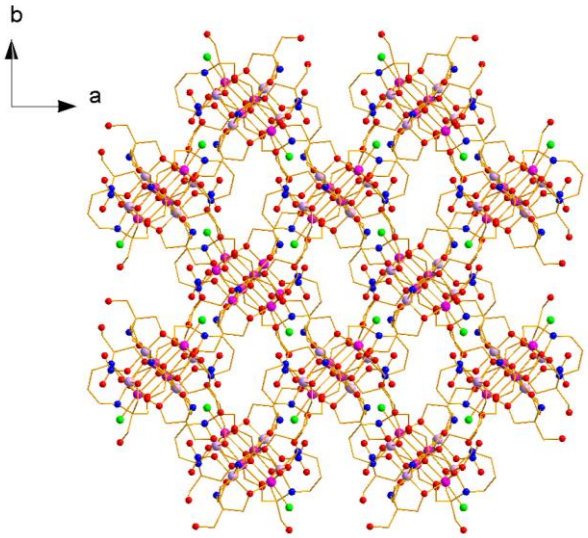

Figure 5-6 Packing diagrams of 17 viewed along *a*-, *b*-, and *c*-axes.

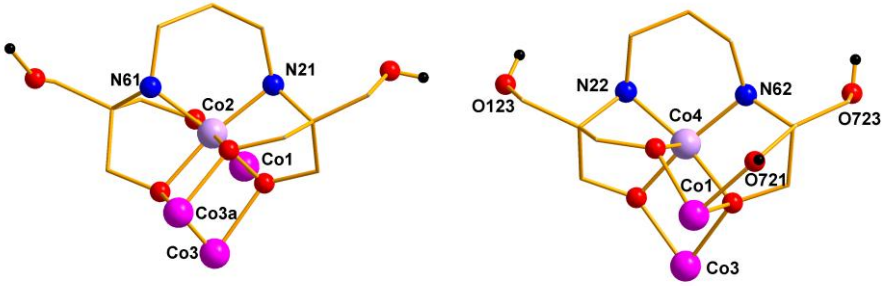

$\eta^1:\eta^1:\eta^2:\eta^2:\eta^3:\eta^3:\mu_4$ (a) $\eta^1:\eta^1:\eta^1:\eta^2:\eta^2:\eta^3:\mu_3$ (b)

Figure 5-7 Different binding modes of BTP ligand in 17, (the protons shown on the O123 and O723 are half occupancy).

There are two different binding modes of btp present in the complex. Type (a) bridges between three unique metal centres and one symmetry equivalent metal centre (Figure 5-7). Two ligand arms remain unbound and protonated, two bridge between three metal centres, and two bridge between two metal centres. This ligand has an overall 4- charge. In type (b) the ligand bridges between three different metal centres. Two of the oxygen donors bridge between two metal centres, a further one bridges between three metal centres and lastly one which remains fully protonated binds to only one metal centre. The two unbound arms of this ligand share a single proton. The shared protons are between atoms O123 and O723 on neighbouring clusters, the distance between these atoms is only 2.53 (2) Å (Figure 5-8).

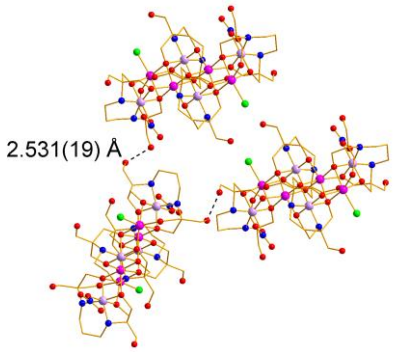

Figure 5-8 Diagram showing distance between O atoms that share a proton.

The binding mode type (a) exhibited in this complex has been found in the following complex $[Co_5(btpH_2)_2(acac)_3(MeOH)]$.[33] Type (b) is very similar to the second type of binding mode found in the same complex however in complex **17** one bridging arm of the ligand remains protonated. Other binding modes for bis-tris propane have been seen in other polynuclear complexes, examples where it binds six metal centres,[34] five metal centres[35], and four metal centres (in a different way to that seen here).[33]

Due to poor yields magnetic measurements could not be carried out on this complex.

Table 5-1 Crystallographic data table for 17.

Empirical Formula	$C_{44}H_{88}Co_8Cl_2N_{10}O_{30}$
Fw (g mol^{-1})	1779.6
Crystal system	Monoclinic
Space group	$P2_1/n$
a (Å)	13.429(1)
b (Å)	13.088(1)
c (Å)	20.726(2)
β (deg)	104.291(5)
V (Å^3)	3530.1(6)
Z	2
T (K)	100(2)
λ (Å)	0.71073
ρ_{calcd} (Mg m^{-3})	1.674
μ (mm^{-1})	1.992
R_1[a]	0.1194
wR_2[b]	0.2261*
Goodness of fit	1.043

*There was some disordered solvent present in the crystal structure of this complex, PLATONsqueeze[36,37] was applied to remove this, it was found that there were 219 unassigned electrons per unit cell and a void space of 627.4 Å^3, this could equate to 8 molecules of MeOH and 8 molecules of H_2O. The high R-factor is due to poor crystal quality.

[a] $R_1 = \Sigma \left| |F_o| - |F_c| \right| / \Sigma |F_o|$ [b] $wR_2 = \left[\Sigma \left[w\left(F_o^2 - F_c^2\right)^2 \right] - \Sigma \left[\left(F_o^2\right)^2 \right] \right]^{1/2}$ where $w = 1/\left[\sigma^2\left(F_o^2\right) + \left(0.2P\right)^2\right]$ and $P = \left[F_o^2 + 2F_c^2\right]/3$

Table 5-2 Selected metal-ligand bond lengths for 17.

Bond	Distance (Å)	Bond	Distance (Å)
Co1–Cl1	2.337(3)	Co3–O712a	2.183(6)
Co1–O111	2.273(6)	Co3–O112a	1.999(7)
Co1–O711	1.980(7)	Co3–O111	2.102(7)
Co1–O121	2.033(8)	Co3–O712	2.155(7)
Co1–O721	2.105(8)	Co3–O122	2.051(7)
Co1–O722	2.194(8)	Co3–O722	2.123(7)
Co2–N21	1.90(1)	Co4– N22	1.95(1)
Co2–N61	1.94(1)	Co4–N62	1.934(8)
Co2–O111	1.895(7)	Co4–O1	1.987(8)
Co2–O112	1.879(6)	Co4–O121	1.851(8)
Co2–O711	1.895(7)	Co4–O122	1.880(7)
Co2–O712	1.918(7)	Co4–O722	1.899(7)

Table 5-3 Selected bond angles for 17.

Atoms	Angle (°)
Co1-O111-Co2	95.4(3)
Co1-O711-Co2	105.9(3)
Co1-O111-Co3	92.4(2)
Co1-O722-Co3	94.1(3)
Co1-O121-Co4	103.1(3)
Co1-O722-Co4	95.8(3)
Co3-O111-Co2	97.5(3)
Co3a-O112-Co2	102.7(3)
Co3-O122-Co4	98.5(3)
Co3a-O712-Co2	95.0(3)
Co3-O712-Co2	95.1(3)
Co3-O712-Co3a	92.6(2)
Co3-O722-Co4	95.5(3)

Table 5-4 BVS results[38] for Co ions in 17.

Atom	Co^{II}	Co^{III}
Co1	2.073	2.157
Co2	3.922	3.972
Co3	2.008	2.052
Co4	3.803	3.853

The underlined value is that closest to the charge for which it was calculated, overestimation for Co^{III} will be discussed in appendix one.

5.2 Complex with ten cobalt centres

5.2.1 Synthesis of $[Co^{II}_6Co^{III}_4(btpH_2)_4Cl_8]$(18)

$CoCl_2.6H_2O$ (0.95 g, 3.99 mmol) was added to 10 mL of MeOH, bis-tris propane (0.57g, 2.02 mmol) was then added followed by $NMe_4OH.5H_2O$ (0.15 g, 0.83 mmol). The reaction was stirred overnight and then filtered. After approximately three weeks in a sealed vial, purple crystals formed in 12% yield of monoclinic complex. Air dried crystals analyse as $\mathbf{C_{45.5}H_{98}N_8O_{27.5}Cl_8Co_{10}}$, analysis (%) calc. (found) C, 26.61 (26.40); H, 4.47 (4.77); N, 5.64 (5.41). Selected IR data: υ = 3379, 3153, 2918, 2868, 1637, 1481, 1452, 1429, 1377, 1294, 1257, 1220, 1149, 1080, 1051, 1020, 989, 935, 869, 844, 794, 742, 686, 663, 615, 603 cm^{-1}.

Synthesis of **18a**·4MeOH (orthorhombic form of **18**), provided by Dr Milway.

Bis-tris propane (0.288 g, 1.02 mmol) was suspended in MeOH (30 mL) and stirred at ambient temperature for 1 hour. $CoCl_2.6H_2O$ (0.485 g, 2.04 mmol) was added and the clear pink solution was stirred at ambient temperature for 30 hours. The resulting clear purple solution was filtered. Purple crystals, suitable for single crystal X-ray diffraction form in 15% yield over several days. Air dried crystals analyse as $\mathbf{C_{44}H_{95}N_8O_{27.5}Cl_8Co_{10}}$, analysis (%) calc. (found) C, 25.79 (25.83); H, 4.67 (4.45); N, 5.47(5.36); Cl, 13.84 (13.36).

5.2.2 Discussion of crystal structure

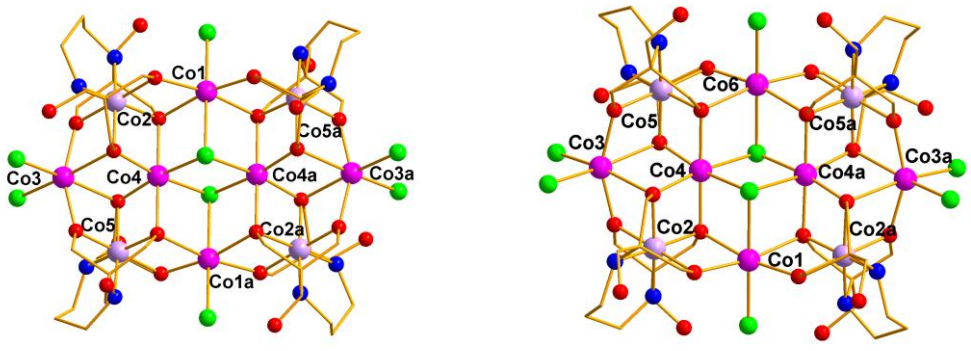

Figure 5-9 Comparison of structures of 18 (disorder in unbound OH group has been omitted) and 18a, (H atoms omitted for clarity) Co^{II} pink; Co^{III} lilac; O red; N blue; Cl bright green.

In both complexes there are six Co^{II} centres and four Co^{III} centres, the metal centres are arranged in a plane and all have distorted octahedral arrangement. The overall configuration of the complex could be described as two overlapping Co7 discs. The ligand in this complex is again bis-tris propane, with chloride acting as a bridging and terminal ligand. In **18** there are 5 independent Co ions and they all have symmetry equivalents, and in **18a** there are 6 different Co ions, Co2, Co3,

Co4 and Co5 have symmetry equivalents; Co1 and Co6 do not. This difference is due to the different space groups, *C*2/*c* which has a two-fold axis and a two-fold screw axis, and *Pbnm* which has a two-one screw axis with a centre of inversion on the axis and two glide planes. All Co^{II} ions have an $\{O_4Cl_2\}$ ligand environment. For Co1 and Co6, the Cl are in the axial positions and for Co3 and Co4 (and their symmetry equivalents) they are equatorial, and the octahedral arrangement is much more distorted in these cases. The four Co^{III} ions have an $\{N_2O_4\}$ ligand donor set, each of these ions is encapsulated by one BTP ligand. The charge on the metals was assigned on the basis of bond valence sum calculations, consideration of bond lengths and charge balance.

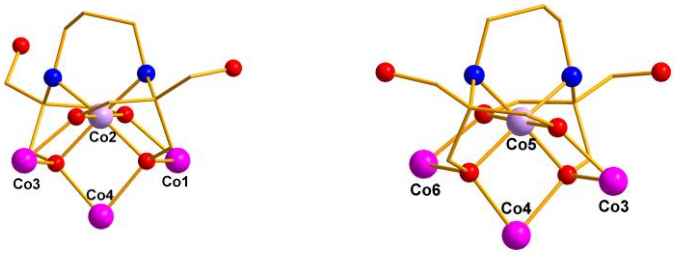

Figure 5-10 Binding mode $\eta^1:\eta^1:\eta^2:\eta^2:\eta^3:\eta^3:\mu_4$ of btp in 18a.

This complex was isolated in two different space groups, one monoclinic (**18**) and one orthorhombic (**18a**). The orthorhombic example was synthesised by Dr Milway, and is included here for comparison, and due to the fact the original reaction method which synthesised the complex in the monoclinic space group was found to give poorer crystal quality. The monoclinic example shows disorder in the unbound oxygen of the two ligands and their symmetry equivalents and in the central carbon of the propane backbone of one ligand and its symmetry equivalent. The binding mode (Figure 5-10) for each of the ligands is the same in this complex and is also the same as the first binding mode described for complex **17**.

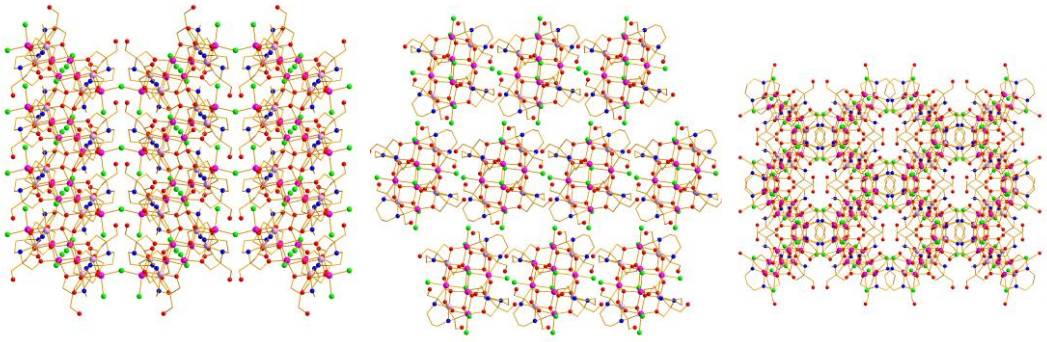

Figure 5-11 Packing diagram for monoclinic complex 18 viewed along *a*-, *b*- and *c*-axes.

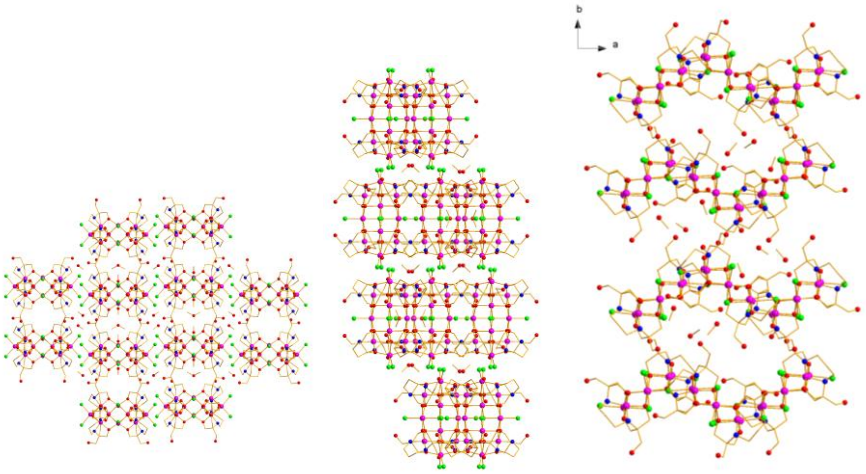

Figure 5-12 Packing diagram for orthorhombic complex 18a viewed along *a*-, *b*-, and *c*-axes.

There are four molecules of MeOH found in the lattice for **18a**, these are found in the small pockets between complexes which can be seen in Figure 5-12 when viewing along the *c*-axis. There are hydrogen bond interactions between the unbound ligand arms and the chloride ligands in a complex and also between neighbouring complexes. Within one complex the unbound ligand arm with O113 is hydrogen bonded to Cl1 (O(H)···Cl 3.582(4) Å), on the opposite side of the complex the unbound ligand arm with O723 has a long interaction with Cl1′, this time on a neighbouring complex, (O(H)···Cl 3.721(4) Å). There are also interactions between O723 and Cl6 (on the same complex) and O113 and Cl6 (on neighbouring complexes). There are also hydrogen bond interactions between O123 and Cl3 (O(H)···Cl 3.176(6) Å) (Figure 5-13). The nearest Co···Co distance between neighbouring complexes is between Co6 and Co1′ and is 9.425(1) Å.

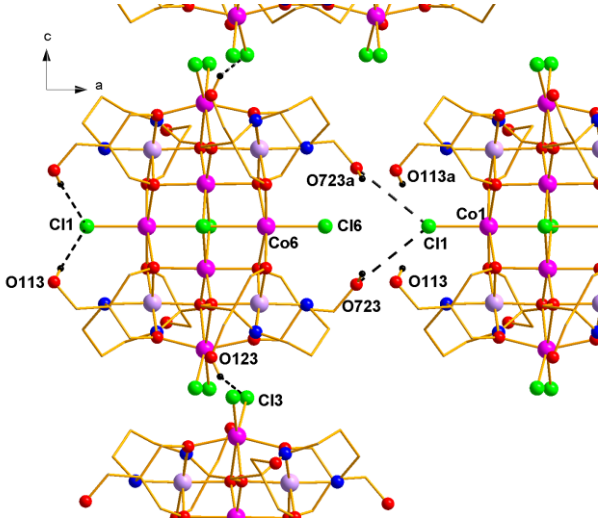

Figure 5-13 Diagram showing hydrogen bonding interactions within and between complexes for 18a.

Table 5-5 Data for crystal structure determination of complexes 18 and 18a·4MeOH.

Empirical Formula	$C_{44}H_{88}Co_{10}Cl_8N_8O_{24}$ (**18**)	$C_{48}H_{104}Co_{10}Cl_8N_8O_{28}$ (**18a·4MeOH**)
Fw (g mol^{-1})	1986.18	2114.35
Crystal system	Monoclinic	Orthorhombic
Space group	*C*2/*c*	*Pbnm*
a (Å)	21.418(3)	13.6466(1)
b (Å)	13.920(2)	21.1881(2)
c (Å)	27.357(5)	26.6690(2)
β (deg)	108.914(5)	90
V (Å^3)	7716(2)	7711.2(1)
Z	4	4
T (K)	100(2)	100(2)
λ (Å)	0.71073	0.71073
ρ_{calcd} (Mg m^{-3})	1.704	1.853
μ (mm^{-1})	2.437	2.451
R_1[a]	0.0617	0.0561
wR_2[b]	0.0910	0.0997
Goodness of fit	1.005	1.038

PLATON squeeze[36,37] was applied to complex **18**, it found a potential solvent accessible void of 1446.7 Å^3 and 473 electrons per unit cell, this could equate to 16 molecules of MeOH and 16 of water.

[a] $R_1 = \Sigma \left| |F_o| - |F_c| \right| / \Sigma |F_o|$ [b] $wR_2 = \left[\Sigma \left[w\left(F_o^2 - F_c^2\right)^2 \right] - \Sigma \left[\left(F_o^2\right)^2 \right] \right]^{1/2}$ where $w = 1/\left[\sigma^2\left(F_o^2\right) + \left(0.2P\right)^2\right]$ and $P = \left[F_o^2 + 2F_c^2\right]/3$

Table 5-6 Results of BVS calculations[38] for Co atoms in 18 and 18a.

Complex **18**	Co^{II}	Co^{III}	Complex **18a**	Co^{II}	Co^{III}
Co1	<u>1.896</u>	1.993	Co1	<u>1.881</u>	1.979
Co2	3.884	<u>3.933</u>	Co2	3.794	<u>3.843</u>
Co3	<u>1.970</u>	2.081	Co3	<u>1.891</u>	1.995
Co4	<u>1.992</u>	2.097	Co4	<u>1.981</u>	2.083
Co5	3.872	<u>3.921</u>	Co5	3.807	<u>3.856</u>
			Co6	<u>1.812</u>	1.910

The underlined value is that closest to the charge for which it was calculated, overestimation for Co^{III} will be discussed in appendix one.

Table 5-7 Selected metal-ligand bond lengths for 18.

Bond	Distance (Å)	Bond	Distance (Å)
Co1–O122	2.198(4)	Co3–O712	2.350(4)
Co1–O721	2.061(4)	Co3–O121	1.982(4)
Co1–Cl1	2.404(2)	Co3–O722	2.334(4)
Co1– Cl2	2.505(2)	Co4–Cl2	2.411(2)
Co1–O111	2.241(4)	Co4–Cl2	2.427(2)
Co1–O711	2.027(4)	Co4–O111	2.108(4)
Co2–O111	1.925(4)	Co4–O712	2.090(4)
Co2–O112	1.878(4)	Co4–O122	2.117(4)
Co2–N21	1.921(5)	Co4–O722	2.084(4)
Co2–N61	1.921(6)	Co5–N22	1.922(5)
Co2–O711	1.893(4)	Co5–N62	1.914(5)
Co2–O712	1.909(4)	Co5–O121	1.882(4)
Co3–Cl3	2.368(2)	Co5–O122	1.923(4)
Co3–Cl4	2.400(2)	Co5–O722	1.906(4)
Co3–O112	1.998(4)	Co5–O721	1.906(4)

Table 5-8 Selected bond angles for complex 18.

Atoms	Angle (°)	Atoms	Angle (°)
Co1-Cl2-Co4	84.55(6)	Co4-O122-Co5	93.2(2)
Co1-Cl2-Co4a	84.29(6)	Co1-O711-Co2	105.0(2)
Co4-Cl2-Co4a	88.24(6)	Co3-O712-Co2	94.9(2)
Co1-O111-Co2	96.3(2)	Co4-O712-Co2	93.8(2)
Co1-O111-Co4	99.4(2)	Co4-O712-Co3	92.7(2)
Co4-O111-Co2	92.7(2)	Co1a-O721-Co5	102.2(2)
Co3-O112-Co2	108.7(2)	Co3-O722-Co5	95.2(2)
Co3-O121-Co5	108.9(2)	Co4-O722-Co3	93.3(2)
Co1a-O122-Co4	99.7(2)	Co4-O722-Co5	94.8(2)
Co1a-O122-Co5	96.9(2)		

Table 5-9 Selected metal-ligand bond lengths 18a.

Bond	Distance (Å)	Bond	Distance (Å)
Co1–Cl1	2.398(2)	Co4–Cl2	2.442 (1)
Co1– Cl2	2.505 (2)	Co4–Cl5	2.429(1)
Co1–O111	2.219(3)	Co4–O111	2.096(3)
Co1–O711	2.039(3)	Co4–O712	2.090(3)
Co1–O111a	2.219(3)	Co4–O121	2.111(3)
Co1–O711a	2.039(3)	Co4–O721a	2.082(3)
Co2–N21	1.950(4)	Co5–N22	1.913(4)
Co2–N61	1.913 (4)	Co5–N62	1.942(4)
Co2–O111	1.915(3)	Co5–O121	1.919(3)
Co2–O112	1.890(3)	Co5–O122	1.899(3)
Co2–O711	1.900(3)	Co5–O722	1.888(3)
Co2–O712	1.920(3)	Co5–O721a	1.919(3)
Co3–Cl3	2.440(1)	Co6–Cl5	2.562 (2)
Co3–Cl4	2.380(1)	Co6–Cl6	2.371(2)
Co3–O112	1.983(3)	Co6–O122	2.029(3)
Co3–O712	2.358(3)	Co6–O721	2.251(3)
Co3–O121	2.369(3)	Co6–O122a	2.029(3)
Co3–O722	2.005(3)	Co6–O721a	2.251(3)

Table 5-10 Selected bond angles 18a.

Atoms	Angle (°)	Atoms	Angle (°)
Co1-Cl2-Co4	84.32(5)	Co4-O111-Co2	93.6(1)
Co1-Cl2-Co4a	84.32(5)	Co4-O121-Co3	92.2(1)
Co1-O111-Co2	95.9(1)	Co4-O121-Co5	93.2 (1)
Co1-O111-Co4	100.6(1)	Co4-O712-Co2	93.7(1)
Co1-O711-Co2	102.7(2)	Co4-O712-Co3	93.0 (1)
Co3-O112-Co2	110.1(2)	Co4a-O721-Co5a	94.0(1)
Co3-O121-Co5	95.2(1)	Co6-Cl5-Co4	84.3 (5)
Co3-O712-Co2	95.3(1)	Co6-Cl5-Co4a	84.31(5)
Co3-O722-Co5	109.6(2)	Co6-O122- Co5	104.3(2)
Co4-Cl2-Co4a	88.04(6)	Co6-O721-Co4a	100.2(1)
Co4-Cl5-Co4a	88.64(6)	Co6-O721-Co5a	95.8(1)

5.2.3 Magnetic Susceptibility Measurements for (18a)

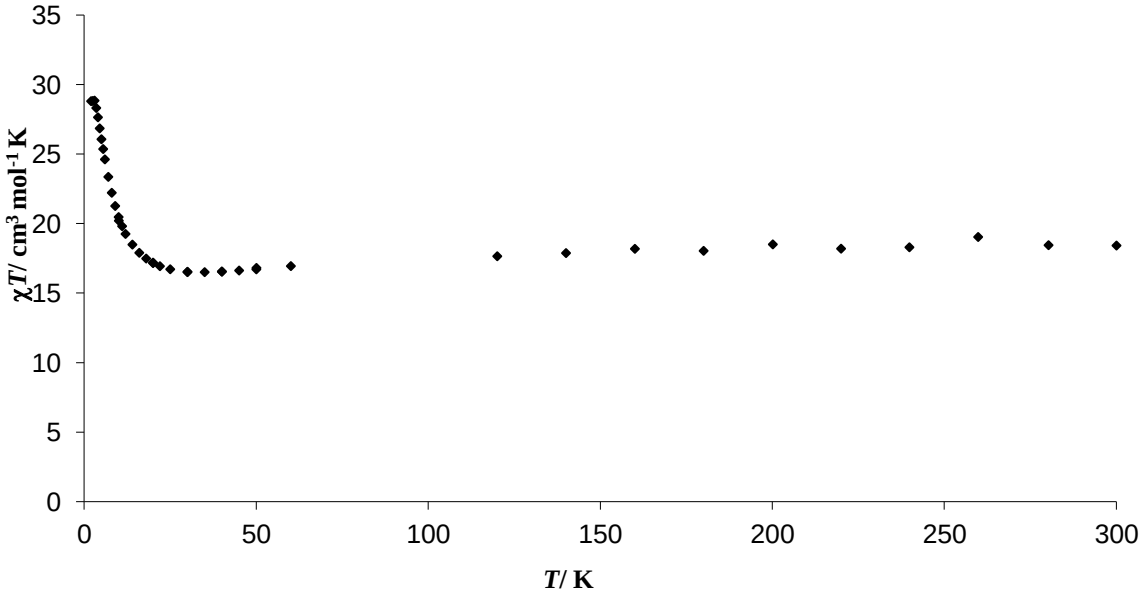

Figure 5-14 Temperature dependence of χT measured for 18a from 1.8-300 K in an applied field of 1000 G. These data was collected at Manchester and some temperatures were not measured.

Magnetic susceptibility measurements were carried out on an air dried sample of **18a** which analysed as **18a·4H$_2$O**. The χT value at 300 K is 18.4 cm^3 mol^{-1} K (Figure 5-13), which is consistent for six uncoupled Co^{II} ions with g = 2.56. There is a gradual decrease of χT to 16.5 cm^3 mol^{-1} K at approximately 30 K, there is then a sharp increase to 28.8 cm^3 mol^{-1} K at 2 K. The value of χT at 2 K is consistent with an effective spin ground state of S' = 3 with g = 4.3 arising from ferromagnetic coupling between six effective S' = ½ Co^{II} centres. The magnetisation was measured as a function of the applied field at 4 K and 2 K (Figure 5-14). At 7 T, M/ Nβ equals 12.9, consistent with S'= 3 and g > 4, this is in agreement with the χT data.

The bridging angles between Co^{II} ions in this complex range from 84°–100° suggesting there could be competing interactions between the Co^{II} centres. The more acute angles (84°–88°) occur when Cl is the bridging atom and the larger angles (92°–100°) are bridged by O atoms. However, from the magnetic data it can be seen that ferromagnetic interactions are dominant; the largest bridging angles (

Table **5-10**) which would perhaps promote antiferromagnetic interactions through O occur where there is also an acute bridging angle through Cl.

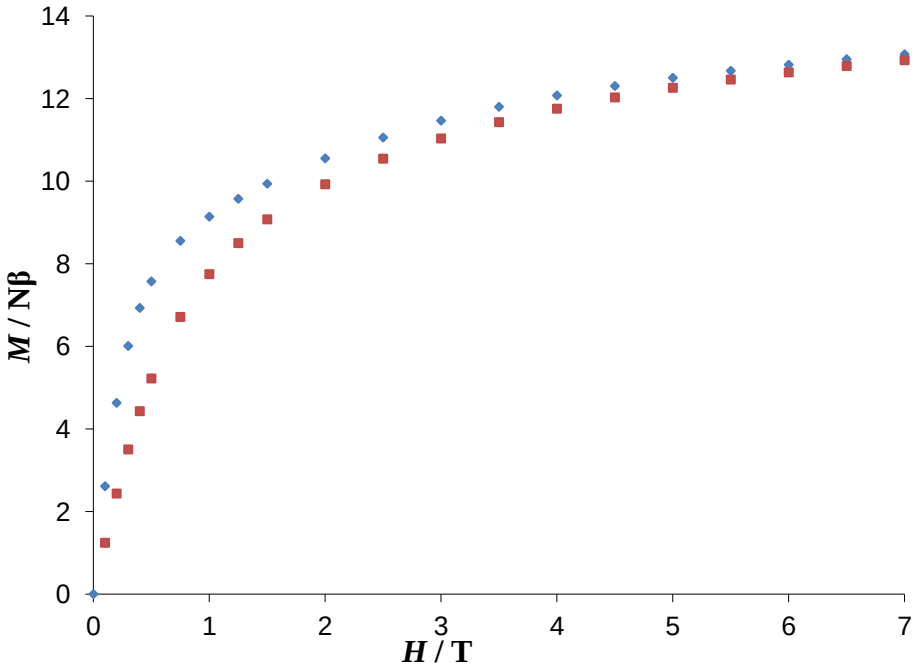

Figure 5-15 Magnetisation *vs.* field for 18a measured at 2 K (◆) and 4 K (■).

5.3 "Double disc" complex

5.3.1 Synthesis of $[Co_{12}Mn_2(NO_3)_4(dea)_{12}Cl_2][Cl]_2[NO_3]_2$ (19)

(where $deaH_2$ = diethanolamine)

$CoCl_2.6H_2O$ (0.24 g, 1.01 mmol) and $Mn(NO_3)_2.4H_2O$ (0.25 g, 1.00 mmol) were dissolved in 20 mL of a 1:1 solution of MeOH and 2-propanol. Diethanolamine (0.10 mL, 1.04 mmol) was added followed by $NMe_4OH.5H_2O$ (0.18 g, 1.00 mmol). The reaction was stirred overnight at room temperature, then filtered to remove a small amount of green precipitate and stored in an open vial, small dark blue-green crystals form after approximately one week in approximately 44% yield. Air dried crystals analyse as $\mathbf{C_{55}H_{136}N_{18}O_{49}Cl_4Co_{11.4}Mn_{2.6}}$, analysis (%) calc. (found) C, 23.67 (23.07); H, 4.91 (4.74); N, 9.04 (8.49); Cl, 5.08 (5.05); Co, 24.07 (23.43); Mn, 5.12 (4.88). Selected IR data: υ = 3390, 3203, 3136, 2935, 2872, 1635, 1469, 1448, 1311, 1278, 1147, 1107, 1062, 1037, 887, 827, 808, 783, 694, 626 cm^{-1}.

5.3.2 Discussion of crystal structure of $[Co_{12}Mn_2(NO_3)_4(dea)_{12}Cl_2][Cl]_2[NO_3]_2$ (19)

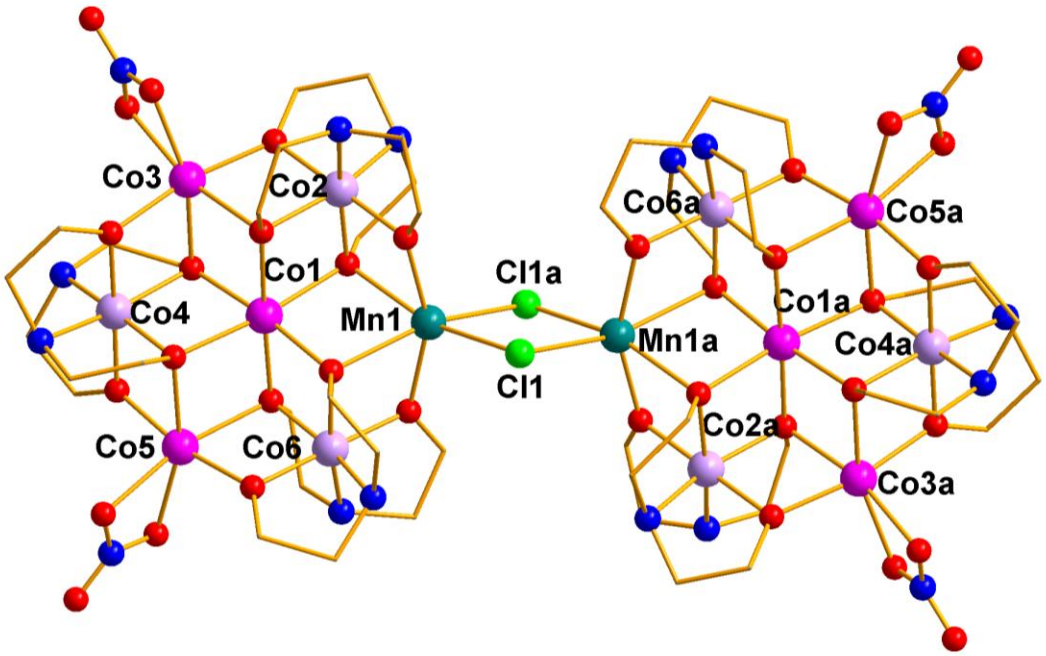

Figure 5-16 Structure of 19 Co^{II} pink; lilac; Mn^{II} teal; Cl bright green; O red; N blue (H atoms omitted for clarity)

This complex is related to those discussed in Chapter four, Sections 4.2.2.2 and 4.3.2.2; it consists of two seven metal centre discs linked by two chloride bridges. However, this complex has a unique structural motif, and each individual disc consists of six cobalt ions and one manganese ion. The outer Co^{II} ions have an $\{O_6\}$ ligand environment, provided by a bidentate nitrate anion and

four diethanolamine ligands arranged in a distorted octahedral arrangement. The central Co^{II} ions of each disc (Co1), has an $\{O_6\}$ ligand environment from six diethanolamine ligands each providing one oxygen atom. The Co^{III} ions are surrounded by two diethanolamine ligands in a distorted octahedral arrangement and have a $\{N_2O_4\}$ ligand donor set. The Mn^{II} ion was assigned on the basis of BVS results and metal analysis. This ion has an $\{O_4Cl_2\}$ ligand environment in a distorted octahedral arrangement, the bridging chloride ligands are in one plane, with the plane of the two oxygens bridging to Co1 offset approximately 30°; the angle between the other oxygen ligands is approximately 157°. The metals were assigned on the basis of bond lengths, consideration of charge balance and BVS calculations.[38]

Microanalysis data suggests that the structure may not be as simple as first thought. The results of metal analysis suggest that there may be some mixing of Mn^{II} into Co^{II} sites within the complex. The complex has an overall 4+ charge that is balanced by anions in the lattice, from the crystallographic data one unbound chloride anion has been modelled in the asymmetric unit which equates to two per cluster. This anion can be seen in the packing diagram (Figure 5-18) in the spaces between complexes, when viewed along the *a*-axis. The remaining 2- charge on the complex must be balanced by further anions which can not be modelled from the crystallographic data.

PlatonSQUEEZE[36,37] was applied to the data and suggests that the other anions could be found within the remaining disordered electron density. There is a potential solvent accessible void of 1923.1 $Å^3$ with 459 electrons per cell not modelled. Chloride analysis suggests that not all the anions within the lattice are chloride, if we assume two anions are nitrate groups and the remaining two are chloride reasonable agreement is found between the theoretical formula and the analytical results. It is particularly difficult to differentiate between cobalt and manganese using typical single crystal X-ray diffraction experiments due to their similar atomic numbers; in this case bond valence sum calculations (Table 5-13) give reasonably clear results allowing the assignment of the metal ions. ICP metal analysis was also carried out to confirm the assignment, and showed that there is some small mixing of the metal sites ($Co_{11.4}Mn_{2.6}$).

The closest Co···Co distance between neighbouring clusters is 7.552(2) Å between Co3 and Co4′, the closest distance between Co^{II} ions on neighbouring complexes is Co3···Co5′ 8.108(3) Å. There are hydrogen bonding interactions between the unbound Cl anion (and symmetry equivalents) and the complex of approximately 3.2 Å (Figure 5-17).

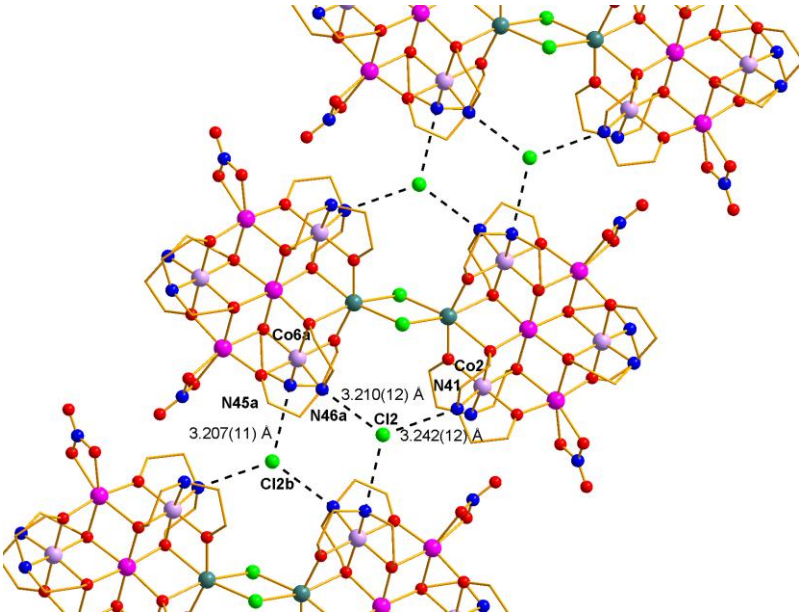

Figure 5-17 Hydrogen bonding between unbound Cl anion and complexes. Symmetry equivalents are labelled a and b; a = (1-x, 1-y, 1-z), b = (-0.5+x, 0.5-y, 0.5+z).

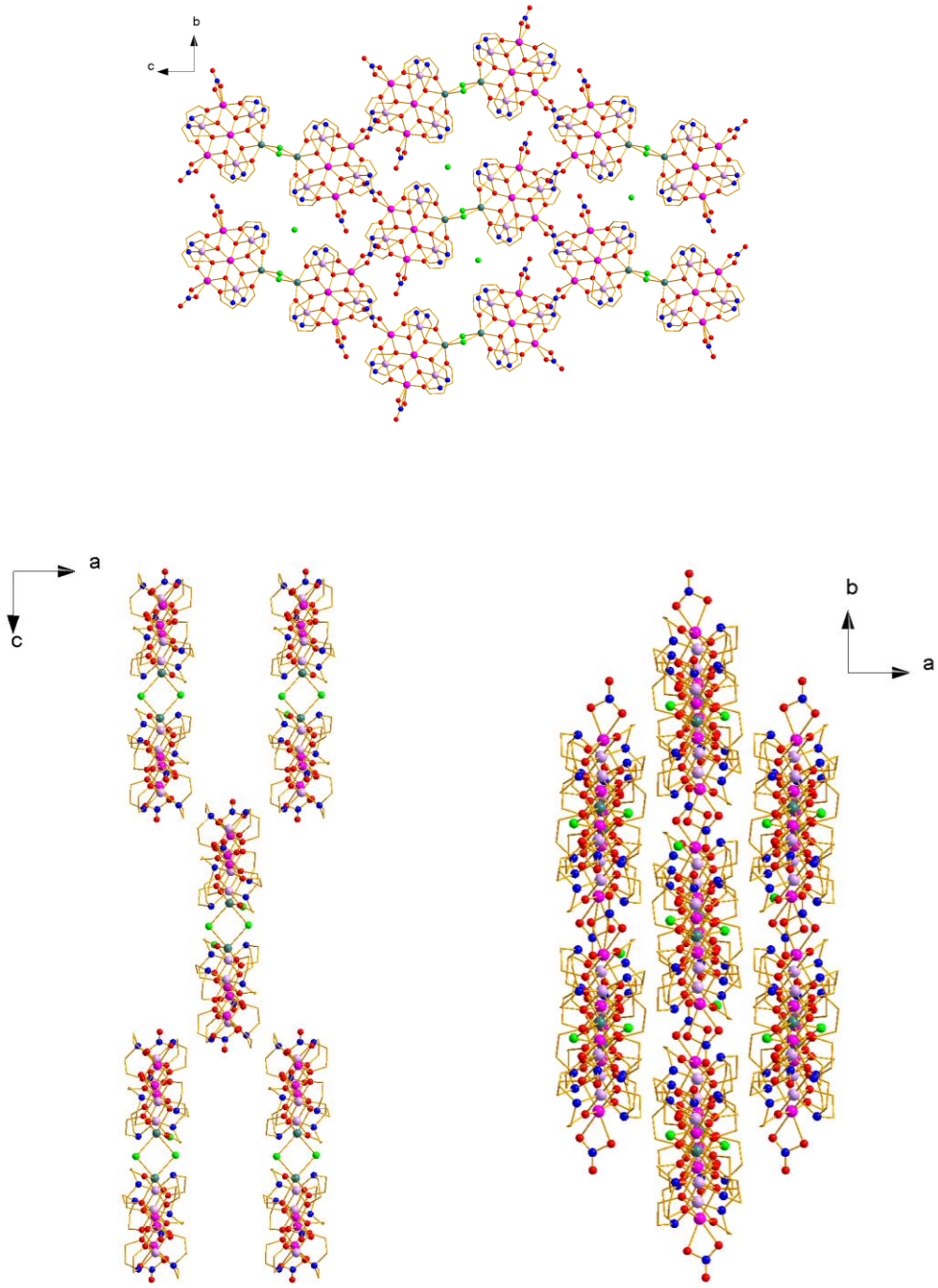

Figure 5-18 Packing diagrams for 19 viewed along *a*-, *b*- and *c*-axes.

Table 5-11 Crystallographic information table for 19.

Empirical Formula	$C_{48}H_{108}Cl_4Co_{12}Mn_2N_{16}O_{36}$*
Fw (g mol^{-1})	2444.36
Crystal system	Monoclinic
Space group	$P2_1/n$
a (Å)	11.5265(6)
b (Å)	12.8748(6)
c (Å)	37.711(2)
β (deg)	90.646(3)
V (Å^3)	5596.0(5)
Z	4
T (K)	100(2)
λ (Å)	0.71073
ρ_{calcd} (Mg m^{-3})	1.449
μ (mm^{-1})	2.108
R_1[a]	0.0983
wR_2[b]	0.0999
Goodness of fit	1.108

*This is the formula from single crystal X-ray diffraction data, using metal analysis and microanalysis data the formula is found to be $C_{55}H_{136}Cl_4Co_{11.4}Mn_{2.6}N_{18}O_{49}$. This structure was refined against F.

[a] $R_1 = \Sigma \left| |F_o| - |F_c| \right| / \Sigma |F_o|$ [b] $wR_2 = \left[\Sigma \left[w\left(F_o^2 - F_c^2\right)^2 \right] - \Sigma \left[\left(F_o^2\right)^2 \right] \right]^{1/2}$ where $w = 1/\left[\sigma^2\left(F_o^2\right) + \left(0.2P\right)^2\right]$ and $P = \left[F_o^2 + 2F_c^2\right]/3$

Table 5-12 Selected bond lengths for 19.

Bond	Distance(Å)	Bond	Distance(Å)
Co1–O11	2.093(8)	Co4–O14	1.975(8)
Co1–O12	2.095(8)	Co4–O73	1.893(8)
Co1–O13	2.143(7)	Co4–O74	1.91(1)
Co1–O14	2.134(8)	Co5–O14	2.151(9)
Co1–O15	2.042(8)	Co5–O15	2.129(8)
Co1–O16	2.124(8)	Co5– O4	2.13(1)
Co2–N41	2.01(1)	Co5–O5	2.09(1)
Co2–N42	1.95(1)	Co5–O73	1.966(8)
Co2–O11	1.925(8)	Co5–O76	1.969(8)
Co2–O12	1.908(8)	Co6–N45	1.97(1)
Co2–O71	1.914(8)	Co6–N46	1.98 (1)
Co2–O72	1.855(8)	Co6–O15	1.925(8)
Co3–O1	2.17(1)	Co6–O16	1.954(9)
Co3–O12	2.151(7)	Co6–O75	1.902(8)
Co3–O13	2.158(8)	Co6–O76	1.896(9)
Co3–O2	2.18(1)	Mn1–Cl1a	2.560(4)
Co3–O71	1.989(9)	Mn1–Cl1	2.547(4)
Co3–O74	1.992(9)	Mn1–O11	2.315(8)
Co4–N43	1.95(1)	Mn1–O16	2.298(8)
Co4–N44	1.97(1)	Mn1–O72	2.036(8)
Co4–O13	1.906(8)	Mn1–O75	2.050(8)

Table 5-13 BVS calculation results for 19.[38]

Atom	Co^{II}	Co^{III}	Mn^{II}	Mn^{III}
Co1	2.010	2.054	2.620	2.416
Co2	3.519	3.565	4.278	4.064
Co3	1.977	2.020	2.577	2.376
Co4	3.589	3.638	4.378	4.153
Co5	1.974	2.017	2.573	2.372
Co6	3.837	3.887	4.659	4.428
Mn1	1.552	1.632	2.062	1.973

Underlined value is that which is closest to the value for which it was calculated, overestimations for Co^{III} will be discussed in appendix one.

Table 5-14 Selected bond angles for 19.

Atoms	Angle (°)	Atoms	Angle (°)
Co1-O11-Co2	96.1(3)	Co3-O74-Co4	102.8(4)
Co1-O11-Mn1	97.9(3)	Co5-O14-Co1	94.7(3)
Co1-O12-Co2	96.6(4)	Co5-O14-Co4	95.8(3)
Co1-O13-Co4	98.2(3)	Co5-O15-Co1	98.2(3)
Co1-O14-Co4	96.4(3)	Co5-O15-Co6	99.8(4)
Co1-O15-Co6	98.4(3)	Co5-O73-Co4	105.1(4)
Co1-O16-Co6	94.8(4)	Co5-O76-Co6	106.8(4)
Co1-O16-Mn1	97.5(4)	Mn1-Cl1-Mn1a	99.6(1)
Co3-O12-Co1	96.3(3)	Mn1-O11-Co2	98.7(3)
Co3-O12-Co2	98.2(4)	Mn1-O16-Co6	98.3(4)
Co3-O13-Co1	94.7(3)	Mn1-O72-Co2	112.0(4)
Co3-O13-Co4	96.9(3)	Mn1-O75-Co6	109.3(4)
Co3-O71-Co2	103.9(4)		

5.3.3 Magnetic Susceptibility Measurements for $[Co_{11.4}Mn_{2.6}(NO_3)_4(dea)_{12}Cl_2][Cl]_2[NO_3]_2$ (19)

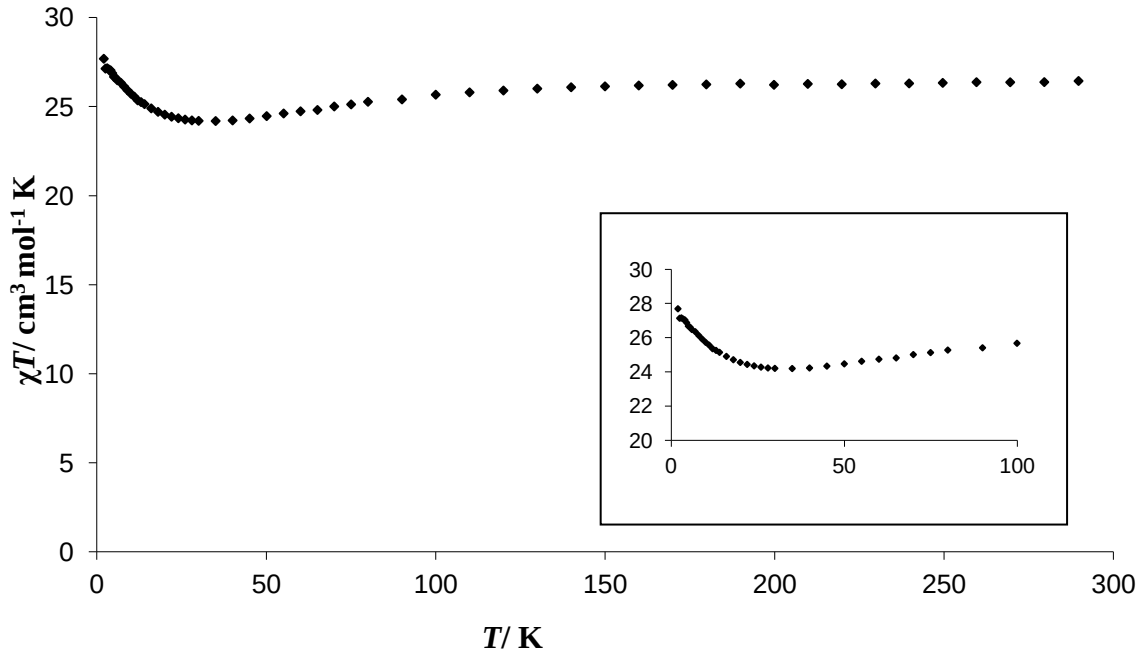

Figure 5-19 Temperature dependence of χT for 19 from 1.8-290K measured in an applied field of 1000 G. Inset highlight view showing decrease in χT at 29 K.

Magnetic susceptibility measurements were carried out on an air dried sample of **19** $\mathbf{[Co_{11.4}Mn_{2.6}(NO_3)_4(C_4NO_2H_9)_{12}Cl_2][Cl]_2[NO_3]_2}$. The χT value at 290 K is 26.4 $cm^3\ mol^{-1}$ K. The calculated value for a complex containing six Co^{II} ions and two Mn^{II} ions is 24.95 $cm^3\ mol^{-1}$ K with g = 2.4 for Co and g = 2 for Mn. As previously stated there is some small mixing of Co and Mn sites if we assume that the oxidation states remain the same and there are 2.6 Mn^{II} centres and 5.4 Co^{II} centres the calculated χT value becomes 25.96 $cm^3\ mol^{-1}$ K with g = 2.4 for Co and g = 2 for Mn, which is much closer to the value observed. There is a gradual slight decrease in χT towards 30 K to 24.2 $cm^3\ mol^{-1}$ K followed by an increase to 27.7 $cm^3\ mol^{-1}$ K at 2 K (inset Figure 5-19). The slight decrease is typical of complexes in which there is spin-orbit coupling; at lower temperature this effect is quenched by ferromagnetic coupling between the Co^{II} and Mn^{II} centres, resulting in the increase in χT.

The magnetisation of the sample was measured as a function of applied field at 2 K and 4K (Figure 5-20). At 7 T the magnetisation is ~20, for two Mn^{II} ions and six Co^{II} ions which are ferromagnetically coupled (with g = 2 and g = 4.3 respectively) the expected value would be 22.9. Taking into account the small mixing of the metal ions this value would be expected to increase to 24.6 for ferromagnetically coupled metal ions.

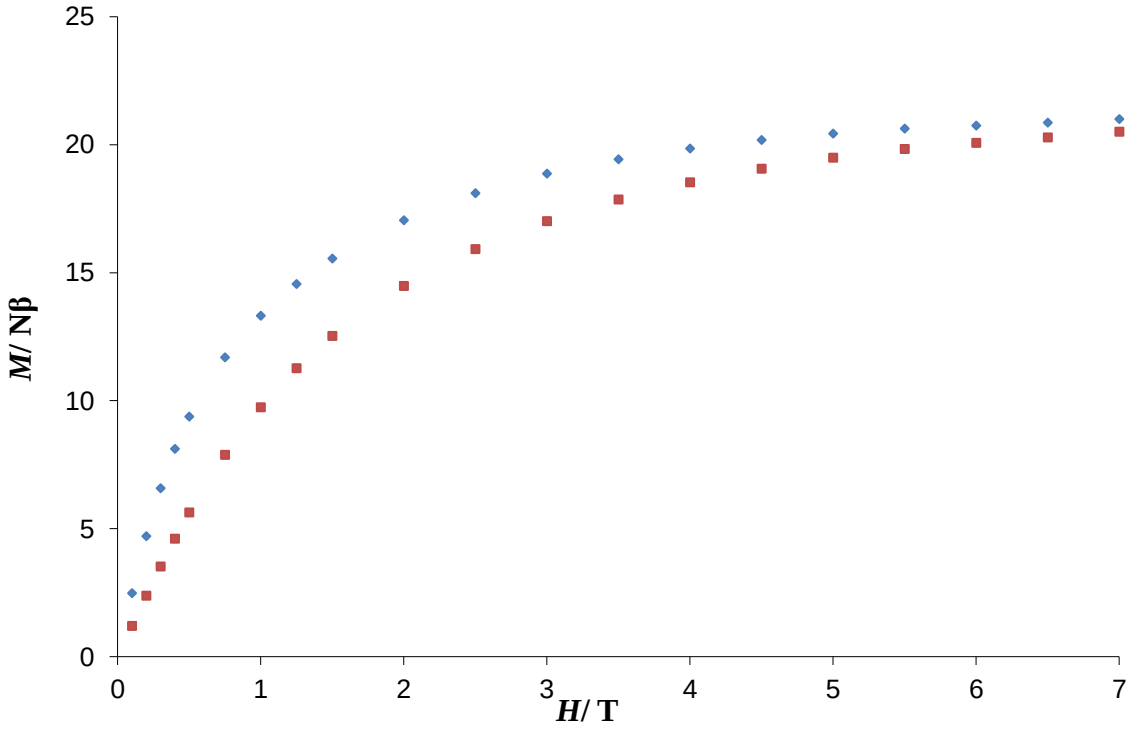

Figure 5-20 Magnetisation *vs.* field measured at 2 K (◆) and 4 K (■).

The bridging angles found for **19** between Co^{II} and Mn^{II} metal centres in this complex are in the range of 95°-97°, which suggests that ferromagnetic coupling should be dominant. However, the observed χT value at low temperature, 27.7 $cm^3\ mol^{-1}$ K, is much lower than the expected value for the number of metal centres if they were ferromagnetically coupled which would be 42.7 $cm^3\ mol^{-1}$ K, with g = 4.3 for Co^{II} with an effective S' = ½. The failure to reach the calculated χT value could be due to the effects of ZFS.

The data collected for this sample are very similar in trend to that measured for the Co_7 and mixed Co and Mn disc complexes described previously (**13** and **16**, Sections 4.2.2.2 and 4.3.2.2). The χT values for **19** are approximately double those for **16** (χT at high temperature 13.6 $cm^3\ mol^{-1}$ K and at low temperature χT 14.6 $cm^3\ mol^{-1}$ K), as might be expected as **16** has the formula $[Co_6Mn_1(dea)_6(NO_3)_3][NO_3]_2$ effectively half of **19**.

5.4 Mixed-valent $\{Co^{II}_2Co^{III}_4Er^{III}_4\}$ complex

The complex described below is a new member of the family of $Co^{II}_2Co^{III}_4Ln^{III}_4$ (Ln = Gd, Y, Dy) complexes published by Powell *et al.*[32] This complex was synthesised using similar methods to those published, and comprises a $\{Co^{II}_2Co^{III}_4Er^{III}_4\}$ cluster formed using the ligands tris, acetate and nitrate. Erbium was chosen to provide a comparison with the already published structures in an attempt to further understand the interactions that occur between the metal centres.

5.4.1 Synthesis of $[Co^{II}_2Co^{III}_4Er^{III}_4(tris)_8(NO_3)_4(OAc)_6(CH_3OH)_2][NO_3]_2 \cdot 2MeOH \cdot H_2O$ (20·2MeOH·H$_2$O)

(where trisH_3 = 2-amino-2-(hydroxymethyl)-propane-1,3-diol

$Co(OAc)_2.4H_2O$ (0.05 g, 0.22 mmol), $Er(NO_3)_3.5H_2O$ (0.10 g, 0.23 mmol) and tris (0.03 g, 0.23 mmol) were dissolved in MeOH (5 mL) at 50 °C and stirred for 10 minutes. Triethylamine (0.015 mL, 0.108 mmol) was then added and the reaction was stirred for a further 10 minutes at 50 °C, the solution was then stirred for 30 minutes at room temperature. The reaction was filtered and the filtrate stored in a sealed vial. Small pink square plate crystals from after approximately three weeks in 28% yield. Air dried crystals analyse as $\mathbf{C_{48}H_{100}N_{14}O_{59}Co_6Er_4}$, analysis (%) calc. (found) C, 18.92 (18.74); H, 3.73 (3.55); N, 6.72 (6.67). Selected IR data: ν = 3267, 3238, 2937, 2854, 1552, 1442, 1417, 1350, 1313, 1107, 1082, 1066, 1012, 813, 790, 746, 678, 601 cm^{-1}.

5.4.2 Discussion of crystal structure of $[Co^{II}_2Co^{III}_4Er^{III}_4(tris)_8(NO_3)_4(OAc)_6(CH_3OH)_2][NO_3]_2$ (20)

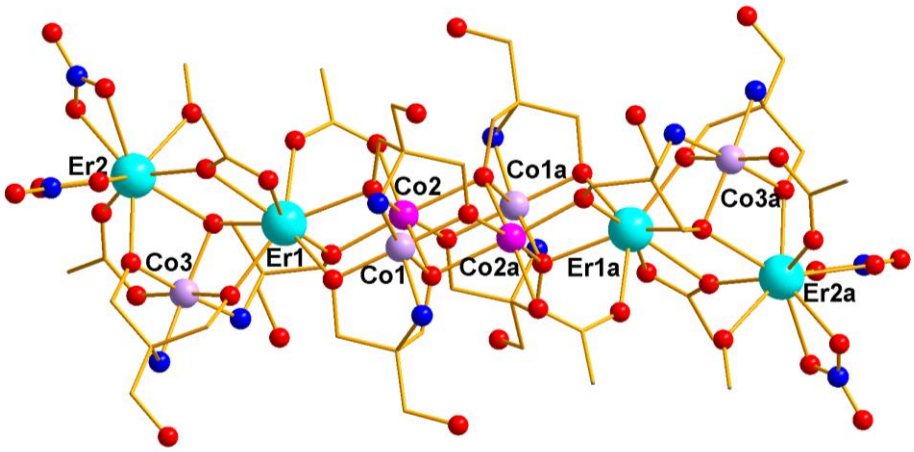

Figure 5-21 Structure of 20 atom label a signifies symmetry equivalent (a = 2-x, 2-y, -z) (H-atoms and anions omitted for clarity) Er^{III} cyan; Co^{II} pink; Co^{III} lilac; O red; N blue.

The complex consists of four Er^{III} ions, two Co^{II} and four Co^{III} ions. The central section of the complex comprising Er1, Co1 Co2 and their symmetry equivalents form a planar core; Er1 and Er1a form one corner of $Er^{III}_2Co^{III}$ triangles, the planes of the triangles sit almost perpendicular to the core, the dihedral angle between the planes is 86.23(2)°.

The Er1 ion is eight coordinate, with distorted dodecahedral geometry, whereas Er2 is nine coordinate with distorted capped square-antiprismatic geometry (Figure 5-22), the coordination spheres in both cases are filled by oxygen. For Er1 the ligand environment is made up of oxygen donors from two acetate groups, and three different tris ligands. Er2 is capped by two bidentate nitrate groups, and bound to two acetate groups and a tris ligand, with methanol completing the coordination sphere. The Co^{III} ions Co1 and Co3 have an $\{N_2O_4\}$ ligand donor set in a distorted octahedral geometry, and Co2, (Co^{II}) has a $\{O_6\}$ ligand environment also in a distorted octahedral geometry.

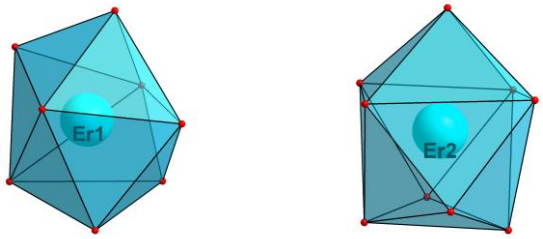

Figure 5-22 Diagram showing geometry of Er1 (distorted dodecahedron) and Er2 (distorted capped square anti-prism).

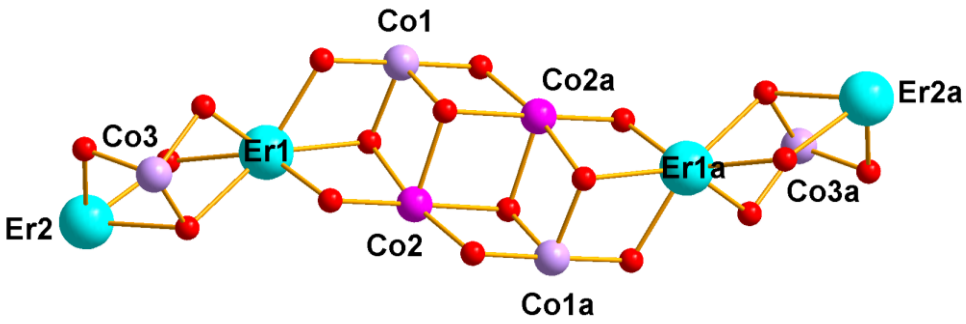

Figure 5-23 Metal-oxygen core structure of the cation of 20 Er^{III} cyan; Co^{II} pink; Co^{III} lilac; O red; N blue.

The four ligands of tris in the asymmetric unit each display different binding modes, shown in Figure 5-24, bridging between different combinations of three and four metal centres. Acetate also acts as a ligand between two metal centres either one Co and one Er or two Er ions. In the case of two Er ions, one oxygen of the acetate group binds to one metal and the other oxygen bridges between two metal centres.

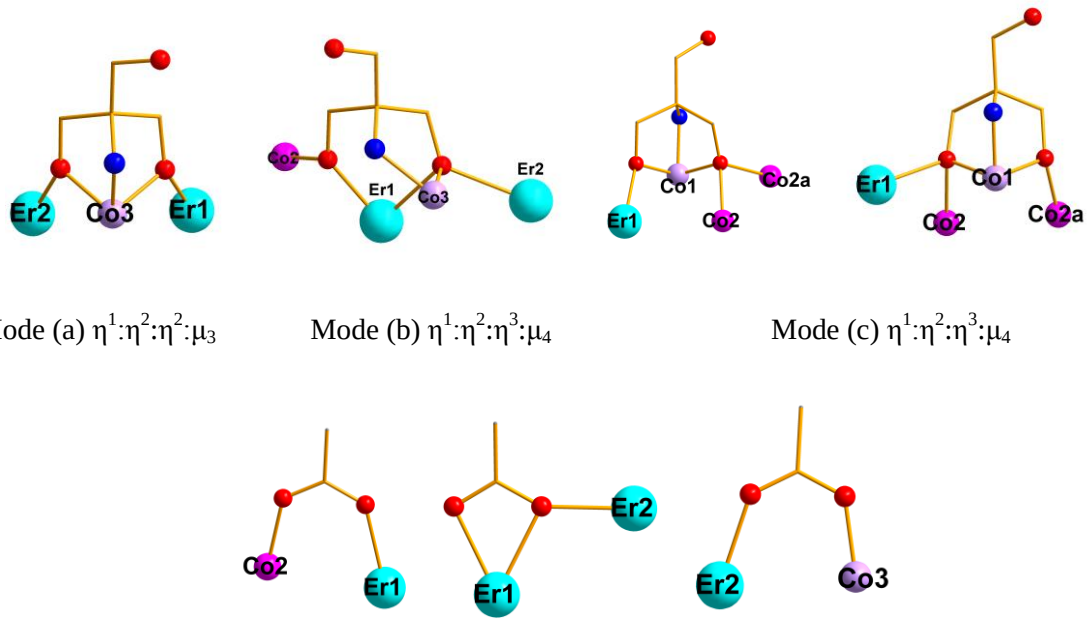

Mode (a) $\eta^1:\eta^2:\eta^2:\mu_3$ Mode (b) $\eta^1:\eta^2:\eta^3:\mu_4$ Mode (c) $\eta^1:\eta^2:\eta^3:\mu_4$

Figure 5-24 Different binding modes of tris and acetate in 20.

Other than the family of complexes related to the one described above[39] tris has been used previously with transition metal ions.[40-43] Binding modes (b) and (c) (Figure 5-24) both bridge four metal ions. In binding mode (b) the metal ion coordinated to both of the coordinating oxygen atoms is not coordinated to the nitrogen atom of the same ligand. This is different to both binding modes (a) and (c). Modes (a) and (b) have only been seen in the related family of complexes, however (c) has also been seen in a Co_7 complex.[43] The unbound nitrate anion has a short contact with an NH of tris on one cluster and the unbound arm of the same ligand on a neighbouring cluster (N(H)···O 3.22 (1) Å; O(H)···O 2.87 (2)Å and 3.330(3)Å). Bound nitrate with N5 has a short contact again with the unbound arm of a tris ligand on a neighbouring cluster (O(H)···O 2.986(9) Å) (Figure 5-25). From the packing diagram, the solvent and unbound anions can be found in rows between rows of complexes (Figure 5-26).

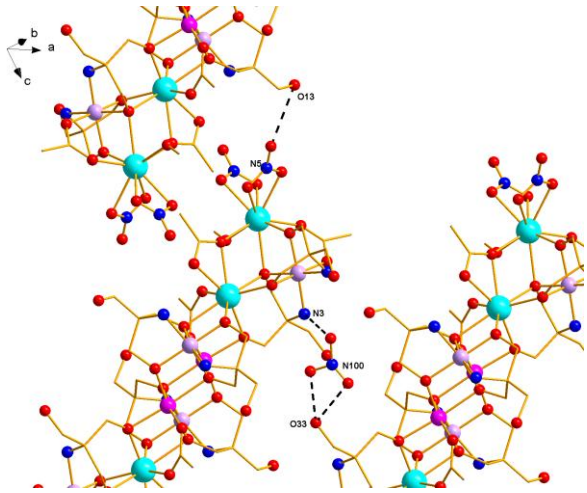

Figure 5-25 Diagram showing hydrogen bonding in 20.

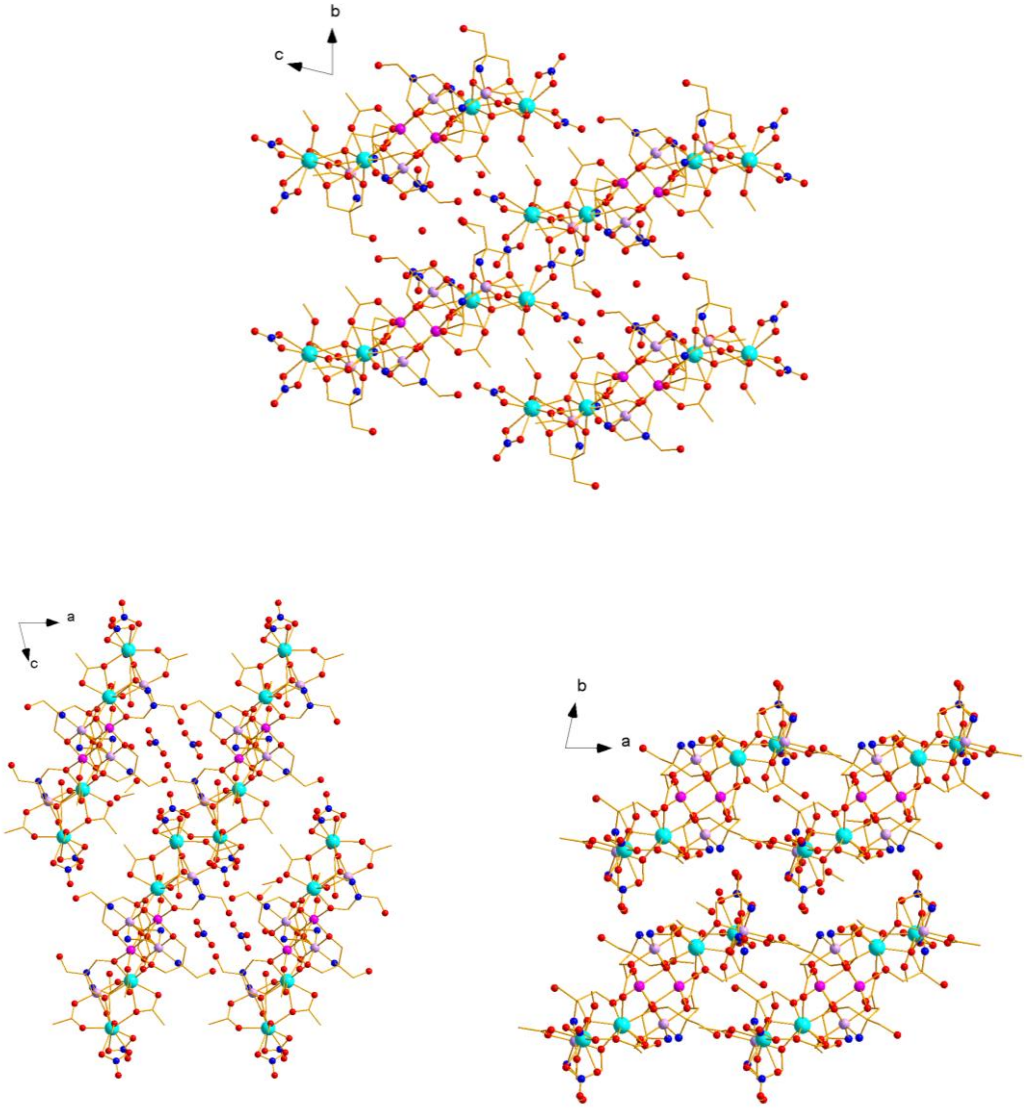

Figure 5-26 Packing diagrams for 20 viewed along *a*-, *b*-, *c*-axes.

Table 5-15 Data for the crystal structure determination of 20·4MeOH·2H_2O.

Empirical Formula	$C_{50}H_{110}Co_6Er_4N_{14}O_{62}$
Fw (g mol^{-1})	2922.12
Crystal system	Triclinic
Space group	*P*-1
a (Å)	12.7340(2)
b (Å)	13.6036(2)
c (Å)	16.1943(2)
α (deg)	72.172(1)
β (deg)	71.896(1)
γ (deg)	73.169(1)
V ($Å^3$)	2479.11(6)
Z	1
T (K)	100(2)
λ (Å)	0.71073
ρ_{calcd} (Mg m^{-3})	1.957
μ (mm^{-1})	4.429
R_1[a]	0.0492
wR_2[b]	0.1139
Goodness of fit	1.051

[a] $R_1 = \Sigma \left| |F_o| - |F_c| \right| / \Sigma |F_o|$ [b] $wR_2 = \left[\Sigma \left[w\left(F_o^2 - F_c^2\right)^2 \right] - \Sigma \left[\left(F_o^2\right)^2 \right] \right]^{1/2}$ where $w = 1/\left[\sigma^2\left(F_o^2\right) + \left(0.2P\right)^2\right]$ and $P = \left[F_o^2 + 2F_c^2\right]/3$

Table 5-16 Selected metal-ligand bond lengths for 20.

Bond	Distance (Å)	Bond	Distance (Å)
Er1–O12	2.429(5)	Co1–N1	1.941(7)
Er1–O22	2.279(5)	Co1–O11	1.896(5)
Er1–O31	2.447(5)	Co1–O12	1.899(5)
Er1–O32	2.171(5)	Co1–N2	1.936(6)
Er1–O41	2.256(5)	Co1–O21	1.902(5)
Er1–O20	2.385(5)	Co1–O22	1.894(5)
Er1–O50	2.462(5)	Co2–O21a	2.220(5)
Er1–O60	2.437(6)	Co2–O11a	1.985(5)
Er2–O31	2.496(5)	Co2–O12	2.135(5)
Er2–O42	2.230(5)	Co2–O21	2.125(5)
Er2–O51	2.487(6)	Co2–O32	2.085(5)
Er2–O52	2.454(6)	Co2–O10	2.056(5)
Er2–O61	2.450(7)	Co3–N3	1.932(6)
Er2–O62	2.459(6)	Co3–O31	1.908(5)
Er2–O40	2.294(5)	Co3–N4	1.936(6)
Er2–O50	2.305(5)	Co3–O41	1.885(5)
Er2–O70	2.371(6)	Co3–O42	1.897(5)
		Co3–O30	1.923(5)

Table 5-17 Selected bond angles for 20.

Atoms	Angle (°)	Atoms	Angle (°)
Co1-O22-Er1	107.5(2)	Co2-O32-Er1	99.7(2)
Co2-O11-Co1	104.0(2)	Co3-O41-Er1	106.4(2)
Co2-O12-Co1	96.8(2)	Co3-O42-Er2	103.6(2)
Co2-O12-Er1	90.7 (2)	Er1-O12-Co1	101.7(2)
Co2-O21-Co1	97.0(2)	Er1-O31-Co3	98.7 (2)
Co2-O21-Co1a	95.5(2)	Er1-O50-Er2	114.4(2)
Co2-O21-Co2a	93.9(2)	Er2-O31-Co3	94.2(2)
		Er2-O31-Er1	108.4(2)

Table 5-18 Bond valence sum results for Co ions in 20.[38]

Atom	Co^{II}	Co^{III}
Co1	3.825	<u>3.875</u>
Co2	<u>2.024</u>	2.068
Co3	3.832	<u>3.881</u>

The underlined value is that closest to the value for which it was calculated, overestimations for Co^{III} will be discussed in appendix one.

5.4.3 Magnetic Susceptibility Measurements for $[Co^{II}_2Co^{III}_4Er^{III}_4(tris)_8(NO_3)_4(OAc)_6(CH_3OH)_2][NO_3]_2$ (20)

Magnetic measurements were carried out on this sample in order to compare the magnetic properties with the structures published by Powell *et al.* of the form $Co^{II}_2Co^{III}_4Ln^{III}_4$ (Ln = Gd, Y, Dy).[39] The published results show that the analogues with yttrium and gadolinium displayed no out-of-phase ac-signal but that the $\{Co^{II}_2Co^{III}_4Dy^{III}_4\}$ complex did display out-of-phase signals below 10 K.[39]

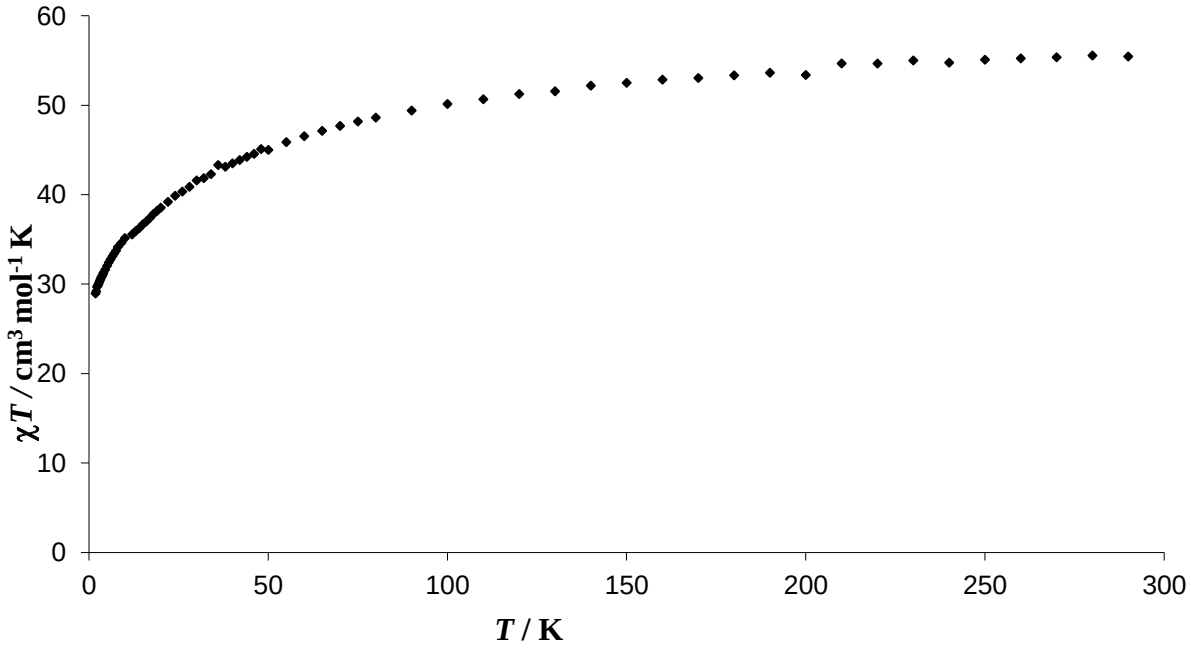

Figure 5-27 Temperature dependence of χT for 20 from 1.8-300 K measured in an applied field of 1000 G.

Magnetic susceptibility measurements were carried out on an air dried sample of **20·2MeOH·H_2O**.The χT value at 300 K is 55.4 $cm^3\ mol^{-1}$ K, this is higher than the expected value for two uncoupled Co^{II} ions and four Er^{III} ions, which would be 51.0 $cm^3\ mol^{-1}$ K (g = 2.3 for Co^{II}; g = 6/5, S = 3/2 and J = 15/2 for Er^{III}). This is possibly a result of significant orbital contributions. As the temperature is decreased, the χT value gradually decreases to 28.9 $cm^3\ mol^{-1}$ K at 1.8 K. The magnetic behaviour of this complex is a result of Co^{II}-Co^{II}, Co^{II}-Er^{III} and Er^{III}-Er^{III} interactions, and also the spin-orbit coupling effects and magnetic anisotropy of the Co^{II} and Er^{III} ions.

The magnetisation was measured as a function of applied field at 2 K and 5 K (Figure 5-28), at 5 T M/ Nβ is equal to ~23.0.

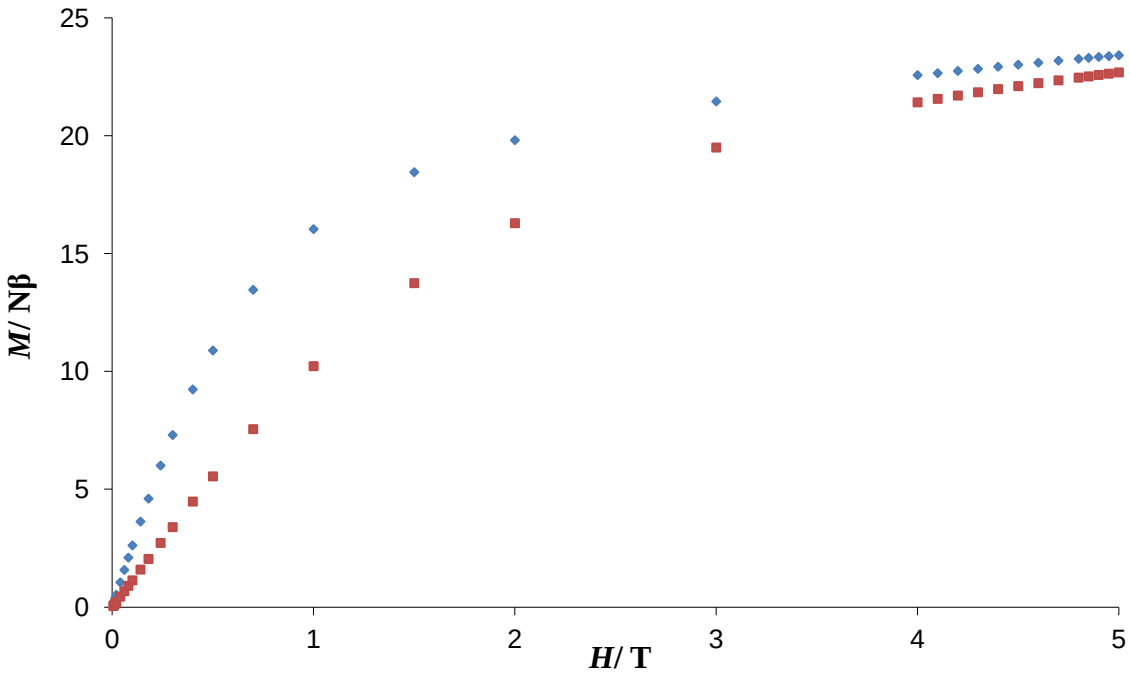

Figure 5-28 *M vs. H* for 20 measured at 2 K (◆) and 5 K (■) up to 5 T.

Powell *et al.* studied the magnetic properties of the yttrium, gadolinium and dysprosium cobalt complexes. The Y^{III} and Co^{III} ions are diamagnetic allowing the magnetic data from this complex to be approximated to a simple Co^{II} dimer. From their measurements they concluded there is weak ferromagnetic coupling between the Co^{II} ions, probably as a result of the Co^{II}-O-Co^{II} bridging angle which is 93.8°. The data from this yttrium complex were then subtracted from the χT vs. T plots for the Gd and Dy complexes, effectively removing the contribution due to the Co^{II}-Co^{II} interactions allowing Co^{II}-Ln^{III} interactions to be studied, assuming that the Ln^{III}-Ln^{III} would be much weaker.[44] By doing this Powell *et al.* were able to conclude that the Co^{II}-Gd^{III} and Co^{II}-Dy^{III} interactions are antiferromagnetic. Ac susceptibility measurements showed an out-of-phase signal for only the $\{Co^{II}_2Co^{III}_4Dy^{III}_4\}$ complex, as all the three complexes published are approximately isostructural it suggests this slow relaxation of magnetisation is due to the anisotropy of the Dy^{III} ions.

Comparing the data for complex **20** to the published work it is most similar to that for the $\{Co^{II}_2Co^{III}_4Gd^{III}_4\}$ complex. This suggests that there is an antiferromagnetic interaction between the Co^{II} and Er^{III} ions. Ac susceptibility measurements carried out on this complex showed no frequency dependent signals.

5.5 Conclusions

Four complexes with more than seven metal centres have been synthesised, two homometallic complexes and two heterometallic complexes. Where possible magnetic measurements have been undertaken.

The Co_8 complex **17** has an unusual structural motif and is a new member of a family of cobalt complexes that utilise the btp ligand. Further work and magnetic studies could provide interesting results as the bridging angles between Co^{II} ions (92-94°) could favour ferromagnetic intereactions.

The two examples of Co_{10} complex **18** and **18a** which again utilise the BTP ligand have a structure which is comparable to overlapping Co_7 discs, and magnetic susceptibility measurements show that there are ferromagnetic interactions between the Co^{II} ions.

The 'double disc' complex **19** has a unique structural motif. Despite the many Co_7 discs that exist, this bridged heterometallic form has not been seen before. Future work could be to synthesise the homometallic complex, and as with the heterometallic complexes described in Section 4.3.2 it would be desirable if the Co^{III} ions could be replaced by alternative M^{III} (Cr^{III}, Fe^{III}, Ln^{III}) ions with improved magnetic performance.

The $Co^{II}_2Co^{III}_4Er^{III}_4$ complex **20** is a new addition to the family of related complexes,[39] one of very few mixed valent Co-Ln examples. It displays similar magnetic properties to the Gd analogue suggesting an antiferromagnetic interaction between Co^{II} and Er^{III}.

5.6 References

(1) Li, B.-W.; Zhou, Y.-L.; Chen, Q.; Zeng, M.-H. *Polyhedron* **2010**, *29*, 148.

(2) Aromí, G.; Batsanov, A. S.; Christian, P.; Helliwell, M.; Parkin, A.; Parsons, S.; Smith, A. A.; Timco, G. A.; Winpenny, R. E. P. *Chemistry – A European Journal* **2003**, *9*, 5142.

(3) Dimitrou, K.; Sun, J.-S.; Folting, K.; Christou, G. *Inorganic Chemistry* **1995**, *34*, 4160.

(4) Beattie, J. K.; Hambley, T. W.; Klepetko, J. A.; Masters, A. F.; Turner, P. *Polyhedron* **1997**, *16*, 2109.

(5) Grillo, V. A.; Sun, Z.; Folting, K.; Hendrickson, D. N.; Christou, G. *Chemical Communications* **1996**, 2233.

(6) Clegg, W.; Garner, C. D.; Al-Samman, M. H. *Inorganic Chemistry* **1983**, *22*, 1534.

(7) Benelli, C.; Blake, A. J.; Brechin, E. K.; Coles, S. J.; Graham, A.; Harris, S. G.; Meier, S.; Parkin, A.; Parsons, S.; Seddon, A. M.; Winpenny, R. E. P. *Chemistry – A European Journal* **2000**, *6*, 883.

(8) Wei, L.-Q.; Li, B.-W.; Hu, S.; Zeng, M.-H. *Crystal Engineering Communications* **2011**, *13*, 510.

(9) Li, B.-W.; Zhou, Y.-L.; Chen, Q.; Zeng, M.-H. *Polyhedron* **2010**, *29*, 148.

(10) Zeng, M.-H.; Yao, M.-X.; Liang, H.; Zhang, W.-X.; Chen, X.-M. *Angewandte Chemie International Edition* **2007**, *46*, 1832.

(11) Cooper, G. J. T.; Newton, G. N.; Kögerler, P.; Long, D.-L.; Engelhardt, L.; Luban, M.; Cronin, L. *Angewandte Chemie International Edition* **2007**, *46*, 1340.

(12) Wang, L.; Li, Y.; Peng, Y.; Liang, Z.; Yu, J.; Xu, R. *Dalton Transactions* **2012**, *41*, 6242.

(13) Li, Q.; Qian, J.; Tian, C.; Lin, P.; He, Z.; Wang, N.; Shen, J.; Zhang, H.; Chu, T.; Yuan, D.; Yang, Y.; Xue, L.; Du, S. *Dalton Transactions* **2014**, *43*, 3238.

(14) McLellan, R.; Reze, J.; Taylor, S. M.; McIntosh, R. D.; Brechin, E. K.; Dalgarno, S. J. *Chemical Communications* **2014**, *50*, 2202.

(15) K. Brechin, E.; G. Harris, S.; Harrison, A.; Parsons, S.; Gavin Whittaker, A.; E. P. Winpenny, R. *Chemical Communications* **1997**, 653.

(16) Mori, F.; Nyui, T.; Ishida, T.; Nogami, T.; Choi, K.-Y.; Nojiri, H. *Journal of the American Chemical Society* **2006**, *128*, 1440.

(17) Ako, A. M.; Mereacre, V.; Clerac, R.; Wernsdorfer, W.; Hewitt, I. J.; Anson, C. E.; Powell, A. K. *Chemical Communications* **2009**, 544.

(18) Stamatatos, T. C.; Teat, S. J.; Wernsdorfer, W.; Christou, G. *Angewandte Chemie International Edition* **2009**, *48*, 521.

(19) Baniodeh, A.; Hewitt, I. J.; Mereacre, V.; Lan, Y.; Novitchi, G.; Anson, C. E.; Powell, A. K. *Dalton Transactions* **2011**, *40*, 4080.

(20) Chandrasekhar, V.; Pandian, B. M.; Azhakar, R.; Vittal, J. J.; Clérac, R. *Inorganic Chemistry* **2007**, *46*, 5140.

(21) Chandrasekhar, V.; Pandian, B. M.; Vittal, J. J.; Clérac, R. *Inorganic Chemistry* **2009**, *48*, 1148.

(22) Costes, J.-P.; Vendier, L.; Wernsdorfer, W. *Dalton Transactions* **2011**, *40*, 1700.

(23) Gómez, V.; Vendier, L.; Corbella, M.; Costes, J.-P. *European Journal of Inorganic Chemistry* **2011**, *17*, 2653.

(24) Gómez, V.; Vendier, L.; Corbella, M.; Costes, J.-P. *Inorganic Chemistry* **2012**, *51*, 6396.

(25) Le Roy, J. J.; Korobkov, I.; Murugesu, M. *Chemical Communications* **2014**, *50*, 1602.

(26) Silva, M. R.; Martin-Ramos, P.; Coutinho, J. T.; Pereira, L. C. J.; Martin-Gil, J. *Dalton Transactions* **2014**, *43*, 6752.

(27) CSD search 2013 September.

(28) Allen, F. *Acta Crystallographica Section B* **2002**, *58*, 380.

(29) Deng, Y.-F.; Chen, M.-S.; Zhang, C.-H.; Tan, X.-W. *Acta Crystallographica Section E* **2011**, *67*, m1478.

(30) Sun, F. *Acta Crystallographica Section E* **2010**, *66*, m1615.

(31) Cui, Y.; Chen, J.-T.; Long, D.-L.; Zheng, F.-K.; Cheng, W.-D.; Huang, J.-S. *Journal of the Chemical Society, Dalton Transactions* **1998**, 2955.

(32) Xiang, H.; Lan, Y.; Li, H.-Y.; Jiang, L.; Lu, T.-B.; Anson, C. E.; Powell, A. K. *Dalton Transactions* **2010**, *39*, 4737.

(33) Ferguson, A.; Schmidtmann, M.; Brechin, E. K.; Murrie, M. *Dalton Transactions* **2011**, *40*, 334.

(34) Milway, V. A.; Tuna, F.; Farrell, A. R.; Sharp, L. E.; Parsons, S.; Murrie, M. *Angewandte Chemie International Edition* **2013**, *52*, 1949.

(35) Ferguson, A.; Darwish, A.; Graham, K.; Schmidtmann, M.; Parkin, A.; Murrie, M. *Inorganic Chemistry* **2008**, *47*, 9742.

(36) Sluis, P. v. d.; Spek, A. L. *Acta Crystallographica Section A* **1990**, *A46*, 194.

(37) Spek, A. *Journal of Applied Crystallography* **2003**, *36*, 7.

(38) Brese, N. E.; O'Keeffe, M. *Acta Crystallographica Section B* **1991**, *47*, 192.

(39) Xiang, H.; Lan, Y.; Li, H.Y.; Jiang,L.; Lu,T.B.; Anson,C.E.; Powell, A.K. *Dalton Transactions* **2010**, *39*, 4737.

(40) Tsyba, I.; Mui, B. B.-k.; Bau, R.; Noguchi, R.; Nomiya, K. *Inorganic Chemistry* **2003**, *42*, 8028.

(41) Masi, D.; Mealli, C.; Sabat, M.; Sabatini, A.; Vacca, A.; Zanobini, F. *Helvetica Chimica Acta* **1984**, *67*, 1818.

(42) Marcoux, Pierre R.; Hasenknopf, B.; Vaissermann, J.; Gouzerh, P. *European Journal of Inorganic Chemistry* **2003**, *13*, 2406.

(43) Ferguson, A.; Parkin, A.; Sanchez-Benitez, J.; Kamenev, K.; Wernsdorfer, W.; Murrie, M. *Chemical Communications* **2007**, 3473.

(44) Benelli, C.; Gatteschi, D. *Chemical Reviews* **2002**, *102*, 2369.

6. Conclusions

Simple ligands have been utilised to form a wide variety of complexes, with different structural forms, valencies and nuclearity ranging from one metal centre to the largest complex which has fourteen metal centres.

6.1 The Tris, Bis-tris and Bis-tris propane ligands

This family of ligands has been used to synthesise eleven complexes, ranging in size from one to ten metal centres. These ligands can display varying degrees of deprotonation and several of these are found in the complexes which have been isolated.

6.1.1 Tris (trisH$_3$)

Two complexes were synthesised with this ligand, both heterometallic, one a seven membered disc incorporating manganese with the formula $[Co_{4.7}Mn_{2.3}(trisH)_6(NO_3)_3(H_2O)_3][NO_3]_2$ (**15**) and the other utilising erbium, $[Co^{II}_2Co^{III}_4Er^{III}_4(tris)_8(NO_3)_4(OAc)_6(CH_3OH)_2][NO_3]_2$ (**20**). Magnetic susceptibility measurements were carried out on the cobalt and erbium complex, which on comparison with published data, suggested the Co^{II}-Er^{III} interactions are antiferromagnetic.

6.1.2 Bis-tris (btH$_5$)

Using this ligand four monomeric complexes were synthesised, one of which $[Co^{II}(btH_5)Cl][Cl]$ (**1**) was subsequently used to form two larger complexes. A homometallic complex with the formula $[Co^{II}_6Co^{III}_4(OH)_2(btH)_3(btH_2)Cl_7(CH_3OH)(MeCN)(H_2O)]$ (**4**) with Co^{II} in a range of geometries octahedral, tetrahedral, trigonal bipyramidal and square pyramidal all distorted. The second complex is heterometallic $[Mn^{II}_5Co^{III}_4Cl_6(OH)_2(btH)_2(btH_2)_2(CH_3OH)(H_2O)]$ (**5**), in this example the Mn^{II} ions display a variety of geometries which are all distorted, octahedral, square pyramidal and trigonal bipyramidal. Magnetic susceptibility measurements were carried out on both the larger complexes. For both of these complexes the magnetic susceptibility measurements are complicated by the effects of octahedral Co^{II} for the first complex, and also the presence of 4- and 5-coordinate Co^{II} and possible second order SOC effects in the second complex possibly due to the distorted geometry of the Mn^{II} ions.

Whilst the ligand remains fully protonated in the monomers, in the larger complexes bis-tris is found in two different states, both tri- and tetra-deprotonated. The possibility for further deprotonation, suggests there is potential for larger complexes to be formed.

6.1.3 Bis-tris propane ($btpH_6$)

Three homometallic mixed valence cobalt complexes were synthesised using btp, one Co_7 disc $[Co^{II}_4Co^{III}_3(btpH_2)_3(NO_3)5EtOH]$ (**12**), a Co_8 complex $[Co^{II}_4Co^{III}_4(btpH_2)_4Cl_2(NO_3)_2]$ (**17**), and a Co_{10} complex $[Co^{II}_6Co^{III}_4(btpH_2)_4Cl_8]$ (**18**) which was isolated in two different crystallographic space groups. Magnetic susceptibility measurements were carried out on the Co_7 disc and the orthorhombic Co_{10} complex, these suggested an effective spin ground state $S' = 2$ for the disc and $S' = 3$ for the Co_{10} complex with $g > 4$ in both cases.

Bis-tris propane has the potential to be up to hexa-deprotonated, however in these complexes it is always found in the tetra-deprotonated form (**17** has one btp ligand with half-occupancy protons but remains $btpH_2$ overall). If full deprotonation or more varied deprotonation of the ligand could be achieved, many more complexes could potentially be isolated.

6.2 Diethanolamine and Triethanolamine ligands

Eight complexes were synthesised using these ligands, several small complexes, with two to four metal centres, two seven membered discs and a novel 'double disc' with fourteen metal centres.

6.2.1 Diethanolamine

Diethanolamine has been used to synthesise a mixed valent Co dimer $[Co^{II}Co^{III}(acac)(deaH)_2]$ (**9**), a Co_7 disc $[Co^{II}_4Co^{III}_3(dea)_6(NO_3)_3][NO_3]_2$ (**13**), a mixed metal cobalt and manganese seven membered disc $[Co_6Mn(dea)_6(NO_3)_3][NO_3]_2$ (**16**) and a novel mixed metal 'double disc' complex (**19**). A further Co_7 disc $[Co^{II}_4Co^{III}_3(N\text{-}mdea)_6(NO_3)_3][NO_3]_2$ (**14**) was synthesised using N-methyldiethanolamine.

Diethanolamine is perhaps the simplest ligand utilised, and resulted in one of the most interesting structural results. Many seven membered cobalt discs are known, however, the 'double disc' $[Co_{11.4}Mn_{2.6}(NO_3)_4(dea)_{12}Cl_2][Cl]_2[NO_3]_2$ (**19**) has not been seen before. Magnetic susceptibility measurements carried out on the 'double disc' suggests the interactions are similar to those in the related heterometallic disc (**16**).

6.2.2 Triethanolamine

A Co^{II} dimer (**8**), a mixed valent trimer (**10**) and a mixed valent tetramer (**11**) were synthesised utilising triethanolamine. This ligand showed a great deal of flexibility, it is fully protonated in the dimer structure, doubly deprotonated in the trimer and fully deprotonated in the tetramer. Use of the dimer as a starting material could be an interesting future project due to the possibility for further deprotonation of the ligand.

6.3 Further work

The area of Co^{II} SMMs is a promising area of research, the magnetic properties of Co^{II} in octahedral geometry remain complex to understand and will only be fully understood through further synthesis of cobalt complexes and studies of their magnetic properties. Utilising different synthetic methods such as anaerobic preparation to prevent Co^{III} formation in clusters could prove advantageous. The synthesis of bimetallic or higher mixed metal complexes could also be a promising area of research in the search for SMMs, attempting to combine desirable magnetic properties of different elements into one complex.

Appendix One

Values used for BVS calculations

Table 0-1 Bond valence parameters (R_0) utilised in this thesis.[1]

Cation	O	N	Cl	Br
Co^{II}	1.692	1.84	2.01	2.18
Co^{III}	1.70		2.05	
Mn^{II}	1.790	1.87	2.13	2.26
Mn^{III}	1.760		2.14	

BVS calculations rely on the assumption that the valence of an atom or ion, z_j, can be defined as,

$$z_j = \sum s_{ij} \tag{0-1}$$

where s_{ij} are the individual bond valences. Individual bond valences are calculated from observed bond lengths using the following *Equation 0-2*, where R_{ij} is the observed bond length and R_0 is a constant which is dependent on the atoms/ions involved in the bond and b = 0.37.

$$s_{ij} = \exp\left[\left(R_0 - R_{ij}\right)/b\right] \tag{0-2}$$

There has been discussion on whether or not R_0 is dependent upon the oxidation state or only the identity of the two atoms involved in the bond. Over the last few decades several different values for R_0 have been published for Co–O; –N; and –Cl, a summary is given in Table 0-2.

Table 0-2 Bond valence parameter R_0 from different published works.

Cation	O		N	Cl	
Co	1.680[2]		1.84,[1]1.790[2]		
Co^{II}	1.692[1,3]			2.01[1]	
Co^{III}	1.70[1]			2.05[1]	
Mn	1.750[2]		1.87[1]		
Mn^{II}	1.765[4]	1.790[3]	1.849[4]	2.133[3]	2.13[1]
Mn^{III}	1.732[4]	1.760[3]	1.837[4]	2.14[1]	
Mn^{IV}	1.750[4]	1.753[3]	1.822[4]	2.13[1]	

From this table it can be seen that there is considerable variation in the values for R_0. By considering two particular examples (complexes **19** and **12**) it can be seen how the difference in R_0 transfers to a difference in calculated oxidation state. BVS results using various combinations of R_0 values are presented in Table 0-4.

Table 0-3 Bond lengths for Co1 and Co2 from complexes 19 and 12.

Complex **19**	Distance(Å)	Complex **12**	Distance (Å)
Co1–O11	2.093(8)	Co1–O111	2.106(2)
Co1–O12	2.095(8)	Co1–O711	2.137(2)
Co1– O13	2.143(7)	Co1–O121	2.106(2)
Co1–O14	2.134(8)	Co1–O721	2.096(2)
Co1–O15	2.042(8)	Co1–O131	2.099(2)
Co1– O16	2.124(8)	Co1–O731	2.116(2)
Co2– N41	2.01(1)	Co2–O111	1.905(2)
Co2–N42	1.95(1)	Co2–O112	1.880(2)
Co2–O11	1.925(8)	Co2–N21	1.951(3)
Co2–O12	1.908(8)	Co2–N61	1.931(3)
Co2– O71	1.914(8)	Co2–O711	1.903(2)
Co2–O72	1.855(8)	Co2–O712	1.889(2)

Table 0-4 Bond valence sum results using different R_0 values.

Complex	Atom	Co^{II}–O 1.692 Co–N 1.79	Co^{II}–O 1.692 Co–N 1.84	Co^{III}–O 1.70 Co–N 1.79	Co^{III}–O 1.70 Co–N 1.84	Co–O 1.680 Co–N 1.79	Co–O 1.680 Co–N 1.84
19	Co1	2.010	2.010	2.054	2.054	1.946	1.946
	Co2	3.341	3.519	3.387	3.565	3.274	3.452
12	Co1	1.940	1.940	1.982	1.982	1.878	1.878
	Co2	3.647	3.839	3.697	3.889	3.573	3.765

For both these examples Co1 is Co^{II} and Co2 is Co^{III}. From the results it can be seen that while the Co^{II} results are generally quite close to what is expected, within 0.12. The Co^{III} results are much more varied with a wider range of results possible. It was found that when using the oxidation state independent R_0 value for Co bound to O of 1.680, for the BVS result to be close to 3.0 for the complexes reported here, an R_0 value for Co bound to nitrogen of around 1.6 would have to be used, this is much lower than any found in the literature.

Although the result of the BVS calculations for Co^{III} were much higher than expected, this was found to be consistent for all complexes examined, and it was possible to distinguish these results from those for Co^{II}. Difficulties arise with heterometallic structures, where the metals are reasonably similar and the BVS results are not reliable enough to distinguish between them. A much more extensive study comparing complexes with different ligands would need to be undertaken to confidently calculate a more appropriate R_0 value for Co bound to nitrogen.

Appendix Two

Single crystal X-ray data

All crystallographic intensity data were collected using a Bruker APEX2 CCD diffractometer equipped with graphite-monochromated Mo-Kα radiation (λ = 0.71073 Å) and an Oxford Cryosystems low-temperature device.

Structures were solved by using SUPERFLIP[6] and refined using full-matrix least-squares refinement on F^2 or F using CRYSTALS.[7] PLATON SQUEEZE was utilised where disordered solvent was found to be difficult to model satisfactorily.[8,9]

Magnetic Susceptibility Measurements

Magnetic measurements in the temperature range 1.8-300 K were performed on polycrystalline samples constrained in eicosane, using a Quantum Design SQUID magnetometer equipped with a 5 T magnet (the Manchester SQUID is equipped with a 7 T magnet). Data were corrected for the diamagnetism of the compounds by using Pascal's constants and for the diamagnetic contributions of the sample holder and eicosane by measurements.

A diamagnetic correction for the sample was not applied for complexes **12** and **13** (data were corrected for diamagnetism of sample holder). In these cases it was assumed by inspection of the data that there was significant temperature independent paramagnetism (TIP), arising from low-lying excited states, which could be of equal magnitude and opposite sign to the sample diamagnetism.

Appendix Three

As mentioned throughout this thesis there is some difficulty identifying metal centres in the bimetallic complexes that have been synthesized due to the similarities between the ions, cobalt and manganese. Also it is difficult to distinguish between oxidation states of the same element using standard X-ray crystallography techniques.

Currently work is being undertaken by Dr Parois and Dr Cooper at the University of Oxford to overcome this problem. Their method involves targeting specific reflections during the determination of a strategy using multiple wavelengths.[10,11] This data can then be combined with data collected in a standard way, as the rest of the model is unaffected by the questionable metal ions. Samples of complexes **16** and **19** were sent for analysis using this method; however the process is still ongoing.

References

(1) Brese, N. E.; O'Keeffe, M. *Acta Crystallographica Section B* **1991**, *47*, 192.

(2) Palenik, G. J. *Inorganic Chemistry* **1997**, *36*, 122.

(3) Brown, I. D.; Altermatt, D. *Acta Crystallographica Section B* **1985**, *B41*, 244.

(4) Liu, W.; Thorp, H. H. *Inorganic Chemistry* **1993**, *32*, 4102.

(5) Ferguson, A.; Parkin, A.; Sanchez-Benitez, J.; Kamenev, K.; Wernsdorfer, W.; Murrie, M. *Chemical Communications* **2007**, 3473.

(6) Palatinus, L.; Chapuis, G. *Journal of Applied Crystallography* **2007**, *40*, 786.

(7) Betteridge, P. W.; Carruthers, J. R.; Cooper, R. I.; Prout, K.; Watkin, D. J. *Journal of Applied Crystallography* **2003**, *36*, 1487.

(8) Spek, A. *Journal of Applied Crystallography* **2003**, *36*, 7.

(9) Sluis, P. v. d.; Spek, A. L. *Acta Crystallographica Section A* **1990**, *A46*, 194.

(10) Parois, P.; Cooper, R. I. *Acta Crystallographica Section A* **2013**, *A69*, s198.

(11) Sutton, K. J.; Barnett, S. A.; Christensen, K. E.; Nowell, H.; Thompson, A. L.; Allan, D. R.; Cooper, R. I. *Journal of Synchrotron Radiation* **2013**, *20*, 200.